



FFI-RAPPORT

21/00127

A study of the Browning M2 Quick Change Barrel and problems experienced in the Norwegian Armed Forces

Svein Morten Bergsrud
Pål Martin Greni

A study of the Browning M2 Quick Change Barrel and problems experienced in the Norwegian Armed Forces

Svein Morten Bergsrud
Pål Martin Greni

Keywords

Maskingeværer
Ammunisjon
Våpenfunksjon
Våpen
Sprekkdannelse

FFI report

21/00127

Project number

5271

Electronic ISBN

978-82-464-3317-2

Approvers

Halvor Ajer, *Director of Research*
Morten Huseby, *Research Manager*

The document is electronically approved and therefore has no handwritten signature.

Copyright

© Norwegian Defence Research Establishment (FFI). The publication may be freely cited where the source is acknowledged.

Summary

Norway has used the Browning M2 heavy machine gun for decades. The first guns were US weapons given to us through the Mutual Defence Assistance Program. They were M2 Heavy Barrel (HB) versions. All weapons were converted to a so-called Quick Change Barrel (QCB) in the early 1990s. Around year 2000 some weapons were rebuilt from a closed-bolt to an open-bolt action. The open-bolt weapons were named NM218 and the closed-bolt weapons were named NM214.

Severe weapon failures have occurred in recent years with the QCB-weapons, and a lot of weapons show cracks in the threaded area on both barrel and barrel extension. Much work has previously been done to investigate these failures, but no clear answers have been found.

The Norwegian Defence Research Establishment (FFI) have been tasked to do a kinematic analysis of the weapon system together with chamber pressure measurements, and an analysis of non destructive crack detection methods.

From the kinematic analysis it was found that the barrel, barrel extension and bolt do not behave as one piece in the milliseconds after shot initiation; this is due to backlash in the system and gives rise to high forces on the parts. It was also found a very good correlation between maximum chamber pressure (P_{max}) and forces acting in the coupling between the barrel and barrel extension.

The crack analysis shows almost all cracks are situated in only two of the three threaded segments. This indicates that the forces between barrel and barrel extension are mainly transferred through two of the segments. This results in an highly asymmetric and increased load on the barrel and barrel extension compared to if the load was evenly distributed over all segments.

The best and easiest way to reduce the forces acting on the barrel and barrel extension would be to use ammunition with temperature-insensitive powder, like the NM241F2 when available. Reduced backlash/smaller tolerances in the threaded area of the barrel and barrel extension and small design and material improvements should also greatly reduce the risk of fatigue failures in the barrel and barrel extension.

Crack analysis shows that neither Magnetic Particle nor Dye Penetrant testing detects all cracks that are shown from microscopic examination of cross section cut. Due to the higher fail rate of the Penetrant testing, it is recommended to continue to use the Magnetic Particle testing for discarding barrels, but other test methods for non-destructive testing should be assessed and tested. Ultrasound is one possible alternative.

Sammendrag

Norge har brukt Browning M2 maskingevær i flere tiår. De første våpnene var amerikanske og ble gitt gjennom USAs våpenhjelp til Norge. Dette var såkalte M2 Heavy Barrel (HB). Alle de norske våpnene ble konvertert til såkalt hurtig pipeskift (Quick change barrel, QCB) på begynnelsen av 1990-tallet. Rundt år 2000 ble en del våpen bygget om fra lukket til åpen bolt mekanisme. Våpnene med åpen bolt mekanisme ble kalt NM218, og våpnene med lukket bolt mekanisme ble kalt NM214.

Alvorlige våpenbrekkasjer har forekommet med QCB-våpnene i de senere år, og veldig mange våpen viser seg å ha sprekker i innfestingen mellom løp og låseramme. Mye arbeid har tidligere blitt utført for å komme til bunns i årsakene til våpenbrekkasjene, men ingen klare og sikre svar er funnet.

Forsvarets forskningsinstitutt (FFI) har i denne sammenheng gjennomført en kinematisk studie av våpensystemet sammen med kammertryksmålinger. En analyse av ikke-destruktiv sprekkanalyse er også utført.

Fra den kinematiske studien ble det funnet at pipe, låseramme og sluttstykke ikke beveger seg som én solid del i de første millisekunder etter antenning av skuddet. Dette skyldes slark/toleranser mellom delene, og dette er med på å skape ekstra store krefter mellom løp og låseramme. Det ble også funnet en meget god korrelasjon mellom maksimalt kammertrykk (PMax) og kreftene som virker i koblingen mellom løp og låseramme.

Sprekkanalyser av det gjengede partiet på pipen viser at nesten alle sprekker ligger i kun to av de tre gjengede segmentene. Dette indikerer at kreftene mellom pipe og låseramme i hovedsak blir overført kun via to gjengesegmenter. Dette gir en asymmetrisk belastning og en kraftig økt belastning på deler av pipen og låserammen, sammenliknet med om kreftene hadde vært jevnt fordelt over alle segmentene.

Den enkleste måten å redusere kreftene som virker på pipe og låseramme, vil være å benytte ammunisjon med temperaturstabil krutt, slik som NM241F2 når denne blir tilgjengelig. Redusert slark/mindre toleranser i det gjengede partiet på løpet og låserammen, sammen med små design- og materialforbedringer, burde også kraftig redusere sannsynligheten for utmattelsesbrudd i pipe og låseramme.

Sprekkanalysen viser at hverken Magnetic Particle- eller Dye Penetrant-testing detekterer alle sprekkeene som ble avdekket med mikroskopi av tverrsnittskutt fra pipen. På grunn av den høye feilprosenten til Dye Penetrant-testen er det anbefalt å fortsette med Magnetic Particle-testing til dette formålet. Vi anbefaler også at man vurderer og tester andre typer ikke-destruktiv sprekkanalyse. Ultralyd er et mulig alternativ.

Contents

Summary	3
Sammendrag	4
1 Introduction	7
2 Description of experiments.	9
2.1 Weapon	9
2.1.1 Basic function of the weapon.	9
2.2 Ammunition	12
2.3 Pressure measurements	12
2.4 Kinematic analysis of main parts	13
2.5 Crack Detection	16
2.5.1 Magnetic Particle Test	17
2.5.2 Dye penetrant Test	18
2.5.3 Microscopic examination of cracks	18
3 Pressure measurements	19
3.1 Robinca gun barrel measurement	22
4 Kinematic analysis of main parts	24
4.1 Positions of main parts	24
4.2 Velocities of main parts	27
4.3 Accelerations of main parts	28
4.4 Forces	30
4.5 Correlation between barrel force and pressure	32
4.5.1 Oiled cartridge cases	34
4.5.2 Temperature stable extruded powder	34
5 Crack detection and measurement of crack depth	38
5.1 Results from Microscopic examination of cracks	48
6 Summary of results	50
6.1 Crack analysis and recommendations on non destructive testing	51
Appendix	
A Pressure measurements	53
B Robinka barrel measurements	58
B.1 Barrel A1	58
B.2 Barrel B1	66

B.3 Barrel C1	73
C Pictures from microscope examination	79
D Brake opening of crack at FOLAT	143
References	150

1 Introduction

The Norwegian Armed Forces have used the Browning M2 heavy machine gun for decades. The first guns were US weapons given to us through the Mutual Defence Assistance Program. They were M2 Heavy Barrel (HB) versions. All weapons were converted to Quick Change Barrel (QCB) in the early 1990s with a conversion kit delivered by FN Herstal. Around year 2000 some weapons were rebuilt to an open bolt action by a company called Vinghøg. The rebuilt was done because some weapons had exploded due to cook-off of the explosive in the Multi-purpose (MP) ammunition. The open bolt weapons were named NM218 and the closed bolt weapons were named NM214.

In 2014 a severe weapon explosion occurred with ordinary Target Practise (TP) ammunition called NM241 (Ball) and NM242 (Tracer). The barrel was teared open and the barrel extension cracked, Figure 1.1. A Technical Investigation Group (TUG) was established to investigate the failure. During their work more weapon failures were discovered. It became obvious that a lot of weapons had cracks in both barrel and barrel extension. The cracks in the barrel were found in the threaded segments at the back end, and the barrel extension showed cracks in the left front part and right back part.

Crack detection on barrel and barrel extension became part of the quarterly maintenance of the weapons. This has shown that a vast majority of the weapons show signs of cracks in these areas. A lot of barrels are therefore discarded to avoid new severe weapon failures. So many that it is a problem to supply enough parts. Naturally a question has arose whether too many barrels are discharged. Completely new weapons are recently procured, but the Norwegian Armed Forces will have to use old weapons in addition for several years.

Despite the work of the Technical Investigation Group, no certain answers could be found to explain the severe weapon failure in 2014 and the other occurring problems.

After reading trough the documentation available from the work of the Technical Investigation Group [11],[7], [9], [10], [6], [3], [5], [4], [1], [2], [8], a brief conclusion on the historic work would be:

- Reduction of threaded area in barrel and barrel extension weakens the QCB configuration as compared to the previous fully threaded M2HB version.
- Poor material quality, especially in barrels, also when compared to the old fully threaded-design. Cracks propagates through inclusions in the barrel.
- Poor machining quality finish. Initiates cracks.
- Uneven load on barrel-extension during firing. Cracks in the left front part and right back part.
- Lack of knowledge on the weapon system among users can have lead to incorrect use. It is of high importance to adhere to the intervals of barrel change and the number of shots in a burst.
- The ball powder used in the NM241 and NM242 is highly temperature sensitive and can, depending on the usage pattern, give high pressures during firing.
- Wet or oiled cartridges can increase the load on the barrel and barrel extension.

The Norwegian Defence Material Agency (NDMA) tasked FFI to further investigate the problems

observed with the weapon system. The task was divided into three separate work packages

1. Kinematic analysis of the weapon together with pressure measurements.
2. Crack analysis of used barrels and an analysis of crack detection methods.
3. Establish a detailed 3D CAD-model of the weapon.

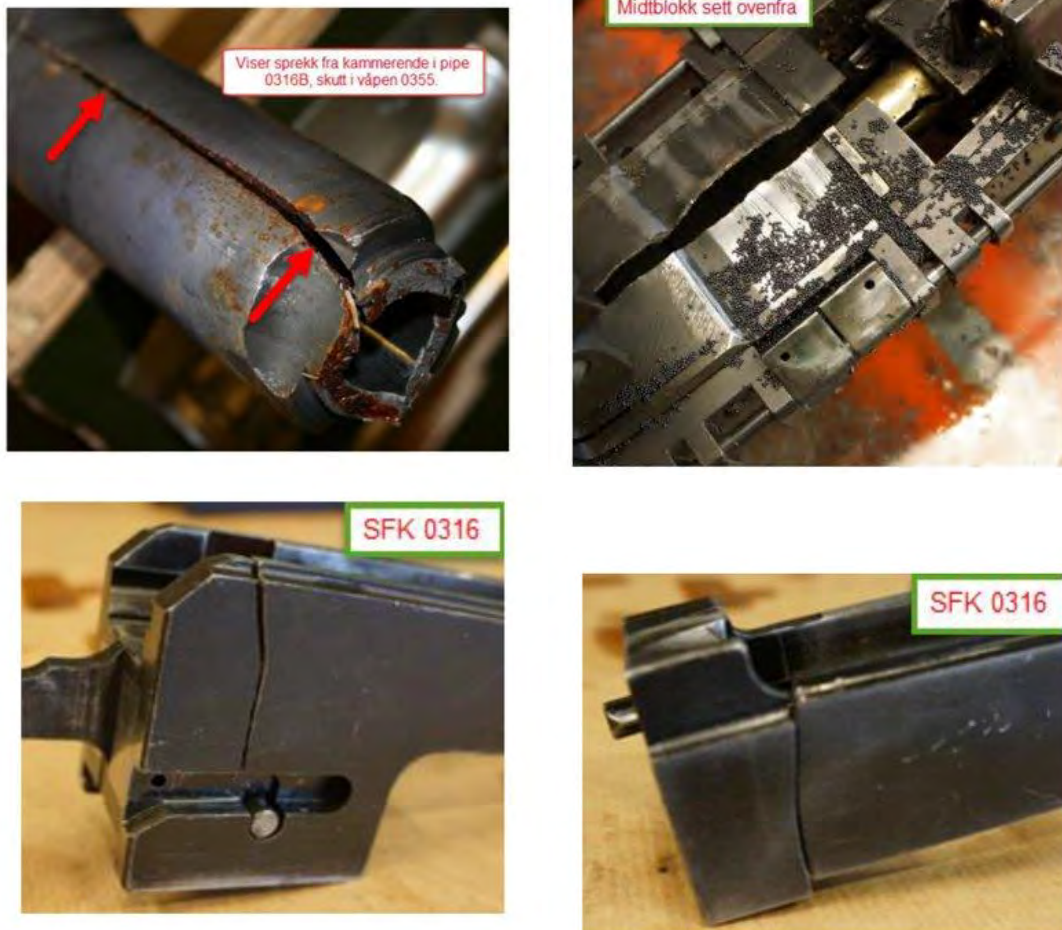


Figure 1.1 Pictures of the weapon with the cracked barrel and barrel extension.

2 Description of experiments.

All handling of weapons, ammunition and other test equipment has been carried out by our two senior research technicians Lasse Sundem-Eriksen and Ole Andreas Haugland.

2.1 Weapon

The weapon used in this study is a FN Herstal Browning M2 Quick Change Barrel (QCB) with a closed bolt operation. Weapon number is 1650517. The Norwegian designation for the closed bolt version with QCB is NM214.

The gun was delivered to us from the Norwegian Defence Material Agency (NDMA) and had three barrels, all modified for pressure measurements according to EPVAT procedures described in MULTI CALIBRE MANUAL OF PROOF AND INSPECTION (M-C MOPI), [12]. The three barrels were pre measured with a caliber gauge and marked with the following numbers:

Barrel	Caliber diameter (mm)
A1	12.54
B1	12.60
C1	12.69

Table 2.1 Pressure modified barrels

The three barrels were chosen by NDMA to represent a unusually tight barrel (A1), a normal barrel (B1) and a unusually wide barrel (C1).

The weapon had some slots cut open in the frame to reveal the barrel extension, breech lock and the bolt during firing.

2.1.1 Basic function of the weapon.

In Figure 2.1 a cut-through of the weapon is shown. The main parts are as follows:

- barrel in beige
- barrel extension in green
- bolt in blue
- barrel buffer body in red
- weapon frame in grey



Figure 2.1 Overview of the weapon with main parts.

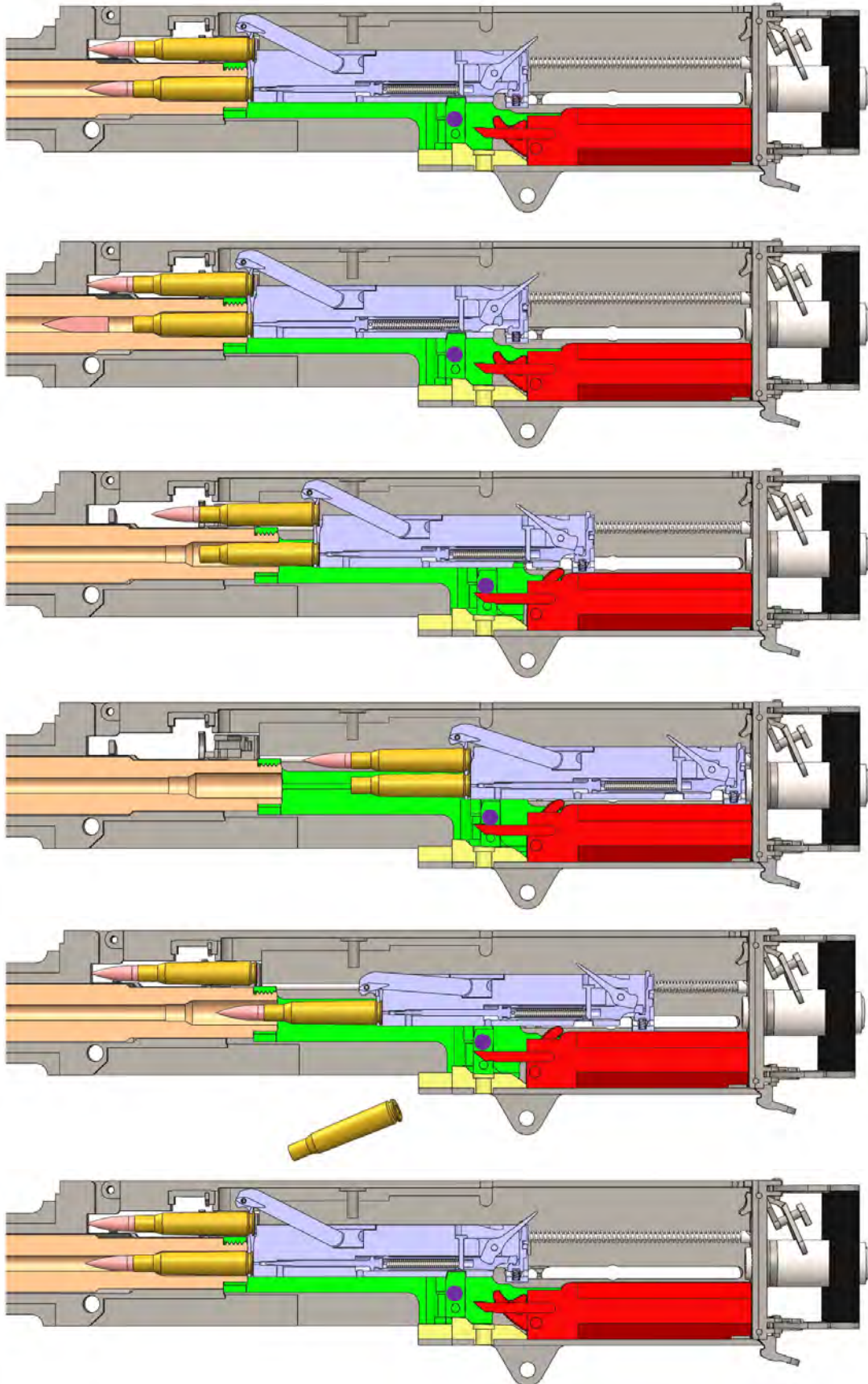


Figure 2.2 Basic operation of the weapon.

In picture 1 of Figure 2.2 the weapon is loaded and ready to fire. The next round is laying on top of the chamber. The barrel is fastened to the barrel extension with locking lugs (on the QCB version). The breach lock (marked with a purple dot) is in the locked position. This means the bolt and the barrel extension are locked together.

In picture 2 the firing pin has struck the primer and the bullet has left the case. The barrel, barrel extension and bolt starts to move backwards in one piece.

In picture 3 the barrel, barrel extension and bolt has moved backwards. The breach lock is pushed down and the bolt is released from the barrel extension and moves backwards against the bolt spring. The barrel and barrel extension has stopped against the barrel buffer and the accelerator has been pushed back.

In picture 4 the bolt has stopped in the backward position. The empty cartridge is ejected and a new round falls into place.

In picture 5 and 6 the bolt moves forward and the new round is loaded into the chamber. When the bolt hits the back of the barrel, the accelerator on the barrel buffer pushes the whole assembly (bolt, barrel extension and barrel) forward and the breach lock is pushed up and locks the assembly together. A new round is ready to be fired.

Figure 2.3 shows how the barrel and barrel extension are coupled together in the QCB version. There are three segments, A, B and C, of locking lugs/threads on the barrel. The barrel is mounted into the barrel extension and rotated 60° to lock.

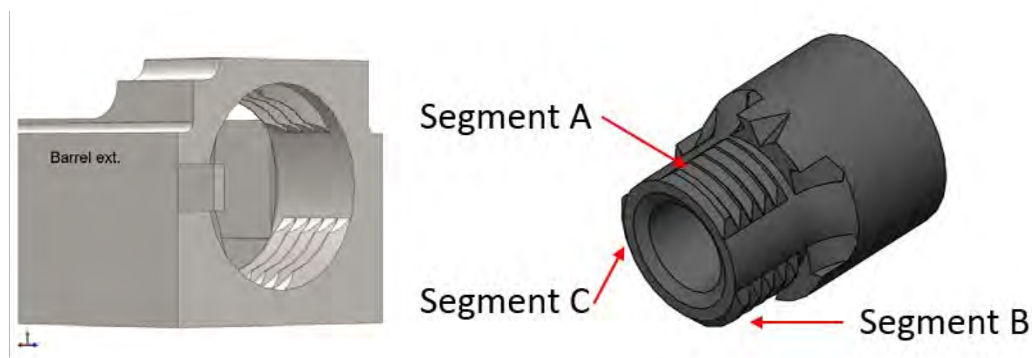


Figure 2.3 The QCB coupling between barrel extension and barrel.

2.2 Ammunition

Ammunition types used in this study are shown in Table 2.2.

Ammunition type	Bullet weight (g)	Lot number
NM241	46	20-RA-10 and 51-RA-12
NM242	43	20-RA-10
NM241 F2	46	T01-RA-18
M33	42	00318-CR1

Table 2.2 Ammunition types

2.3 Pressure measurements

The pressure sensor used was the Kistler Model 6215. The pressure sensor was connected to a Kistler model 5073A charge amplifier, which in turn was connected to a National Instruments PCI-4462 placed in a PC. The sampling rate was 204.8 kHz. A FFI-developed Lab-view program was used to log pressure data.

The barrels were modified for pressure measurements according to MULTI CALIBRE MANUAL OF PROOF AND INSPECTION (M-C MOPI), [12]. Procedures for pressure measurements are described in Section 12 "Combination Electronic Pressure Velocity & Action Time (EPVAT) Test Procedure".

With the EPVAT Test Procedure a hole is drilled in the barrel for the pressure sensor right in front of the cartridge case neck. Using this method of pressure measurement, there are two things to be aware of.

1. The pressure sensor does not register any pressure before the bullet is released from the case and the powder gases start to leak around the bullet, hence the pressure built up before the projectile starts to move is absent. Because of this the pressure rises steeply when the bullet leaves the case mouth.
2. The pressure sensor is mounted in a drilled hole in the barrel, and it doesn't fill the hole all the way through. The pressure already inside the case when the bullets leaves the case mouth, gives a high pressure spike in the measurement. This pressure spike is a result of the powder gases filling up the hole where the sensor sits, giving it a "kick". This again leads to pressure waves moving up and down the mounting hole giving rise to a "sawtooth"-like pressure curve. The raw pressure data must therefore be filtered to remove these effects [12].

A typical pressure measurement is shown in Figure 2.4. Measured pressure is plotted in blue, and filtered pressure is plotted in red.

The maximum pressure (PMax) for all shots fired in this study was read off manually as the maximum value of the filtered curve. The filter used was a moving-average filter. Matlab was used to apply the filter with the following command.

```

windowSize = 10;
b = (1/windowSize) * ones(1, windowSize);
a = 1;
Filtereddata = filter(b, a, Inputdata);

```

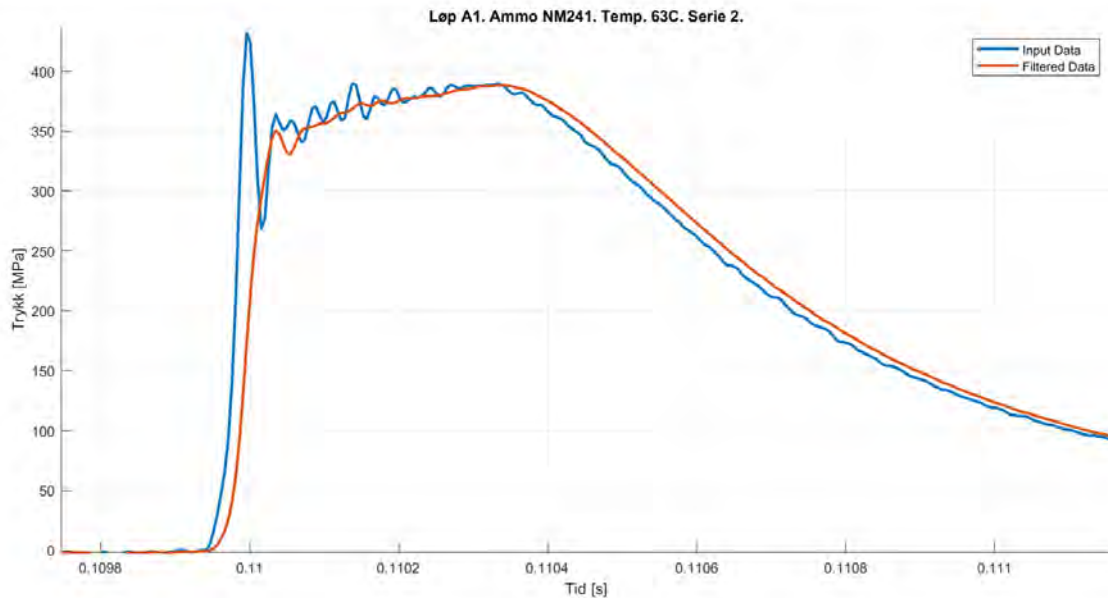


Figure 2.4 Measured pressure in blue, filtered pressure in red.

2.4 Kinematic analysis of main parts

To analyse movement, velocity, acceleration and forces on the weapon parts during firing, high speed cameras together with a motion analysis software have been used. The test setup is shown in Figure 2.5. The two high speed cameras were Photron FASTCAM SA-Z and Photron FASTCAM AX-200. The cameras were in sync and filmed with a picture rate of 20 000 fps. The motion analysis software used was TEMA Defence from IMAGESYSTEMS.

In Figure 2.6 the layout from TEMA Defence is shown. The FASTCAM AX-200 was used to film the barrel and the weapon frame, the FASTCAM SA-Z was used to film the barrel extension and the bolt. All the parts were marked with a small dot of white paint to be the marker for the software. The best tracking algorithm for this analysis were found to be the "Center of gravity". This algorithm tracks the center of gravity of the contour of a marker. The white dots made a perfect contrast and the software had no issues with tracking the points from frame to frame.

To calculate the velocity and acceleration a built in filter of 13 points was used. This means that 13 positions points is used to calculate the velocity at one point. So for point $t = a$, all points between $t = a - 7$ and $t = a + 6$ are used to calculate the slope of the position curve in point $t = a$. The same goes for the acceleration. Hence, in order to capture high accelerations the video frame rate needs to be high.

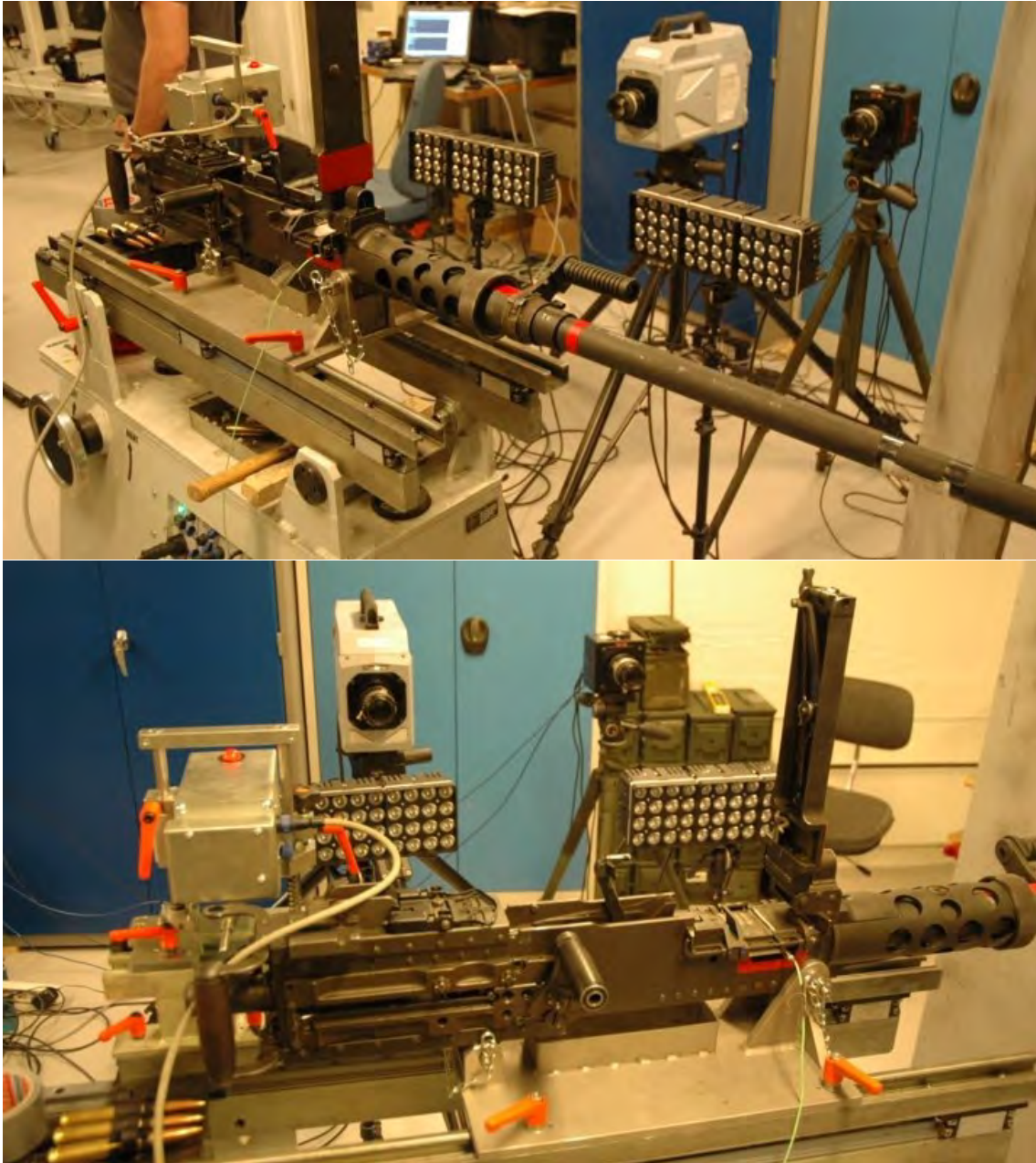


Figure 2.5 Test setup with high speed cameras and pressure measurements.

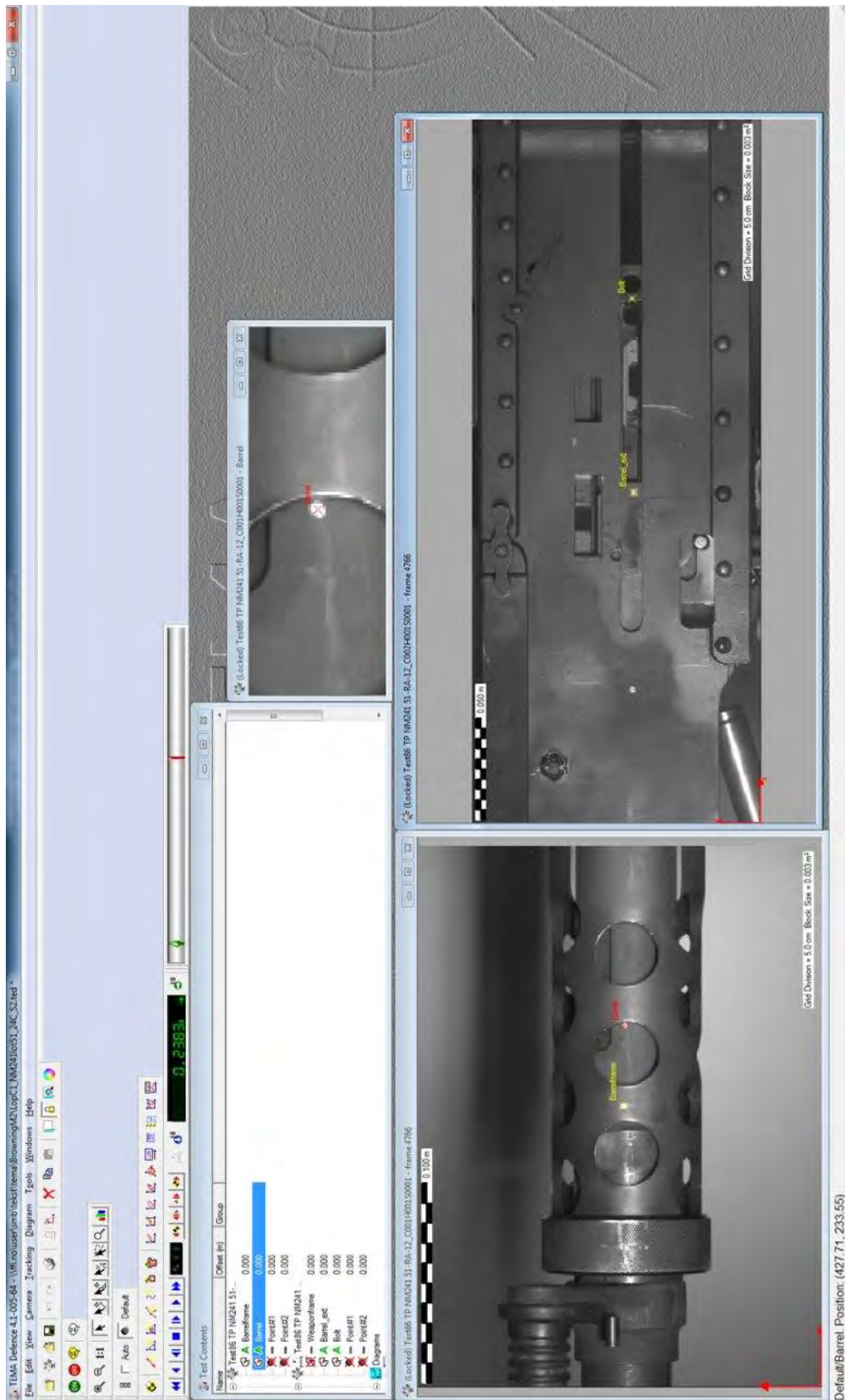


Figure 2.6 Motion Analysis software TEMA Defense.

2.5 Crack Detection

Six barrels were given to FFI for conducting experiments with crack detection. All six barrels were discarded by personnel from the Norwegian Defence Material Agency (NDMA), based on crack detection with Magnetic Particle testing (MT). MT is the standard method for crack detection in the Norwegian Defence. Due to the weapon accidents experienced the recent years, it is decided to perform crack detection on all barrels and barrel extensions when the weapons are into quarterly maintenance. This has shown that a vast majority of the barrels shows signs of cracks on the locking lugs/threads in the three segments. A lot of barrels are of course then discarded, and a question has arisen whether too many barrels are discharged when using the MT method.

It was therefore decided to look into some methods of crack detection to better judge if the Magnetic Particle testing is suitable for this purpose.

The crack detection was done on all six barrels by the three methods; Magnetic Particle Test, Dye Penetrant Test (PT), and examination by microscope (M). Microscope is expected to have 100 % success rate for detecting cracks and is a destructive test. Only the rear end of the barrels where cracks were expected to occur was examined. The rest of the barrels was cut off to make the specimens more easy to handle. The microscopic examination was done at FOLAT (Forsvarets Laboratorietjenester) at Kjeller.

To obtain evidence for the performance of the MT and PT methods, different cameras and setup was used to take pictures.

To get an overview of where the crack is related to the test object, a Nikon D70s was used mounted on a stand where the complete test object could be on one picture. The Nikon camera was used with the setup in Table 2.3.

F-Stop	f/29
Exposure time	8 sec.
Exposure bias	+0.7 step
Focal length	105 mm
Max aperture	4.1
35 mm focal length	157
Equipt with NIKON AF MICRO	
	Limit
	Manual

Table 2.3 Nikon D70s camera setup

For close up view, a AMScope MU1000 camera connected to a Zeiss Stemi 2000-C microscope was used. The following procedure during photo shoot was used to get clear image of the cracks:

1. Place object in field of view for camera.
2. Use white light when adjust focus.
3. Illuminate object with UV-light and take photos.

Figure 2.7 shows the setup when taking pictures from MT-examination.

2.5.1 Magnetic Particle Test

Magnetic particle testing (MT) is done by establishing a magnetic field in the test object and applying a fluorescent magnetic ink. The magnetic ink will be attracted to the magnet poles on the test object. If a crack exist in the test object, the magnetic particles will accumulate at the surface discontinuities. By use of a UV torch light in a dark room the fluorescent magnetic ink will appear clearly. Figure 2.7 shows the setup when taking pictures from MT-examination.

The following equipment was used during testing:

- Fluorescent magnetic ink: Bycotest 101
- UV torch light: Labino UVG3
- Cleaning agent: Bycotest C10
- Pressurized air: Lyreco invertible gas duster
- Electromagnetic yoke: MY-2

This short procedure was used to find cracks:

1. Clean object with Bycotest C10.
2. Wipe dry with a paper tissue.
3. Magnetize object with claws in each end of object.
4. Shake and apply fluorescent magnetic ink (Bycotest 101) on the object.
5. Use compressed air to gently remove excess fluorescent magnetic ink.
6. Use UV-flashlight to light up areas where there is expected to detect cracks.

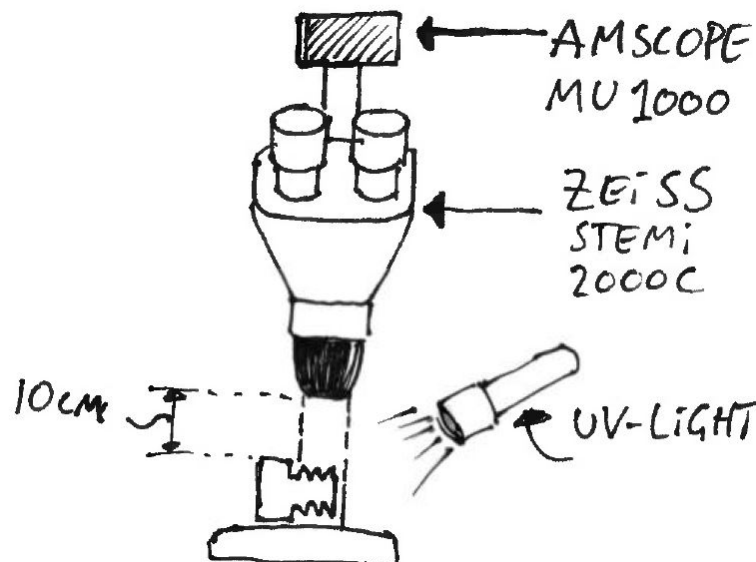


Figure 2.7 Examination with Magnetic Particle Test

2.5.2 Dye penetrant Test

Liquid penetrant test is often foreshortened as PT. This method is known for low cost and easy to perform. The following equipment and procedure was used for PT-inspection.

- Cleaning agent: Bycotest C10
- Dye penetrant spray: Bycotest RP20
- Developer: Bycotest D30A

Temperature of test object during penetrating test must be within 10 °C to 50 °C.

1. Clean object with Bycotest C10 and a paper tissue.
2. Let test object dry for minimum of 2 minutes, to ensure all cleaning agents is evaporated from surface defects.
3. Apply color penetrating spray (Bycotest RP20). A wet surface of penetrating spray is important over the complete area where it is expected to find cracks. The penetrating spray must work for at least 20 minutes.
4. Gently clean surface with water with temperature of approximately 30 °C.
5. Let test object dry for 3 minutes. Within 10 minutes after water cleaning apply developer. The developer shall be applied with short burst of spray to get a thin white evenly thick layer of developer.
6. Examination of test object can start as soon as developer is dry and last for up to 30 minutes.

2.5.3 Microscopic examination of cracks

The microscope examination was done by FOLAT at Kjeller. Each segments was cut out from barrel at FFI and delivered to FOLAT. Then segments were cleaned and cast separately in a cylindrical shape of epoxy. Each cylinder was then grind flat and polished before examination. Some of the specimens was then cut and polished up to six times as shown in figure 2.8, where a measurement of cracks was done for each cut. The results is summarized in table 5.1 to 5.6, and table 5.13.

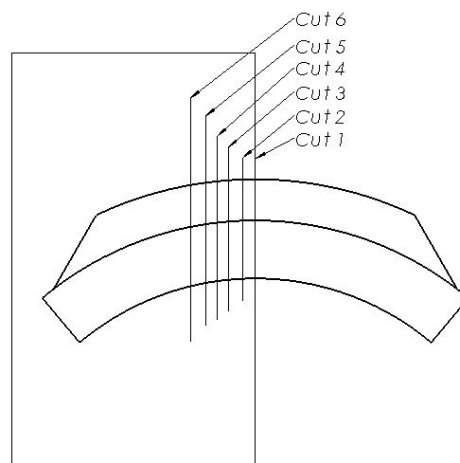


Figure 2.8 Cross section cuts of specimens

3 Pressure measurements

All shots fired were both filmed with high speed cameras and pressure was measured. In this part we only focus on the pressure measurements.

The pressure was measured at different powder temperatures to find how the maximum pressure (Pmax) react to higher temperatures. It is well known that the ammunition can get very warm before being chambered in the Browning M2 during extensive firing. This is because the ammunition rests on top of the chamber. Tests performed by Nammo have shown ammunition temperatures well above 100 °C before the ammunition enter the chamber, and chambered ammunition close to 200 °C, [6].

In Figures 3.2 to 3.5 the average Pmax for all ammunition types in all barrels are shown. As we see, the NM241 has a quite high pressure and the Pmax increases fast with increasing powder temperature. The M33 and NM242 tracer have lower pressures than NM241, but also reacts with increasing PMax with increasing powder temperature. The new NM241F2 clearly has a temperature stable powder. The PMax value is almost constant over the temperature range from 24 °C to 100 °C! The NM241F2 has an extruded powder from Eurenco (NC1394NT) whereas NM241 and NM242 have ball powder from PB Clearmont (PBC-347).

We see that there are small differences in PMax between the barrels, but barrel B1 has a slightly higher average pressure than the two others. The original theory was that tight barrels should give higher pressures than wide barrels. Based on the caliber diameter found by gauging the barrels, this seems not to be the case.

The number of shots fired at each temperature is shown in Figure 3.1. To visualize the spread/variation in data, Box plots of the measurements are shown in Appendix A.

Ammo/Temperature	Number of shots fired at each temperature			
	24 C°	52 C°	63 C°	100 C°
Barrel A1 M33	12	-	-	-
Barrel B1 M33	9	-	-	-
Barrel C1 M33	6	-	6	-
Barrel A1 NM241	6	6	6	-
Barrel B1 NM241	6	6	6	6
Barrel C1 NM241	6	6	6	-
Barrel A1 NM242	5	3	3	-
Barrel B1 NM242	7	-	3	-
Barrel C1 NM242	6	-	3	-
Barrel A1 NM241F2	6	-	6	-
Barrel B1 NM241F2	6	-	6	6
Barrel B1 NM242F2	6	-	6	-

Figure 3.1 Number of shots fired at each temperature.

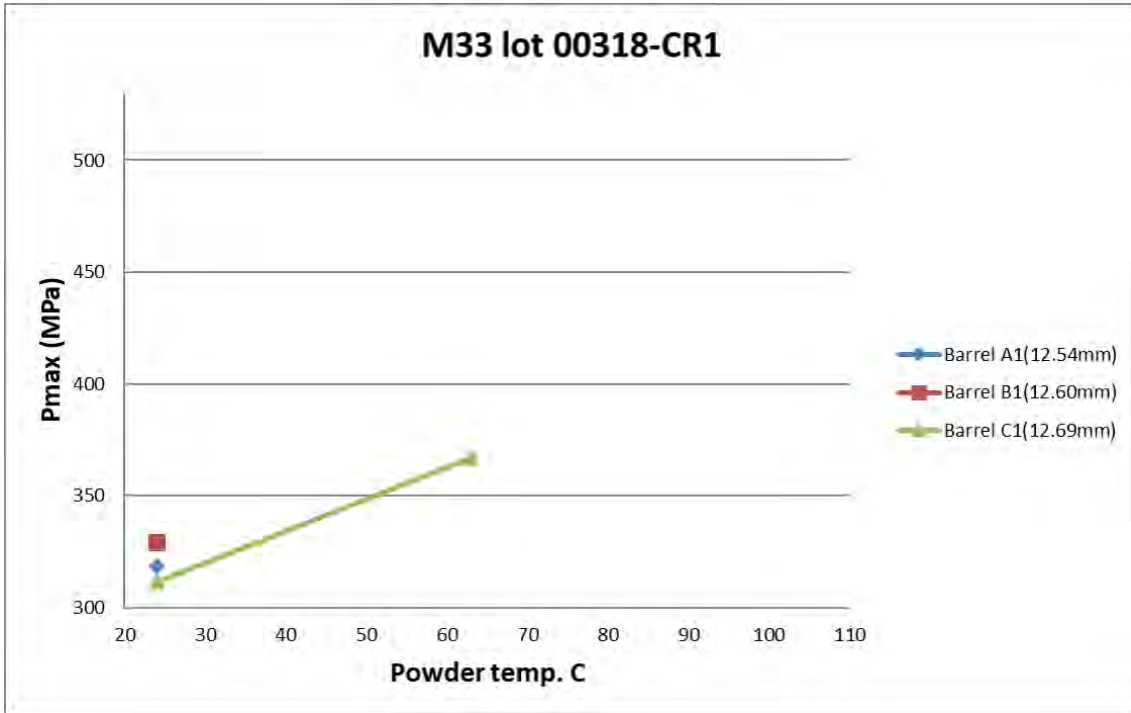


Figure 3.2 M33 lot 00318-CR1

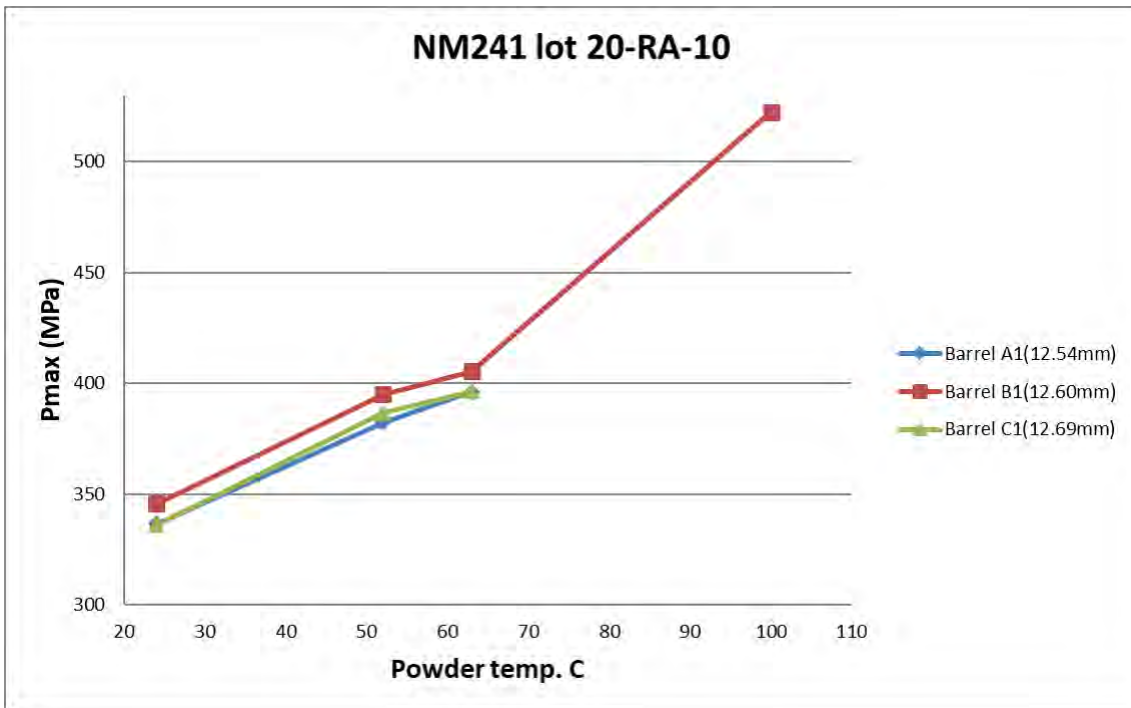


Figure 3.3 NM241 lot 20-RA-10

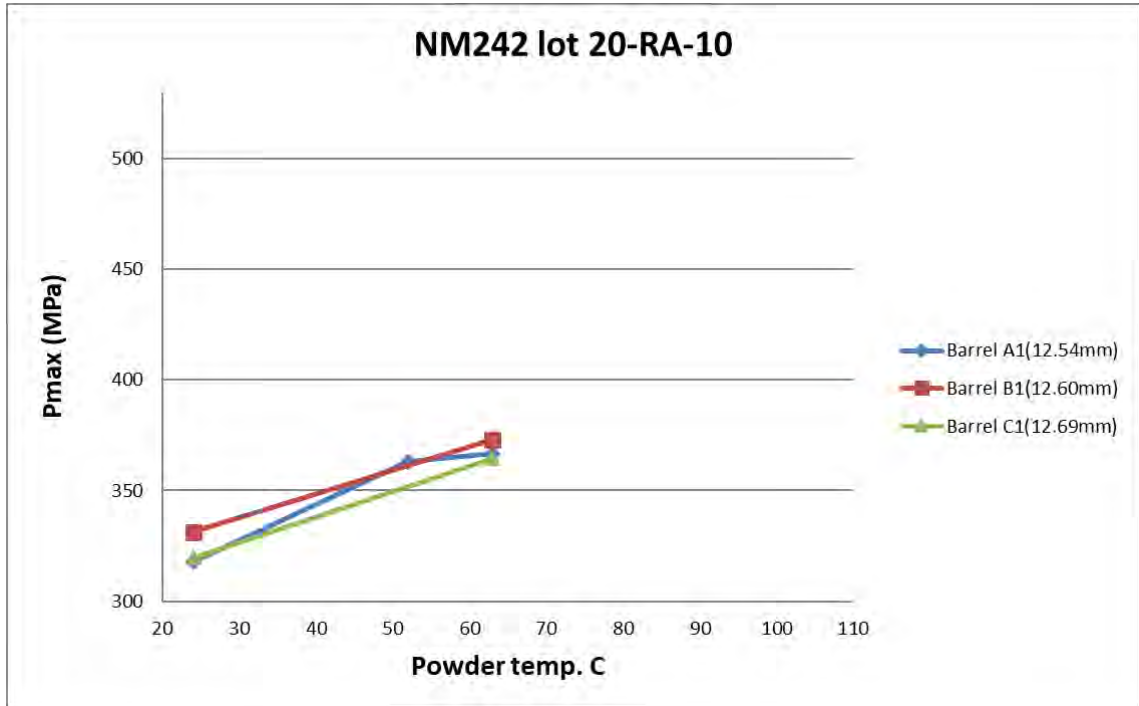


Figure 3.4 NM242 lot 20-RA-10

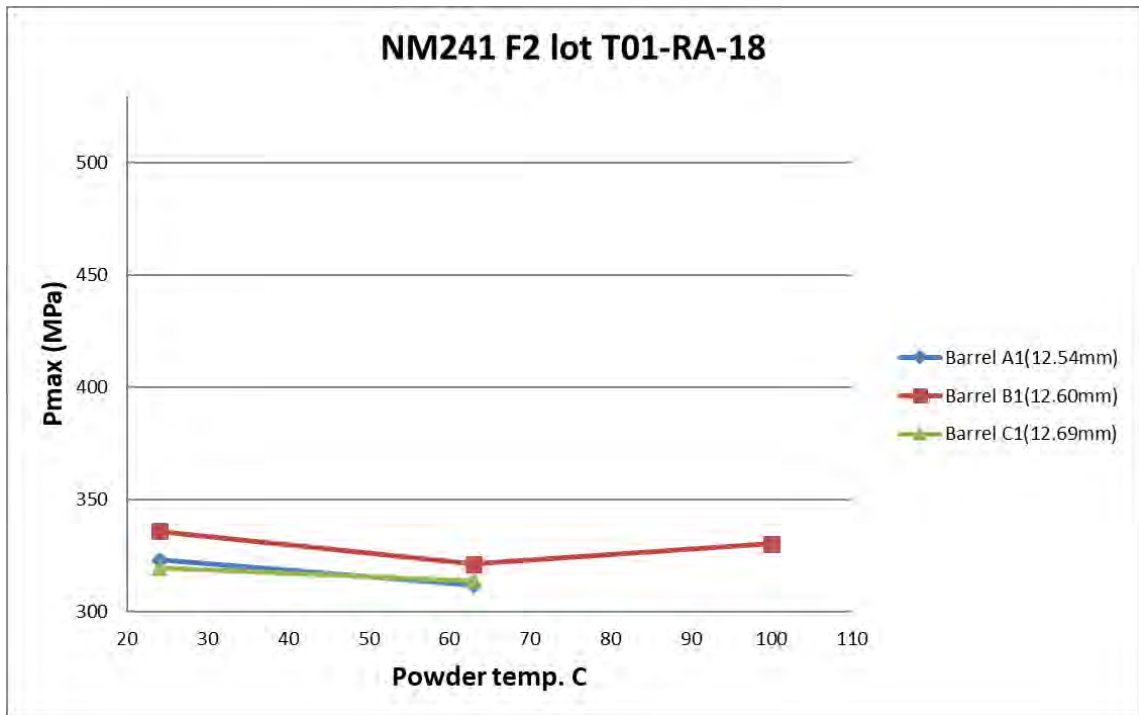


Figure 3.5 NM241F2 lot T01-RA-18

3.1 Robinca gun barrel measurement

As mentioned the three barrels were measured with a caliber gauge to the following minimum caliber diameter:

Barrel	Caliber diameter (mm)
A1	12.54
B1	12.60
C1	12.69

The theory was that tight barrels should give higher pressures than wide barrels. As mentioned the barrels were chosen by NDMA to represent an unusually tight barrel (A1), a normal barrel (B1) and an unusually wide barrel (C1). Based on our pressure measurements there were no large differences in PMax between the barrels, but B1 had a slightly higher average pressure for all ammunition types. To gauge the caliber diameter is however not the best way to judge which barrels are tighter or wider. The grooves diameter is more important. Figure 3.6 shows the difference between the grooves and caliber diameter.

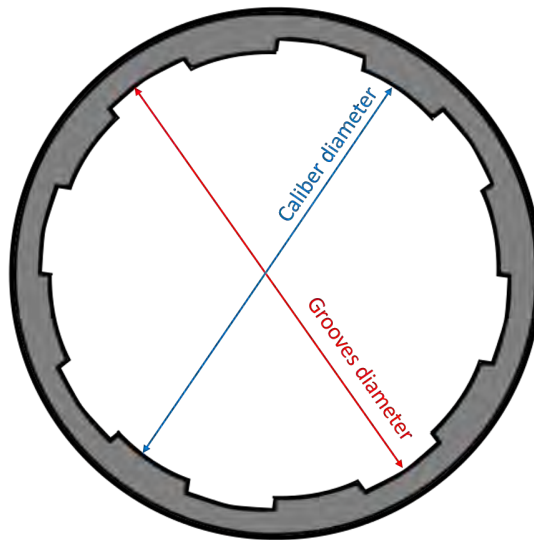


Figure 3.6 Grooves and caliber diameter in a barrel.

To get a better measurement of the inner diameter of the barrels, a Robinca gun barrel measurement was performed at Romerike tekniske verksted (RTV). This system measures both the groove diameter and the caliber diameter. The barrels have eight grooves and lands. There are therefore four measurements for the caliber and the grooves diameter at each position in the barrel. Measurements were taken at 17 positions from the muzzle back to the commencement of rifling. Measurement reports from RTV can be found in Appendix B.

The average groove and caliber diameter at each point down the barrel is plotted in Figure 3.7. The muzzle is at position 0 mm. As seen in the figure, Barrel C1 has the largest diameter for both the grooves and caliber. Barrel A1 is a little bit tighter than B1 from the muzzle and half way in, B1 is then tighter back towards the chamber.

Barrel B1 shows a slightly higher maximum pressure than barrel A1 and C1. This could be due to the barrel being tighter in the area from the chamber and about half way down the barrel, because this is the area where the pressure builds up and reaches its maximum value, but measurements from more barrels would be necessary to conclude on this.

All things considered, it seems safe to conclude that the maximum pressure is not very sensitive to the tightness of the barrel. The main cause of high pressures is the powder temperature.

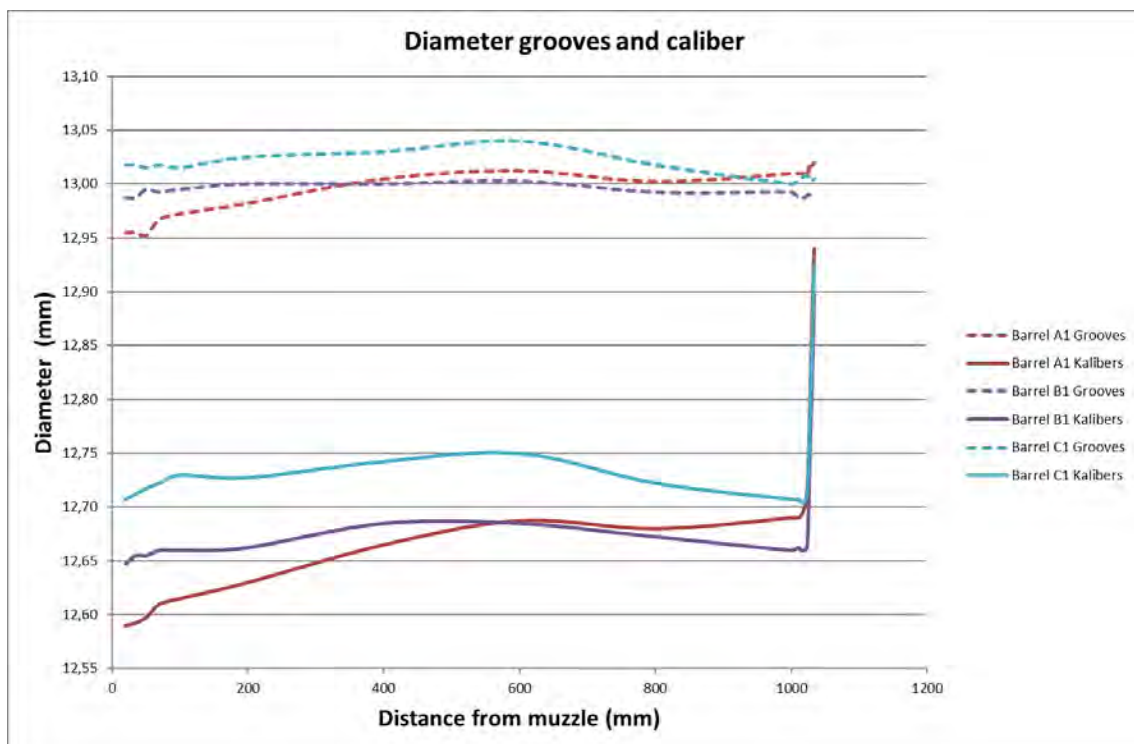


Figure 3.7 Diameter of grooves and caliber measured with Robinca gun barrel measurement system.

4 Kinematic analysis of main parts

Burst of three shots with each ammunition type were filmed in one sequence. Pressure measurements were done simultaneously to be able to correlate the movements of the parts to the pressure.

4.1 Positions of main parts

In Figure 4.1 we see the position of the barrel, barrel extension, bolt and weapon frame as a function of time for the two first shots in a burst. All parts are plotted with a start position of 0 mm. We see how the bolt, barrel and barrel extension moves together for about 25 mm. The bolt then separates and moves backward. The barrel and the barrel extension moves backwards together with the weapon frame before the bolt returns and joins the barrel and barrel extension. The whole assembly then moves forward to the starting position. We see that the whole weapon moves backward due to the recoil forces (yellow line). If we subtract the position of the weapon frame from the others we get the position of the main parts relative to the weapon frame. This is shown in Figure 4.2. The pressure curves are also plotted. The time scale of the plot is approximately 210 ms or 0.21 s.

In Figure 4.3 we have subtracted the position of the bolt from the position of the barrel extension and plotted it together with the pressure curve. The time scale of the plot is now 25 ms. This figure shows that the bolt moves approximately 0.4 mm relative to the barrel extension, immediately as the shot is fired. This means that there are some backlash between the bolt and barrel extension. This has to do with the breach lock tolerances. The bolt can move 0.4 mm before the breach lock is in full contact with both bolt and barrel extension.

In Figure 4.4 we have subtracted the position of the barrel extension from the position of barrel and plotted it together with the pressure curve. This figure shows that the barrel extension moves approximately 0.5 mm relative to the barrel, immediately as the shot is fired. This means that there are some backlash between the barrel extension and barrel as well. This has to do with the tolerances in the locking lugs/threads connecting the barrel and barrel extension.

Based on this we can say that the bolt moves before the barrel extension and the barrel extension moves before the barrel. When the round is initiated, the cartridge has to move backwards and push on the boltface. Backlash between bolt and barrel extension is taken up (breach lock tolerances), then backlash between barrel extension and barrel is taken up (locking lugs/threads tolerances). Hence, most likely friction between cartridge and chamber does not play an important role in this process, because if the cartridge was stuck in the barrel during the shot the barrel should have moved first.

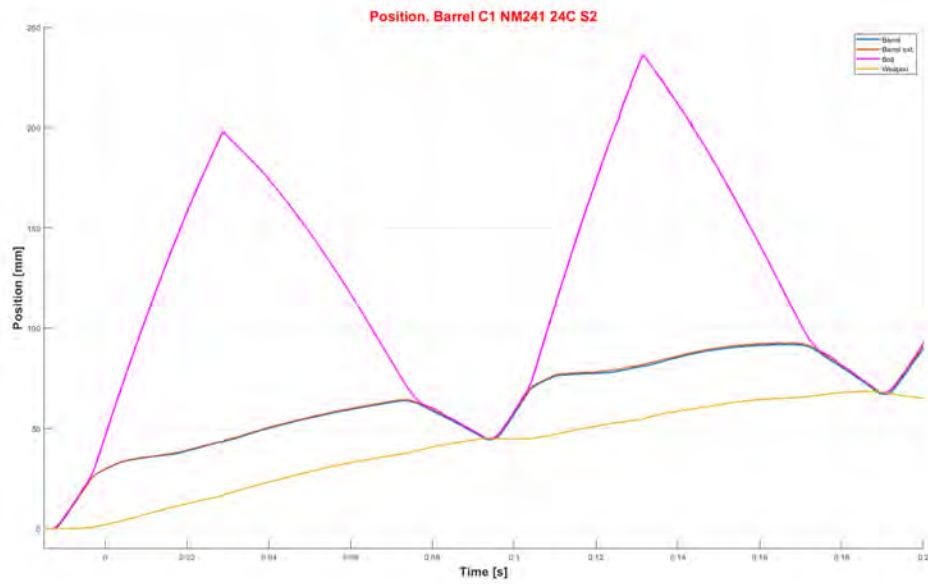


Figure 4.1 Position of main parts.

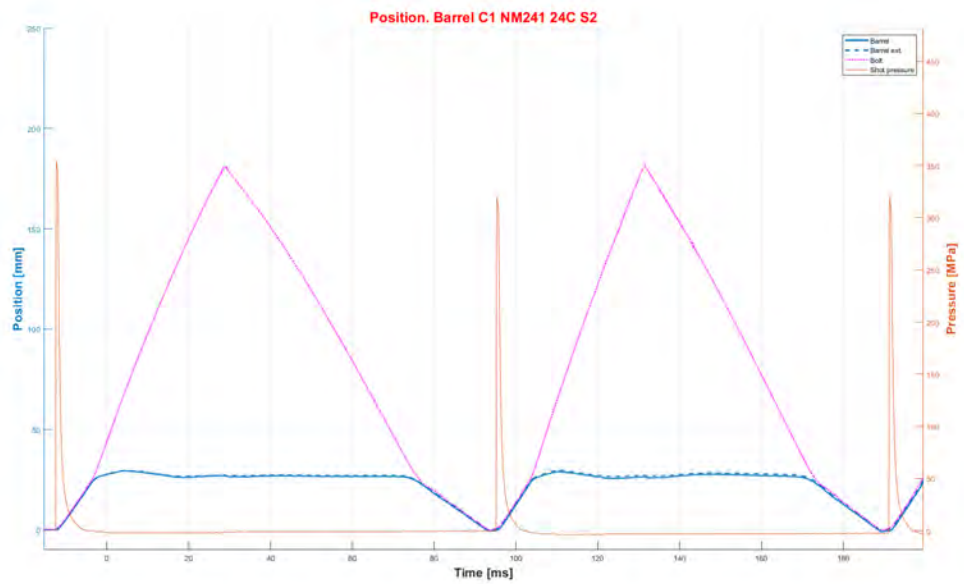


Figure 4.2 Position of main parts relative to weapon frame.

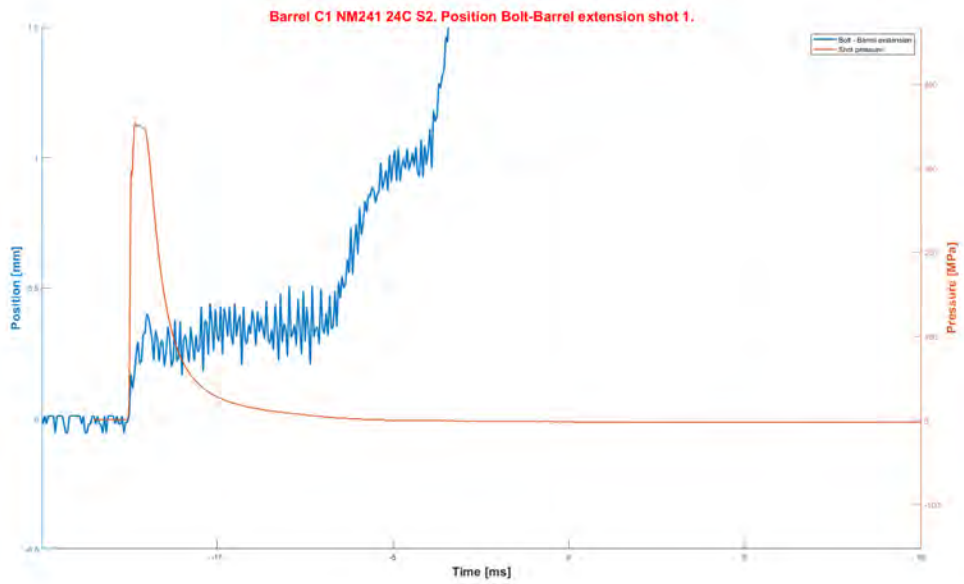


Figure 4.3 Position of the bolt subtracted from the position of the barrel extension.

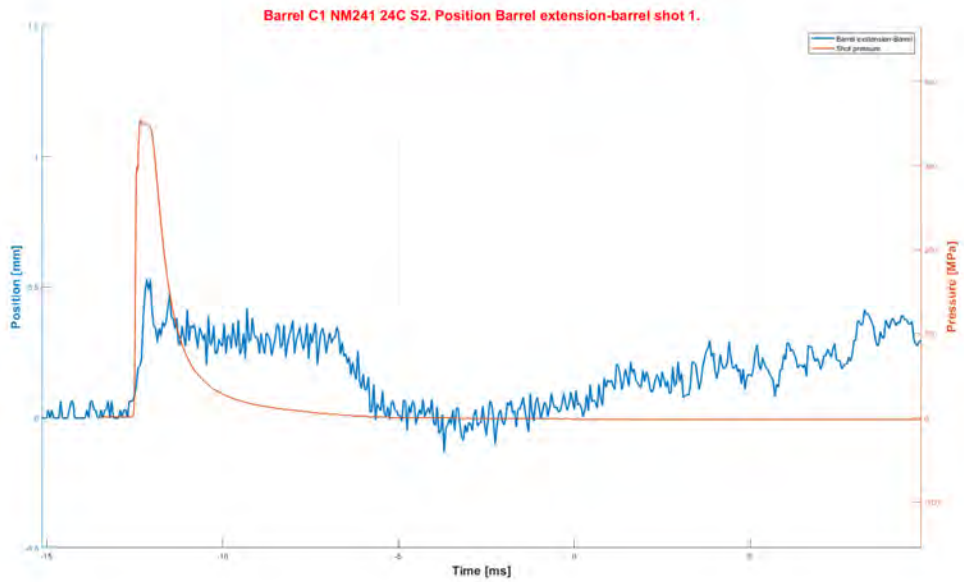


Figure 4.4 Position of the barrel extension subtracted from the position of barrel.

4.2 Velocities of main parts

In Figure 4.5 and 4.6 we see the velocity of the barrel, barrel extension and bolt together with the pressure curve. Figure 4.5 shows the first shot and Figure 4.6 shows the second shot in a three shot burst. The time scale of both plots are 25 ms.

Figure 4.5 shows that the bolt and barrel extension starts to gain velocity first. The bolt moves faster than the barrel extension, and reaches a velocity of almost 2 m/s before the barrel starts to move. We see that the bolt velocity drops at the exact same time as the barrel starts to move. The barrel extension velocity flattens out at the same time. Then after about 1 ms all three parts have reached the same velocity. They then move together with a speed of approximately 3 m/s before the bolt separates and increases its speed to 6 m/s. The barrel extension and barrel loses speed and eventually stops about 20 ms after the shot initiation.

Figure 4.6 shows the second shot. We see all parts are moving forward with a speed of a little bit less than 2 m/s. The barrel extension and barrel stops a fraction of a millisecond before the bolt and they bounce back a little bit. When the shot is initiated all three parts have close to zero velocity. Then the same process as described above starts again.

These figures also shows that there are backlash in the system, making the bolt move first and then the barrel extension before the barrel. When the barrel starts to move, both bolt and barrel extension have reached considerable velocity, and the barrel actually slows down the bolt and barrel extension. We can imagine that this is a brutal process compared to if there were no backlash between the barrel and barrel extension (the case with a fully threaded coupling between barrel and barrel extension).

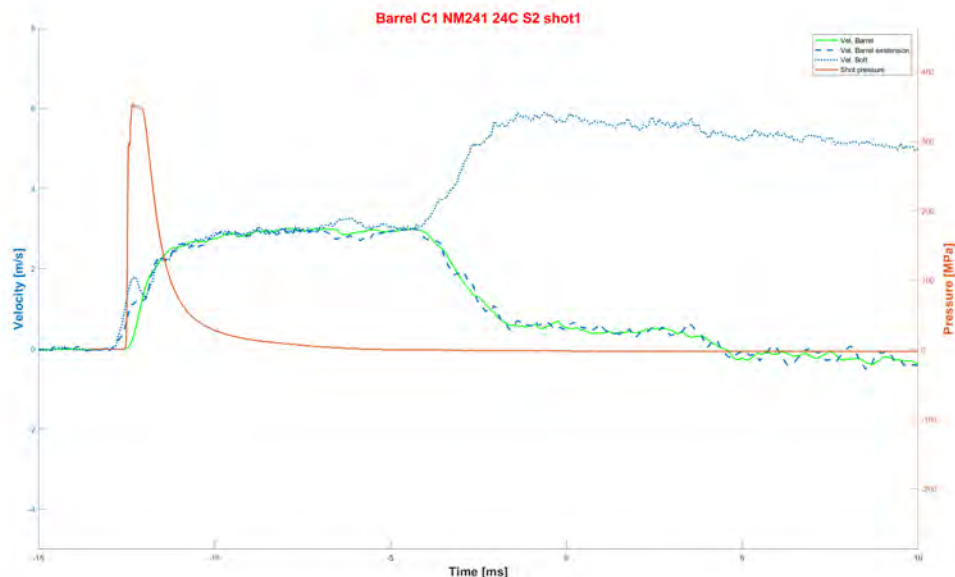


Figure 4.5 Velocity of barrel, barrel extension and bolt together with the pressure curve. 1. shot.

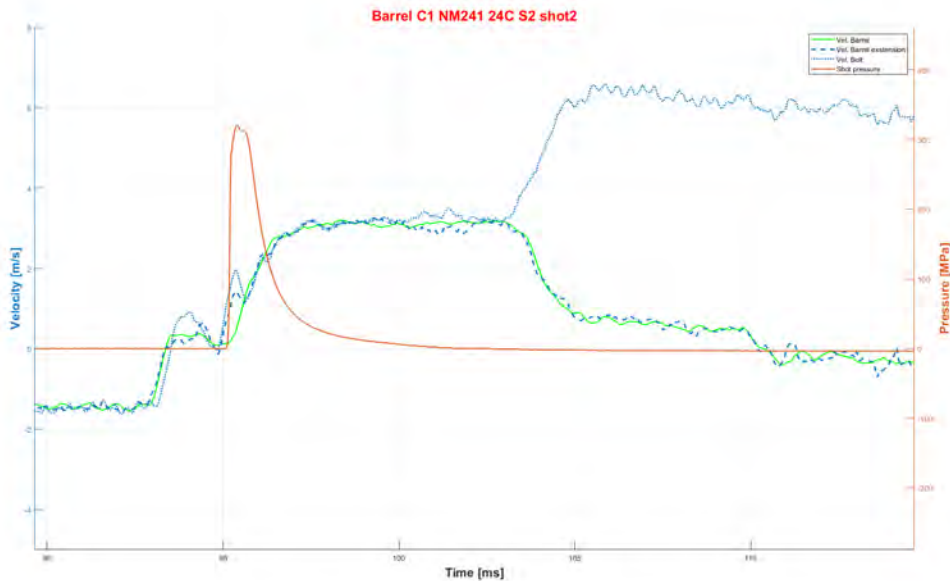


Figure 4.6 Velocity of barrel, barrel extension and bolt together with the pressure curve. 2. shot.

4.3 Accelerations of main parts

In Figure 4.7 and 4.8 we see the acceleration of the barrel, barrel extension and bolt together with the pressure curve. Figure 4.7 shows the first shot and Figure 4.8 shows the second shot in a three shot burst. The time scale of both plots are 10 ms.

From 4.7 we see that the bolt and barrel extension starts to accelerate at the same time and reaches a peak value at the same time as the barrel starts to accelerate. The bolt accelerates faster than the barrel extension. The bolt and barrel extension then have a decreasing acceleration when the barrel acceleration increases. When the barrel reaches its peak acceleration, the bolt and barrel extension reaches a local minimum. In fact the acceleration of the bolt and barrel extension are in perfect antiphase with the barrel. This happens at the same time as the chamber pressure is at its peak value. When the pressure starts to fall, all three parts accelerates with comparable values.

In Figure 4.8 the second shot in the burst is shown. We see that before the shot initiation the parts are accelerated quite brutally, this is when they stop in the forward position. The barrel extension stops first, then the barrel and at last the bolt. Then the shot initiates and the same process as described above starts over again.

The pressure curves in both the velocity and acceleration plots starts later than the movement in the parts. This is due to the measurement method as described in section 2.3. There is pressure in the system, but the bullet has to move past the pressure sensor mounting hole before any pressure is registered.

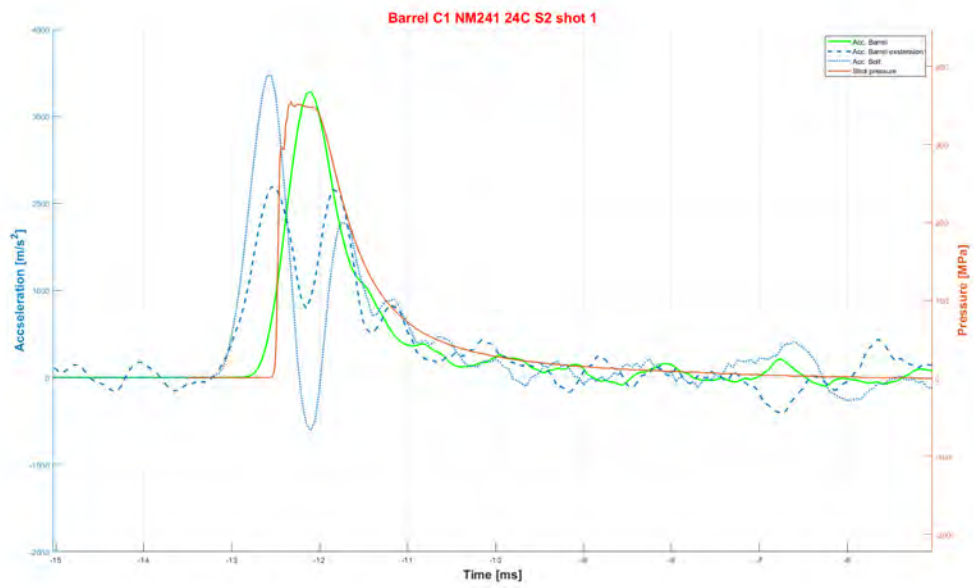


Figure 4.7 Acceleration of barrel, barrel extension and bolt together with the pressure curve. 1. shot.

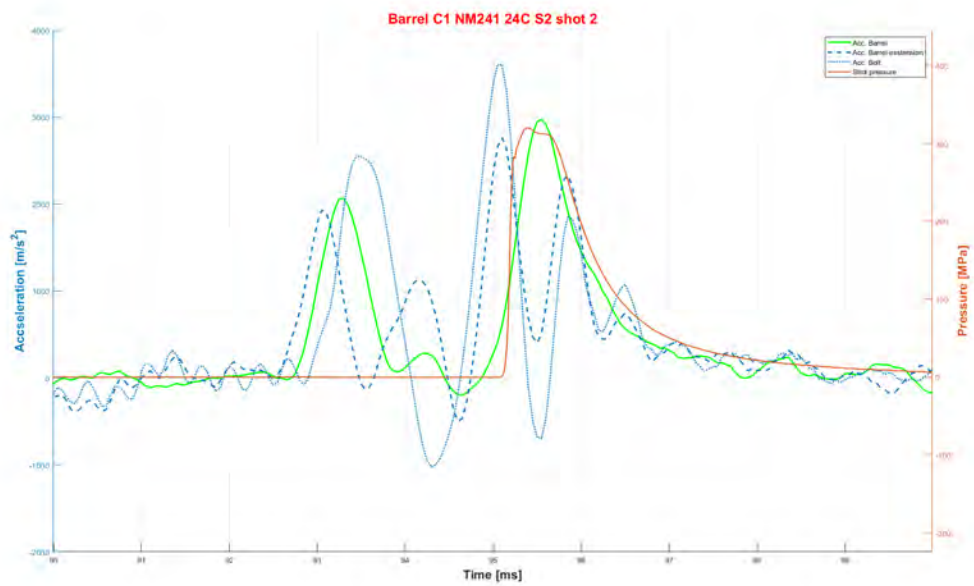


Figure 4.8 Acceleration of barrel, barrel extension and bolt together with the pressure curve. 2. shot.

4.4 Forces

To calculate the sum of forces on each part we have to multiply the acceleration with the mass of each part. The mass of the parts are

- Barrel: 12.30 kg
- Barrel extension: 1.87 kg
- Bolt: 2.32 kg

To calculate the net force from the chamber pressure we assume the net pressure is working on a surface area equal to the case neck area. The case neck has a inner diameter of 13 mm. The case neck area is then 132.73 mm^2 .

When we do this we get the values shown in Figure 4.9.

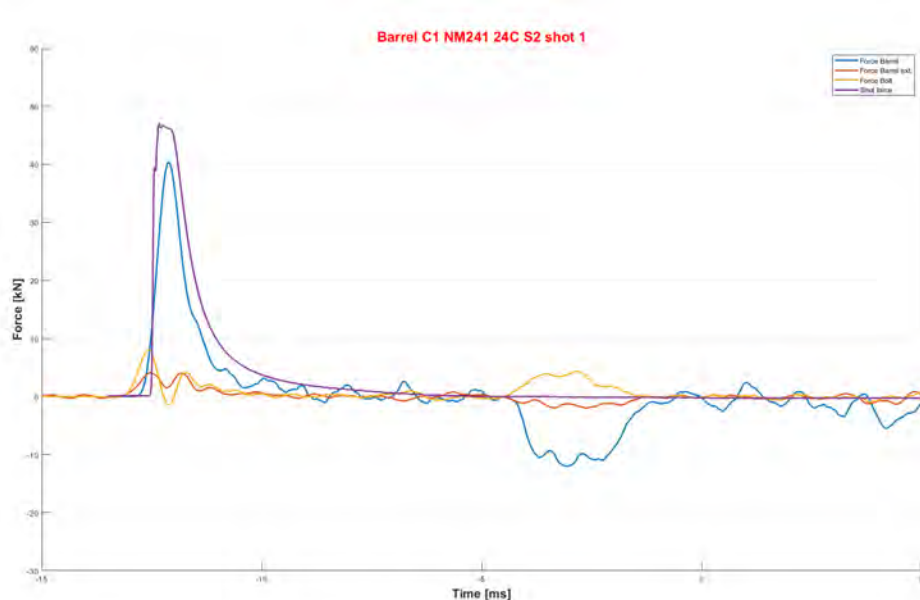


Figure 4.9 Sum of forces on barrel, barrel extension and bolt.

As shown in Figure 4.9, most of the impulse from the shot pressure is transferred to the barrel. This is reasonable because the barrel is the heaviest component in the system and it is free to move because it is only attached to the weapon through the locking lugs/threads.

The most interesting value for this analysis are in fact the forces acting on the locking lugs/threads of the barrel and barrel extension. This is where the cracks and failures are observed. We recognize the following possible forces to act on the barrel during the shot process:

1. The main force working on the barrel during the shot are the force acting on the locking lugs/threads, the force is transferred from the barrel extension. Due to Newtons 3. law the force on the locking lugs in the barrel extension will be exactly the same as the force on the barrel locking lugs.
2. Friction between the cartridge case and the chamber wall might transfer forces to the barrel.

-
-
3. There will be a small force acting on the barrel from the bullet moving down the barrel. This is due to friction between bullet and barrel (pushing the barrel forward). We assume this force to be negligible compared to the force from the chamber pressure.

As discussed earlier, the data indicate that friction between cartridge and chamber does not play a significant role in the shot process. We will assume, for now, that the total force on the barrel is only acting on the locking lugs/threads.

The force on the barrel for the first and second shot in a burst is shown in Figure 4.10 and Figure 4.11. Time scale for both plots are 20 ms.

In Figure 4.10 we see the force acting on the barrel during the first shot. The chamber pressure force and the barrel force are in phase during the shot. Barrel force is about 40 000 N in this example. About 10 ms after the shot initiation the barrel experiences a large negative force. This is when the barrel stops against the barrel buffer.

In Figure 4.11 we see the force acting on the barrel during the second shot. The barrel experiences a large positive force when stopping in the forward position. This force is big, about 25 000 N, but smaller than the force during the shot, which is about 36 000 N in this example. Then after about 10 ms the barrel stops in the backward position to a negative force of approximately 20 000 N.

Hence, the largest forces acting on the barrel during a burst of shots, are the forces from the shot pressure.

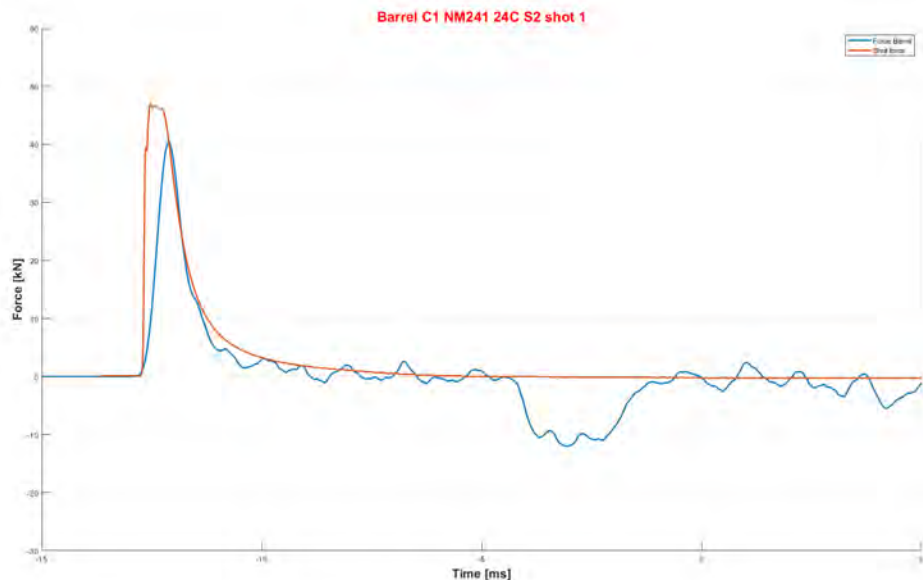


Figure 4.10 Force on barrel together with the chamber pressure force for 1. shot in a burst.

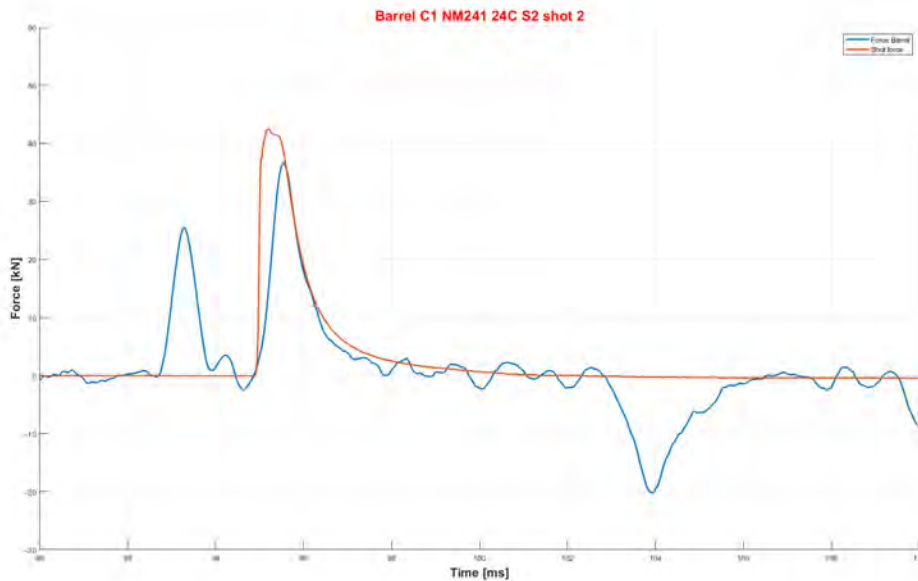


Figure 4.11 Force on barrel together with the chamber pressure force for 2. shot in a burst.

4.5 Correlation between barrel force and pressure

As discussed above, the force acting on the barrel during the shot is transferred from the barrel extension. Due to Newton's 3. law the force on the locking lugs in the barrel extension will be exactly the same as the force on the barrel locking lugs. This area on both the barrel and barrel extension are the most vulnerable to fatigue fracture in the old Norwegian QCB weapons.

The largest force on the barrel during a firing cycle is due to the shot pressure (not stopping force in the backward or forward positions). It is therefore of interest to see how good the peak shot pressure correlates to the peak force on the barrel. In Figure 4.12 all shots filmed and analysed with barrel B1 and ammunition NM241 are plotted with maximum force on barrel on the y-axis, and corresponding peak pressure on the x-axis. The values represent powder temperatures ranging from 24 °C to 100 °C. As the Figure shows, there is a very good linear correlation between maximum force on barrel and peak shot pressure. The linear trend line has a R^2 of 0.91, which means that 91% of the variation in maximum force between shots can be explained by the measured peak pressure. This means we can actually use the measured peak pressure to give a good estimate of the maximum force on barrel by inserting the peak pressure in the formula: $Force = 0.05 * Pmax + 20.676$ (Force is kN and Pmax is MPa).

In Figure 4.13 we have also added all analysed shots with barrel A1 and C1 together with B1 with the NM241. We can see that all shots from all three barrels falls on approximately the same line, hence the correlation between barrel force and shot pressure is most likely not barrel dependent.

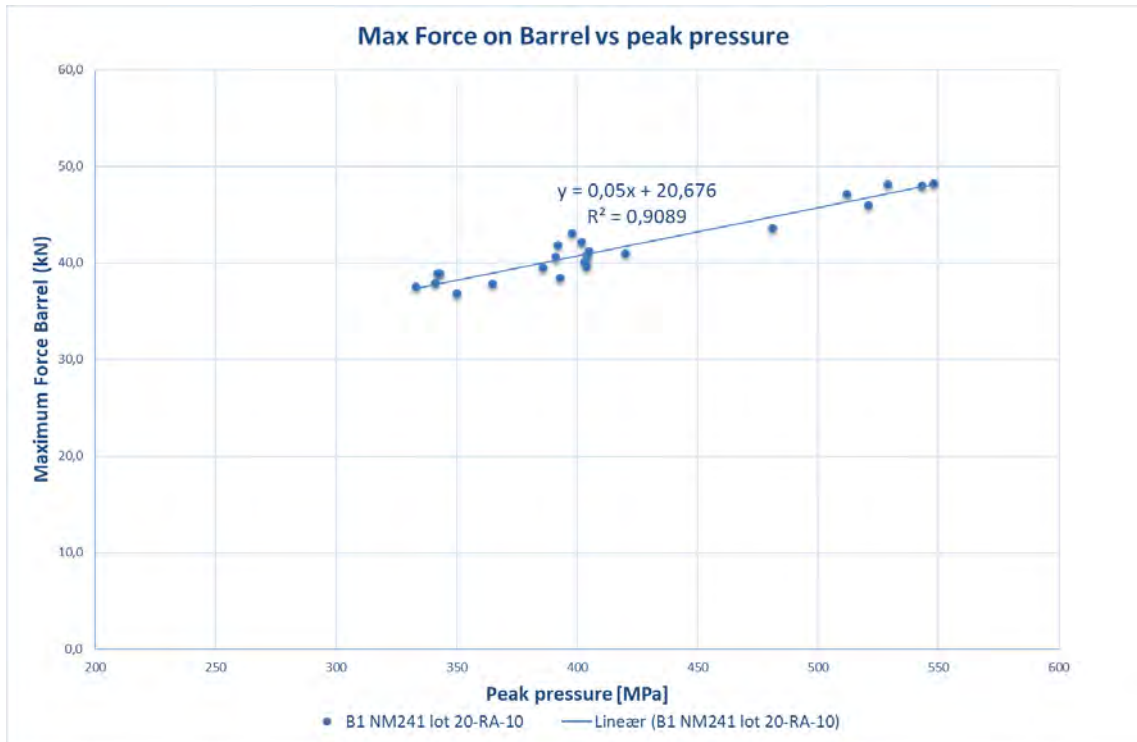


Figure 4.12 Maximum force on barrel vs peak pressure. Barrel B1 with ammunition NM241.

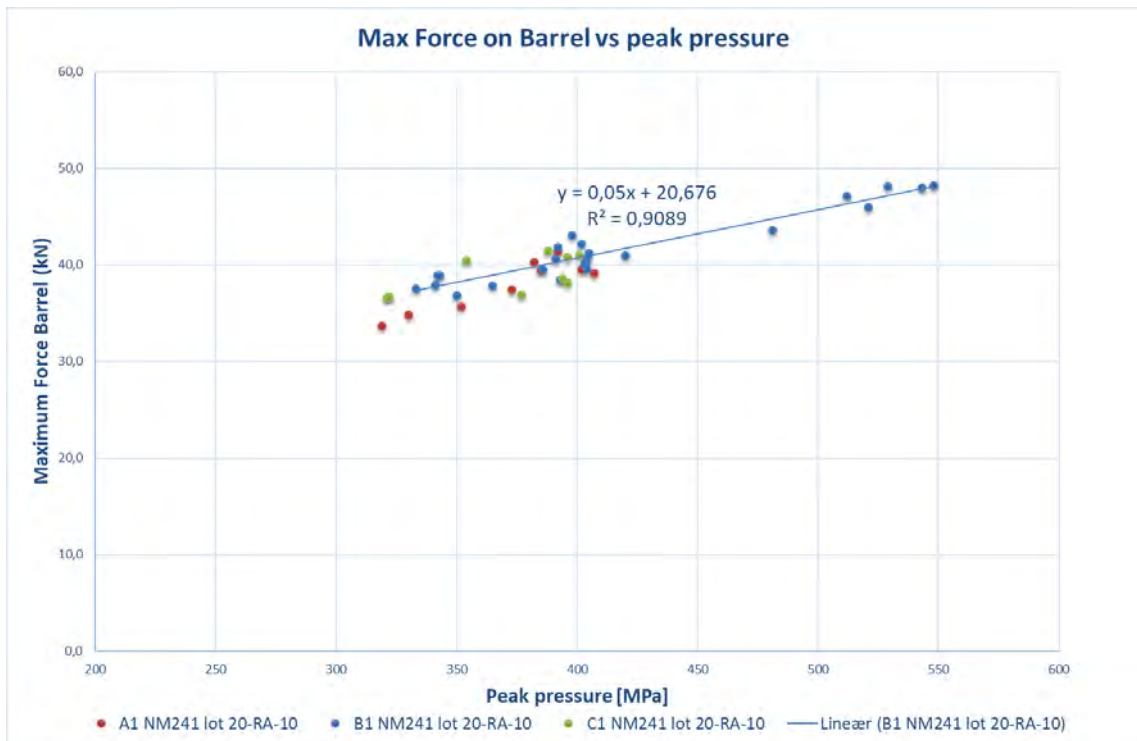


Figure 4.13 Maximum force on barrel vs peak pressure. Barrel A1, B1 and C1 with ammunition NM241.

4.5.1 Oiled cartridge cases

If friction between chamber and cartridge case is a significant part of the measured barrel force, this would of course mean that the force on the barrel and barrel extension locking lugs/threads is smaller than the measured force.

The above analysis show that in the shot process, the bolt moves first, then the barrel extension and at last the barrel. Hence, it seems logic that friction between chamber and cartridge doesn't play a significant part in the transfer of forces to the barrel, at least in the very early process of the shot that is studied here (when the bullet is still in the barrel and the forces are at the maximum values). If it does, we would expect the barrel to move first because the cartridge would be stuck in the chamber.

A second possibility to consider is that the cartridge case is more or less stuck in the chamber during the time the bullet is in the barrel, and the reason the bolt starts to move first is because the case starts to flow (elastic and plastic flow). I.e. the case is stuck in the chamber, but it stretches and fills the head-space gap and hits the bolt before anything else have started to move.

In order to investigate further the possible contribution from friction between cartridge and chamber to the total barrel force, it was decided to analyse some shots with oiled cases. The theory was that the oil will guarantee approximately zero friction between cartridge and chamber. If case friction is a large part of the total barrel force when firing dry cartridges, it is reasonable that the shots with oiled cartridges will give a force vs time plot with higher values over a slightly shorter time frame, because no force will be transferred to the barrel before the backlash between bolt and barrel extension, and barrel extension and barrel are *fully* taken up. This should then lead to a higher peak barrel force at a given peak shot pressure, and the "*barrel force vs peak pressure*" data points should be offset from the one in Figure 4.12 and 4.13.

In Figure 4.14 the shots with oiled cases are plotted together with the shots from Figure 4.12. We see that the data points fits in almost perfectly with the previous shots with dry cases. Hence, this analysis also indicate that friction between chamber and cartridge is not a significant part of the force transferred to the barrel during the shot. I.e. the total force is transferred trough the locking lugs/threads on the barrel and barrel extension.

4.5.2 Temperature stable extruded powder

The new lot named NM241F2 has a extruded temperature stable powder (NC1394NT from Eurenco), as opposed to the old NM241 that has a very temperature sensitive ball powder (PBC-347 from PB Clearmont).

In order to investigate the effect on barrel force from this new type of powder, 9 shots were analysed with the tracking software. The analysed shots were fired with barrel B1 and powder temperatures of 21, 63 and 100 °C, 3 shots at each temperature. In figure 4.15, the maximum force on barrel as a function of peak pressure is shown together with the values for the old NM241 with ball powder.

As seen from the figure these shots don't fall on the same line as the old NM241 ammunition. We see that NM241F2 gives a lower barrel force than the NM241 both due to the fact that it has a lower peak pressure for all temperatures, but also because it gives a lower force for a given pressure. For

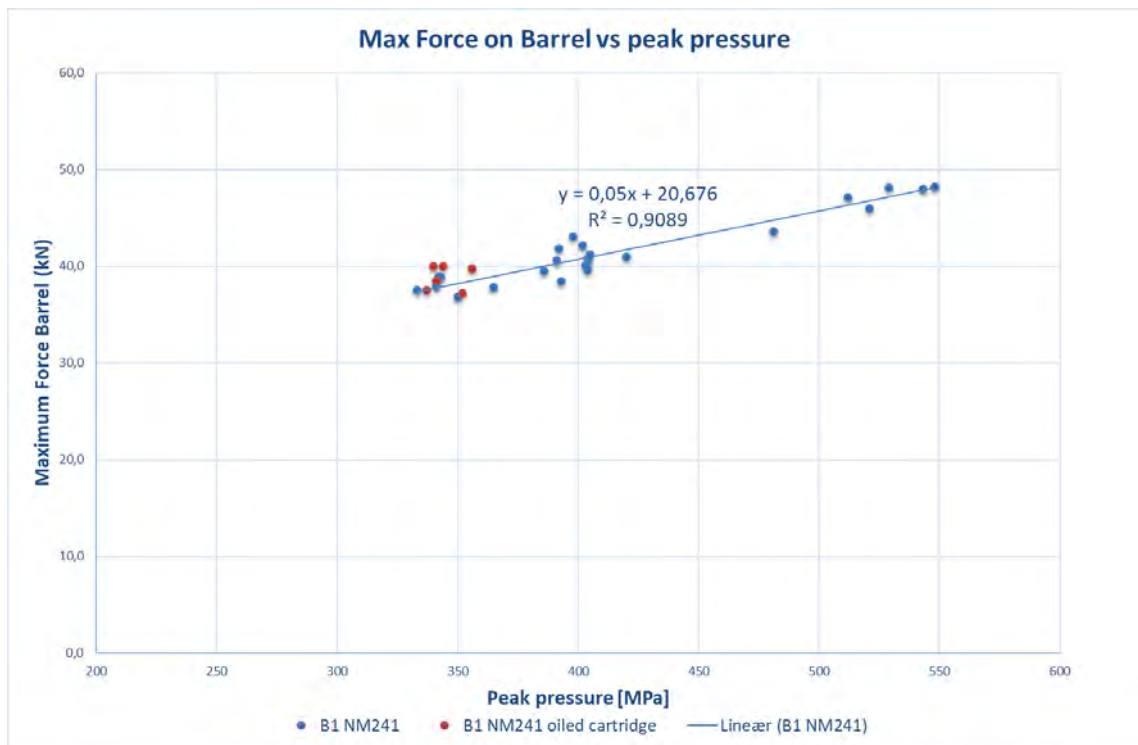


Figure 4.14 Maximum force on barrel vs peak pressure. Barrel B1 with NM241. Dry and oiled cartridges.

the shots with pressure in the area 330-350 MPa, the NM241F2 gives a barrel force about 5 kN lower than the NM241.

Why this new powder doesn't give the same correlation between barrel force and peak pressure is hard to explain. A possible explanation is that it has to do with the burning characteristics of the two powders. The extruded powder and ball powder have different shaped pressure curves. This is shown in Figure 4.16 where the pressure curve from a shot with NM241, NM241F2 and M33 are plotted. Both the NM241 and M33 have ball powder, and as seen they have a much steeper pressure build up than the extruded powder in the NM241F2.

Because the M33 also have ball powder (unknown type and manufacturer), some shots were analysed with the M33. The analysed shots were fired with barrel B1 and C1 and powder temperatures of 21 and 63 °C. In figure 4.17, the maximum barrel force as a function of peak pressure for M33 is shown together with the values for the NM241 and NM241F2. We see that the peak pressure and barrel force for the M33 shots have a correlation comparable to the NM241. This strengthens the theory that the extruded powder is the cause of the observed lower barrel force as a function of pressure.

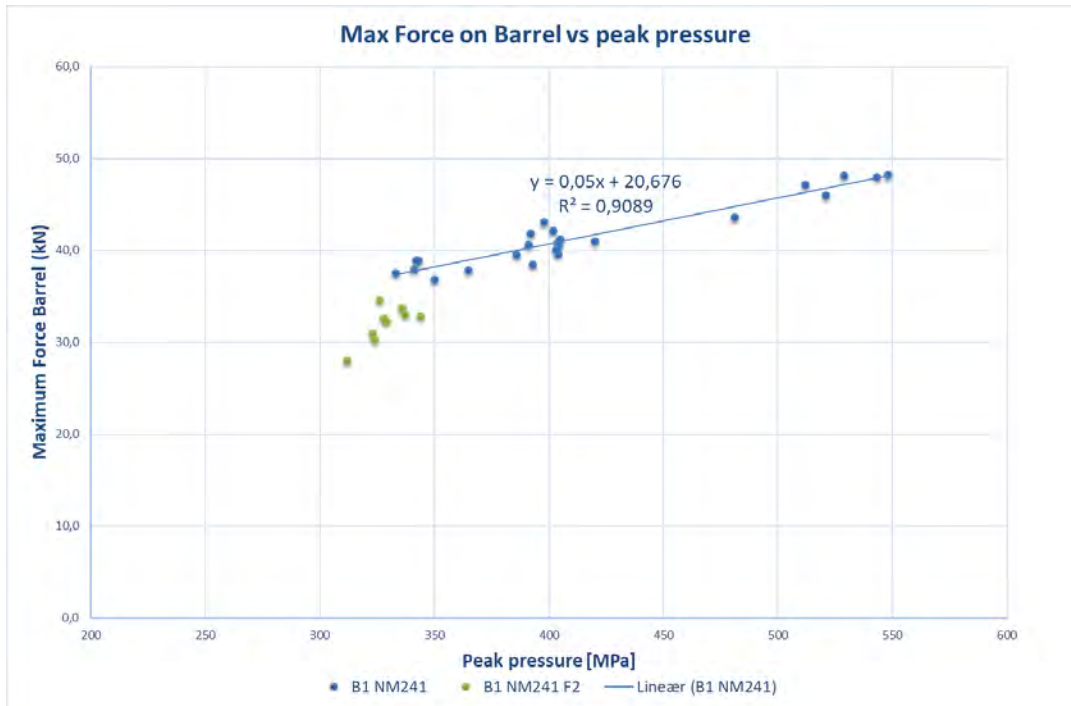


Figure 4.15 Maximum force on barrel vs peak pressure. Barrel B1 with NM241 and NM241F2 with temperature stable powder.

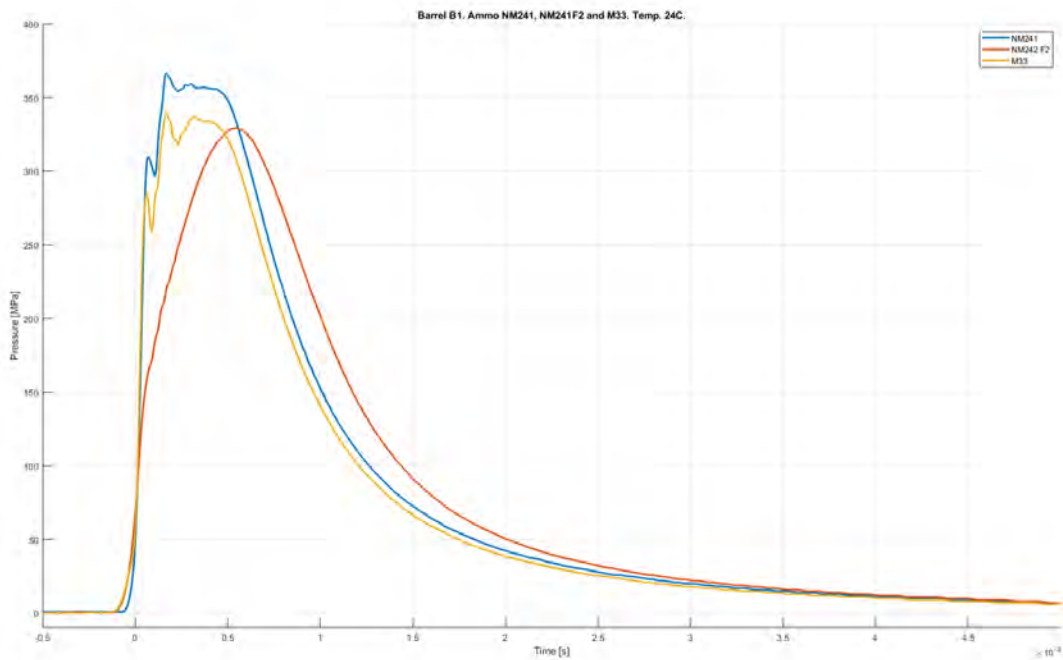


Figure 4.16 Pressure curves for NM241(blue), NM241F2(red) and M33(yellow).

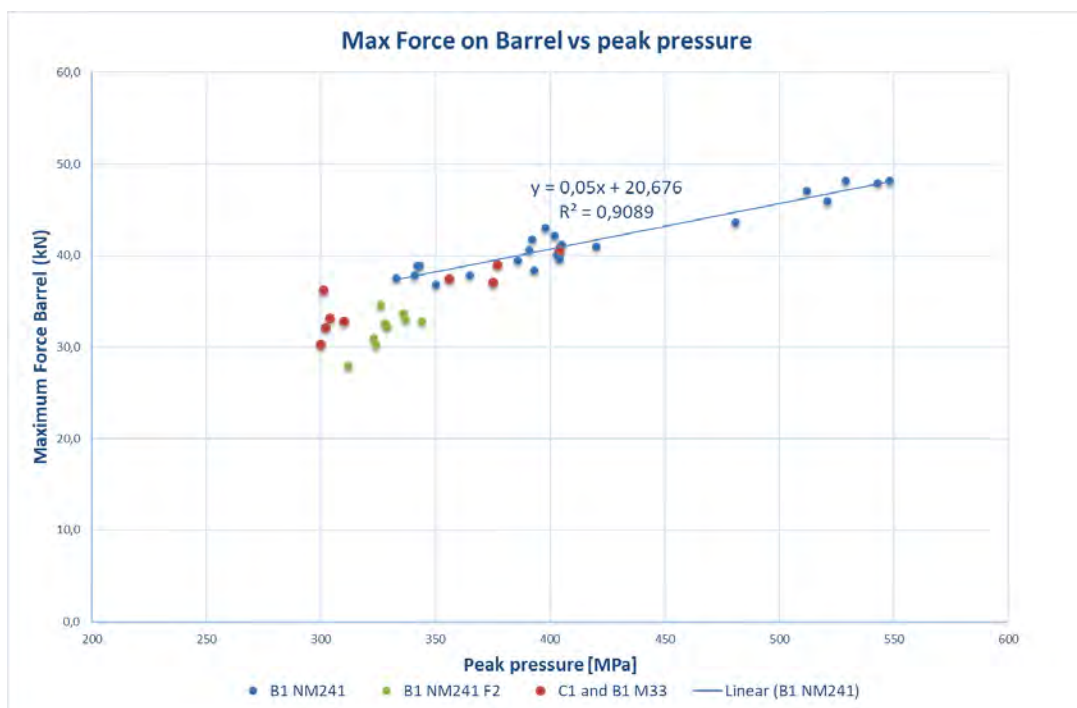


Figure 4.17 Maximun force on barrel vs peak pressure. Barrel B1 with NM241, NM241F2 and M33(also barrel C1).

5 Crack detection and measurement of crack depth

Table 5.1 to 5.6 shows the summary of what method that detected different cracks. For the cases where cracks were found by microscope (M), the depth of the cracks in the center of segment is shown in the tables. The notation used for specifying where cracks were found is shown in figure 5.1. Pictures of all segments with both Magnetic particle and Dye Penetrant applied are shown in Table 5.7 to 5.12.

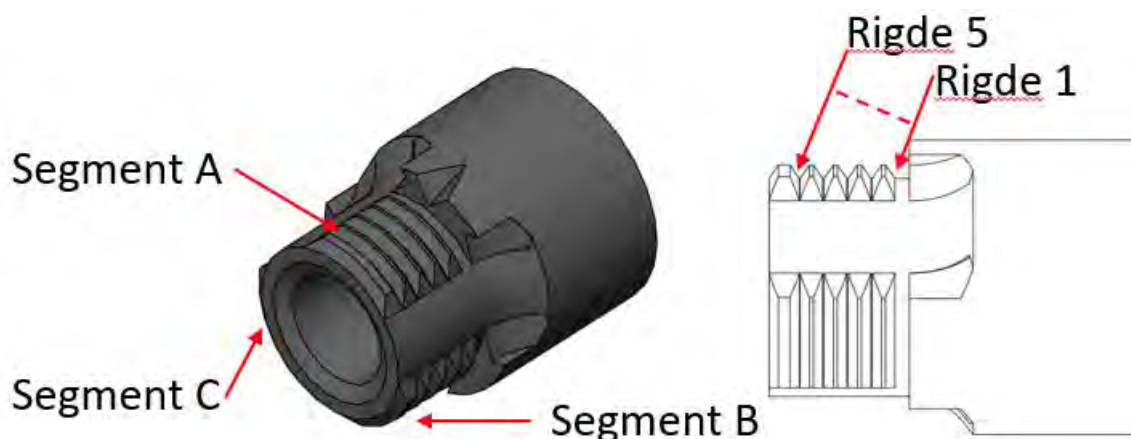


Figure 5.1 Notation used for location for different parts of barrel connection.

	Segment A / 1A		Segment B / 1B		Segment C / 1C	
Ridge 1	MT PT M	1 mm	M	0.73 mm		
Ridge 2	M	0.2 mm	M	0.06 mm	MT M	0.39 mm
Ridge 3	M	0.05 mm	M	0.07 mm		
Ridge 4	M	0.04 mm	M	0.07 mm		
Ridge 5						

Table 5.1 Barrel no. 1613

	Segment A / 1A		Segment B / 1B		Segment C / 1C	
Ridge 1	MT M	0.8 mm	MT M	0.70 mm		
Ridge 2	M	0.28 mm	M	0.32 mm	MT PT M	0.59 mm / 0.25 mm
Ridge 3	M	0.17 mm	MT M	0.37 mm	M	0.02 mm / 0.02 mm
Ridge 4	M	0.05 mm	M	0.11 mm		
Ridge 5	M	0.02 mm				

Table 5.2 Barrel no. SFK0123-A

	Segment A / 3A		Segment B / 3B		Segment C / 3C	
Ridge 1	MT PT M	0.95 mm	MT PT M	0.93 mm		
Ridge 2	M	0.3 mm	M	0.05 mm	MT M	0.42 mm
Ridge 3						
Ridge 4	M	0.08 mm	MT M	0.23 mm		
Ridge 5						

Table 5.3 Barrel no. 8832/6713

	Segment A / 4A		Segment B / 4B		Segment C / 4C	
Ridge 1	MT M	0.79 mm	MT PT M	1 mm		
Ridge 2	MT M	0.38 mm	MT M	0.23 mm	MT M	0.22 mm
Ridge 3	M	0.15 mm	M	0.07 mm / 0.06 mm		
Ridge 4	M	0.04 mm	M	0.03 mm		
Ridge 5						

Table 5.4 Barrel no. SFK 0120-A

	Segment A / 5A		Segment B / 5B		Segment C / 5C	
Ridge 1	MT PT M	0.62 mm	MT M	0.65 mm		
Ridge 2			MT M	0.13 mm	MT M	0.23 mm
Ridge 3	M	0.03 mm				
Ridge 4			M	0.02 mm		
Ridge 5						

Table 5.5 Barrel no. 1393

	Segment A /6A *Kant		Segment B / 6B		Segment C / 6C	
Ridge 1	MT PT M		MT PT M	2.14 mm		
Ridge 2	MT M		M	0.16 mm/0.04 mm	MT PT M	0.89 mm
Ridge 3	M		M	0.02 mm	MT M	0.02 mm
Ridge 4	M		M	0.03 mm		
Ridge 5						

Table 5.6 Barrel no. 14389

As can be seen in Table 5.1 to 5.6 segment A and B have cracks in most of the ridges from 1 to 4. Segment C has significantly fewer cracks. Ridge 1 in segment A and B always has the deepest crack within the segment, whereas segment C never has cracks in ridge 1. The reason for missing cracks in ridge 1 of segment C is a missing ridge/thread in the segment on the barrel extension. This is shown in Figure 5.4. This undoubtedly leads to a significant increased load on segment A and B during firing, especially in ridge 1 which most likely get most of the load during firing. This will undoubtedly also cause an highly uneven/non concentric load on the barrel extension, explaining the previously described cracks in the barrel extension.



Figure 5.2 Segment A B and C from barrel no. 1613

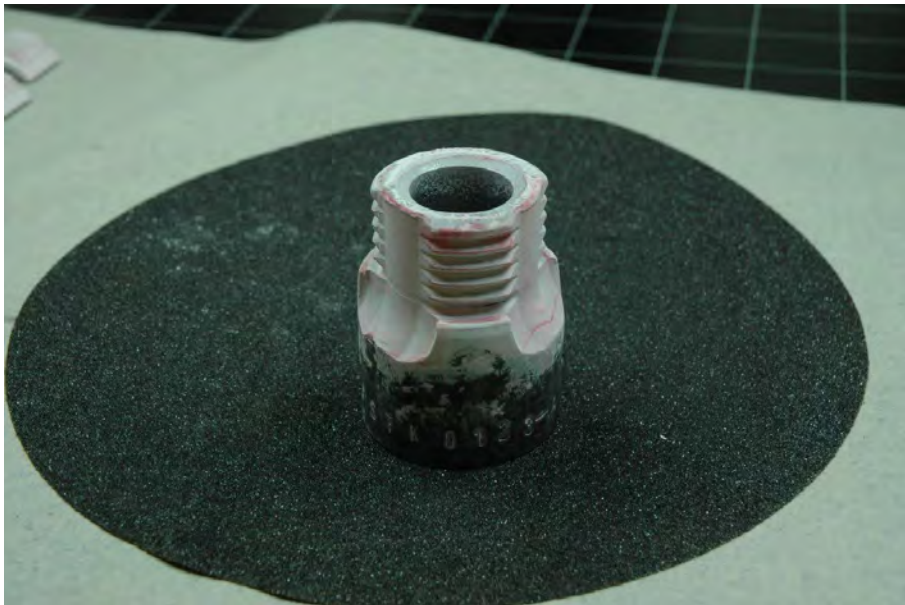


Figure 5.3 Overview of barrel no. SFK 0123-A

Uneven load

Majority of cracks are in segment A and B.

→ Force probably transferred to barrel mainly through segment A and B.

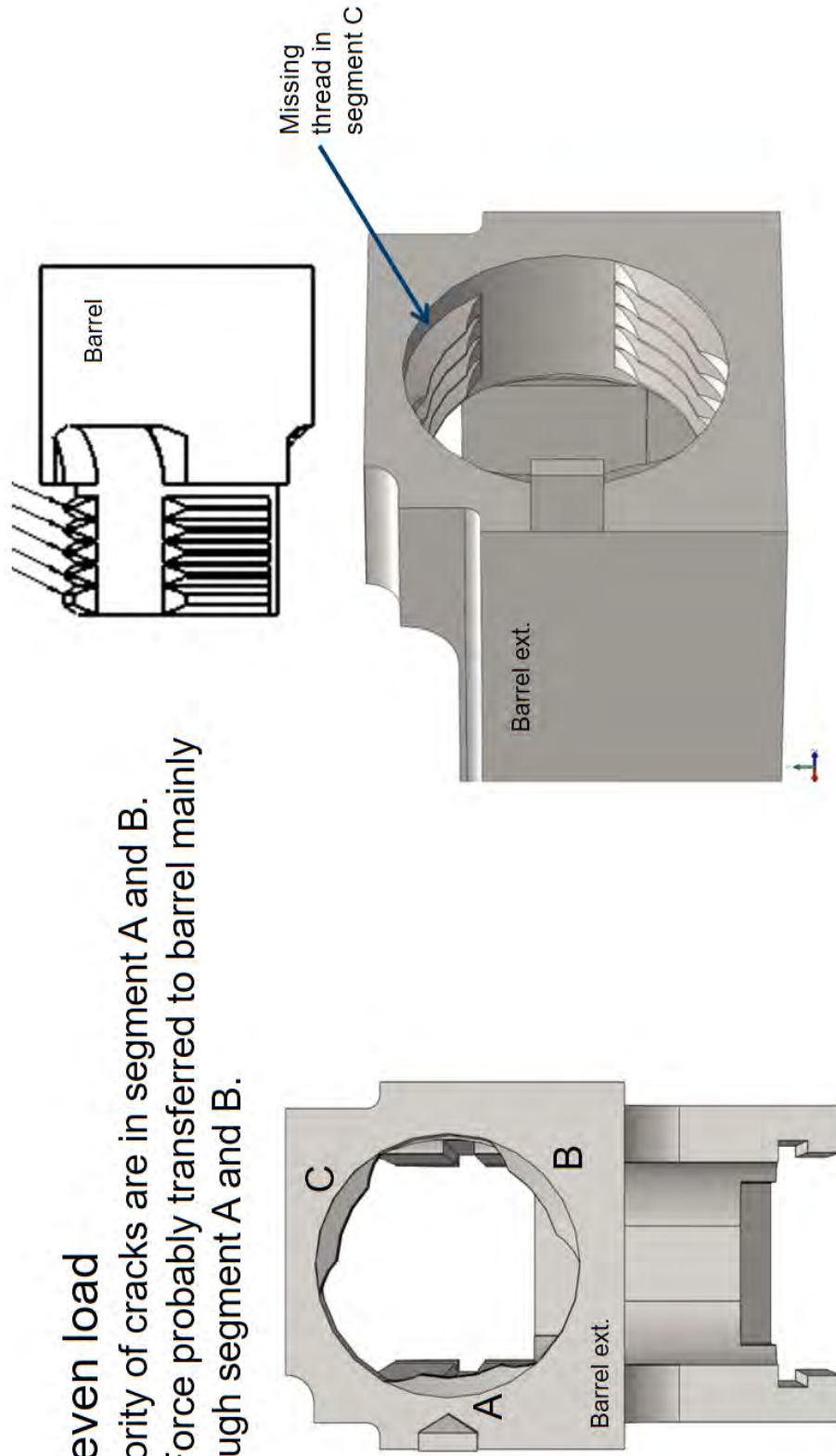


Figure 5.4 Missing I. ridge in segment C of the barrel extension.

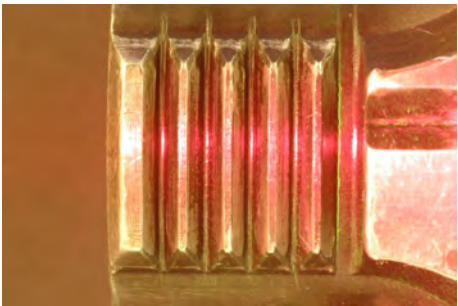
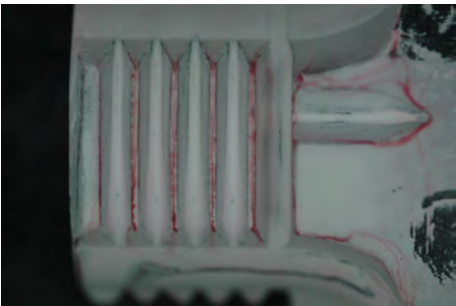
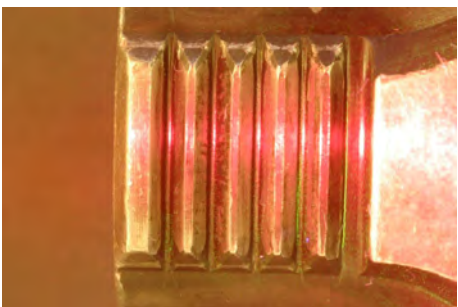

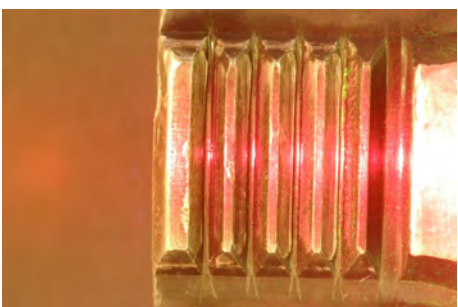

MT	PT	Comment
		<p>Segment A: Both MT and PT show indication of crack at first ridge.</p>
		<p>Segment B: MT shows indication of crack at first and second ridge. PT shows no indication of crack.</p>
		<p>Segment C: MT shows indication of crack at third ridge. No crack detection with PT-method.</p>

Table 5.7 Comparison of test results for barrel no. 1393

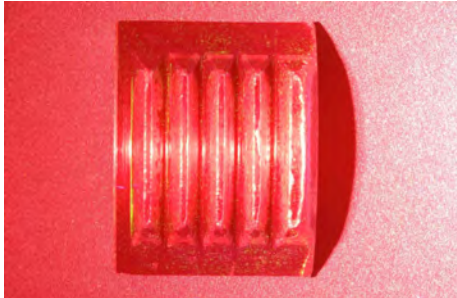





MT	PT	Comment
		<p>Segment A: Both MT and PT shown indication of crack at first ridge.</p>
		<p>Segment B: Only som residual die penetrant on top of ridges shown. No cracks detected.</p>
		<p>Segment C: No crack detected.</p>

Table 5.8 Comparison of test results for barrel no. 1613

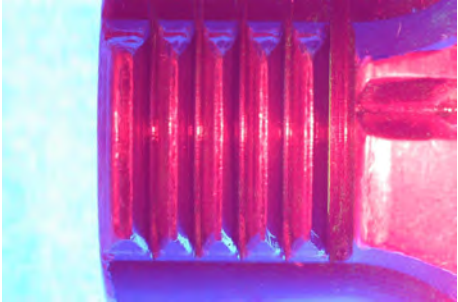

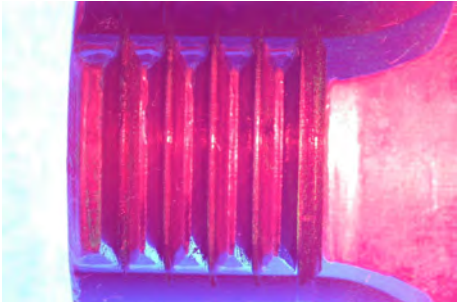

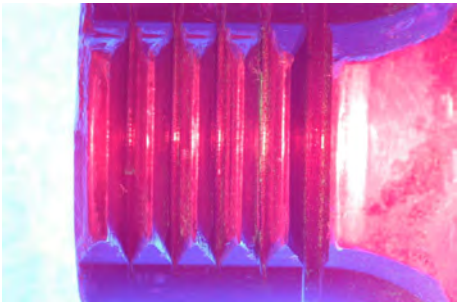
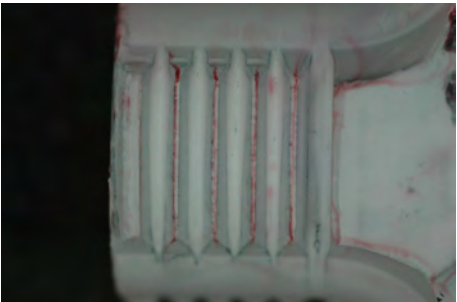
MT	PT	Comment
		<p>Segment A: MT shows clearly a crack at first ridge. No crack detected with PT.</p>
		<p>Segment B: MT shows indication of cracks at ridge no. 1 and 3. No indication of cracks with PT.</p>
		<p>Segment C: PT gives a indication for crack between at 2nd rigde. MT also shows a crack in the same area.</p>

Table 5.9 Comparison of test results for barrel no. SFK0123-A

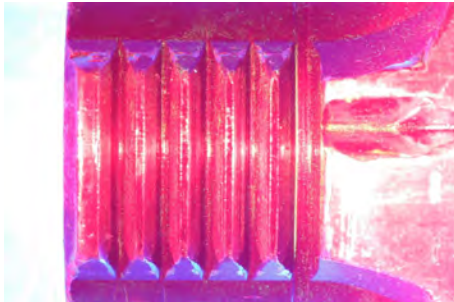
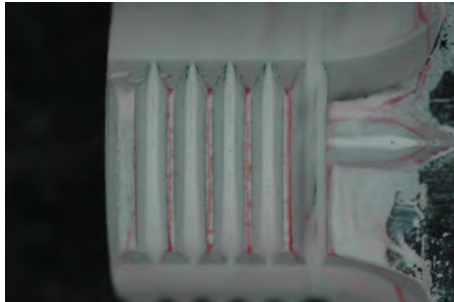
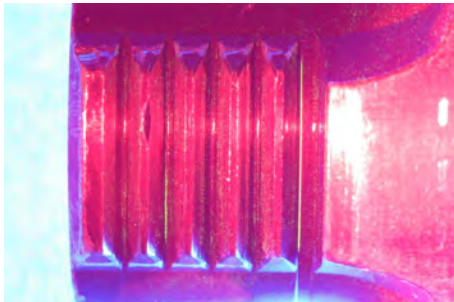

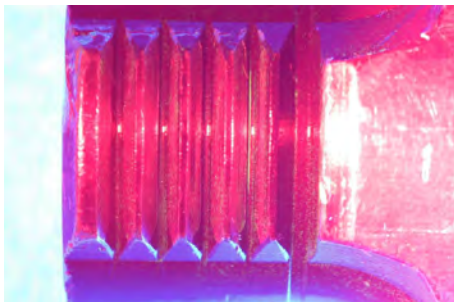

MT	PT	Comment
		<p>Segment A: MT and PT both shows indication of crack at first ridge.</p>
		<p>Segment B: MT and PT both shows indication of crack at first ridge. MT also indicate a crack at fourth ridge.</p>
		<p>Segment C: MT shows indication of crack at second ridge. No cracks detected with PT.</p>

Table 5.10 Comparison of test results for barrel no. 8832/6713

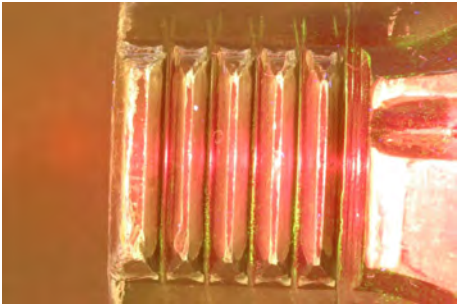
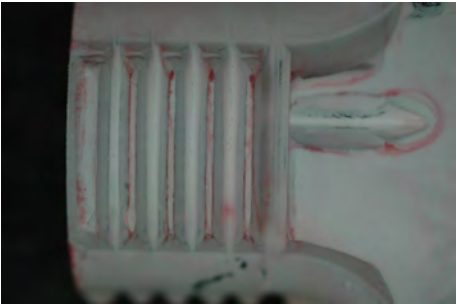
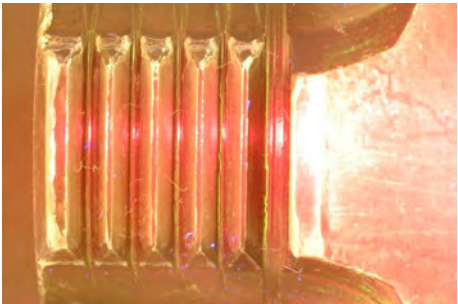

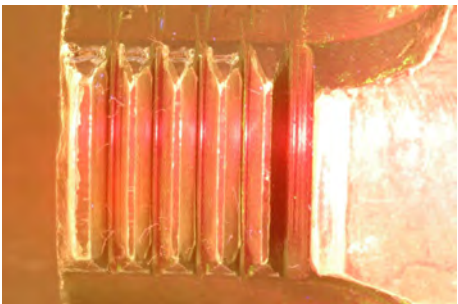

MT	PT	Comment
		<p>Segment A: MT shows indication of crack at first and second ridge. No indication with PT-method.</p>
		<p>Segment B: MT and PT shows indication of crack at first ridge. MT also indicate a crack at the second ridge.</p>
		<p>Segment C: MT shows indication of crack at second ridge. No cracks detected with PT.</p>

Table 5.11 Comparison of test results for barrel no. SFK0120-A

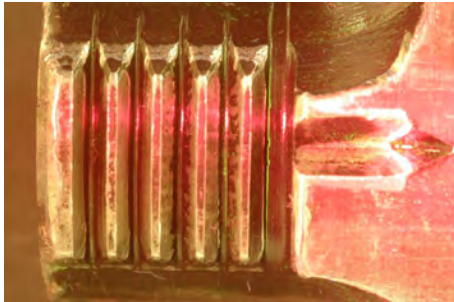
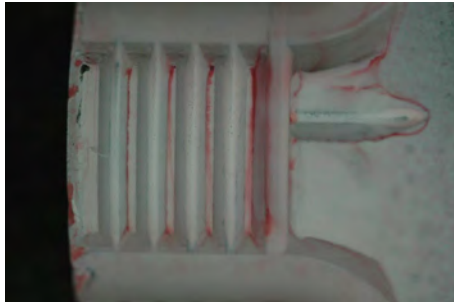
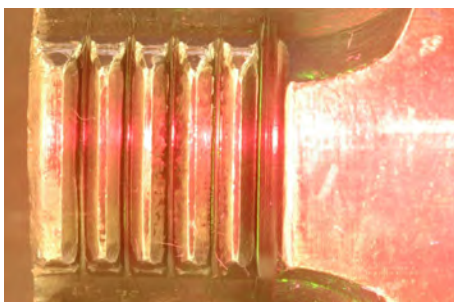

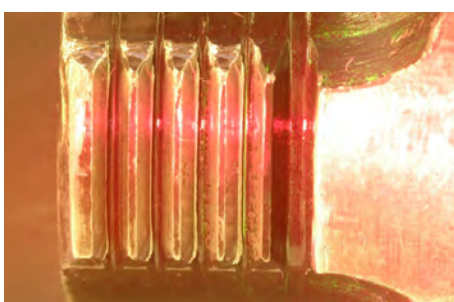

MT	PT	Comment
		<p>Segment A: Both PT and MT shows indication of crack at first ridge. MT also shows indication of crack at second ridge.</p>
		<p>Segment B: Both PT and MT shows indication of crack at first ridge.</p>
		<p>Segment C: MT shows indication of crack at second and third ridge. PT only show indication of crack at the second ridge.</p>

Table 5.12 Comparison of test results for barrel no. 14389

5.1 Results from Microscopic examination of cracks

Three segments from barrel no. SFK 0120-A and 14389 were cut and polished up to six times to get an indication of crack shape (shown in figure 2.8). It was expected that the crack was deepest at the center of crack, but table 5.13 shows not this trend for all cracks. It can be three reasons for this: The epoxy-casts can only be cut in parallel to the first cutting plane, and therefore depth is not measured normal to surface. Second alternative; the crack depth is not measured long enough to get a trend. The total distance from first cut to the last is approximately 5 mm. Depth might vary significantly over this length. Or at last; the crack doesn't grow as expected. In addition to these measurements the crack at first ridge of segment B on barrel no. 14389 was broke open at FOLAT. A presentation of the results of this test is shown in appendix D and figure 5.5. The face of the crack shows that the crack is a typical fatigue crack with a shape as expected.

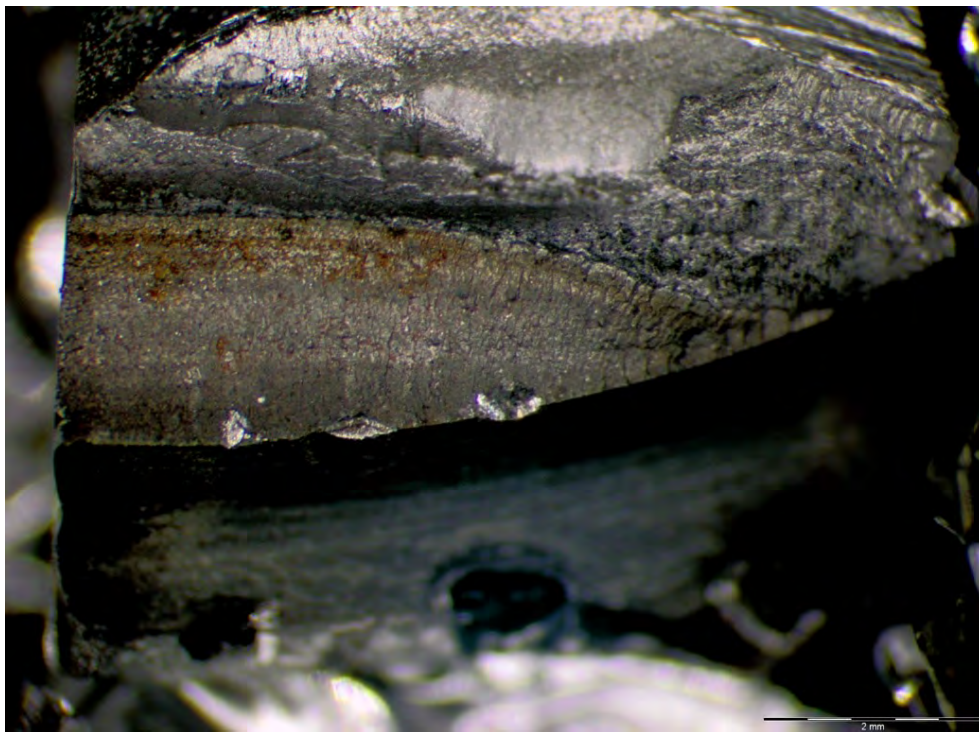


Figure 5.5 Face of fatigue crack at the first ridge at segment B on barrel no. 14389

Cut 1	SFK 0120-A, Segment B	14389, Segment A	14389, Segment C
Ridge 1	1.07 mm	0.14/0.14	
Rigde 2	0.24 mm	0.03 mm	0.94 mm
Rigde 3	0.1 mm	0.01 mm	0.02 mm
Rigde 4	0.03 mm	0.01 mm	
Ridge 5			
Thickness before cutting	20.66 mm	22.04 mm	19.76 mm
Cut 2			
Ridge 1	1.15 mm	0.55 mm	
Rigde 2	0.25 mm	0.05 mm	0.92 mm
Rigde 3	0.06 mm/0.06 mm	0.01 mm	0.01 mm
Rigde 4	0.06 mm	0.01 mm	
Distance from last cut	0.74 mm	0.75 mm	0.72 mm
Cut 3			
Ridge 1	1.13 mm	0.96 mm	
Rigde 2	0.09 mm /0.23 mm	0.06 mm	0.84 mm
Rigde 3	0.03 mm /0.13 mm	0.02 mm	
Rigde 4	0.04 mm	0.01 mm	
Rigde 5		0.01 mm	
Distance from last cut	0.67 mm	0.64 mm	0.98 mm
Cut4			
Ridge 1	1.2 mm	1.24 mm	
Rigde 2	0.28 mm/0.03 mm	0.04 mm/0.07 mm	0.74 mm
Rigde 3	0.16 mm		
Rigde 4	0.07 mm	0.02 mm	
Rigde 5	0.04 mm/0.02 mm	0.01 mm	
Distance from last cut	0.71 mm	0.82 mm	0.56 mm
Cut 5			
Ridge 1	1.19 mm	1.56 mm	
Rigde 2	0.32 mm/0.05 mm	0.12 mm	0.40
Ridge 3	0.16 mm	0.02 mm	0.02 mm
Ridge 4	0.11 mm		
Ridge 5	0.05 mm	0.02 mm	
Distance from last cut	0.91 mm	0.59 mm	0.95 mm
Cut 6			
Ridge 1	1.05 mm	1.81 mm	
Rigde 2	0.36 mm	0.1 mm	0.34 mm
Ridge 3	0.12 mm/0.08 mm		0.01 mm
Ridge 4	0.15 mm	0.02 mm	
Ridge 5	0.06 mm/0.03 mm		
Distance from last cut	1.07 mm	1.04 mm	1.01 mm

Table 5.13 Crack depth in different cross sections cut

6 Summary of results

From the pressure measurements we found that the current Target Practice NM241 and NM242 had a very temperature sensitive powder. The new NM241F2 had very temperature insensitive powder. No large differences in pressure between barrels were found. The inner diameter of the barrels was measured, but the effect on shot pressure (P_{max}) was small.

From the kinematic analysis it was found that the barrel, barrel extension and bolt don't behave as one piece in the milliseconds after shot initiation, this is due to backlash in the system and gives rise to high forces on the parts. It was also found a very good correlation between shot pressure (P_{max}) and force acting on the barrel and barrel extension. Almost all of the force acting on the barrel is believed to be transferred from the barrel extension via the segments in the coupling, not from friction between cartridge and chamber.

Due to this correlation between barrel force and shot pressure the old ammunition with a very temperature sensitive powder will give rise to very high forces. Due to the design of the weapon a lot of heat is transferred to the ammunition before it is chambered and ammunition temperatures well above $100\text{ }^{\circ}\text{C}$ is not unlikely, [6]. Our measurements shows pressures up to 550 MPa at this ammunition temperature. The new ammunition, NM241F2, with a temperature insensitive powder, greatly reduces the forces. Figure 6.1 shows the shots fired with old and new ammunition with powder temperatures varying from $24\text{-}100\text{ }^{\circ}\text{C}$ for both types. We see that the maximum force acting between the barrel and barrel extension is in the range of 34-49 kN with the old NM241 and in the range 28-35 kN with the new NM241F2, a reduction of almost 30 %.

The crack analysis shows almost all cracks are situated in segment A and B on the barrel, and the largest cracks are always at the bottom of the first thread(ridge 1). Almost no cracks are found in segment C. This indicates strongly that segment A and B takes up most of the force transferred to the barrel, and that the first thread within the segment takes up more force than the others. The reason for this is believed to be a missing locking lug/thread in segment C (shown in Figure 5.4) on the barrel extension, resulting in an uneven/non concentric load on both the barrel and barrel extension. Practically 1/3 of the threaded area does not contribute in the transfer of forces between the barrel and barrel extension.

Seeing these findings in combination with some of the findings from the Technical Investigation group, e.g. described in Technical-report 150128-03 from Forsvarets laboratorietjeneste [7], where a 20 % reduction in material strength was found in the new QCB-barrels compared to the old fully threaded barrels, this gives a good and reasonable explanation for the extensive amount of barrels with cracks found in the pool of QCB-weapons.

The easiest way to reduce the forces acting on the barrel and barrel extension on all QCB-weapons in use to day, is to use ammunition with temperature insensitive powder, like the NM241F2. A second possible way could be to slightly adjust the geometry of the threads on the barrel and/or barrel extension, so that the forces could be taken up more evenly over all three segments and distributed over all threads within a segment. With regards to new weapons, a reduced backlash/smaller tolerances in combination with design (ref. Figure 5.4), material and surface finish improvements in the threaded areas, should greatly reduce the

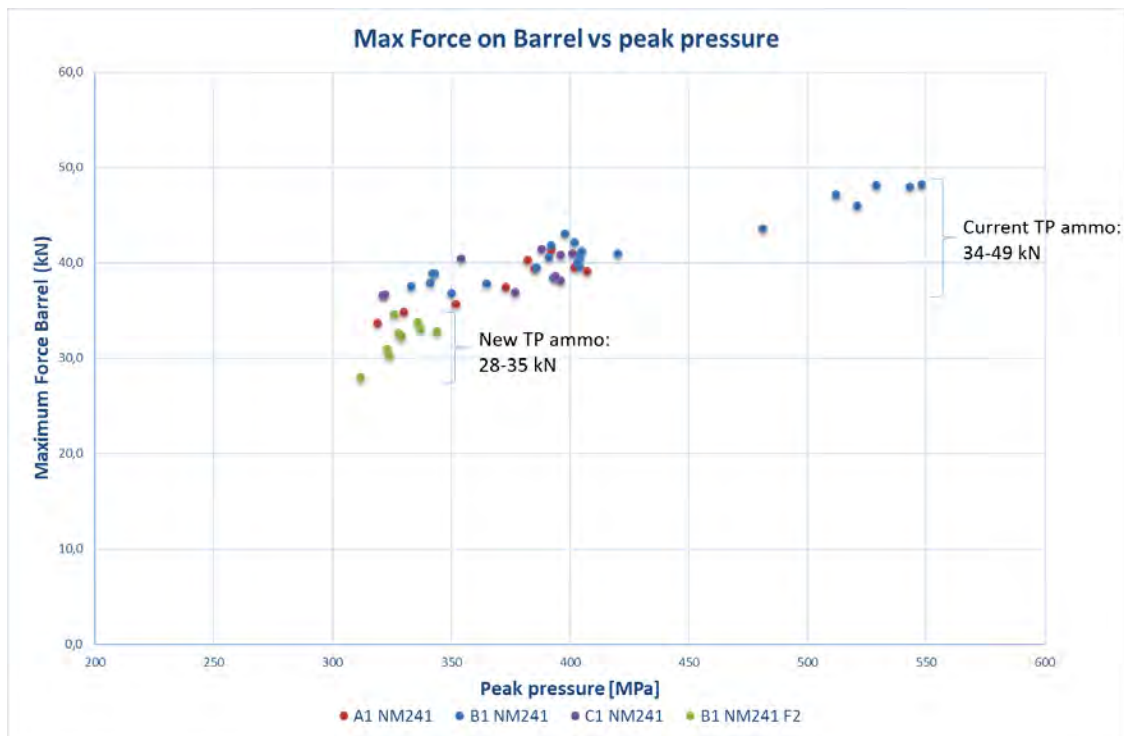


Figure 6.1 Maximum force on barrel vs peak pressure. Barrel A1, B1 and C1 with NM241 and B1 with NM241F2

risk of weapon failure due to fatigue in the barrel and barrel extension.

6.1 Crack analysis and recommendations on non destructive testing

Crack analysis shows that neither MT og PT detects all cracks that is shown from microscopic examination of cross section cut. The percental success rate is shown in table 6.1.

100 %	Microscopic examination (Reference)
48 %	Magnet Particle Testing (MT)
17 %	Dye Penetrate Testing (PT)

Table 6.1 Percentage of cracks detected

The MT procedure was done first. The magnetic particle fluid may fill the cracks, and make it harder for the color penetrate spray to fill the cracks as intended. If the test should be redone ultrasonic cleaning might be a better solution than a typical cleaning agent.

Galling occur on some of the barrels, and the excessive material is gather near the bottom of the grooves as shown in figure C.63 and C.64. This kind of cavity may look like a crack with both MT and PT inspection. For the two figures shown in this example, both MT and PT indicate crack in this area, but it is not known if it was because of the crack or the excessive material with the cavity.

One reason for that the PT fails for a large number of cracks, might be due to the geometry of the test object. It is practically impossible to apply a evenly thick layer of developer on the area where cracks is expected to occur. In the bottom between the ridges the layer is significant thicker than other places as illustrated on figure 6.2.

Due to the high fail rate of the PT, it is recommended to continue to use the MT for discarding barrels, but other test methods for non destructive testing should be assessed and tested. Ultrasound is one possible alternative, and the Norwegian company Dolphitech AS can be contacted for further information on this technology.

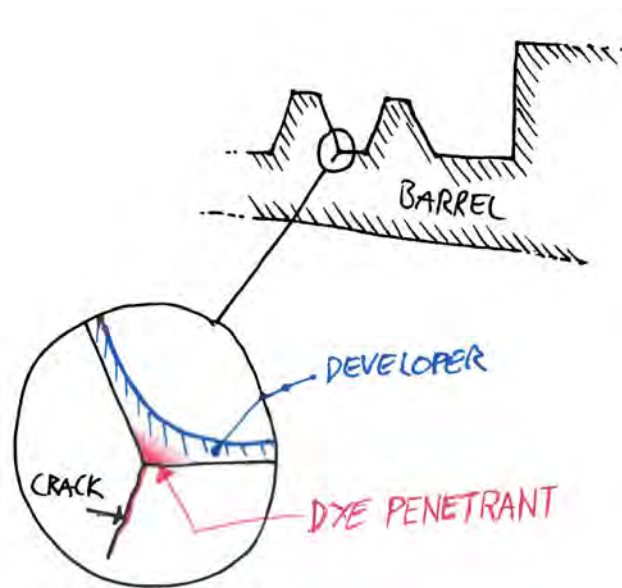


Figure 6.2 Thick layer of developer prevents color penetrant to be visible on the surface

A Pressure measurements

In Figure A.1 to A.4 a Box plot of Pmax as a function of powder temperature for all ammunition types in all three barrels are shown.

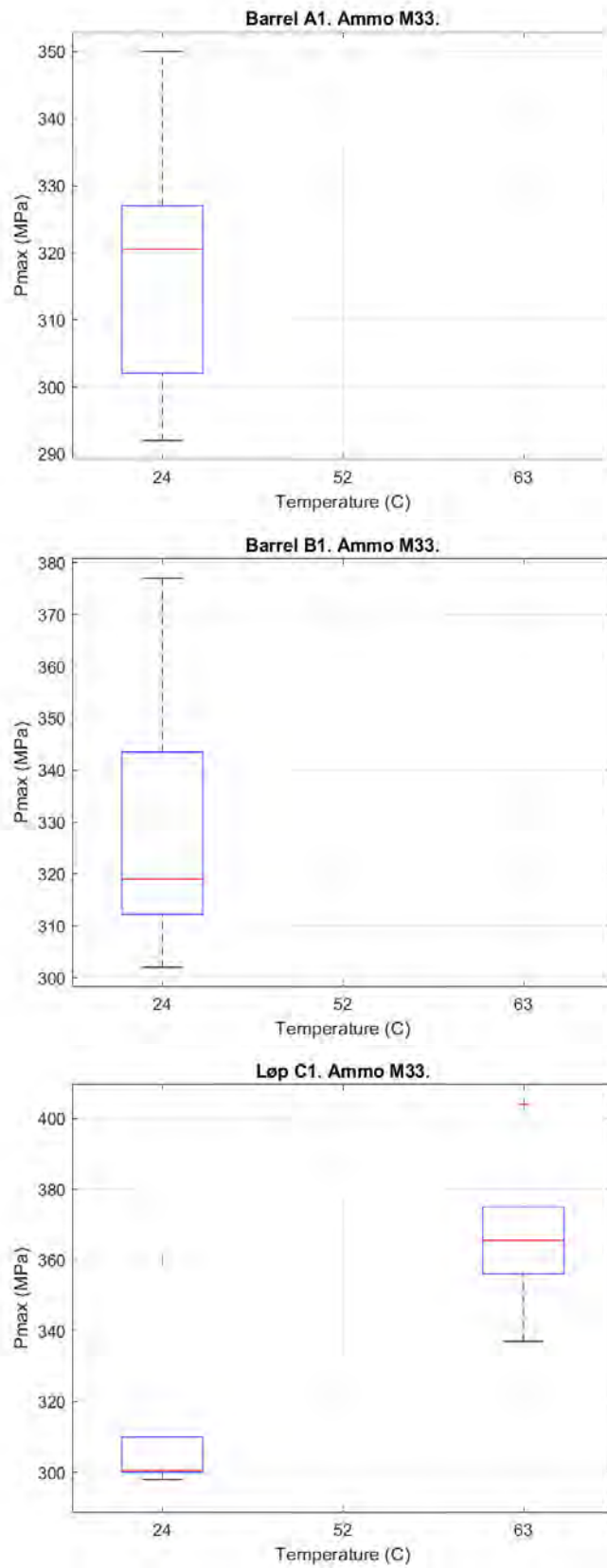


Figure A.1 M33 lot 00318-CR1

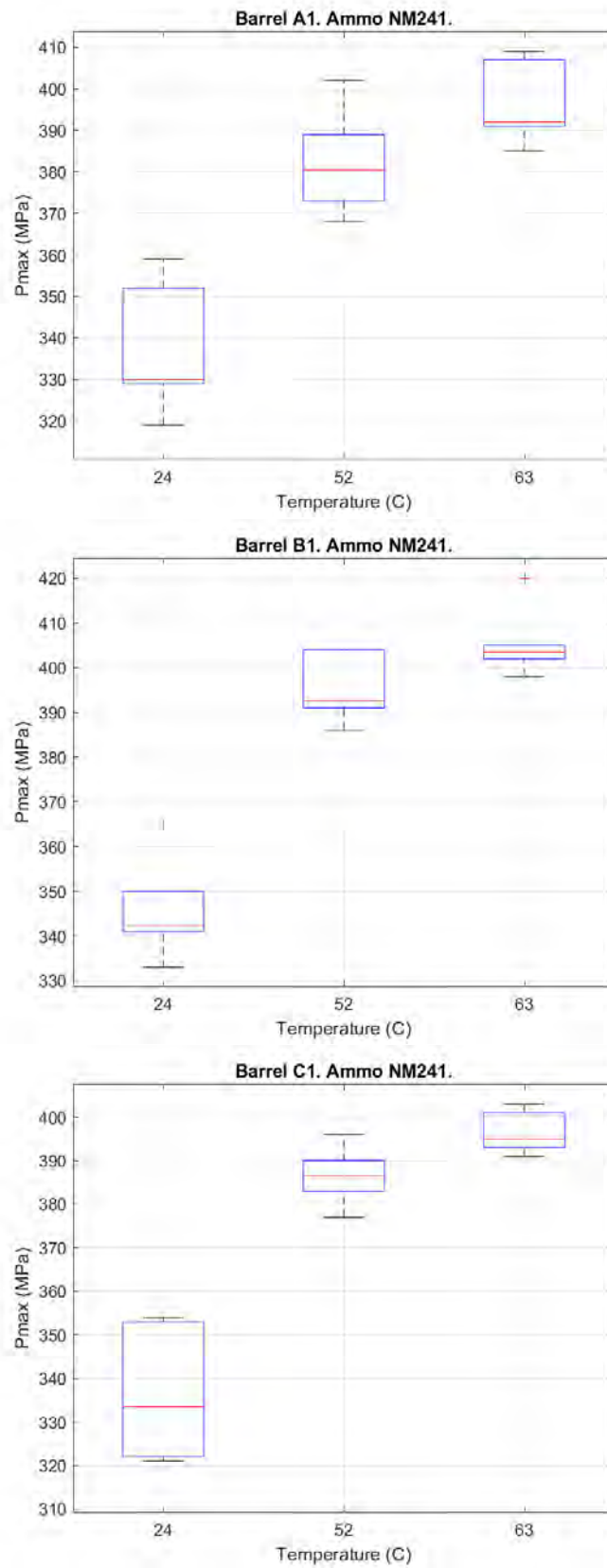


Figure A.2 NM241 lot 20-RA-10

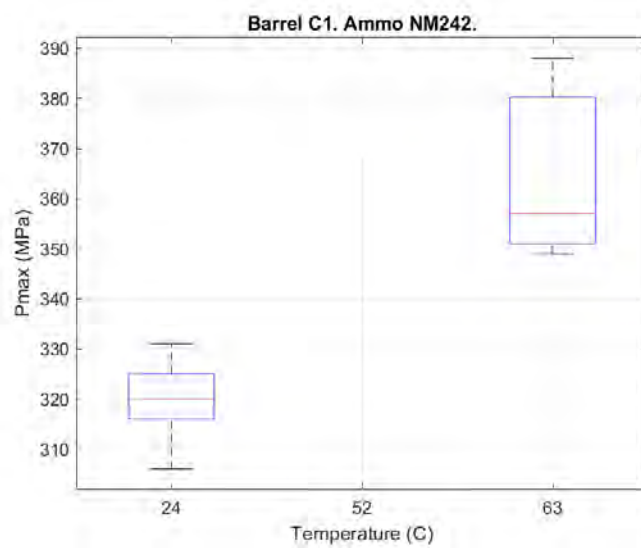
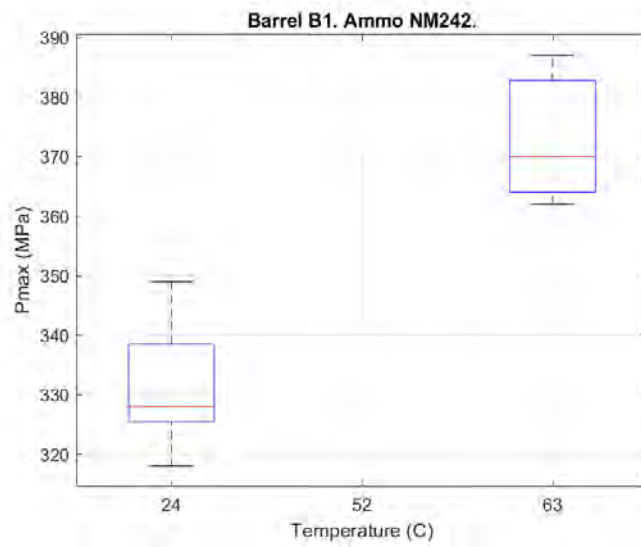
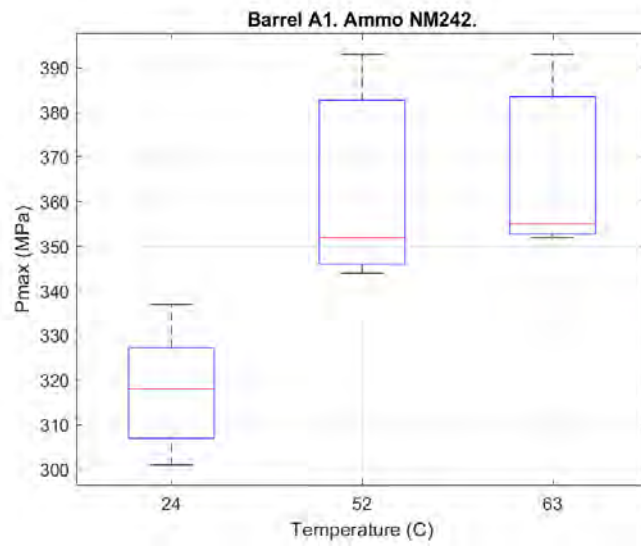


Figure A.3 NM242 lot 20-RA-10

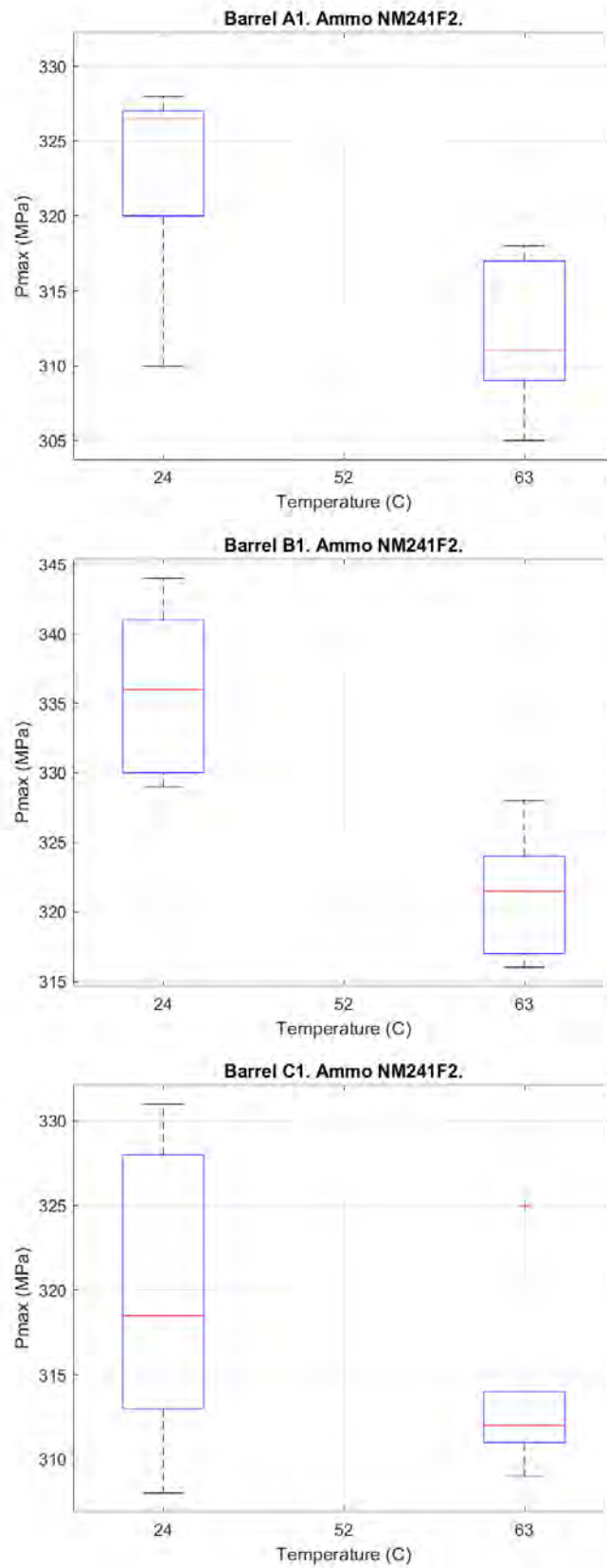


Figure A.4 NM241 F2 lot T01-RA-18

B Robinka barrel measurements

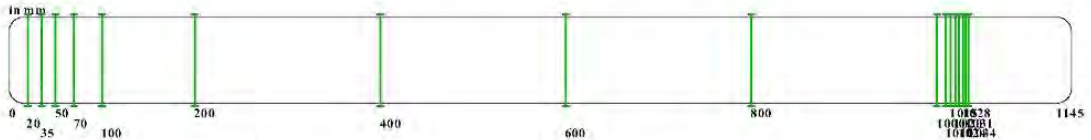
B.1 Barrel A1

BCS result file

Barrel station : 17 / 0 Chamber station : 0 / 0

Pictures : 8 Laser Measures : 0

Max diameter : 13.026 Min diameter : 12.586



Software Revision : QtBCS 1.2.0.30
 Operator : Halvard Heimlund
 NATO stock number :
 Vehicle registration number: Browning
 Shots count: ukjent

Date : 20180228
 Measurement type : station_per_station

Barrel

Tube

Ref : Browning 12.7
 ID : a1
 Length : 1145mm
 Tube Diameter : 12.7mm
 Groove Diameter : 0mm
 Groove Count : 8

Probe

Ref : small_kaliber
 ID : S1570
 Layout : meuframe

Stations (17)

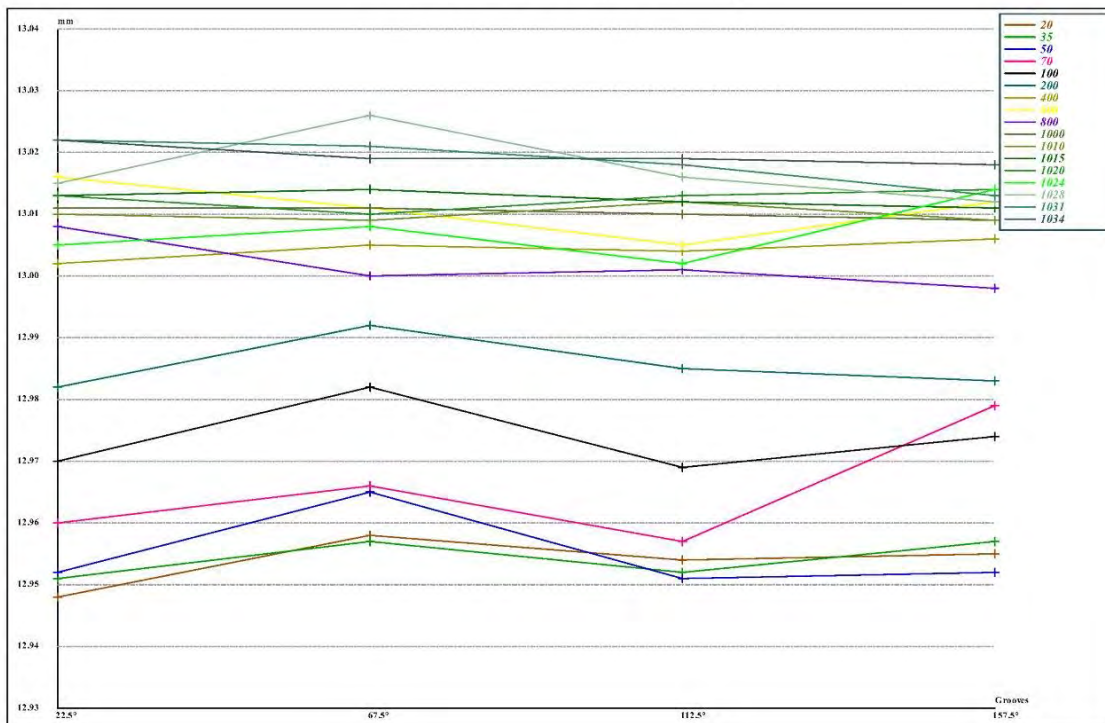
Position (mm)	Radius Mode	Groove Mode	Station Number
20.00	tube centered view	groove per groove radius	1
35.00	tube centered view	groove per groove radius	2
50.00	tube centered view	groove per groove radius	3
70.00	tube centered view	groove per groove radius	4
100.00	tube centered view	groove per groove radius	5
200.00	tube centered view	groove per groove radius	6
400.00	tube centered view	groove per groove radius	7
600.00	tube centered view	groove per groove radius	8
800.00	tube centered view	groove per groove radius	9
1000.00	tube centered view	groove per groove radius	10
1010.00	tube centered view	groove per groove radius	11
1015.00	tube centered view	groove per groove radius	12
1020.00	tube centered view	groove per groove radius	13
1024.00	tube centered view	groove per groove radius	14
1028.00	tube centered view	groove per groove radius	15
1031.00	tube centered view	groove per groove radius	16
1034.00	tube centered view	groove per groove radius	17

Grooves Overview (mm)

Station (mm) / Angular position (degree)

	22.5°	67.5°	112.5°	157.5°
20	12.95	12.96	12.95	12.96
35	12.95	12.96	12.95	12.96
50	12.95	12.96	12.95	12.95
70	12.96	12.97	12.96	12.98
100	12.97	12.98	12.97	12.97
200	12.98	12.99	12.98	12.98
400	13.00	13.01	13.00	13.01
600	13.02	13.01	13.01	13.01
800	13.01	13.00	13.00	13.00
1000	13.01	13.01	13.01	13.01
1010	13.01	13.01	13.01	13.01
1015	13.01	13.01	13.01	13.01
1020	13.01	13.01	13.01	13.01
1024	13.01	13.01	13.00	13.01
1028	13.02	13.03	13.02	13.01
1031	13.02	13.02	13.02	13.01
1034	13.02	13.02	13.02	13.02

Grooves Overview (mm)



Kalibers Overview (mm)

Station (mm) / Angular position (degree)

	0.0°	45.0°	90.0°	135.0°
20	12.59	12.59	12.59	12.59
35	12.59	12.59	12.59	12.60
50	12.59	12.60	12.60	12.60
70	12.61	12.61	12.61	12.61
100	12.61	12.61	12.62	12.62
200	12.63	12.63	12.63	12.63
400	12.66	12.67	12.67	12.66
600	12.68	12.69	12.69	12.69
800	12.68	12.68	12.68	12.68
1000	12.69	12.69	12.69	12.69
1010	12.69	12.69	12.69	12.69
1015	12.69	12.69	12.70	12.69
1020	12.70	12.70	12.70	12.70
1024	12.72	12.72	12.72	12.72
1028	12.80	12.80	12.80	12.80
1031	12.88	12.88	12.88	12.88
1034	12.94	12.94	12.94	12.94

Kalibers Overview (mm)

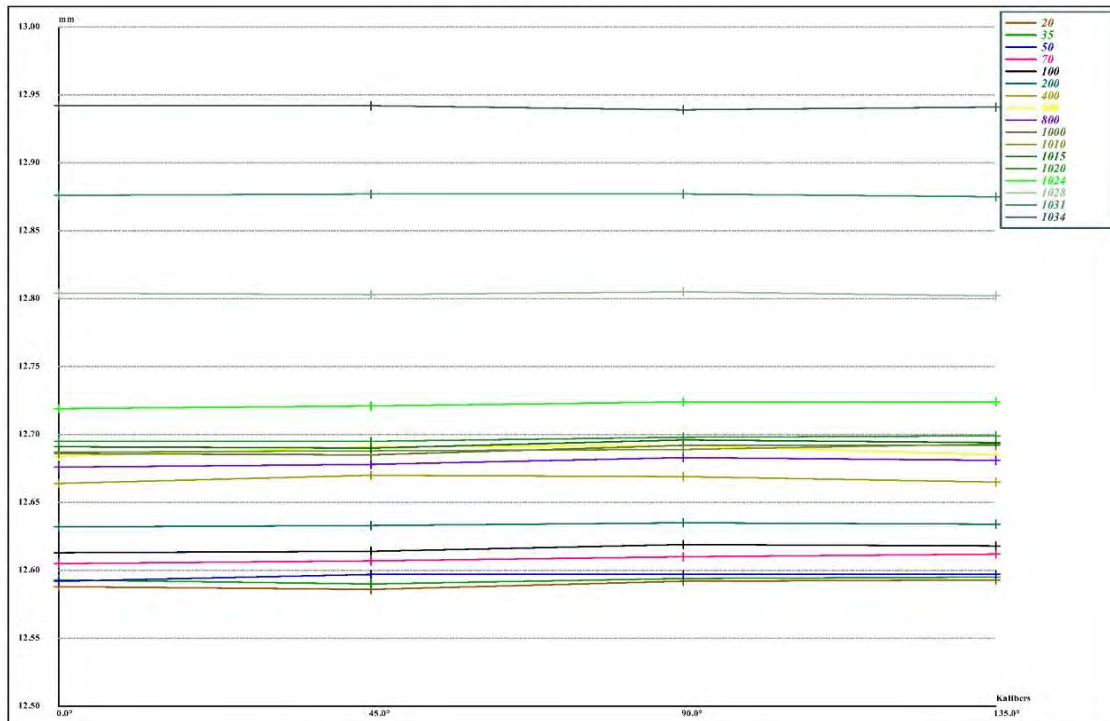








Image 5

12:49 23/04/2018



Position: 810 mm, Rotation: 45°, Tilt: 0°
Area 1: nan mm2, Tag 1: kromslipp bom,
Comments:



Image 6

12:51 23/04/2018



Position: 1002 mm, Rotation: 0°, Tilt: 0°
Area 1: nan mm2, Tag 1: oversiktsbilde mot kammer,
Comments:



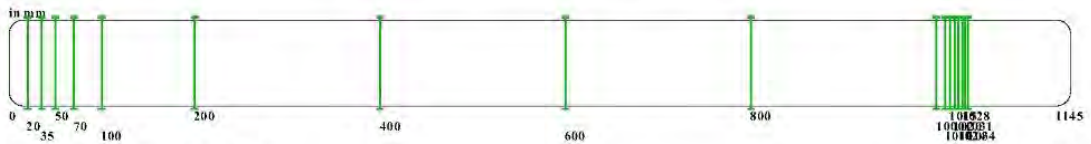
B.2 Barrel B1

BCS result file

Barrel station : 17 / 0 Chamber station : 0 / 0

Pictures : 5 Laser Measures : 0

Max diameter : 13.005 Min diameter : 12.643



Software Revision : QtBCS 1.2.0.30
 Operator : Per Bjortomt
 NATO stock number :
 Vehicle registration number: Browning
 Shots count: ukjent

Date : 20180301
 Measurement type : station_per_station

Barrel

Tube

Ref: Browning 12.7
 ID: b1
 Length: 1145mm
 Tube Diameter: 12.7mm
 Groove Diameter: 0mm
 Groove Count: 8

Probe

Ref: small kaliber
 ID: S1570
 Layout: meuframe

Stations (17)

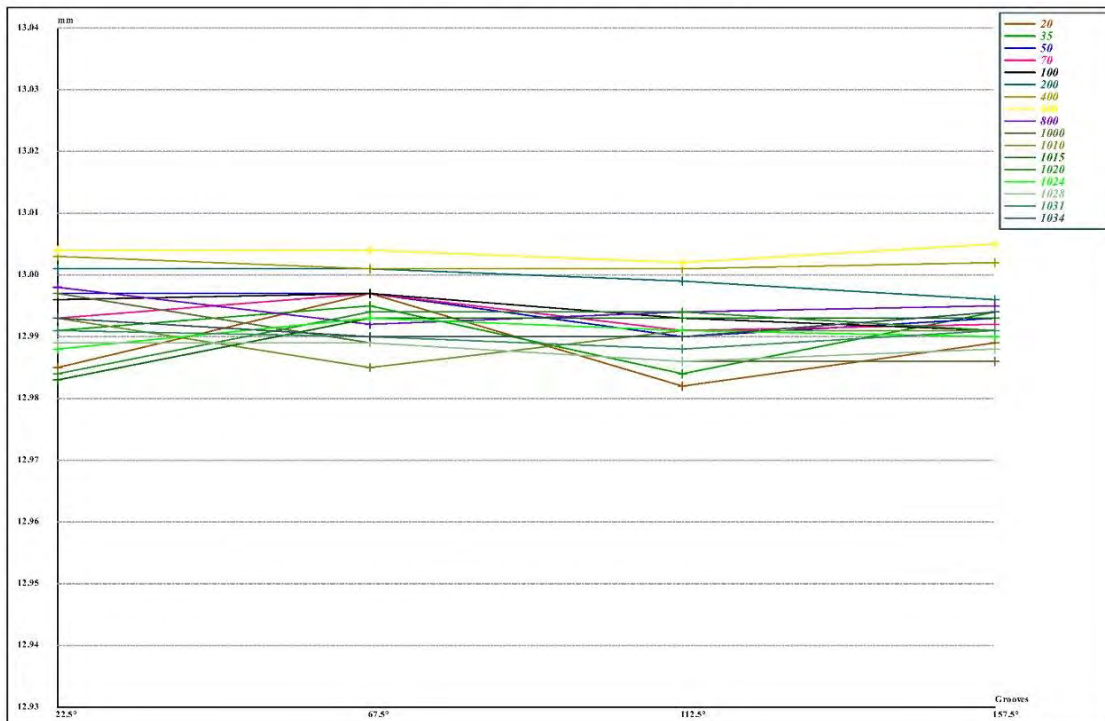
Position (mm)	Radius Mode	Groove Mode	Station Number
20.00	tube centered view	groove per groove radius	1
35.00	tube centered view	groove per groove radius	2
50.00	tube centered view	groove per groove radius	3
70.00	tube centered view	groove per groove radius	4
100.00	tube centered view	groove per groove radius	5
200.00	tube centered view	groove per groove radius	6
400.00	tube centered view	groove per groove radius	7
600.00	tube centered view	groove per groove radius	8
800.00	tube centered view	groove per groove radius	9
1000.00	tube centered view	groove per groove radius	10
1010.00	tube centered view	groove per groove radius	11
1015.00	tube centered view	groove per groove radius	12
1020.00	tube centered view	groove per groove radius	13
1024.00	tube centered view	groove per groove radius	14
1028.00	tube centered view	groove per groove radius	15
1031.00	tube centered view	groove per groove radius	16
1034.00	tube centered view	groove per groove radius	17

Grooves Overview (mm)

Station (mm) / Angular position (degree)

	22.5°	67.5°	112.5°	157.5°
20	12.98	13.00	12.98	12.99
35	12.99	12.99	12.98	12.99
50	13.00	13.00	12.99	12.99
70	12.99	13.00	12.99	12.99
100	13.00	13.00	12.99	12.99
200	13.00	13.00	13.00	13.00
400	13.00	13.00	13.00	13.00
600	13.00	13.00	13.00	13.01
800	13.00	12.99	12.99	12.99
1000	13.00	12.99	12.99	12.99
1010	12.99	12.98	12.99	12.99
1015	12.98	12.99	12.99	12.99
1020	12.98	12.99	12.99	12.99
1024	12.99	12.99	12.99	12.99
1028	12.99	12.99	12.99	12.99
1031	12.99	12.99	12.99	12.99
1034	12.99	12.99	12.99	12.99

Grooves Overview (mm)



Kalibers Overview (mm)

Station (mm) / Angular position (degree)

	0.0°	45.0°	90.0°	135.0°
20	12.65	12.65	12.65	12.64
35	12.66	12.66	12.65	12.65
50	12.65	12.66	12.66	12.65
70	12.66	12.66	12.66	12.66
100	12.66	12.66	12.66	12.66
200	12.66	12.67	12.66	12.66
400	12.68	12.68	12.69	12.69
600	12.68	12.68	12.69	12.69
800	12.67	12.67	12.67	12.68
1000	12.66	12.66	12.66	12.66
1010	12.66	12.67	12.66	12.66
1015	12.66	12.65	12.66	12.67
1020	12.66	12.65	12.66	12.67
1024	12.66	12.66	12.67	12.67
1028	12.76	12.76	12.76	12.76
1031	12.82	12.82	12.82	12.82
1034	12.90	12.90	12.89	12.90

Kalibers Overview (mm)

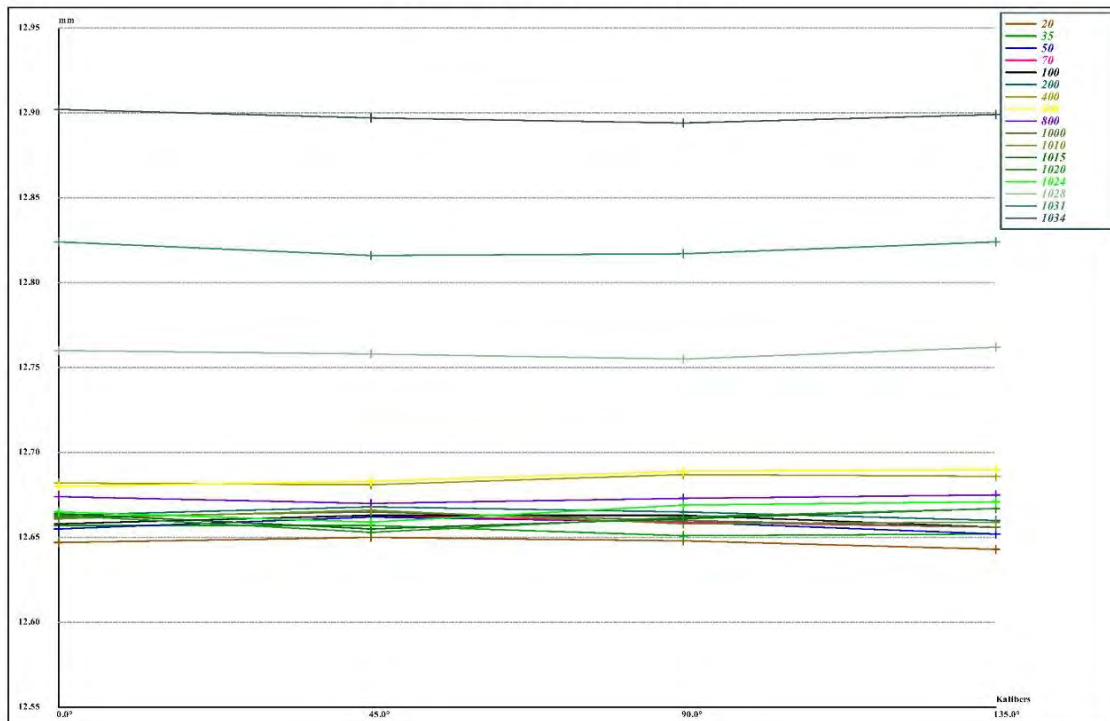








Image 5

08:15 24/04/2018



Position: 1040 mm, Rotation: 0°, Tilt: 0°

Area: 1; nan mm2; Tag: 1; Oversiktsbilde med trykkhull mot bakre bommer/overgangskonus.;

Comments:

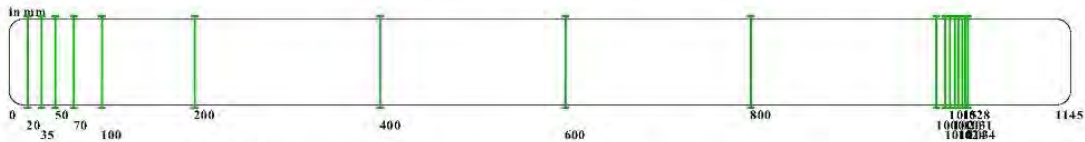
B.3 Barrel C1

BCS result file

Barrel station : 17 / 0 Chamber station : 0 / 0

Pictures : 4 Laser Measures : 0

Max diameter : 13.041 Min diameter : 12.69



Software Revision : QtBCS 1.2.0.30

Operator : Per Bjortomt

NATO stock number :

Vehicle registration number: Browning

Shots count: ukjent

Date : 20180302

Measurement type : station_per_station

Barrel

Tube

Ref : Browning 12.7

ID : b1

Length : 1145mm

Tube Diameter : 12.7mm

Groove Diameter : 0mm

Groove Count : 8

Probe

Ref : small kaliber

ID : S1570

Layout : meuframe

Stations (17)

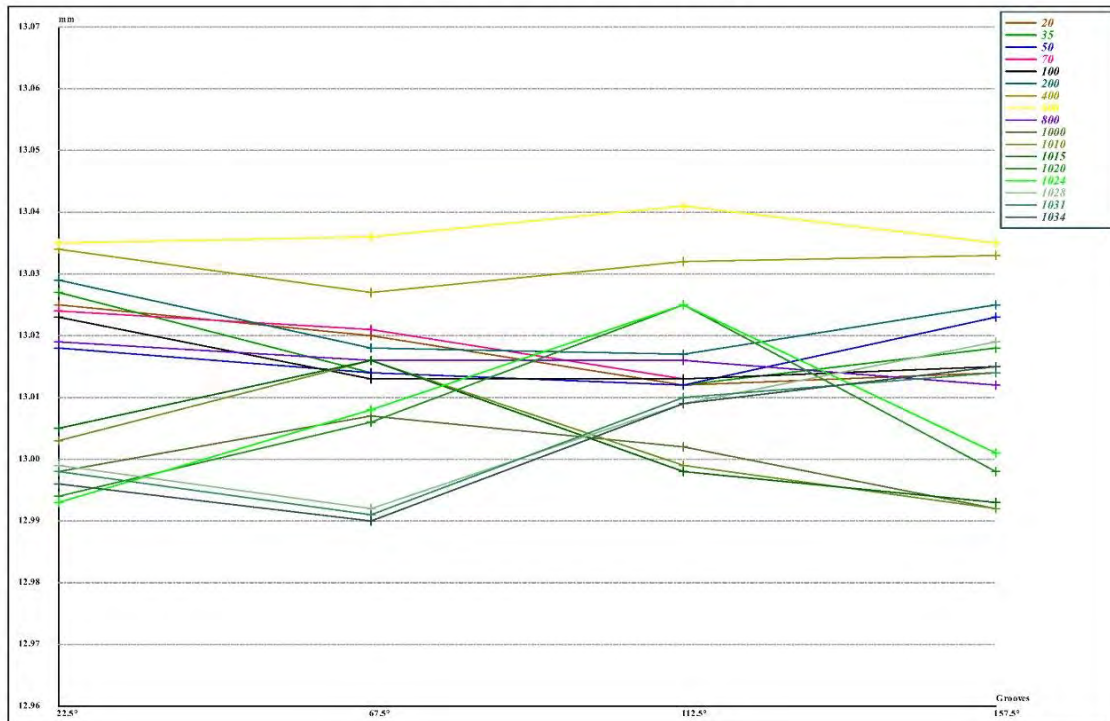
Position (mm)	Radius Mode	Groove Mode	Station Number
20.00	tube centered view	groove per groove radius	1
35.00	tube centered view	groove per groove radius	2
50.00	tube centered view	groove per groove radius	3
70.00	tube centered view	groove per groove radius	4
100.00	tube centered view	groove per groove radius	5
200.00	tube centered view	groove per groove radius	6
400.00	tube centered view	groove per groove radius	7
600.00	tube centered view	groove per groove radius	8
800.00	tube centered view	groove per groove radius	9
1000.00	tube centered view	groove per groove radius	10
1010.00	tube centered view	groove per groove radius	11
1015.00	tube centered view	groove per groove radius	12
1020.00	tube centered view	groove per groove radius	13
1024.00	tube centered view	groove per groove radius	14
1028.00	tube centered view	groove per groove radius	15
1031.00	tube centered view	groove per groove radius	16
1034.00	tube centered view	groove per groove radius	17

Grooves Overview (mm)

Station (mm) / Angular position (degree)

	22.5°	67.5°	112.5°	157.5°
20	13.03	13.02	13.01	13.01
35	13.03	13.01	13.01	13.02
50	13.02	13.01	13.01	13.02
70	13.02	13.02	13.01	13.02
100	13.02	13.01	13.01	13.02
200	13.03	13.02	13.02	13.03
400	13.03	13.03	13.03	13.03
600	13.04	13.04	13.04	13.04
800	13.02	13.02	13.02	13.01
1000	13.00	13.01	13.00	12.99
1010	13.00	13.02	13.00	12.99
1015	13.01	13.02	13.00	12.99
1020	12.99	13.01	13.03	13.00
1024	12.99	13.01	13.03	13.00
1028	13.00	12.99	13.01	13.02
1031	13.00	12.99	13.01	13.01
1034	13.00	12.99	13.01	13.02

Grooves Overview (mm)



Kalibers Overview (mm)

Station (mm) / Angular position (degree)

	0.0°	45.0°	90.0°	135.0°
20	12.71	12.71	12.71	12.70
35	12.72	12.71	12.71	12.71
50	12.72	12.72	12.72	12.71
70	12.72	12.73	12.72	12.72
100	12.73	12.73	12.73	12.73
200	12.73	12.73	12.72	12.73
400	12.74	12.74	12.74	12.75
600	12.75	12.75	12.75	12.75
800	12.72	12.72	12.73	12.72
1000	12.69	12.71	12.72	12.71
1010	12.69	12.71	12.72	12.71
1015	12.69	12.71	12.72	12.70
1020	12.69	12.69	12.72	12.72
1024	12.70	12.70	12.73	12.73
1028	12.79	12.78	12.78	12.80
1031	12.87	12.85	12.85	12.87
1034	12.93	12.91	12.92	12.94

Kalibers Overview (mm)

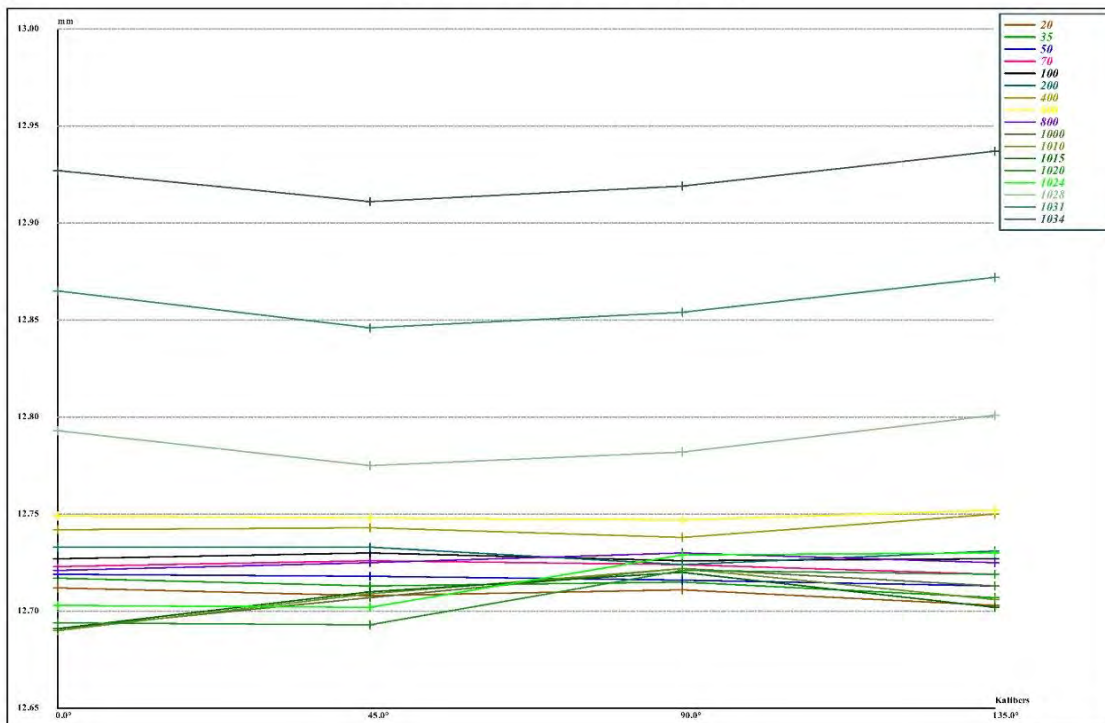






Image 3

14:25 24/04/2018



Position: 1015 mm, Rotation: 0°, Tilt: 0°
Area 1: nan mm2, Tag 1: Oversikt mot kammer.
Comments:



Image 4

14:30 24/04/2018



Position: 1040 mm, Rotation: 0°, Tilt: 0°
Area 1: nan mm2, Tag 1: Oversiktsbilde fra kammer mot bommer, med tryktestehull.
Comments:

C Pictures from microscope examination

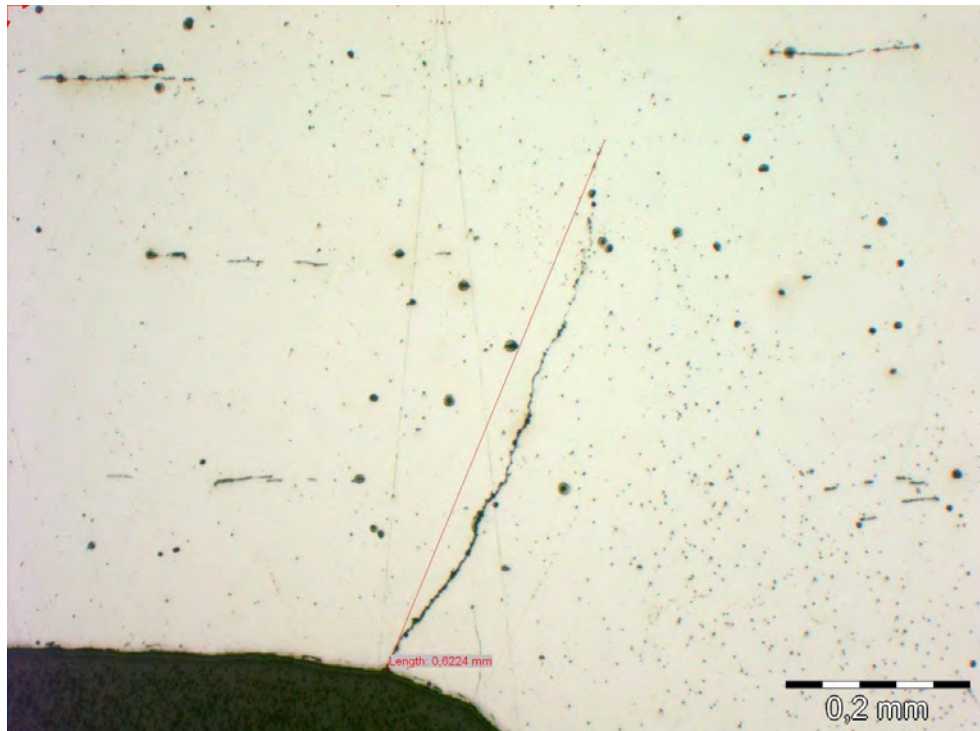


Figure C.1 Crack at segment A, first ridge on barrel no. 1393

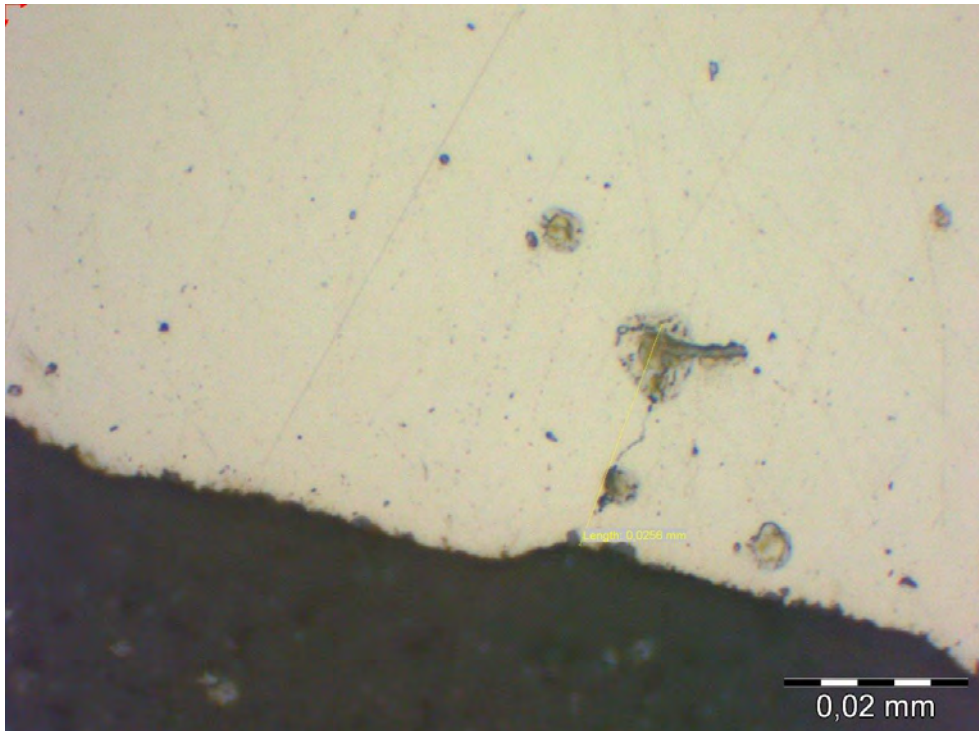


Figure C.2 Crack at segment A, third ridge on barrel no. 1393

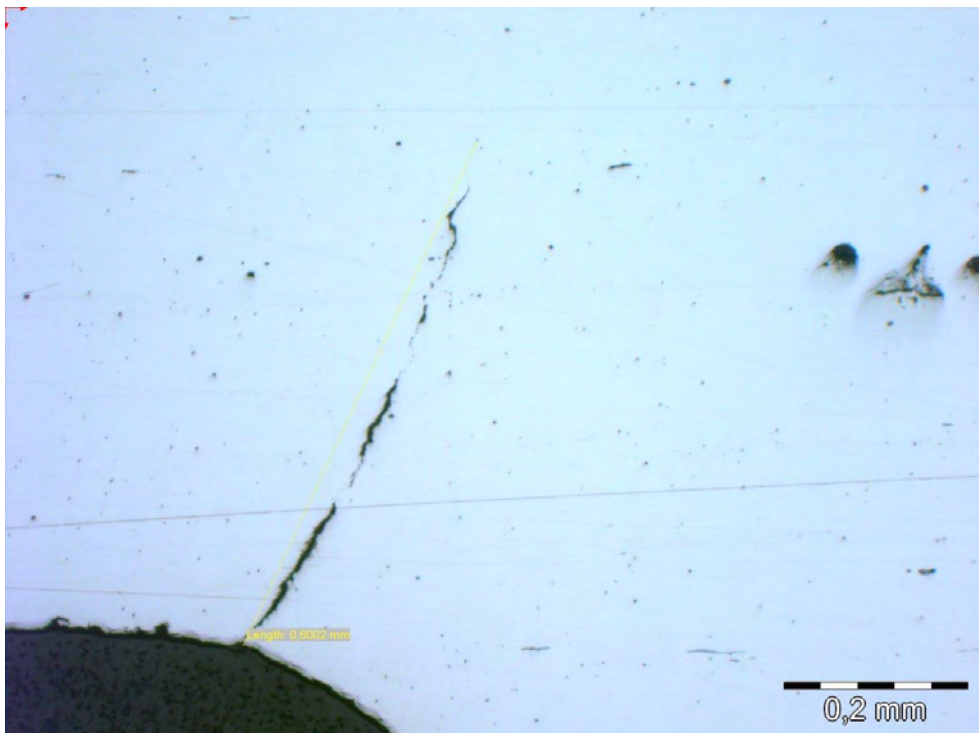


Figure C.3 Crack at segment B, first ridge on barrel no. 1393 (second cut)

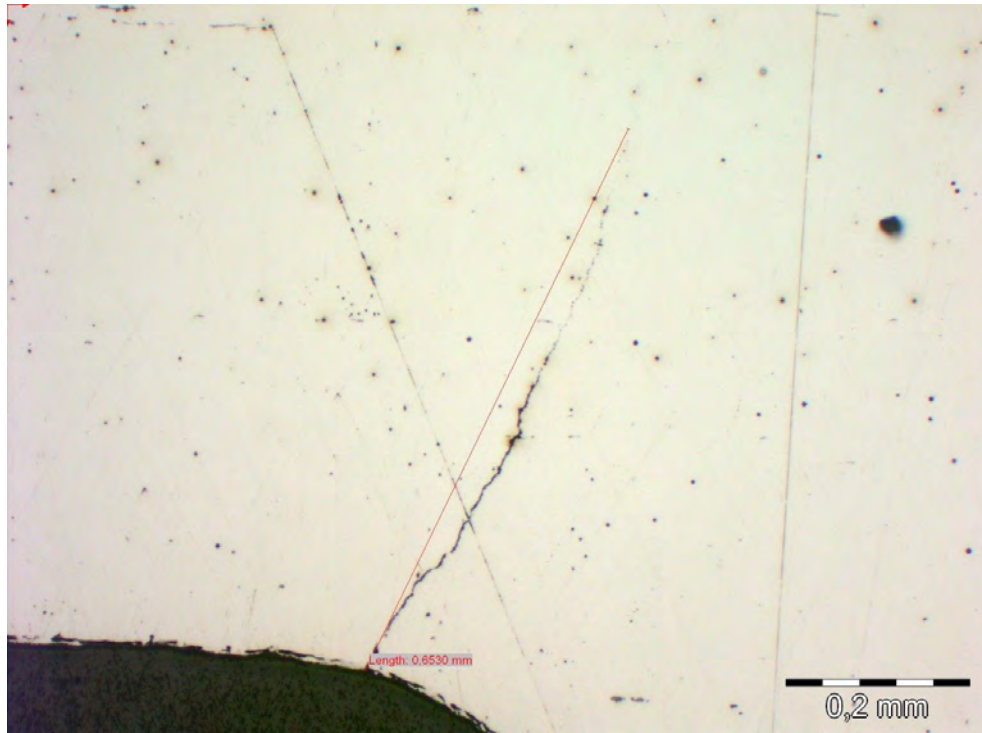


Figure C.4 Crack at segment B, first ridge on barrel no. 1393 (first cut)

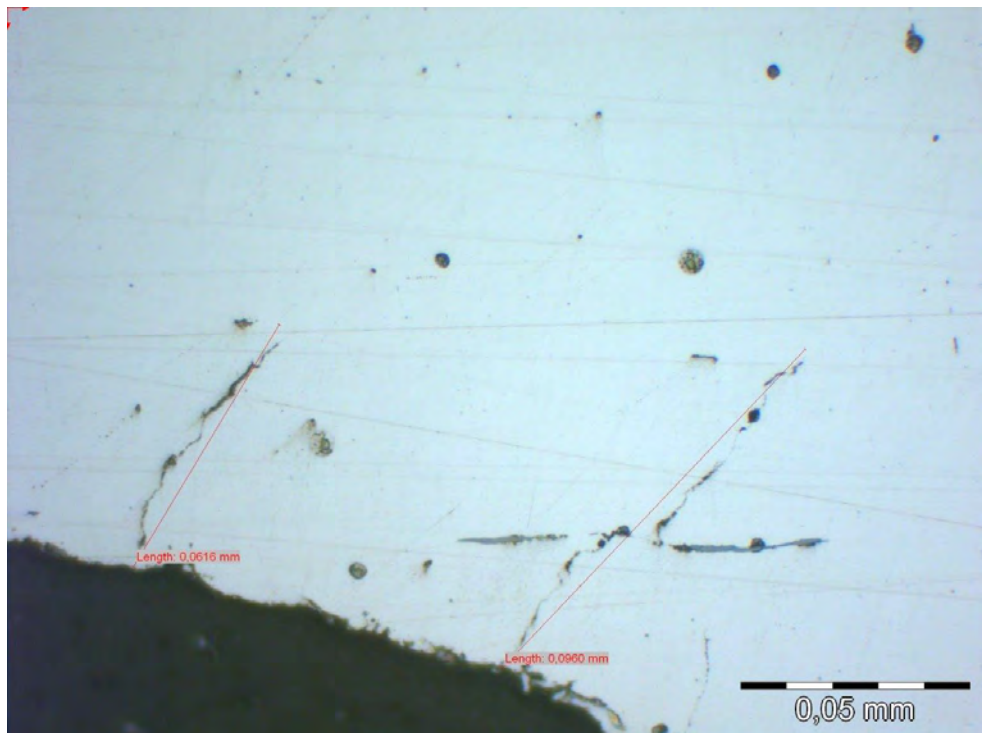


Figure C.5 Crack at segment B, second ridge on barrel no. 1393 (second cut)

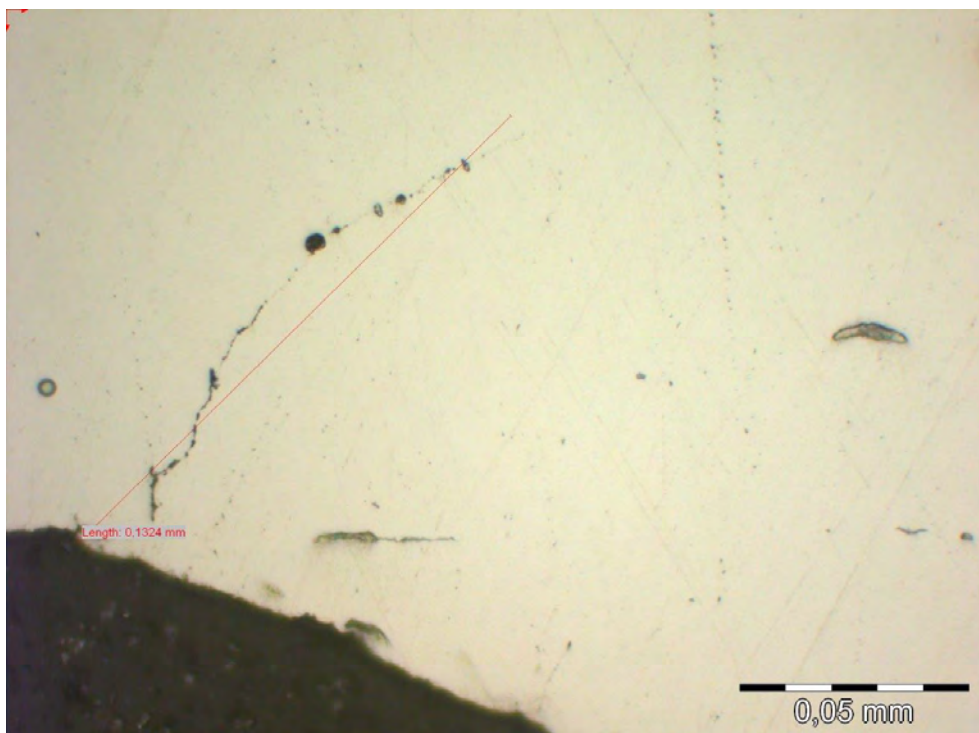


Figure C.6 Crack at segment B, second ridge on barrel no. 1393 (first cut)

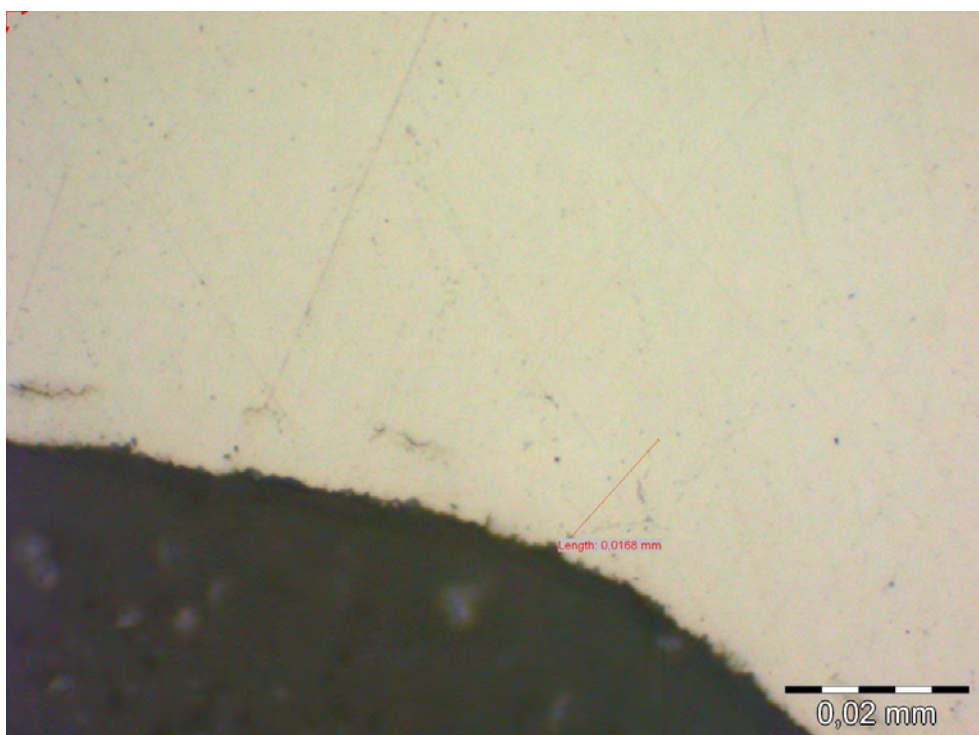


Figure C.7 Crack at segment B, fourth ridge on barrel no. 1393

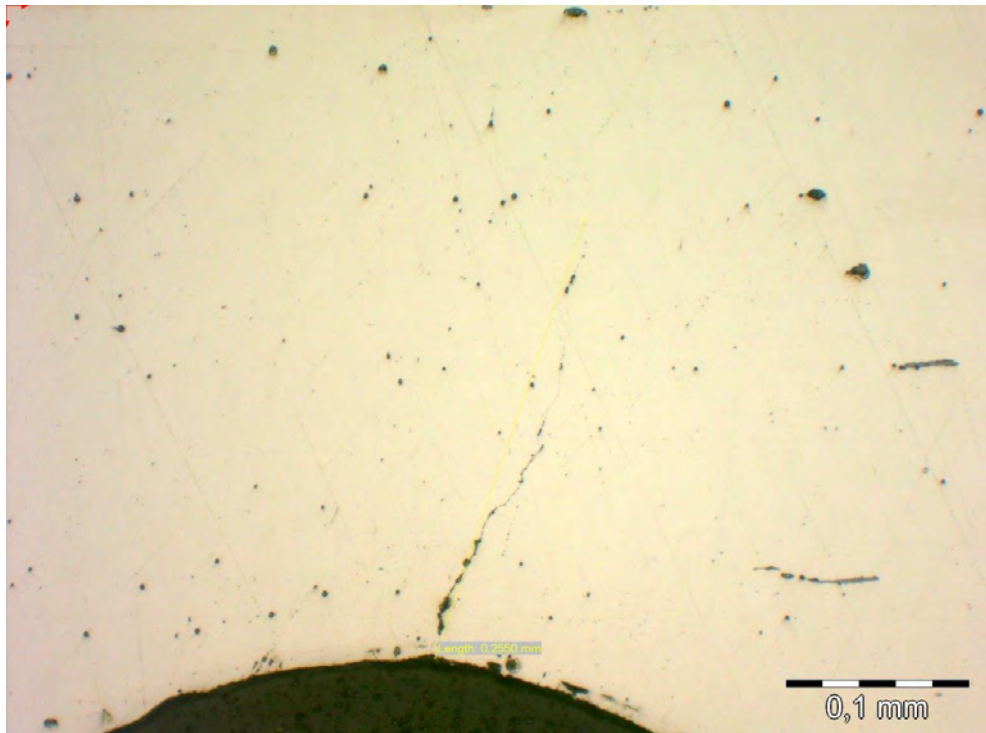


Figure C.8 Crack at segment C, second ridge on barrel no. 1393

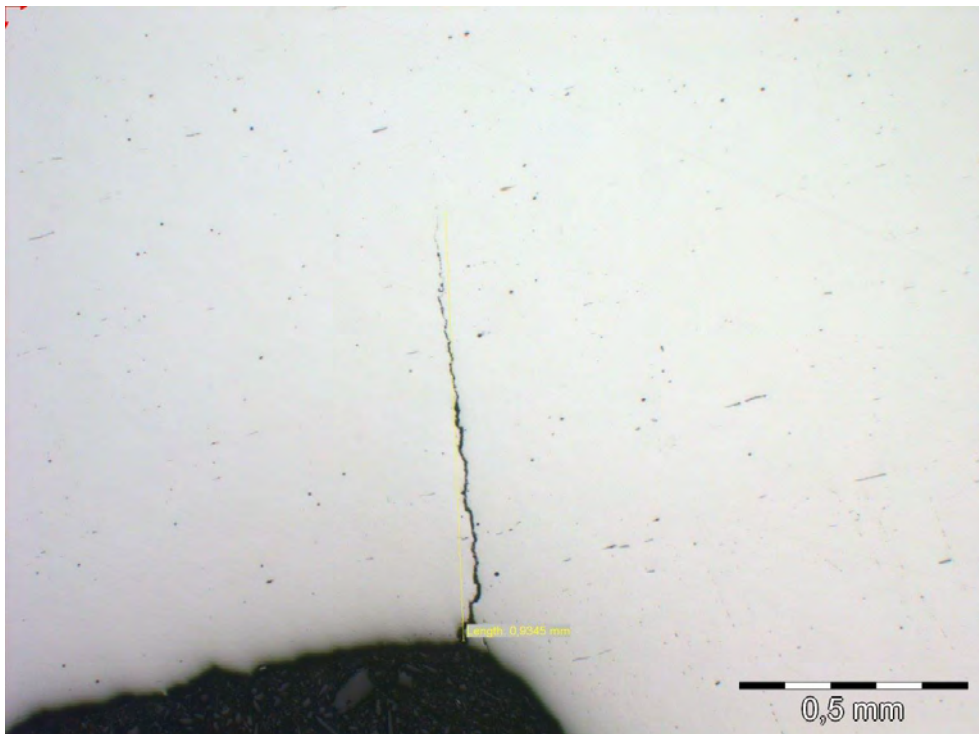


Figure C.9 Crack at segment C, second ridge on barrel no. 1613

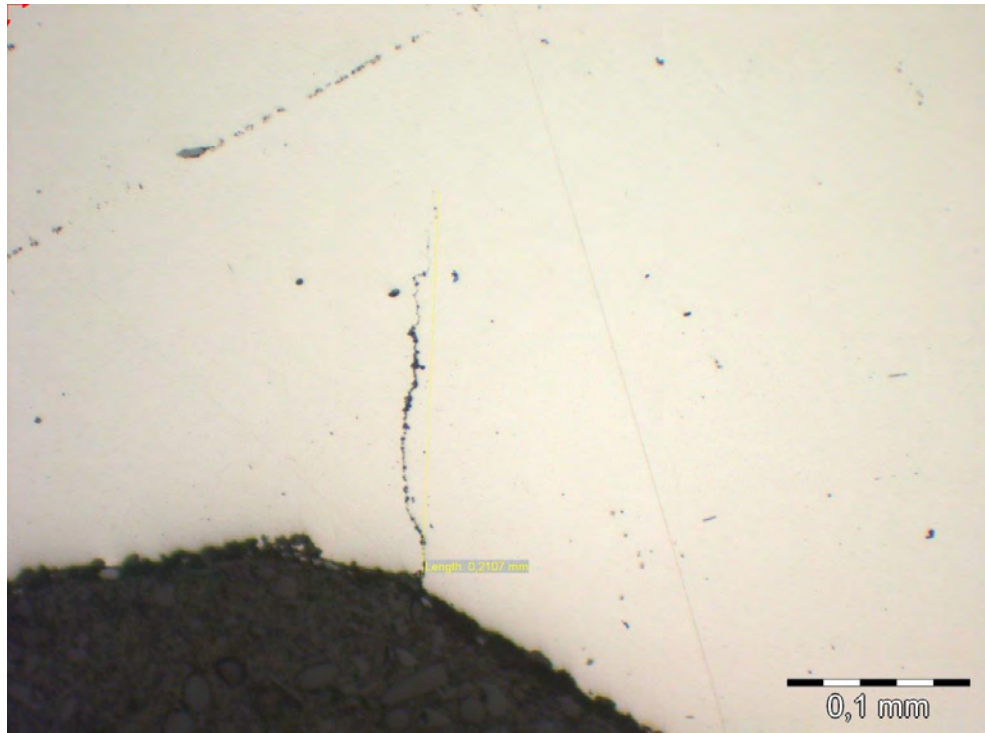


Figure C.10 Crack at segment C, second ridge on barrel no. 1613

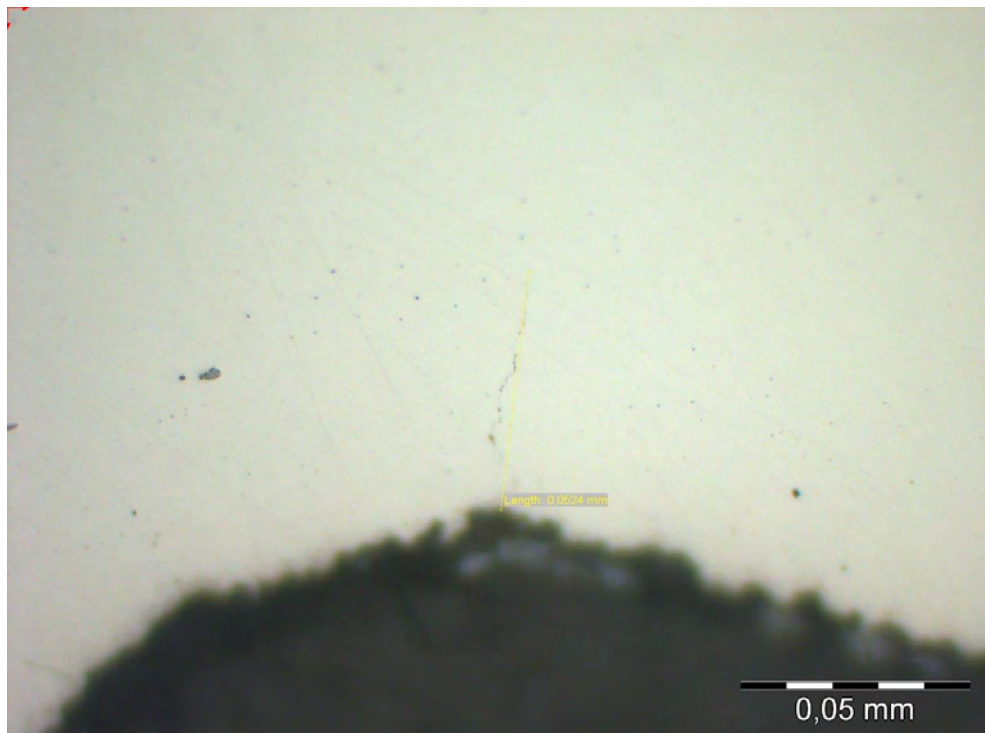


Figure C.11 Crack at segment C, second ridge on barrel no. 1613

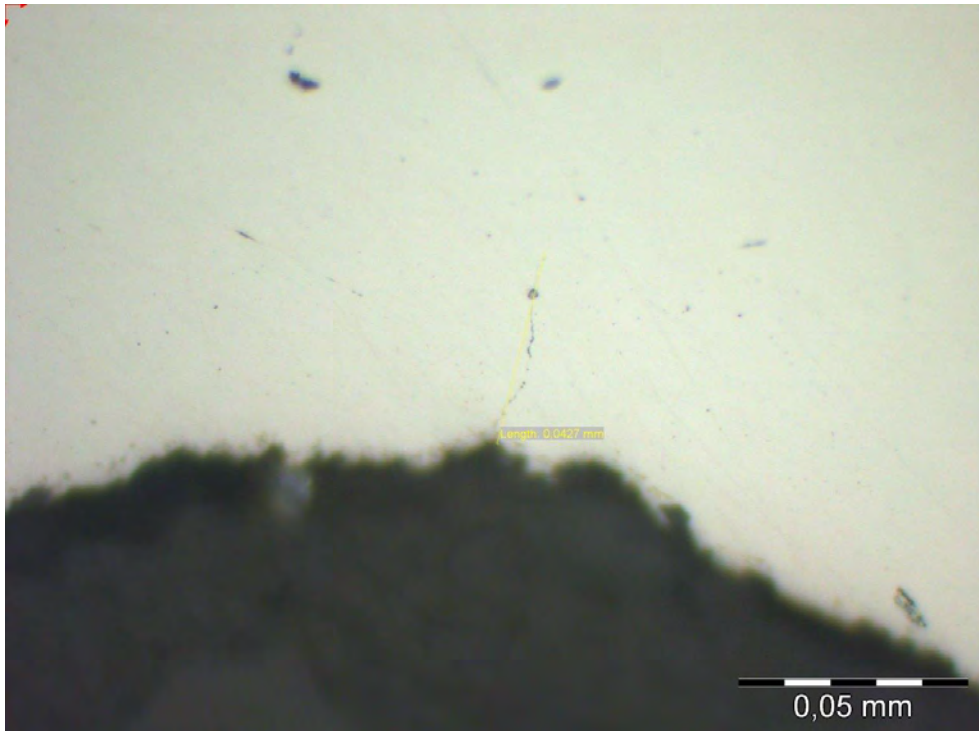


Figure C.12 Crack at segment C, second ridge on barrel no. 1613

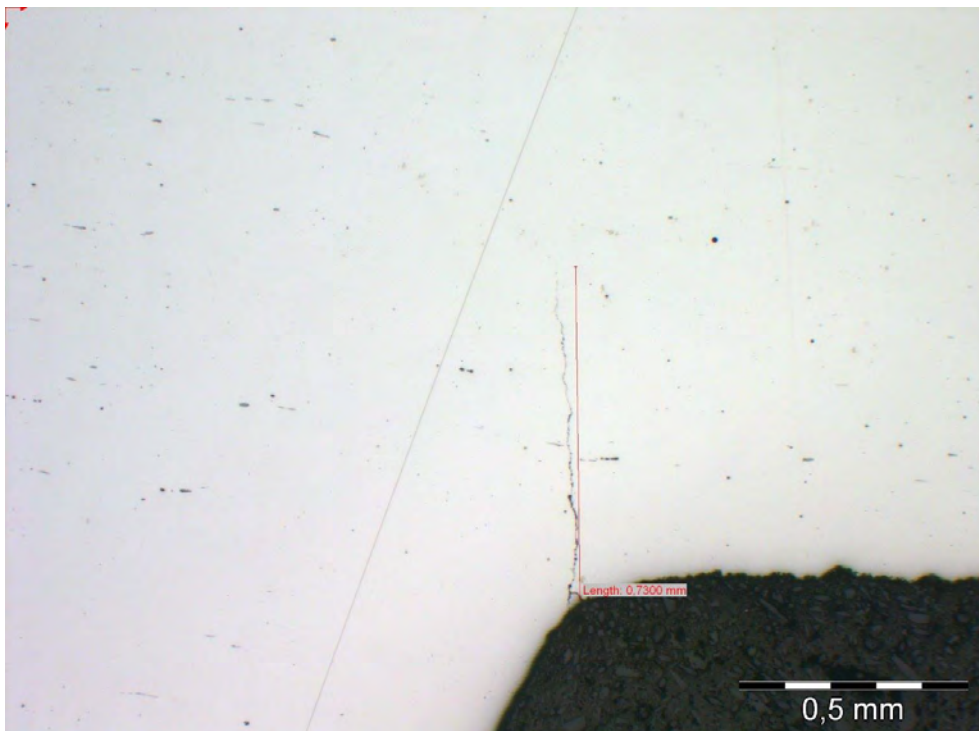


Figure C.13 Crack at segment C, second ridge on barrel no. 1613

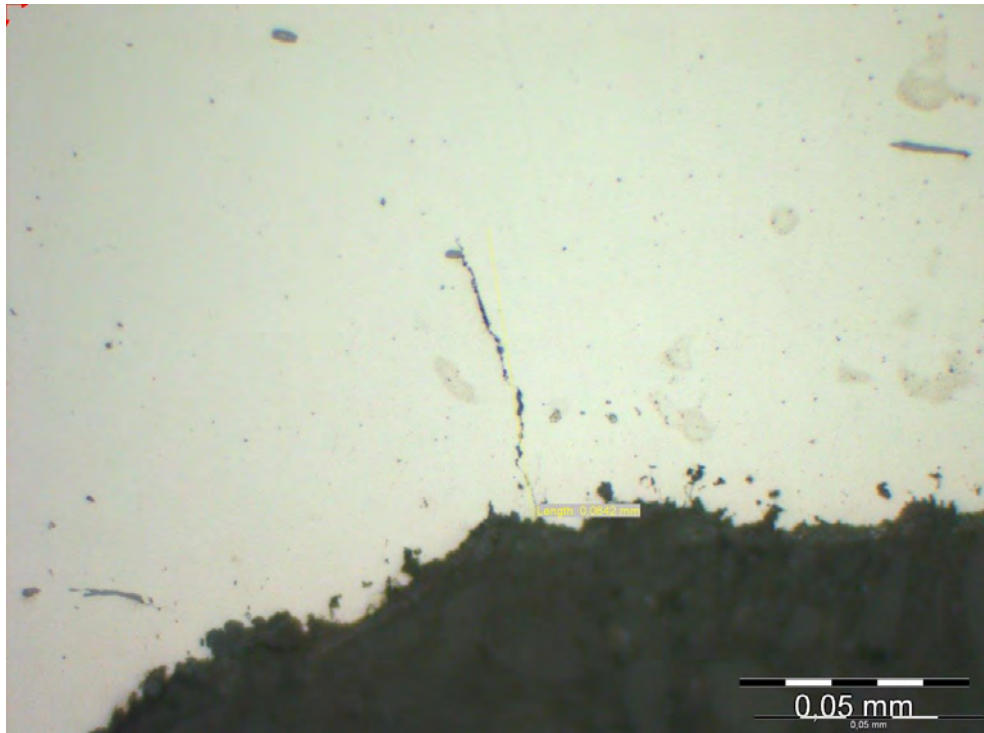


Figure C.14 Crack at segment C, second ridge on barrel no. 1613

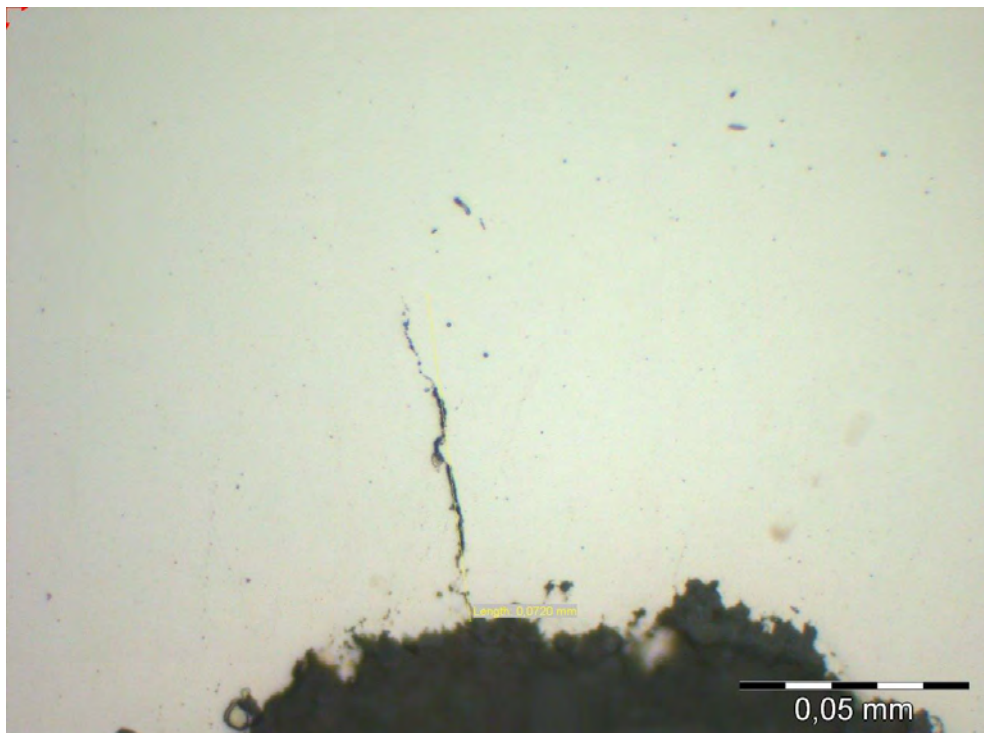


Figure C.15 Crack at segment C, second ridge on barrel no. 1613

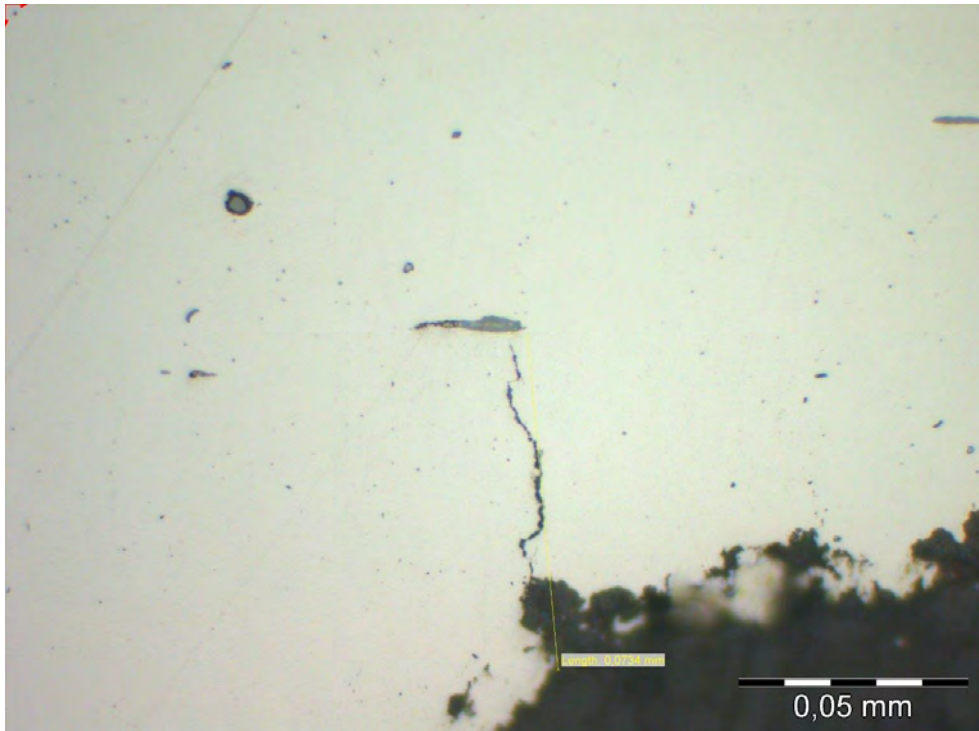


Figure C.16 Crack at segment C, second ridge on barrel no. 1613

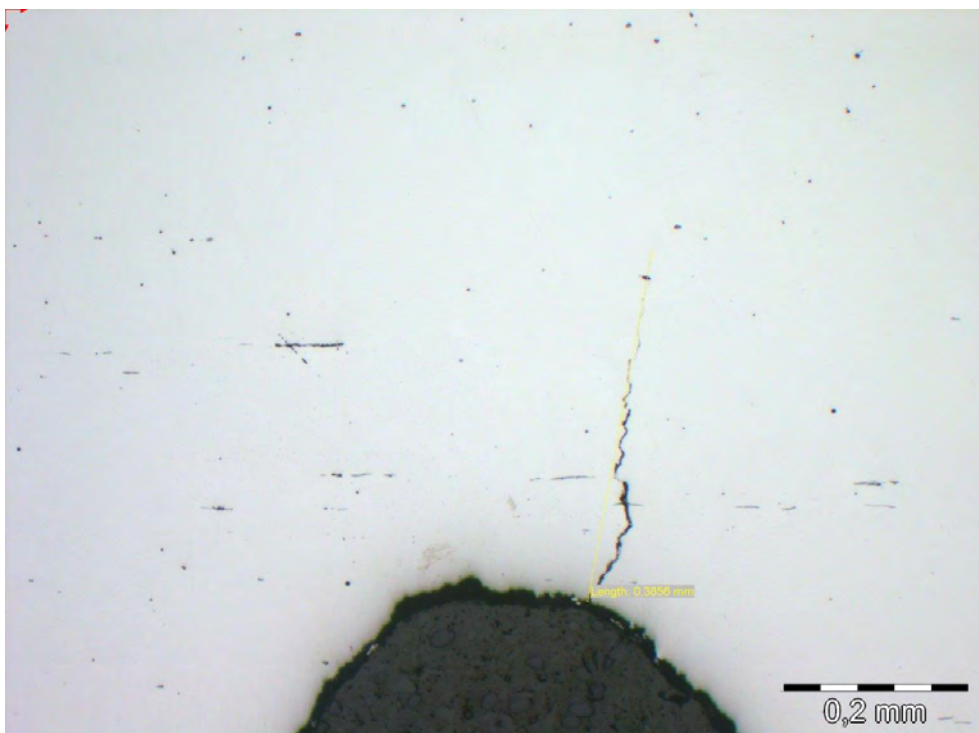


Figure C.17 Crack at segment C, second ridge on barrel no. 1613

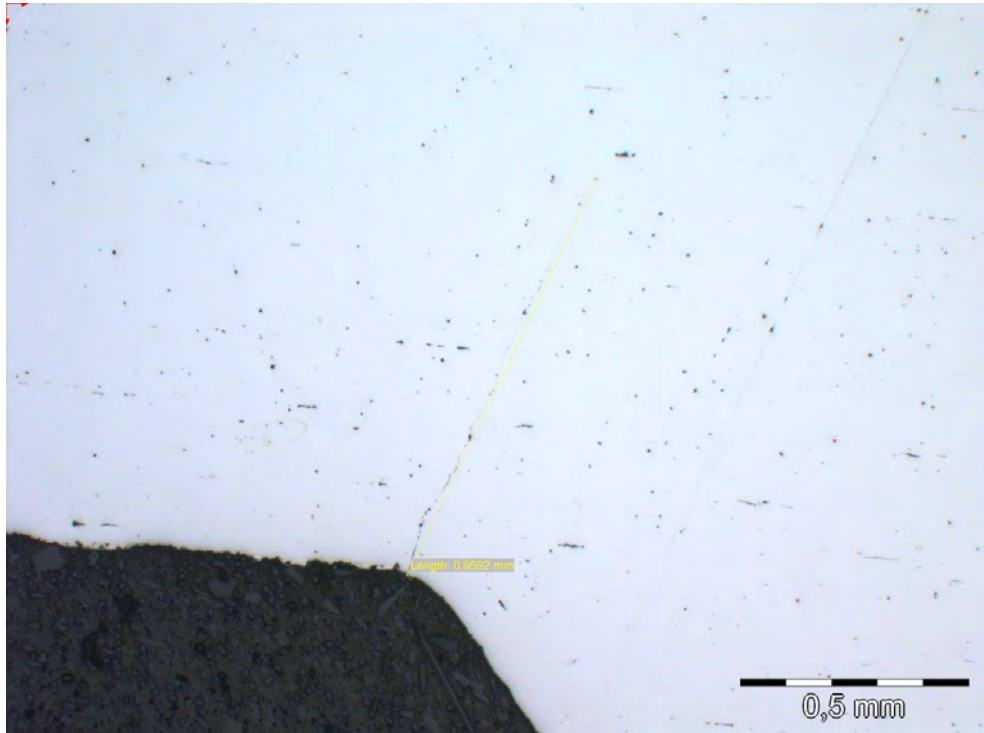


Figure C.18 Crack at segment A, first ridge on barrel no. 8832/6713

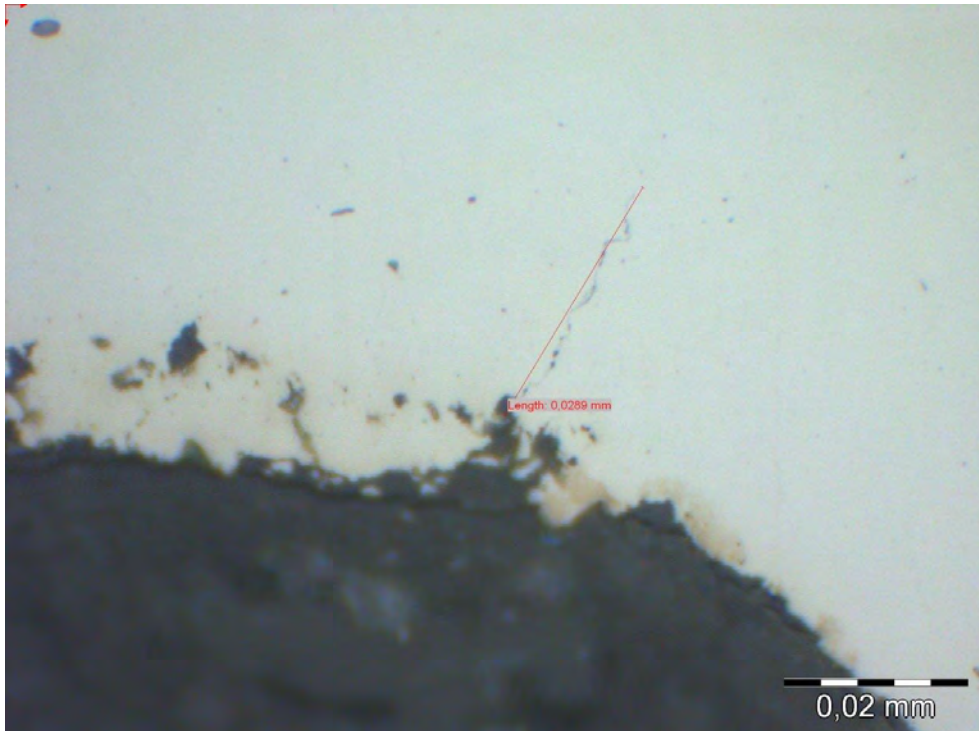


Figure C.19 Crack at segment A, second ridge on barrel no. 8832/6713

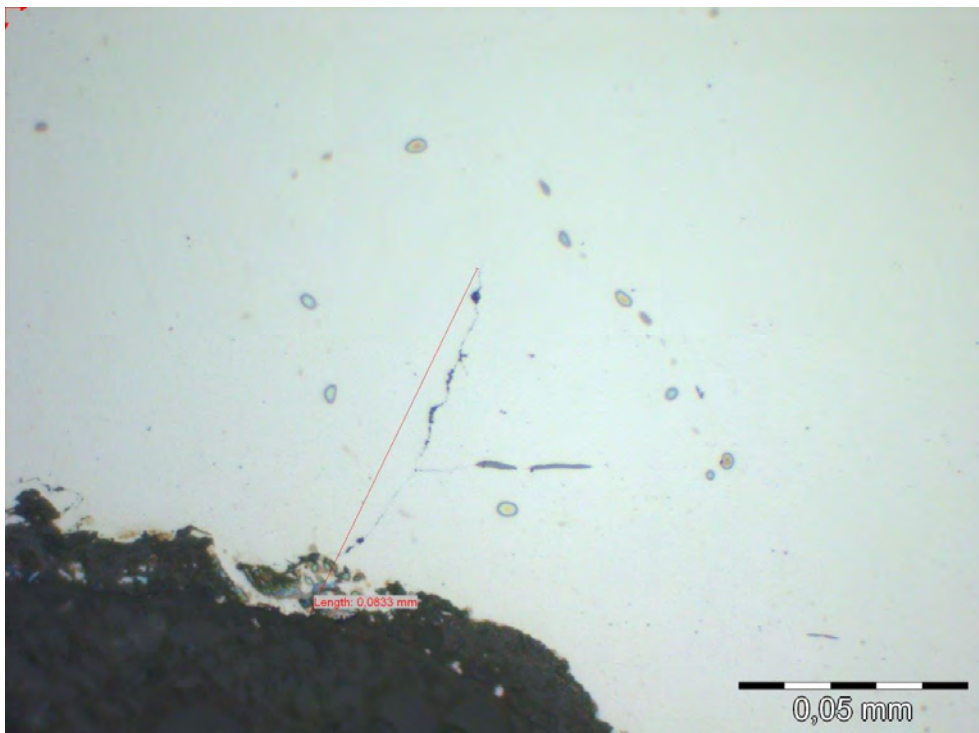


Figure C.20 Crack at segment A, fourth ridge on barrel no. 8832/6713

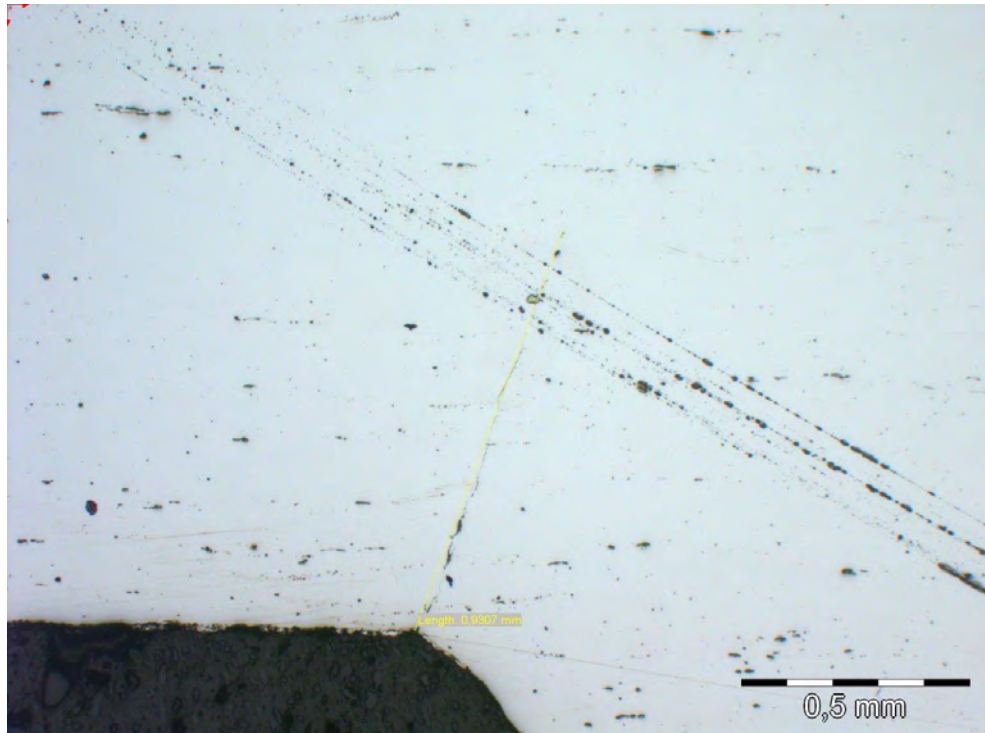


Figure C.21 Crack at segment B, first ridge on barrel no. 8832/6713

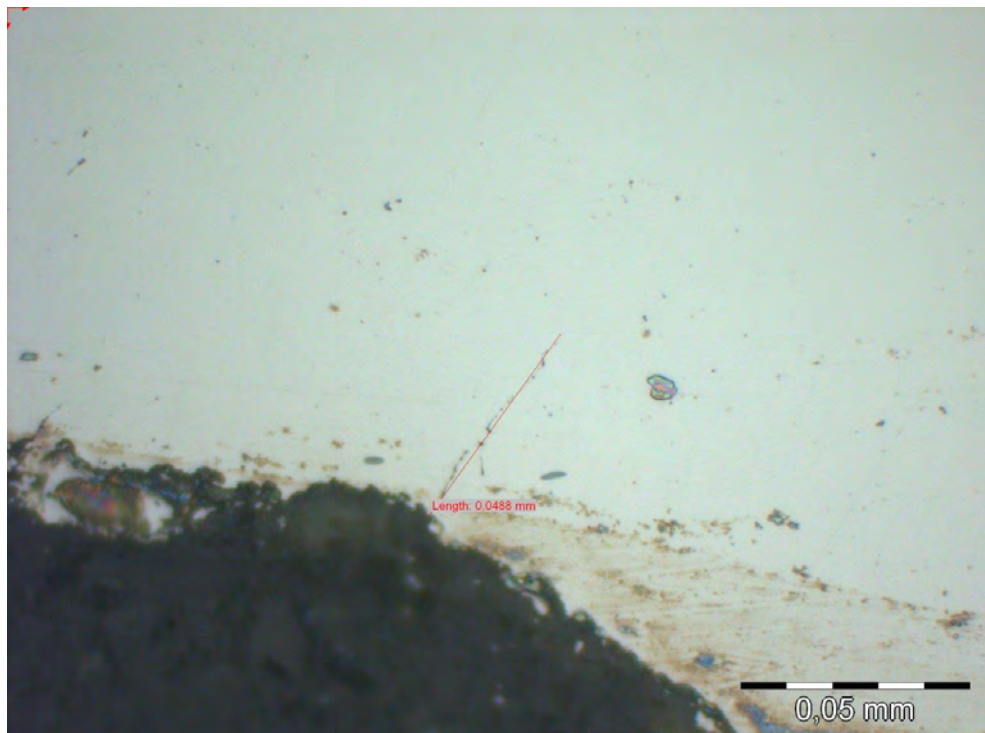


Figure C.22 Crack at segment B, second ridge on barrel no. 8832/6713

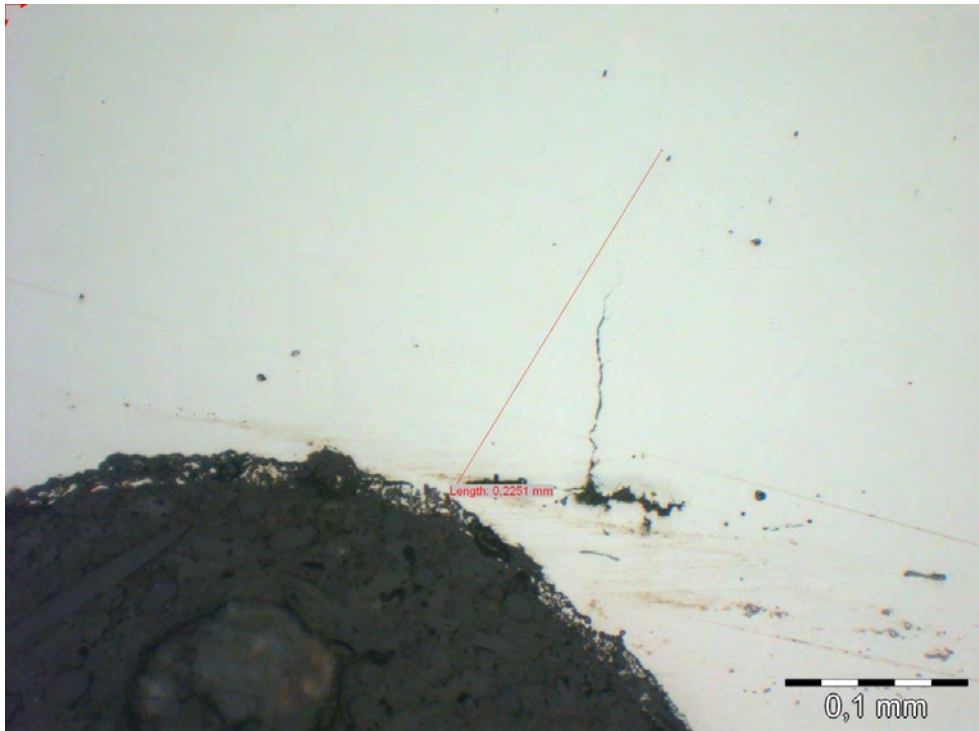


Figure C.23 Crack at segment B, fourth ridge on barrel no. 8832/6713

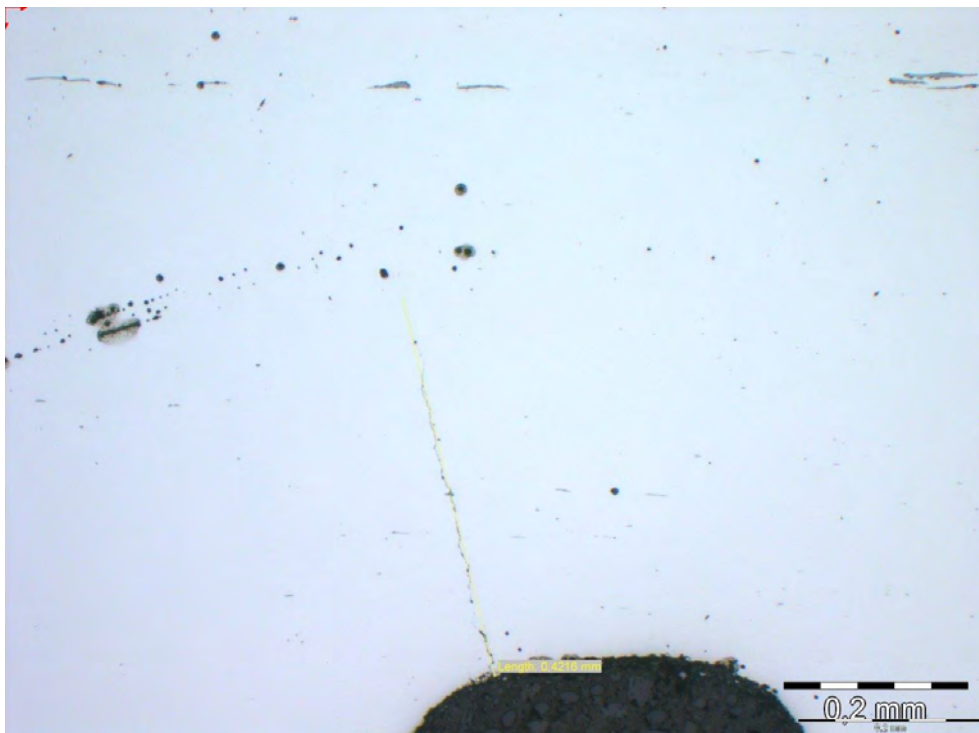


Figure C.24 Crack at segment C, second ridge on barrel no. 8832/6713

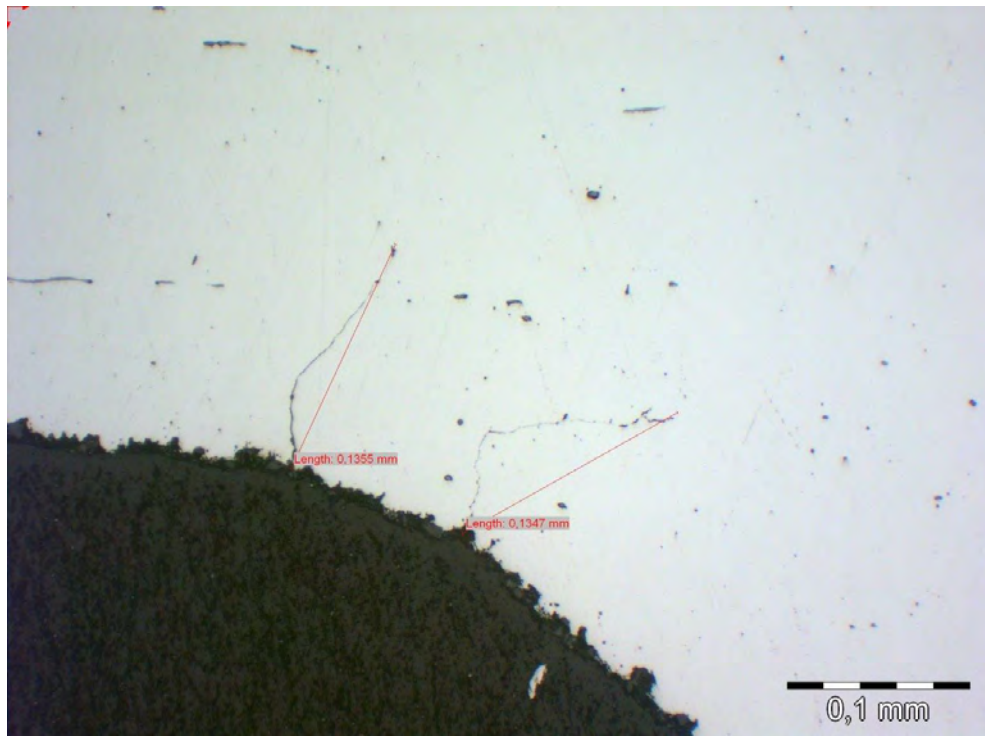


Figure C.25 Cut one in crack at segment A, first ridge on barrel no. 14389

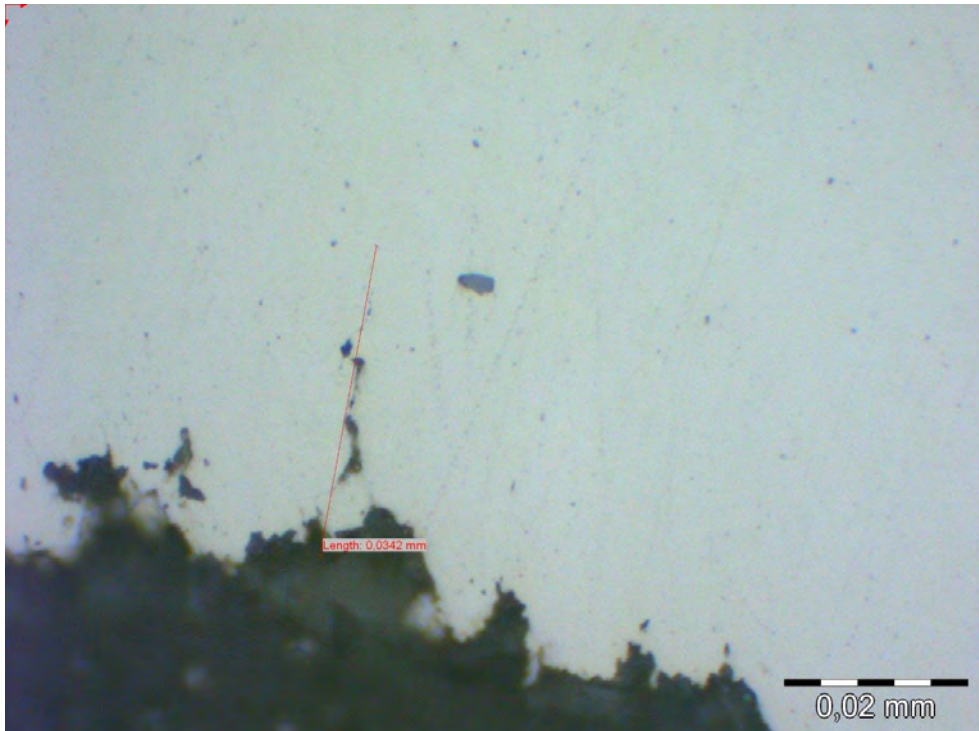


Figure C.26 Cut one in crack at segment A, second ridge on barrel no. 14389

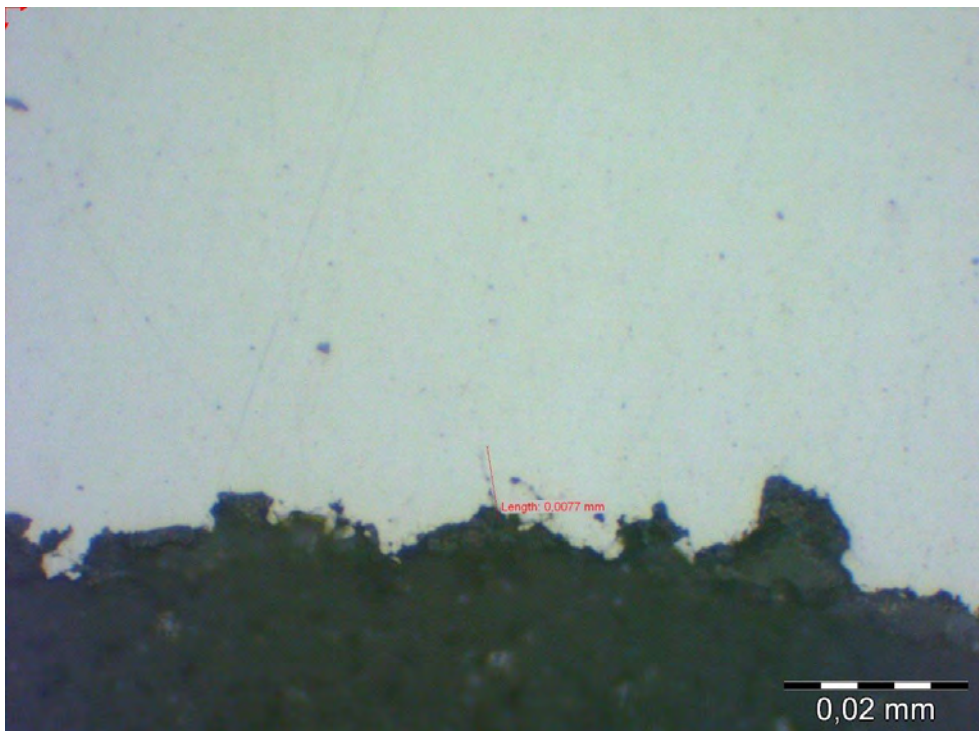


Figure C.27 Cut one in crack at segment A, third ridge on barrel no. 14389

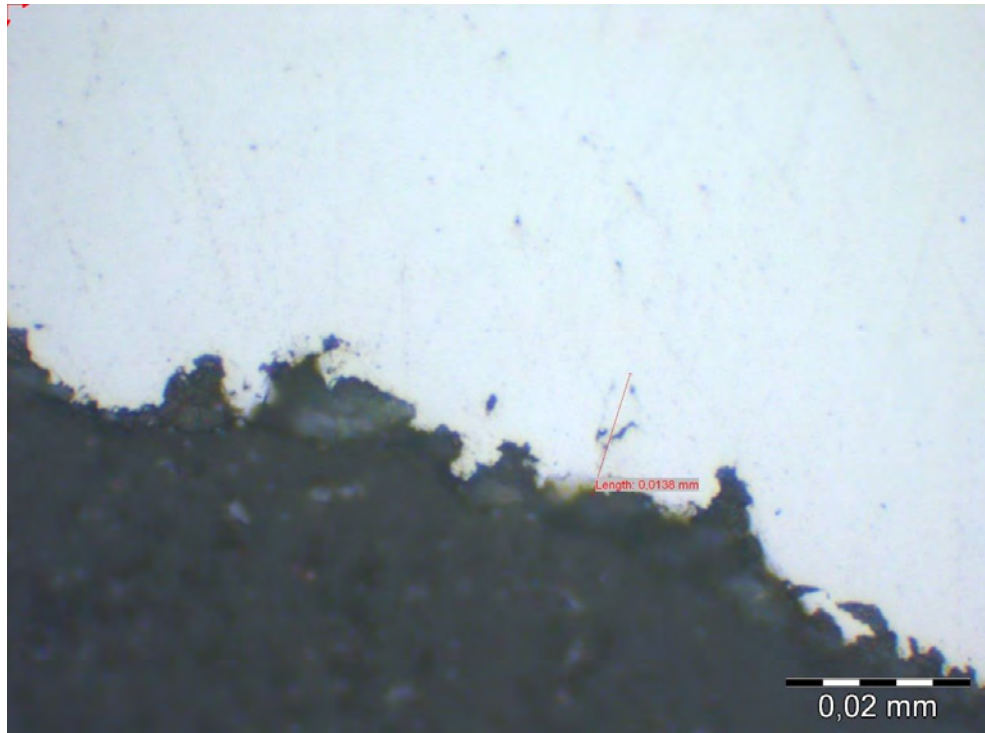


Figure C.28 Cut one in crack at segment A, fourth ridge on barrel no. 14389

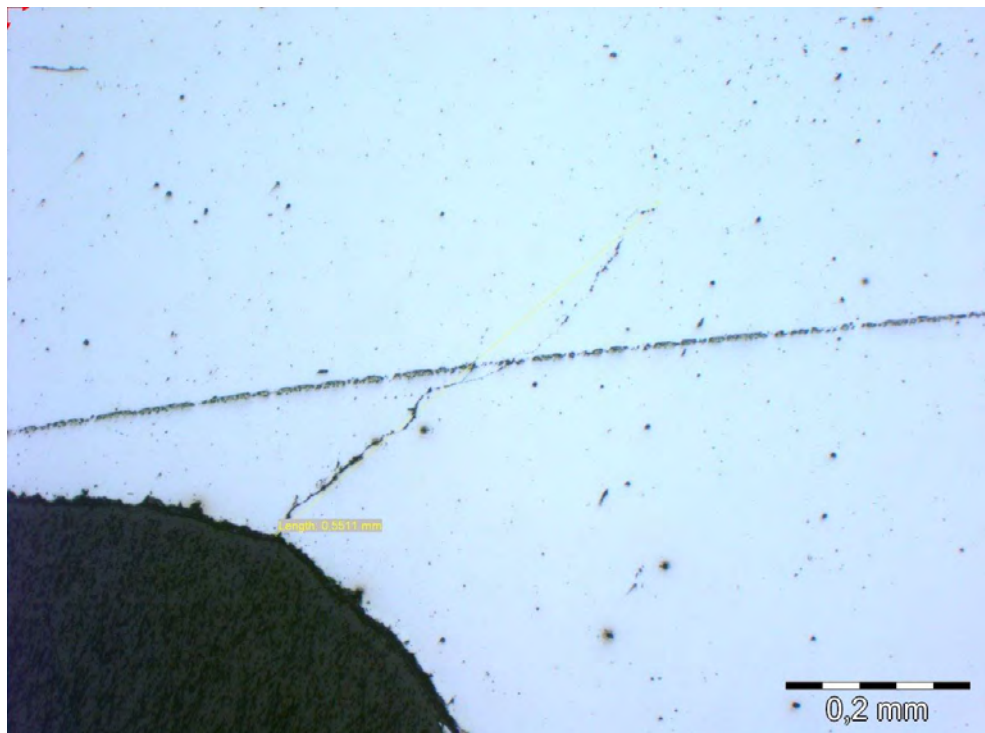


Figure C.29 Cut two in crack at segment A, first ridge on barrel no. 14389

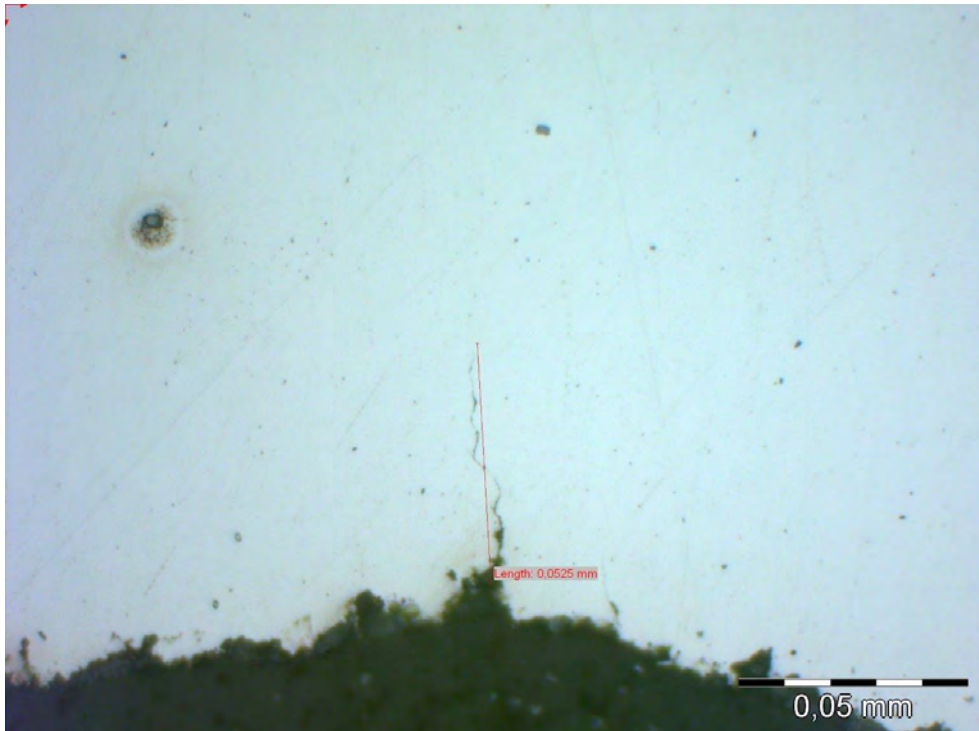


Figure C.30 Cut two in crack at segment A, second ridge on barrel no. 14389

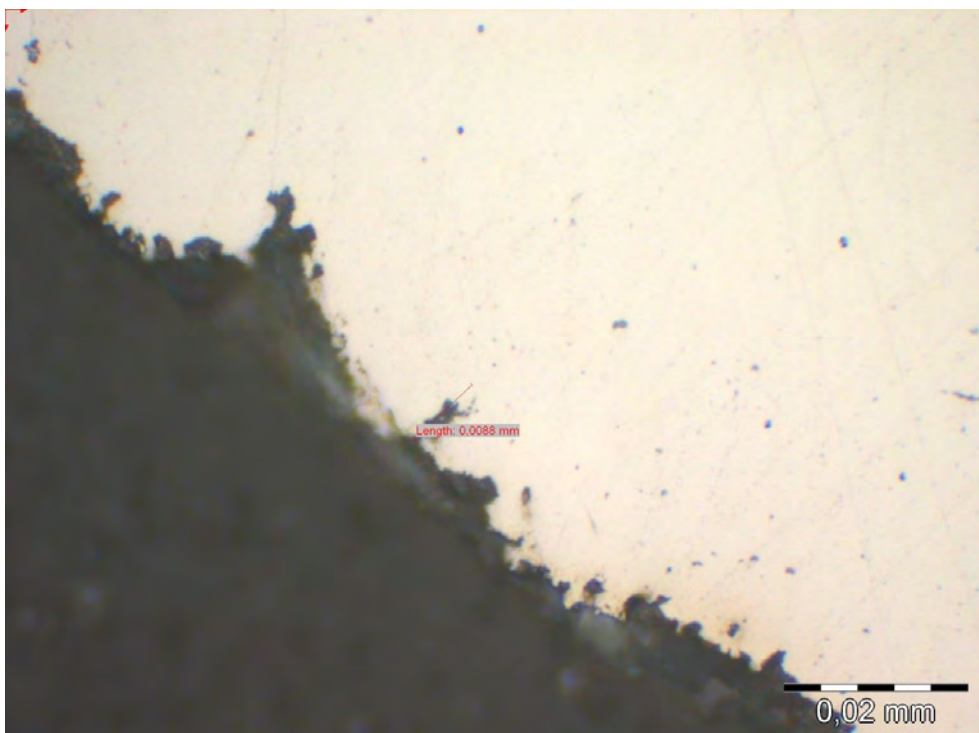


Figure C.31 Cut two in crack at segment A, third ridge on barrel no. 14389

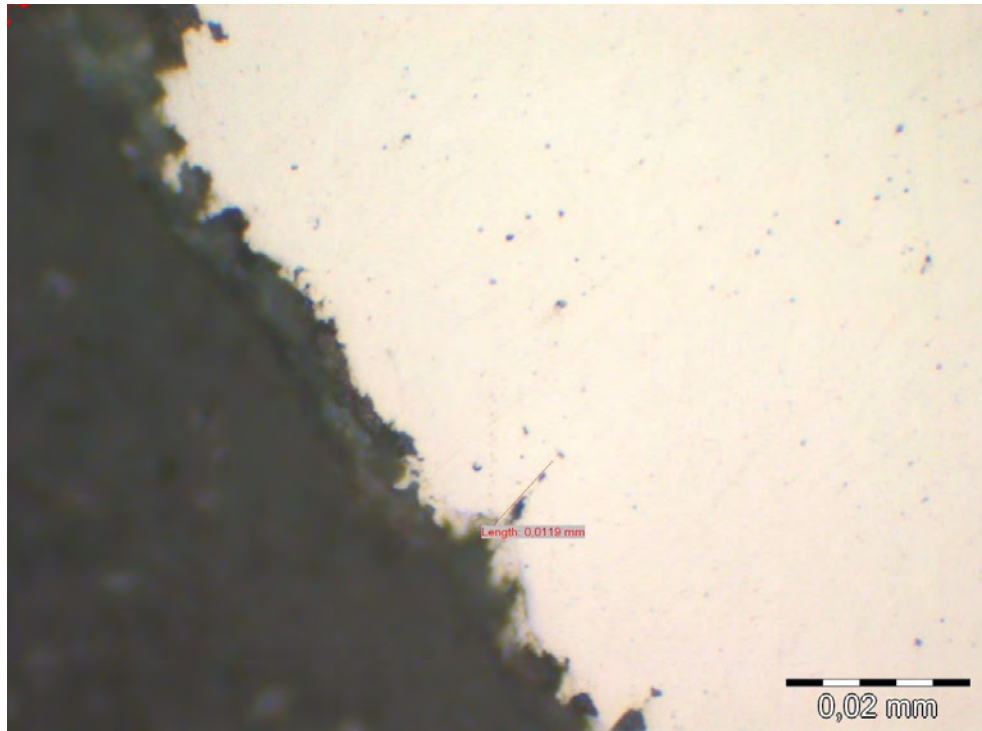


Figure C.32 Cut two in crack at segment A, fourth ridge on barrel no. 14389

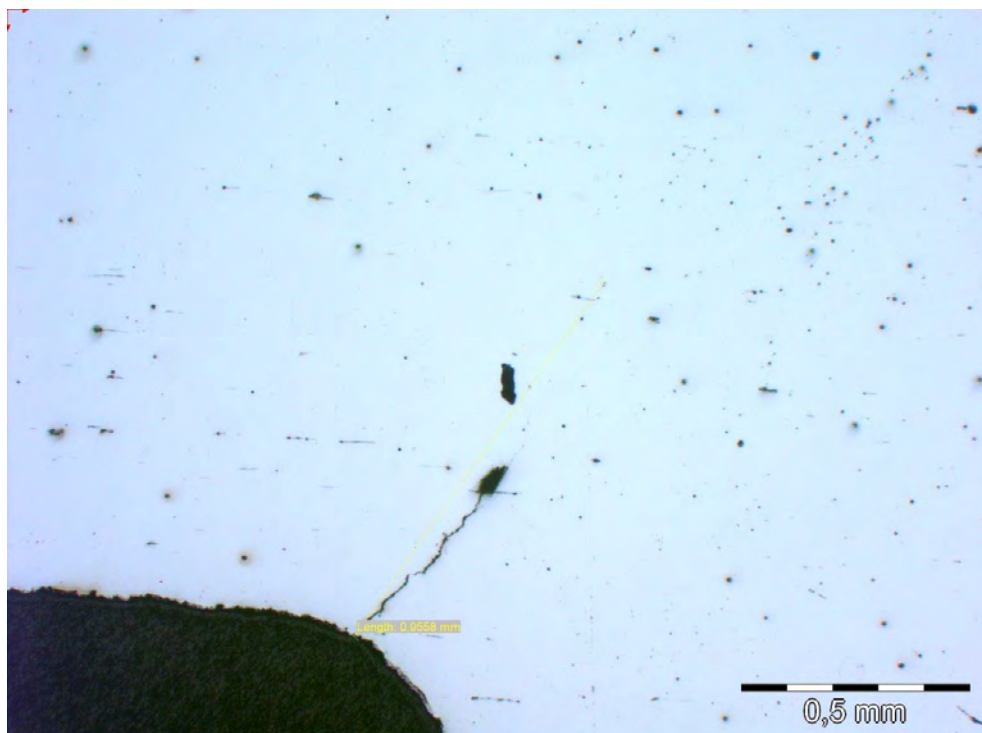


Figure C.33 Cut three in crack at segment A, first ridge on barrel no. 14389

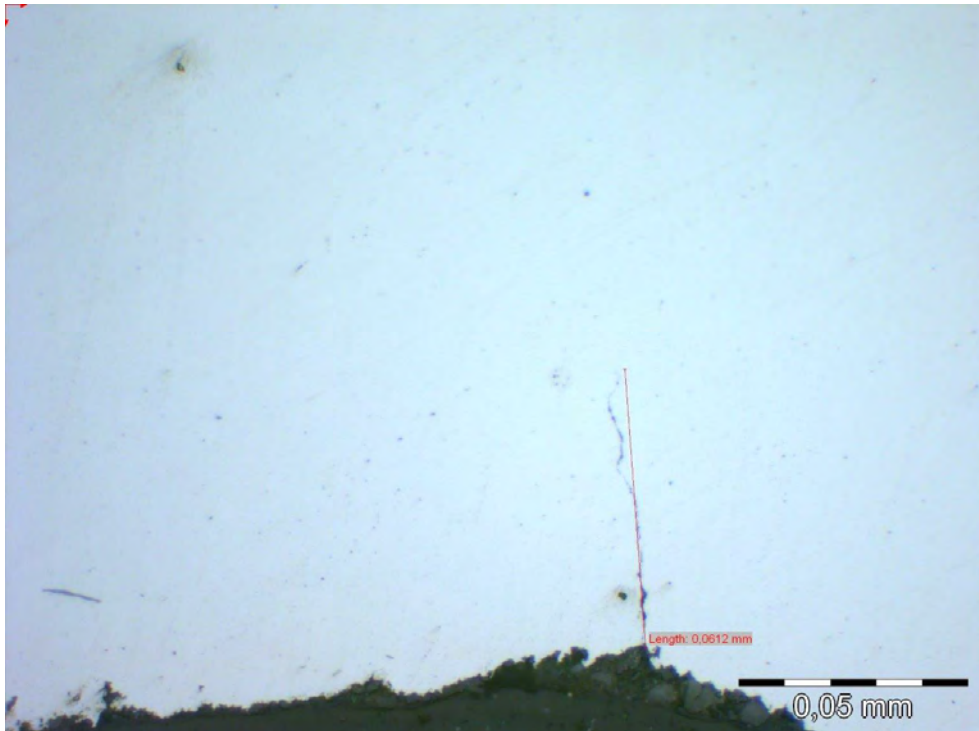


Figure C.34 Cut three in crack at segment A, second ridge on barrel no. 14389

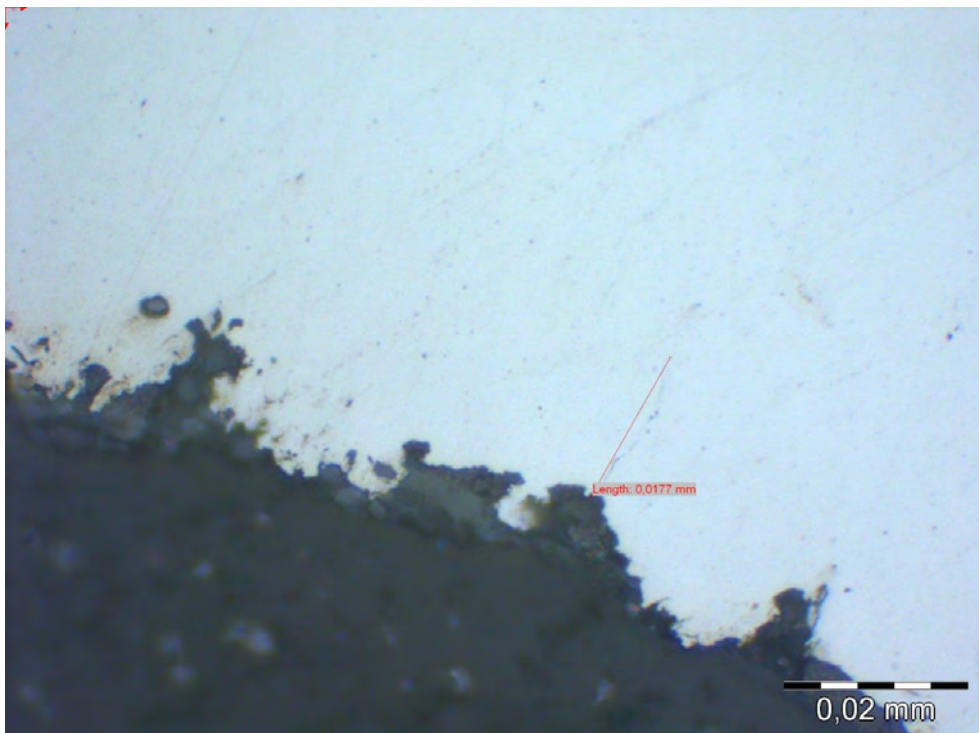


Figure C.35 Cut three in crack at segment A, third ridge on barrel no. 14389

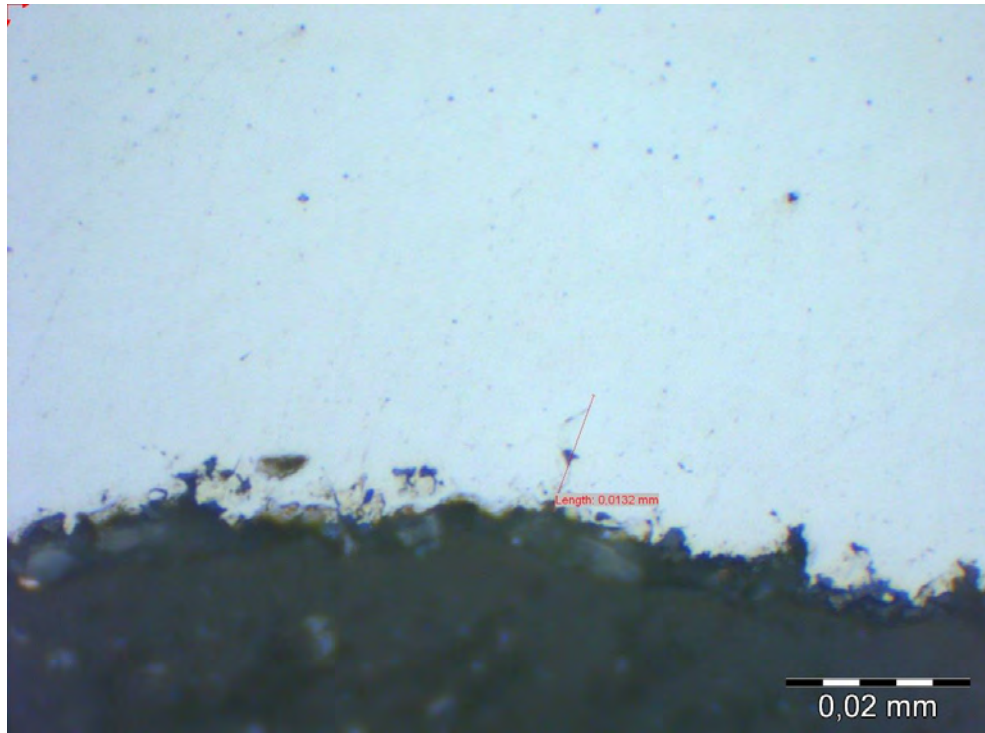


Figure C.36 Cut three in crack at segment A, fourth ridge on barrel no. 14389

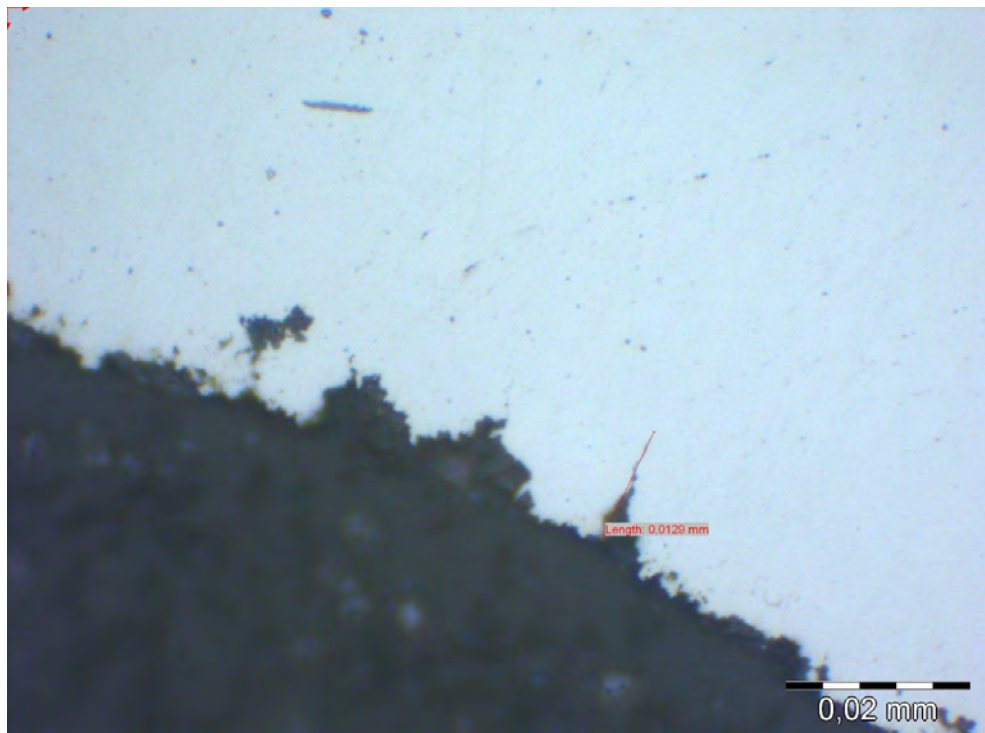


Figure C.37 Cut three in crack at segment A, fifth ridge on barrel no. 14389

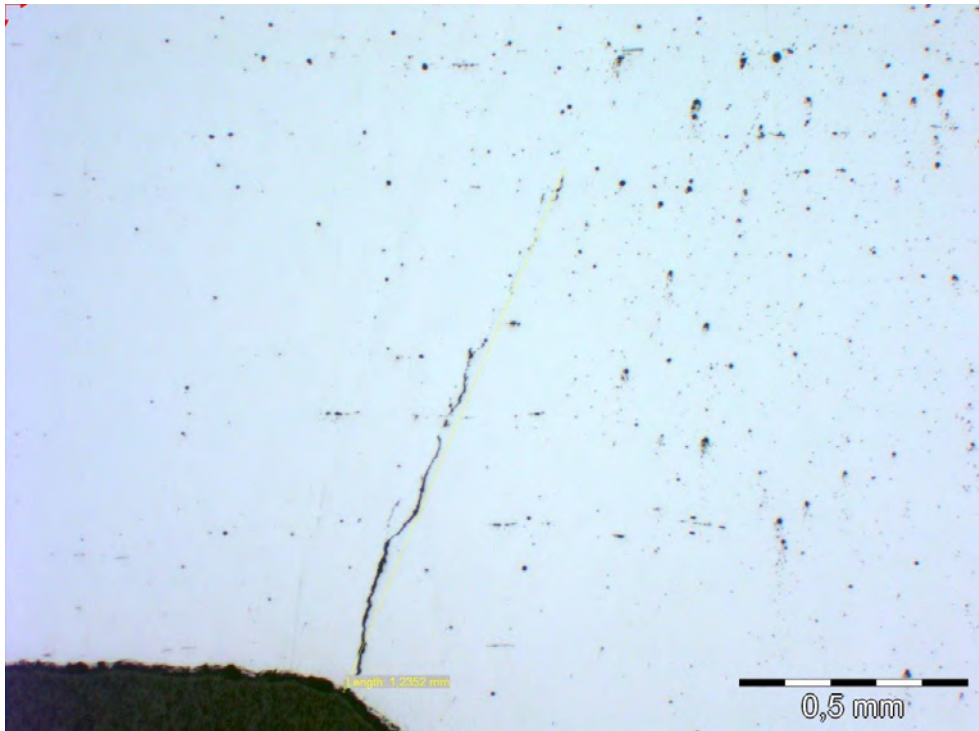


Figure C.38 Cut four in crack at segment A, first ridge on barrel no. 14389

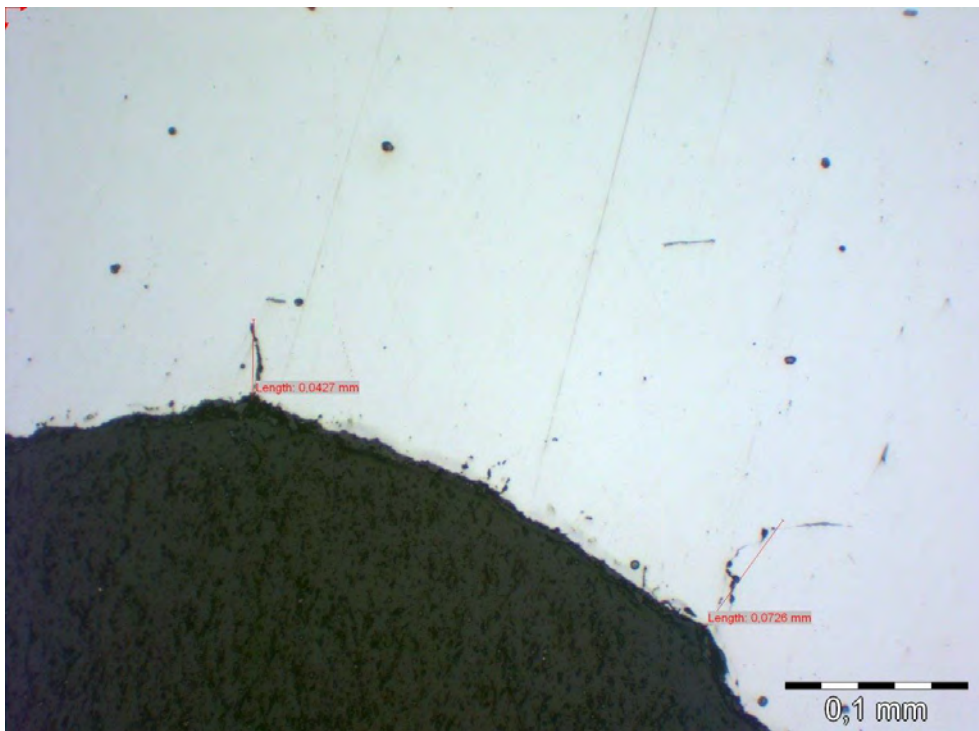


Figure C.39 Cut four in crack at segment A, second ridge on barrel no. 14389

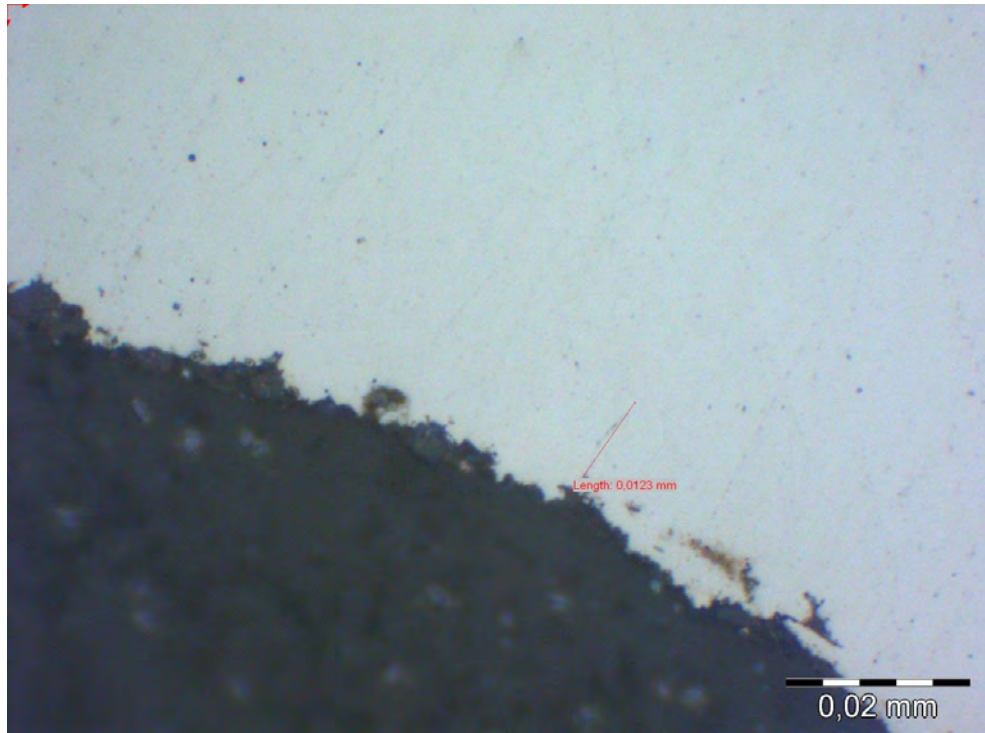


Figure C.40 Cut four in crack at segment A, fifth ridge on barrel no. 14389

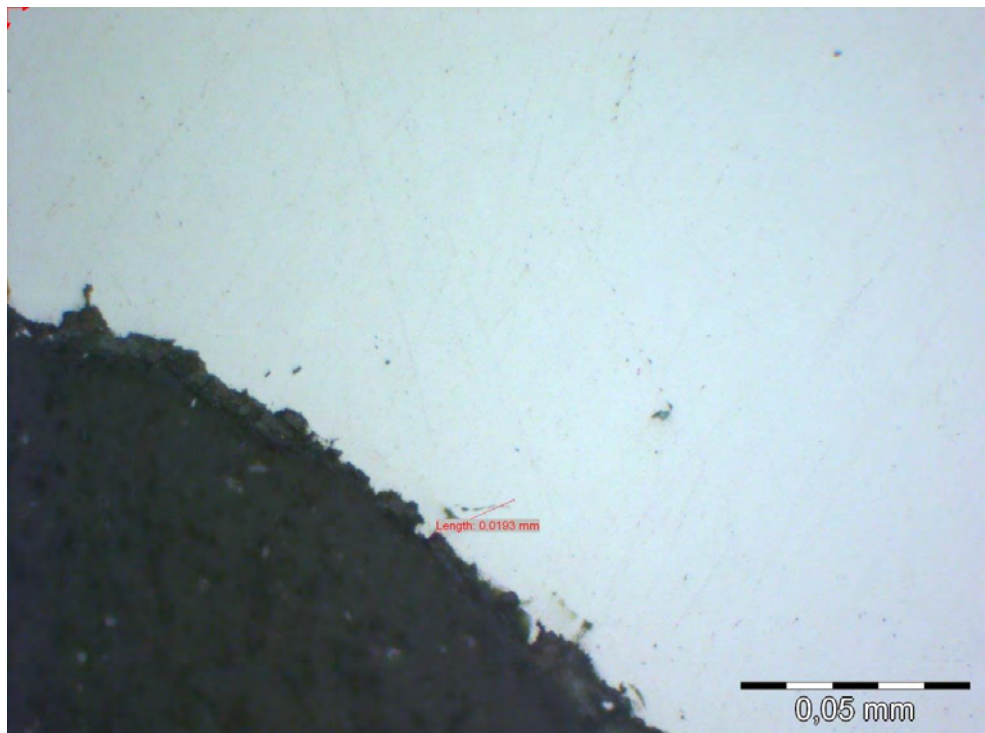


Figure C.41 Cut four in crack at segment A, fourth ridge on barrel no. 14389

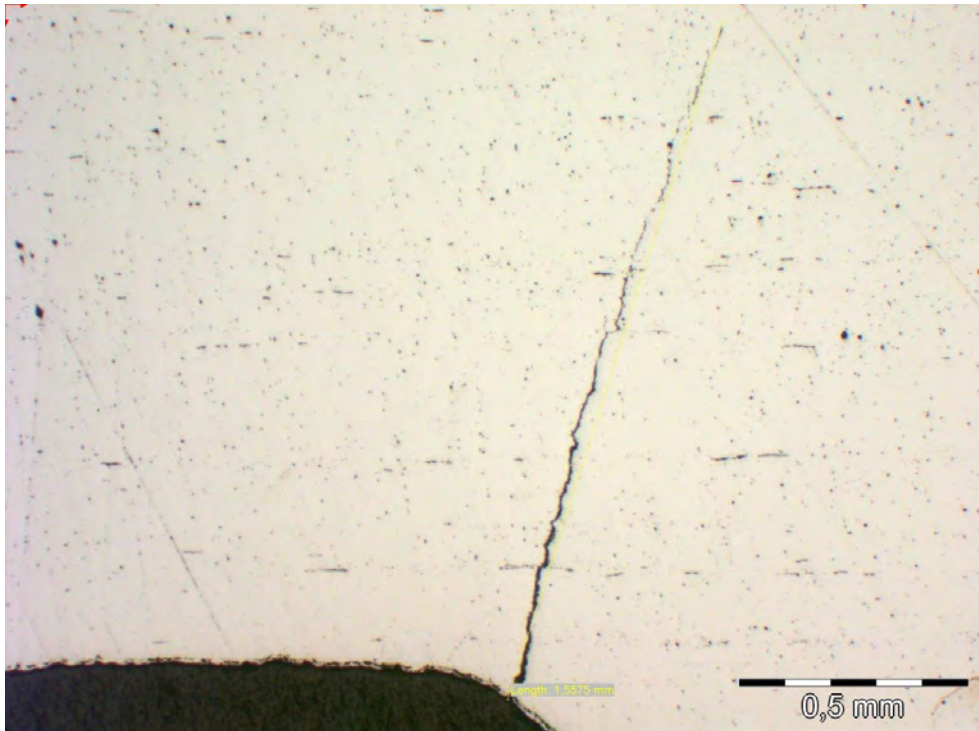


Figure C.42 Cut five in crack at segment A, first ridge on barrel no. 14389

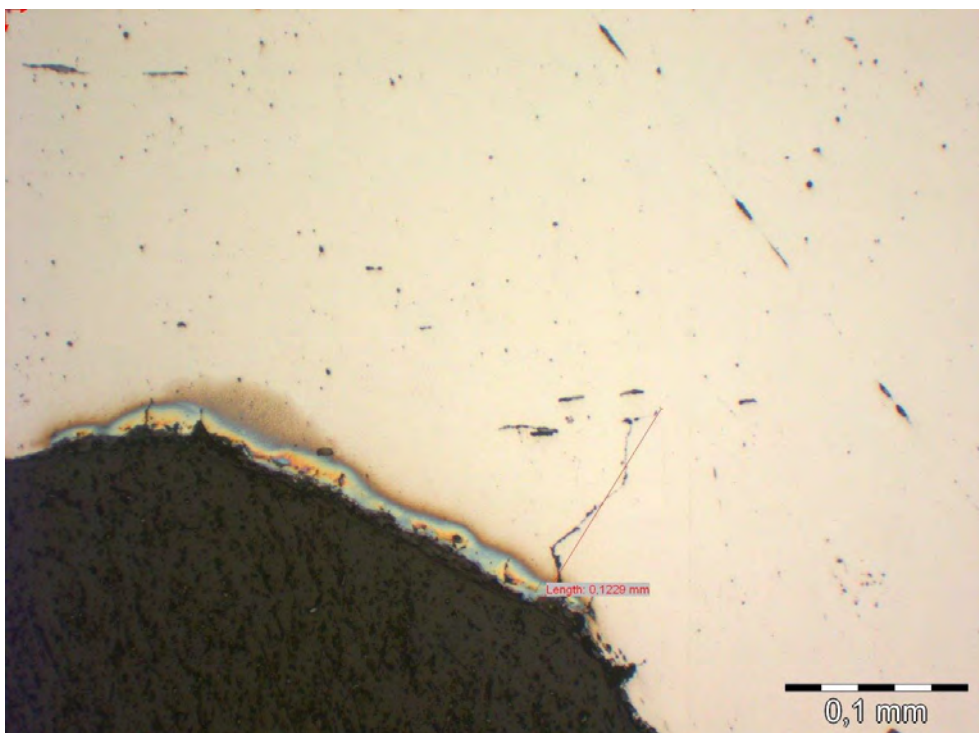


Figure C.43 Cut five in crack at segment A, second ridge on barrel no. 14389

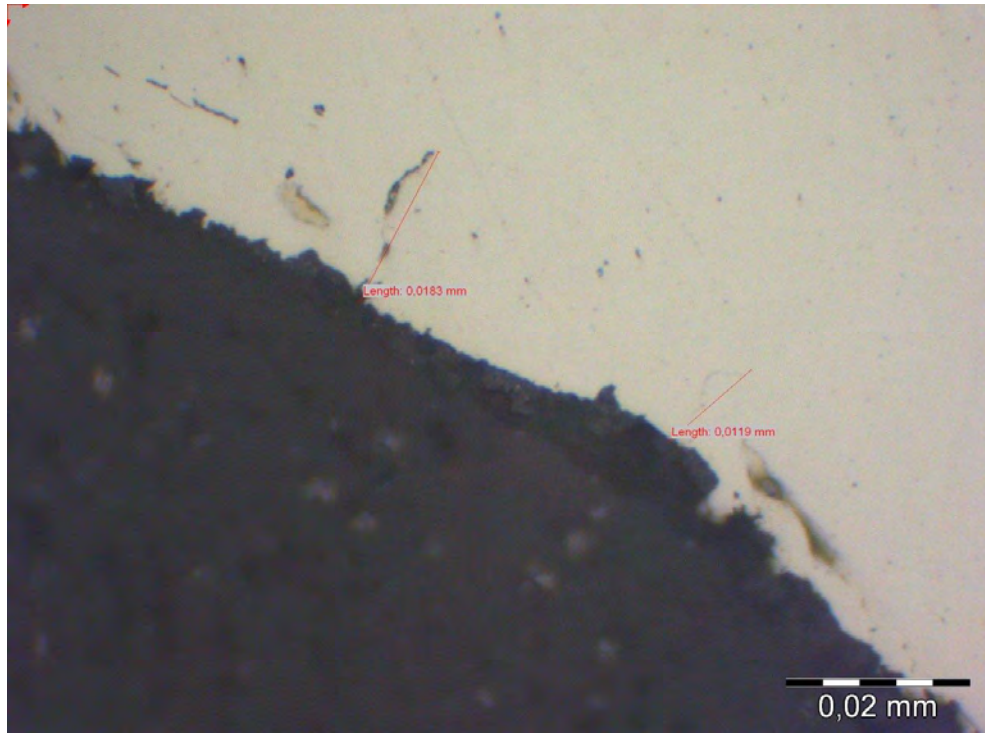


Figure C.44 Cut five in crack at segment A, third ridge on barrel no. 14389

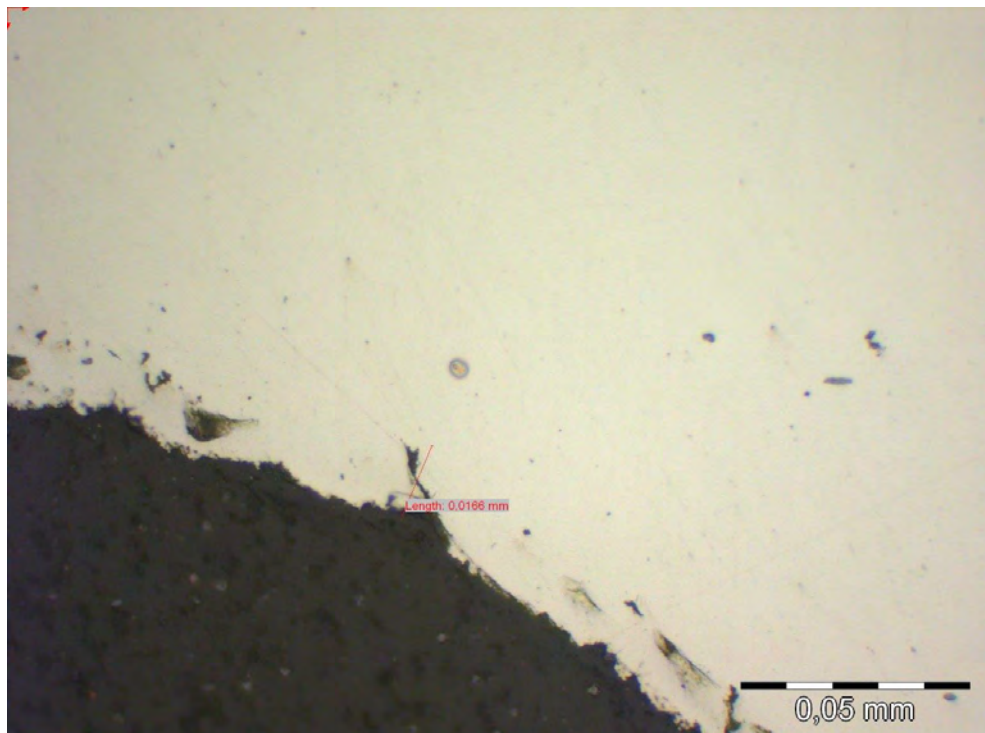


Figure C.45 Cut five in crack at segment A, fifth ridge on barrel no. 14389

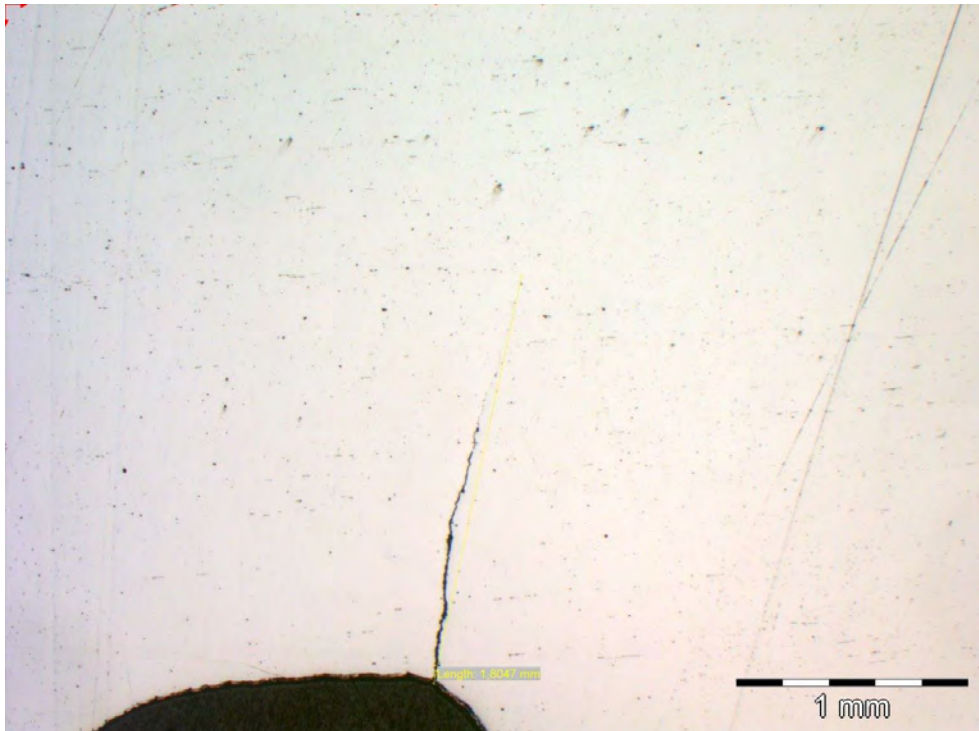


Figure C.46 Cut six in crack at segment A, first ridge on barrel no. 14389

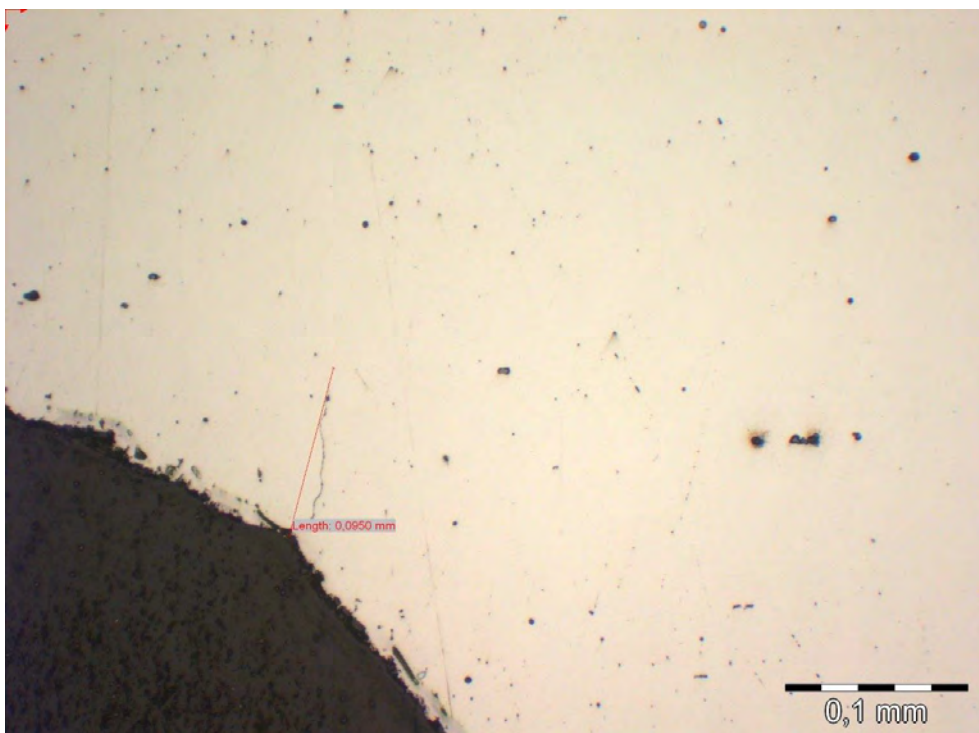


Figure C.47 Cut six in crack at segment A, second ridge on barrel no. 14389

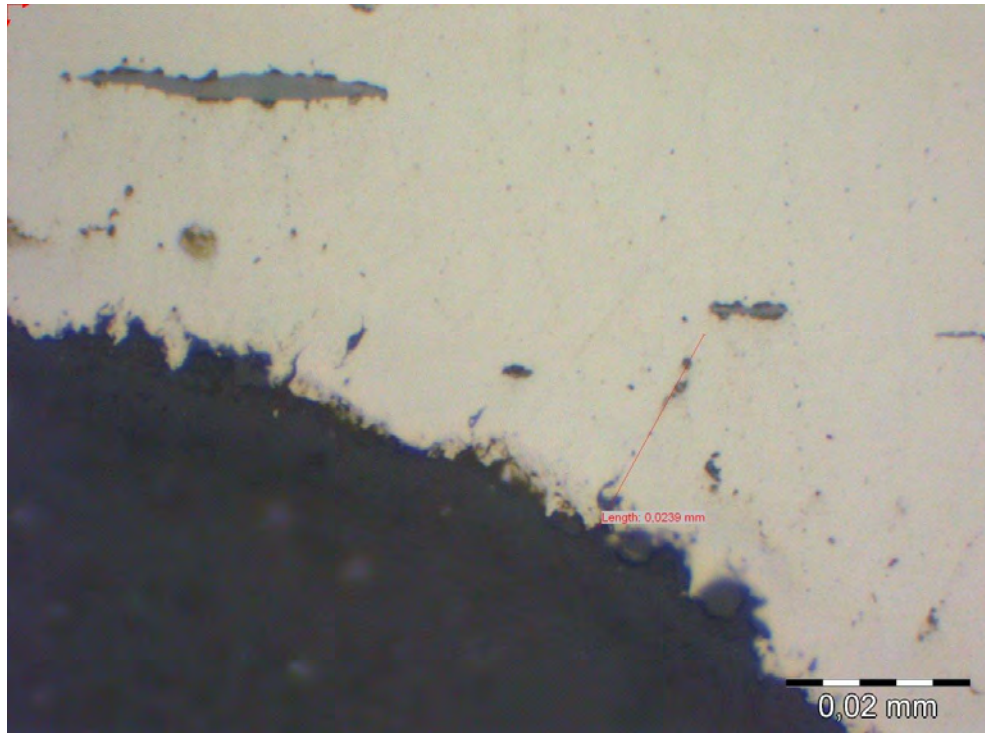


Figure C.48 Cut six in crack at segment A, fourth ridge on barrel no. 14389

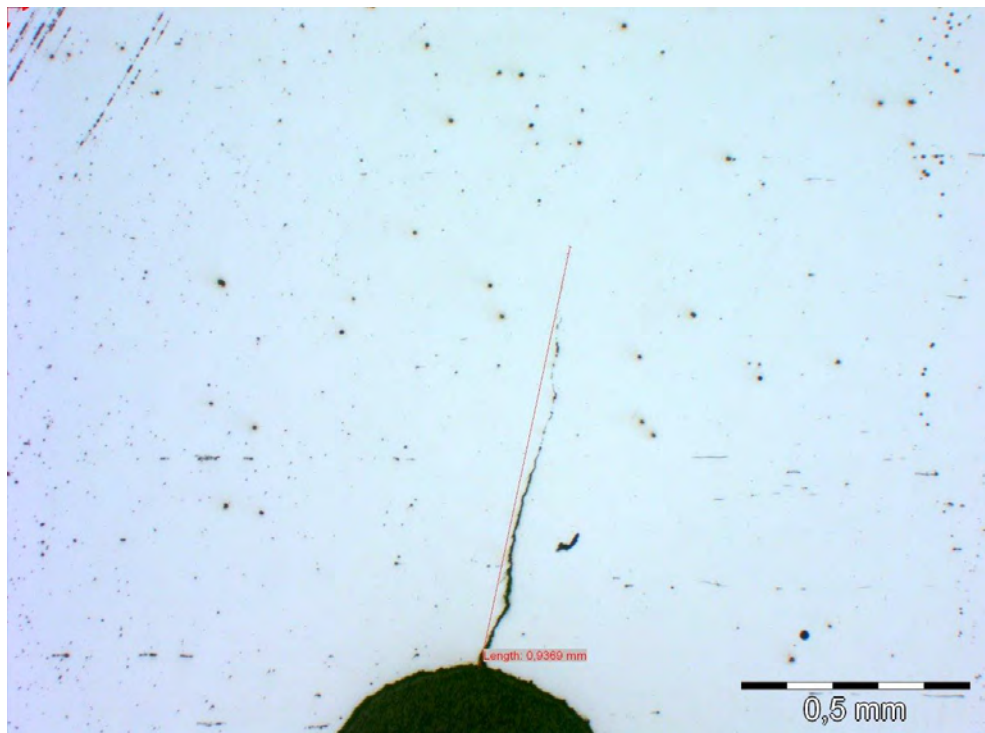


Figure C.49 Cut one in crack at segment C, second ridge on barrel no. 14389

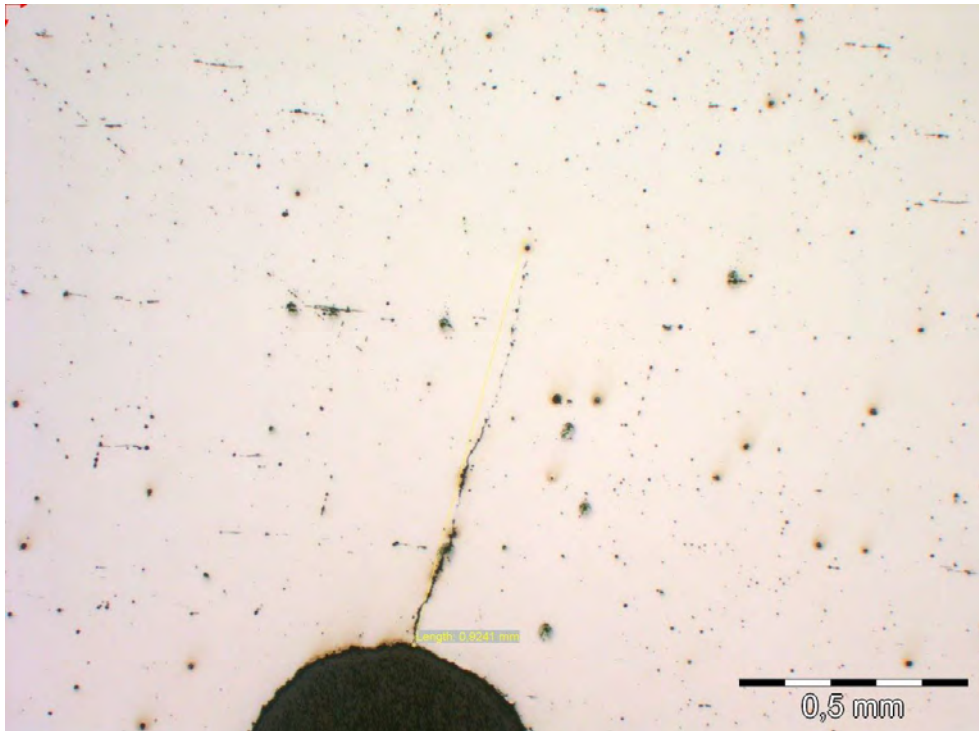


Figure C.50 Cut two in crack at segment C, second ridge on barrel no. 14389

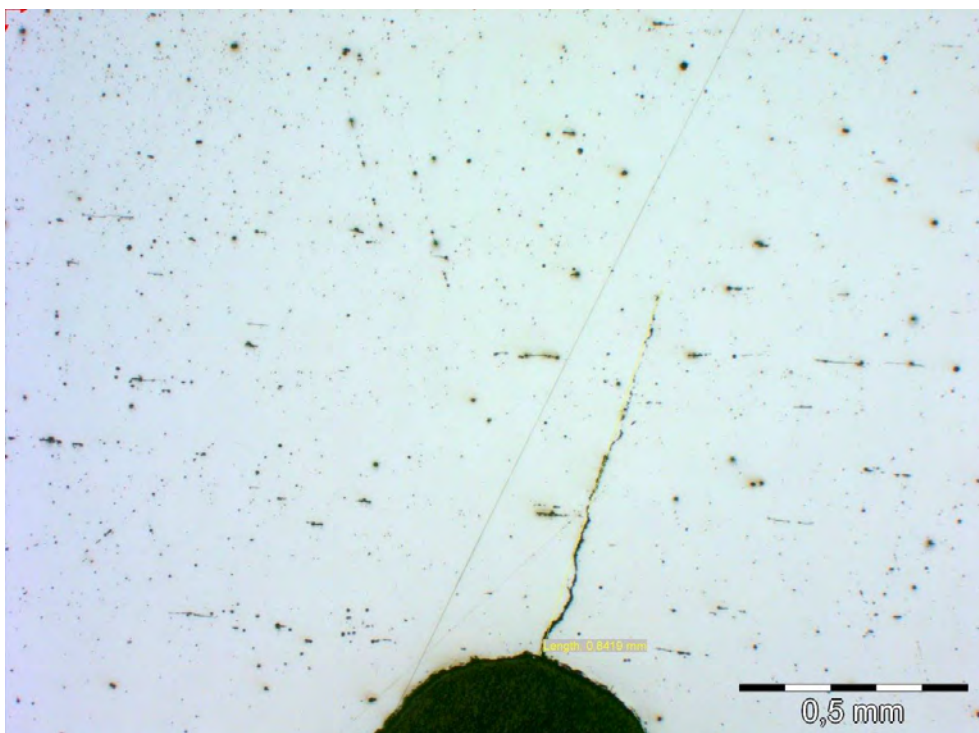


Figure C.51 Cut three in crack at segment C, second ridge on barrel no. 14389

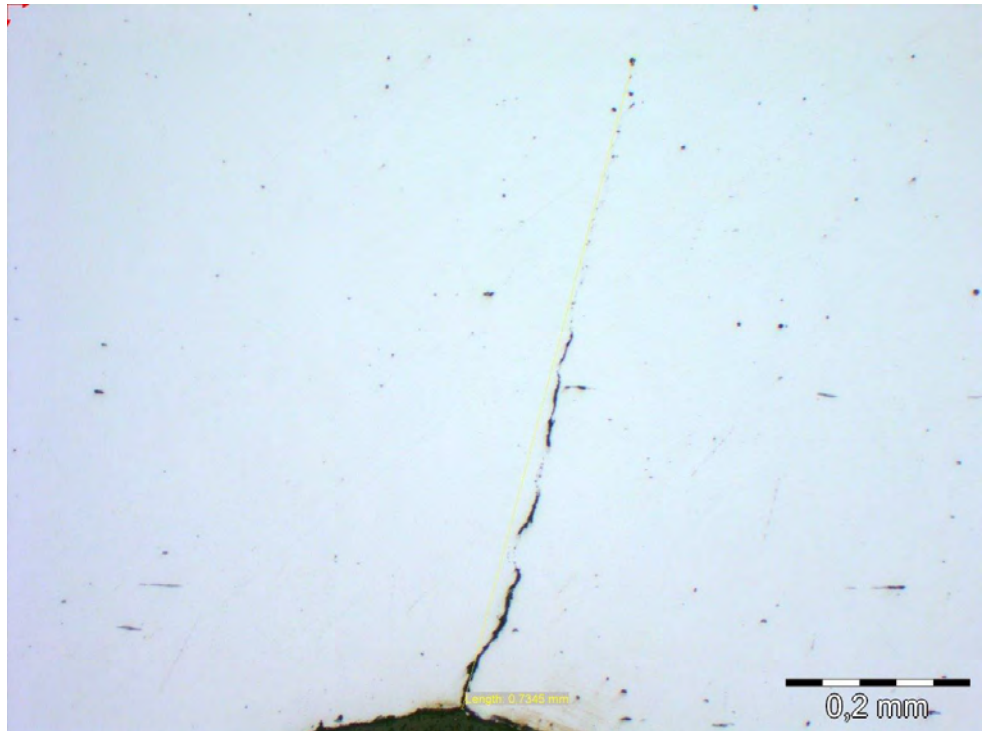


Figure C.52 Cut four in crack at segment C, second ridge on barrel no. 14389

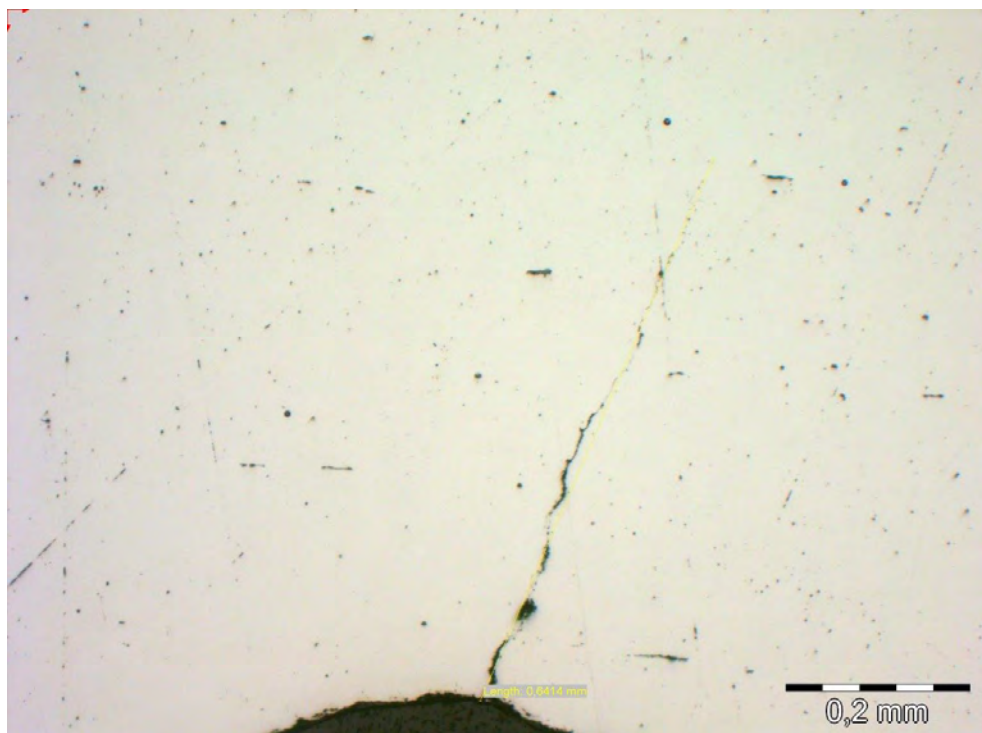


Figure C.53 Cut five in crack at segment C, second ridge on barrel no. 14389

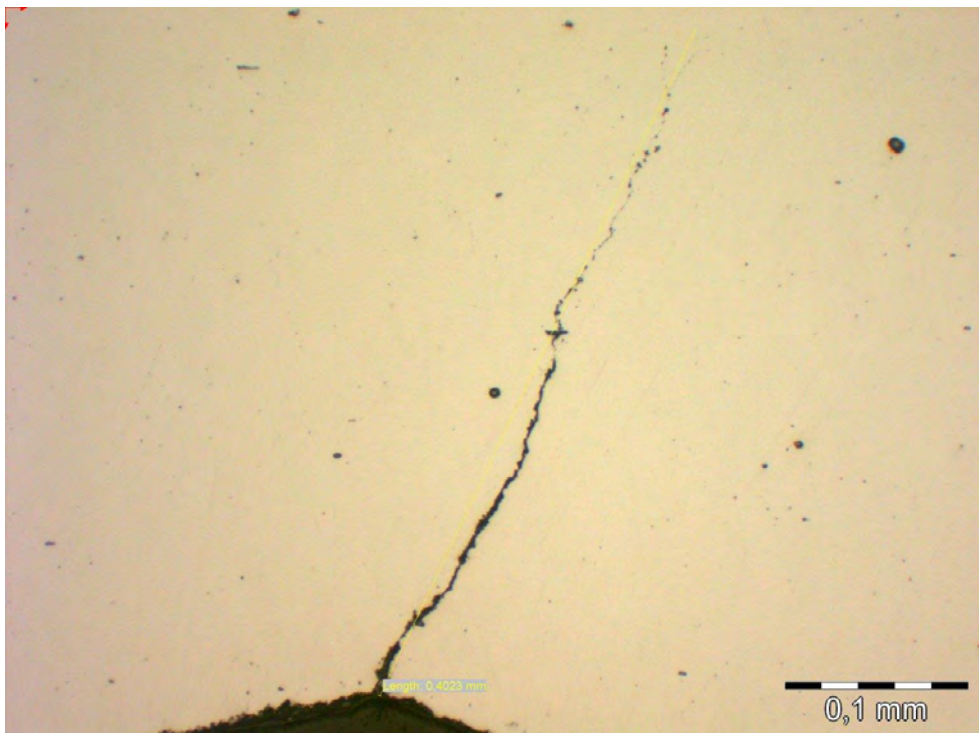


Figure C.54 Cut six in crack at segment C, second ridge on barrel no. 14389

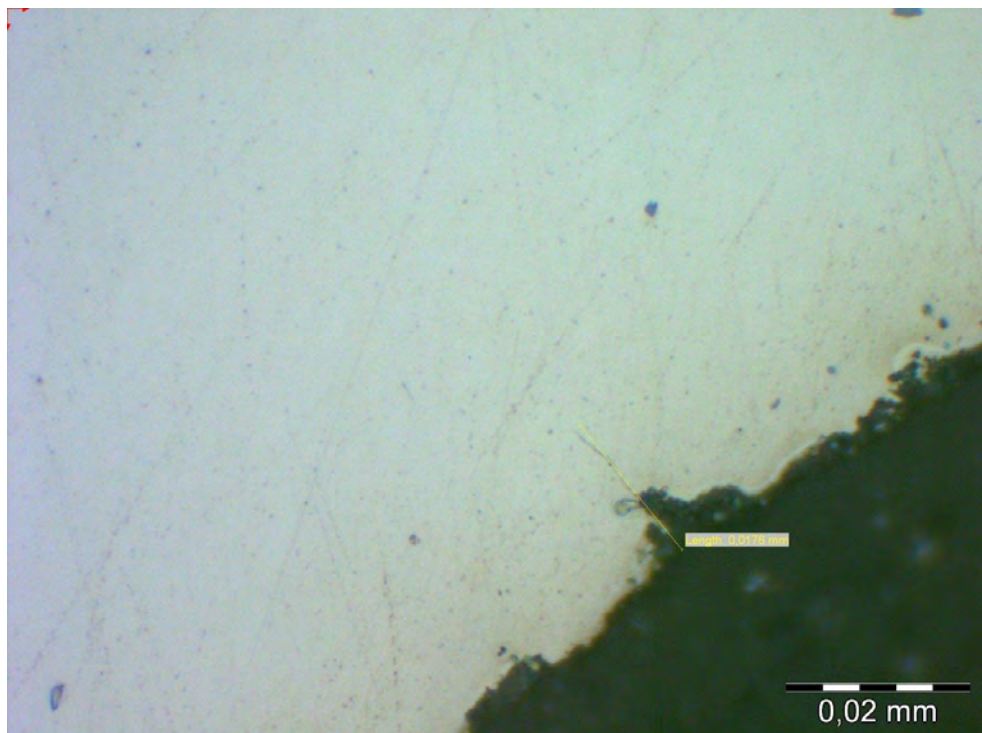


Figure C.55 Cut one in crack at segment C, third ridge on barrel no. 14389

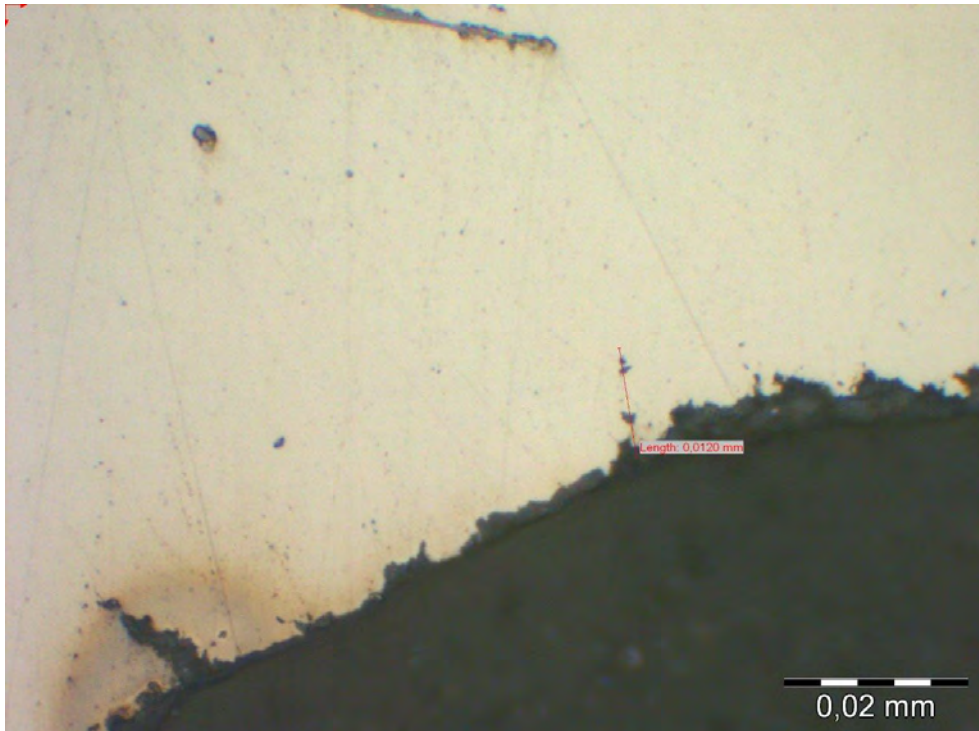


Figure C.56 Cut two in crack at segment C, third ridge on barrel no. 14389

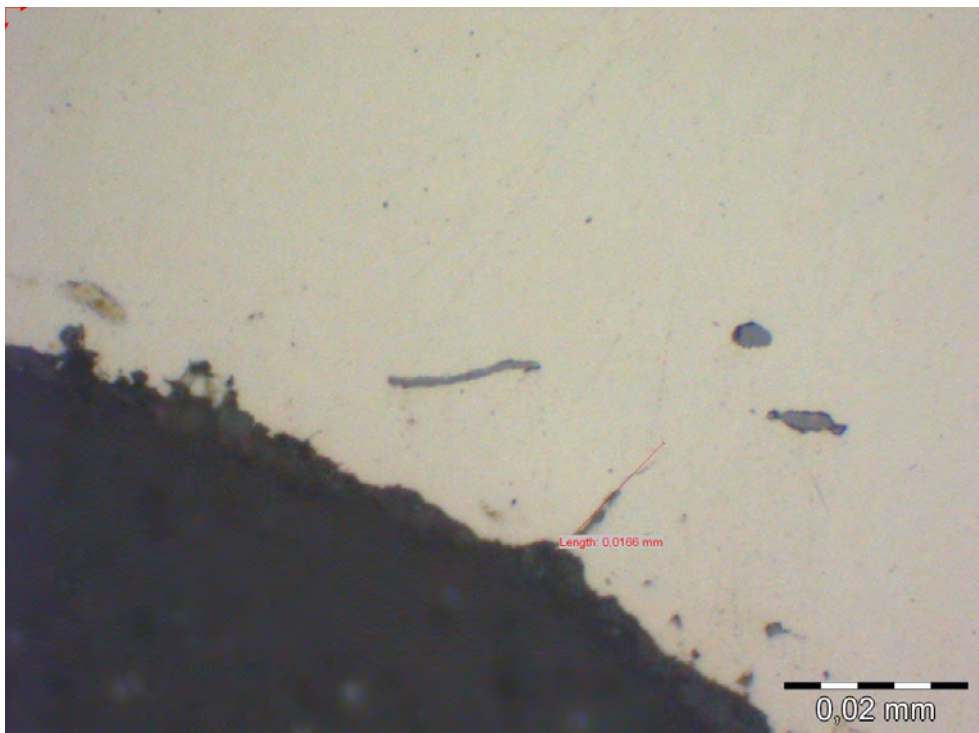


Figure C.57 Cut five in crack at segment C, third ridge on barrel no. 14389

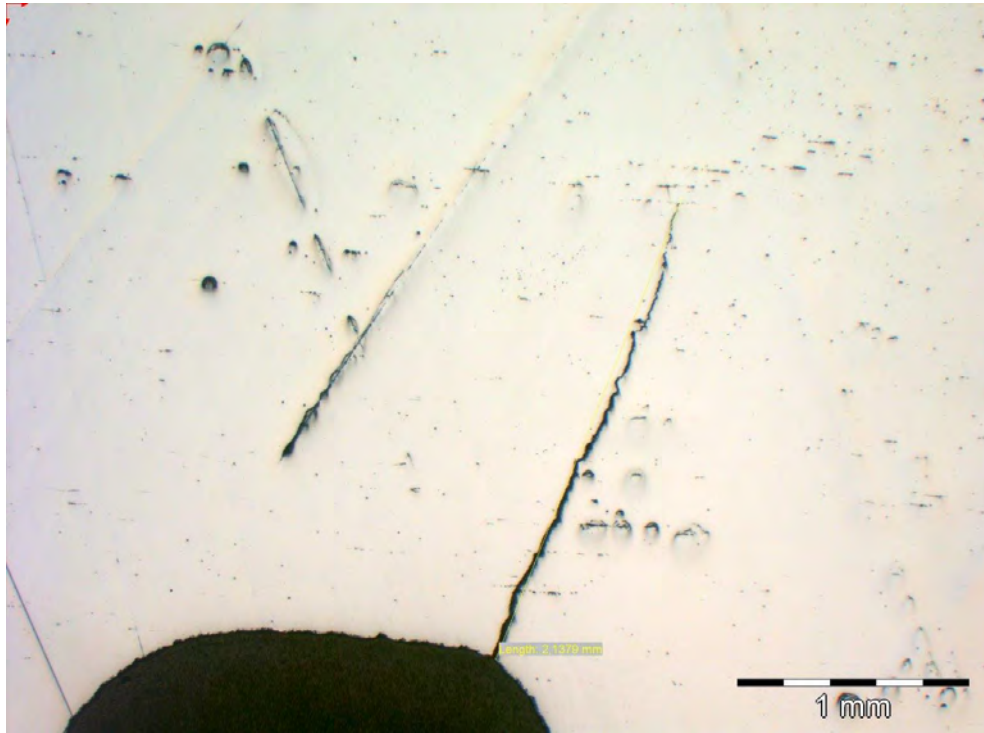


Figure C.58 Crack at segment A, first ridge on barrel no. 14389

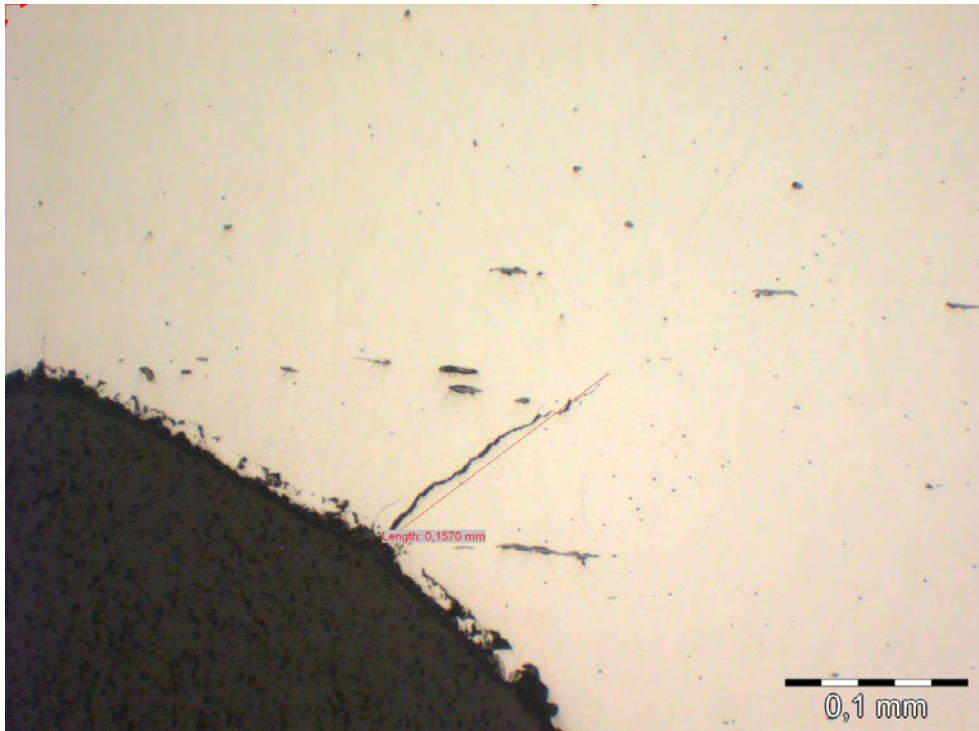


Figure C.59 Crack at segment A, second ridge on barrel no. 14389

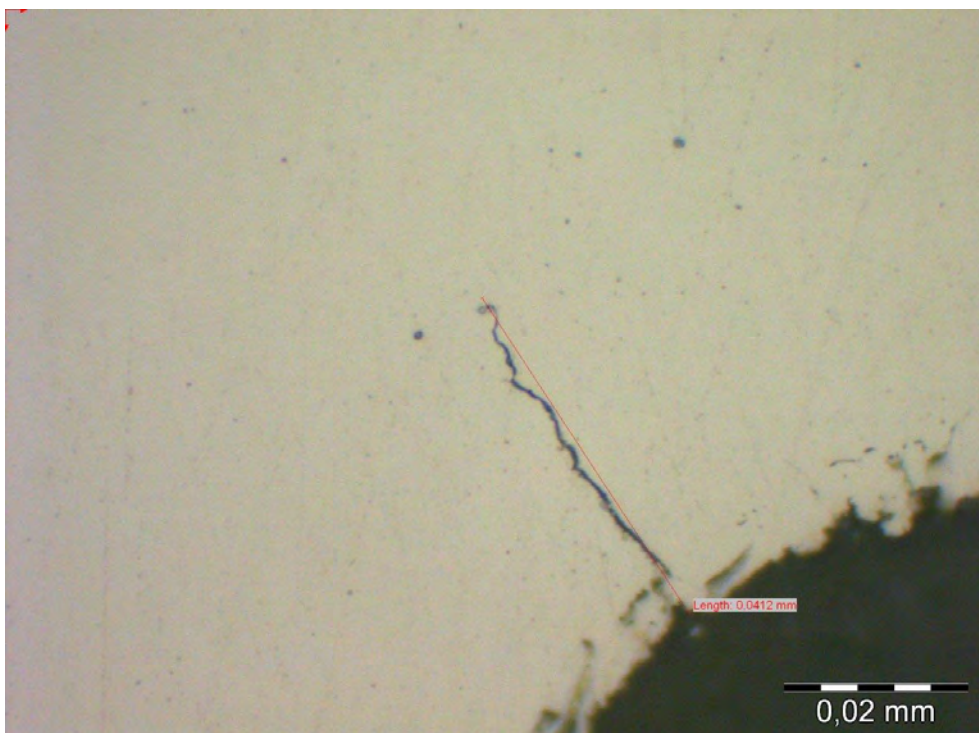


Figure C.60 Crack at segment A, second ridge on barrel no. 14389

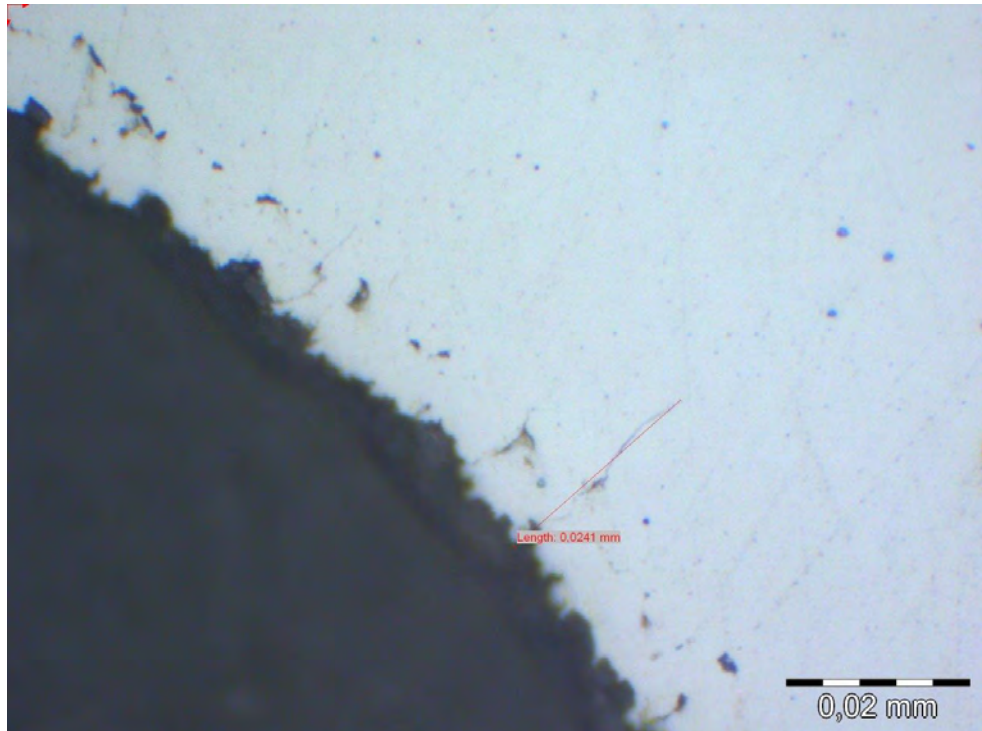


Figure C.61 Crack at segment A, third ridge on barrel no. 14389

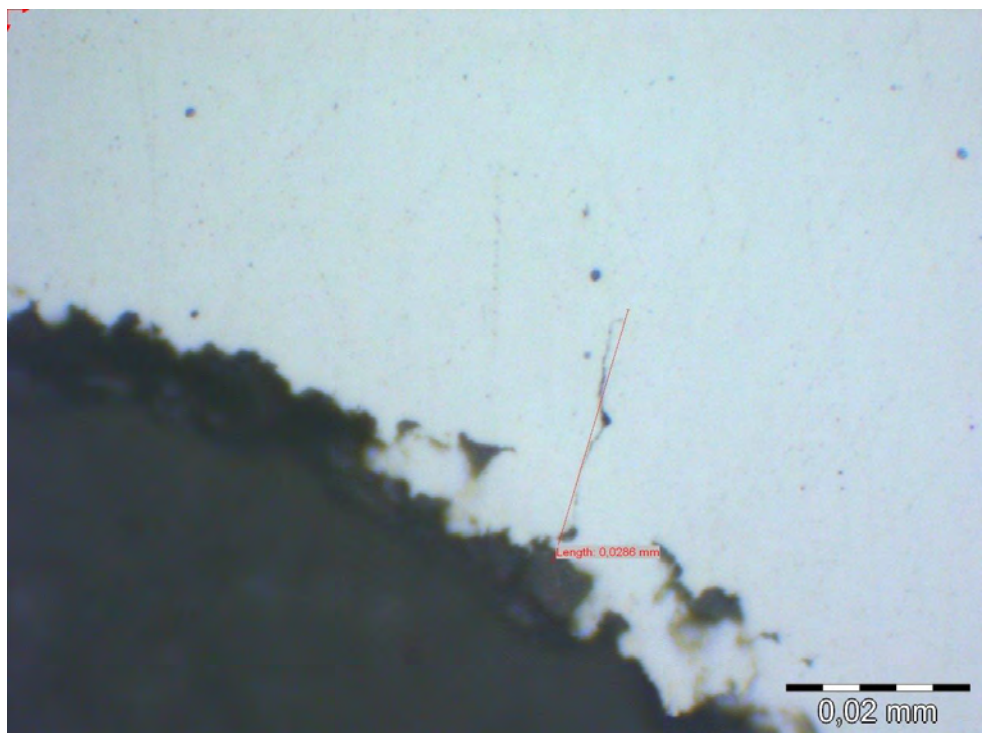


Figure C.62 Crack at segment A, fourth ridge on barrel no. 14389

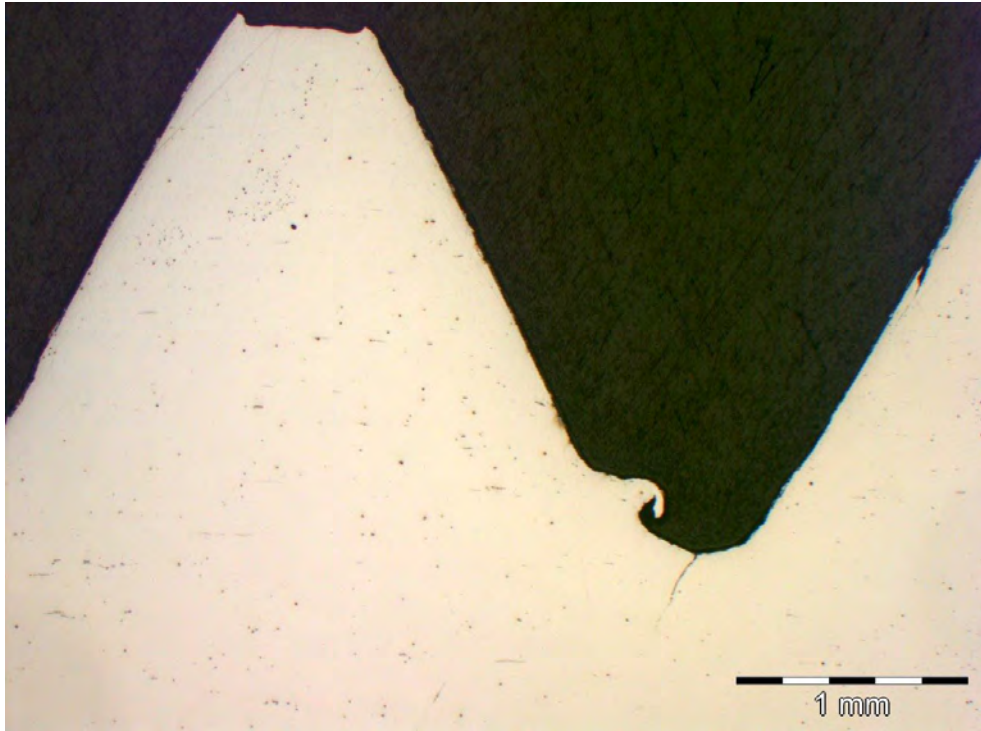


Figure C.63 Large view of cut six in crack at segment C, second ridge on barrel no. 14389

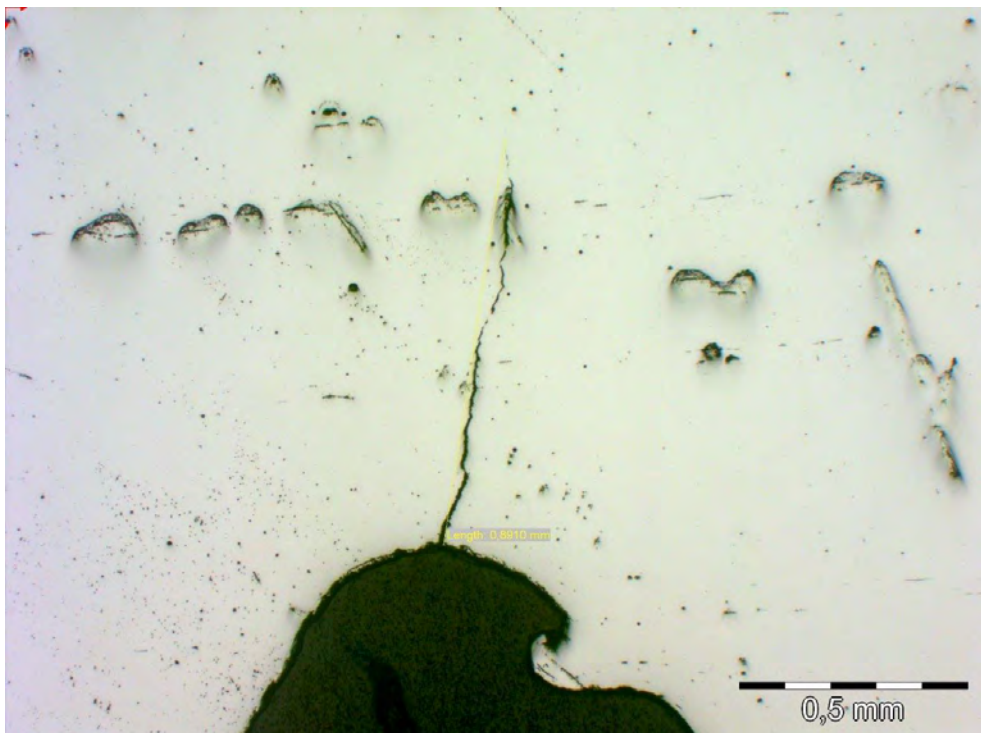


Figure C.64 Crack at segment C, second ridge on barrel no. 14389

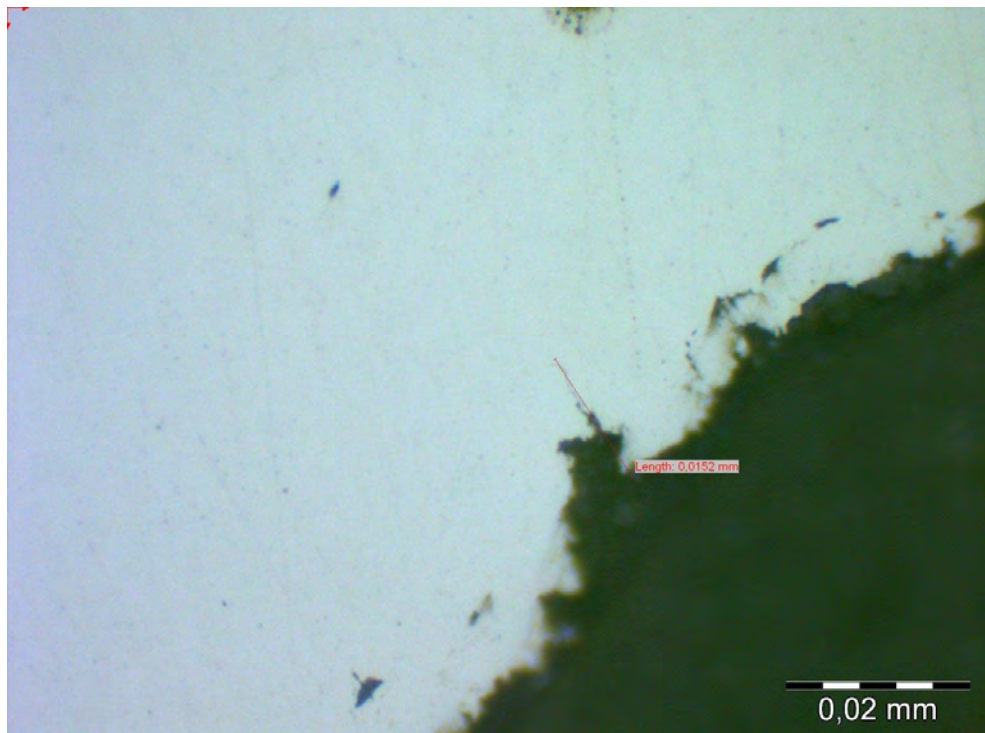


Figure C.65 Crack at segment C, third ridge on barrel no. 14389

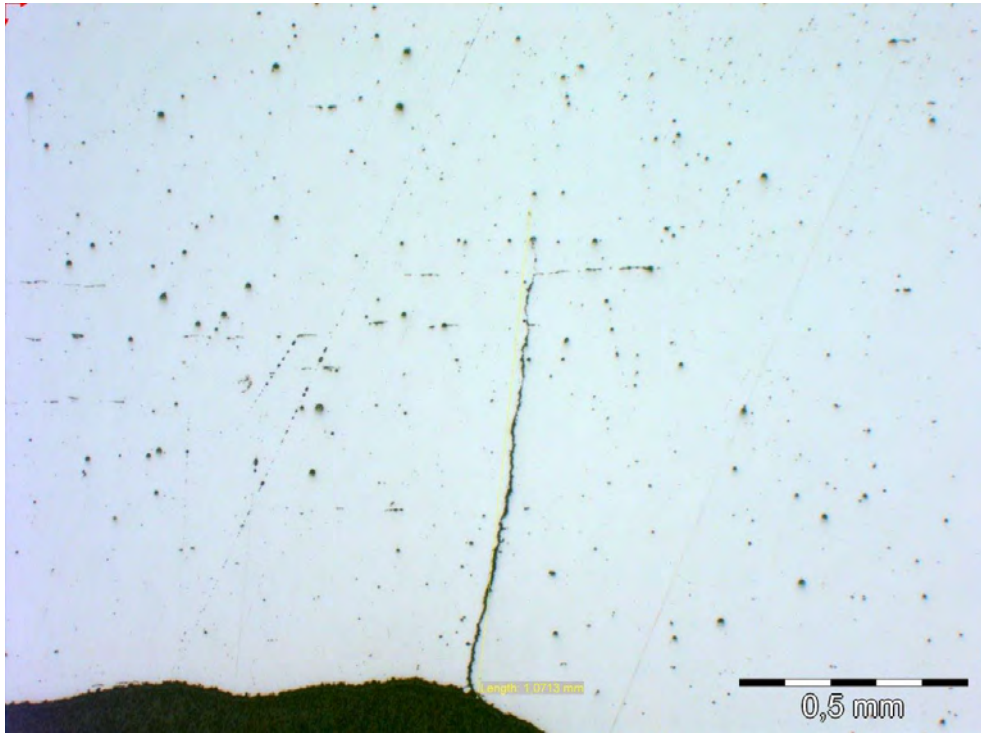


Figure C.66 Cut one in crack at segment A, first ridge on barrel no. SFK 0120-A

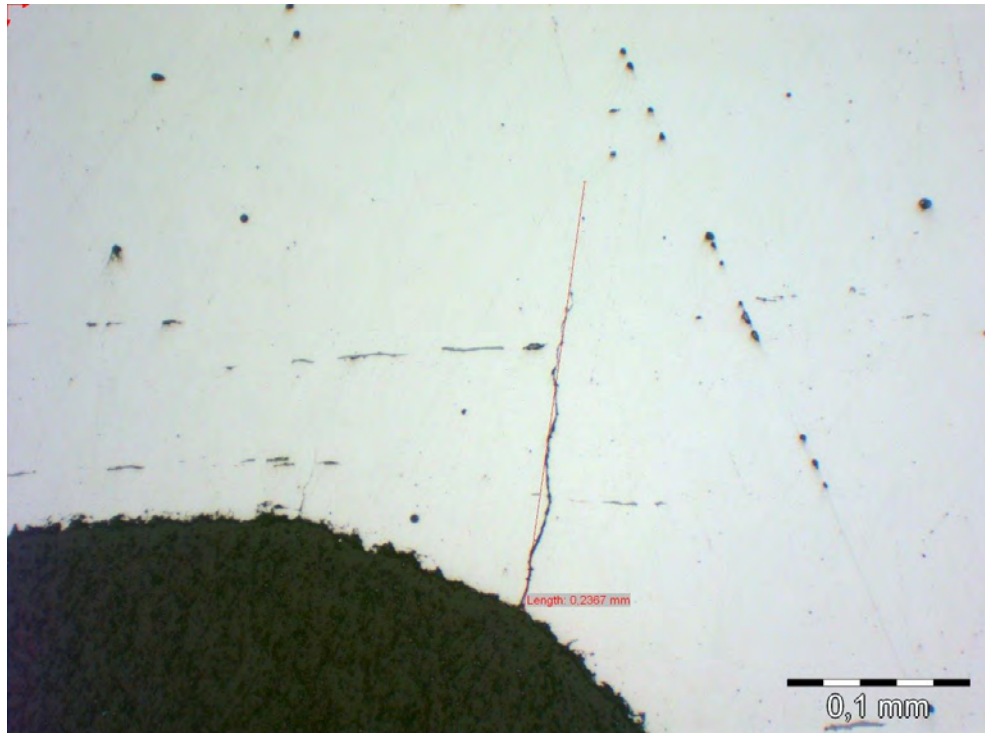


Figure C.67 Cut one in crack at segment A, second ridge on barrel no. SFK 0120-A

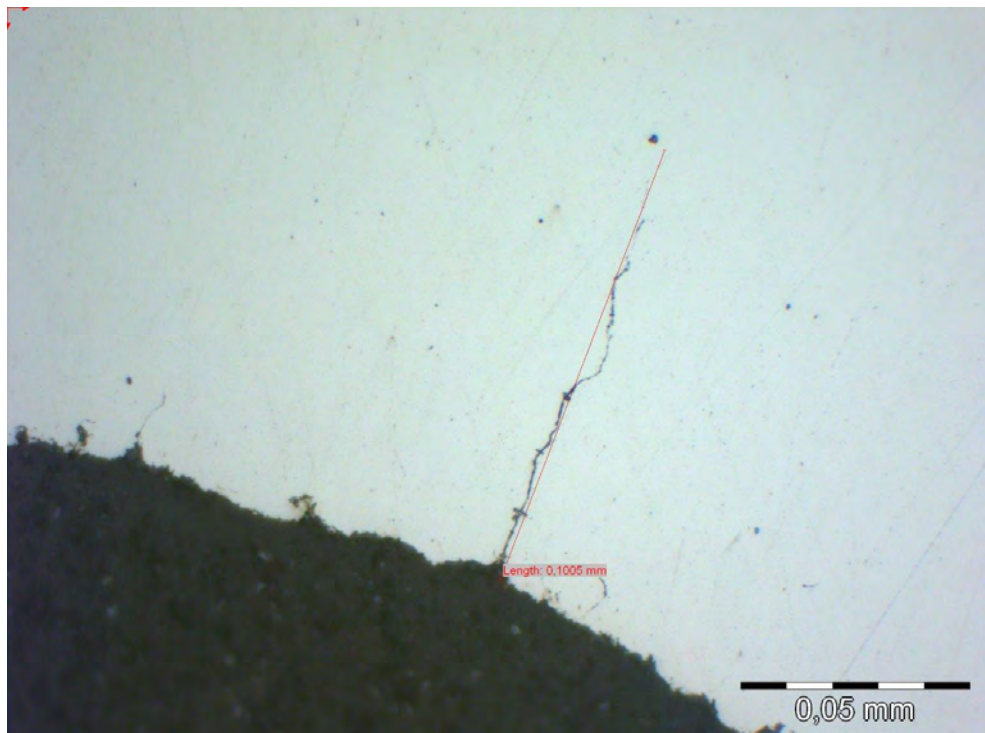


Figure C.68 Cut one in crack at segment A, third ridge on barrel no. SFK 0120-A

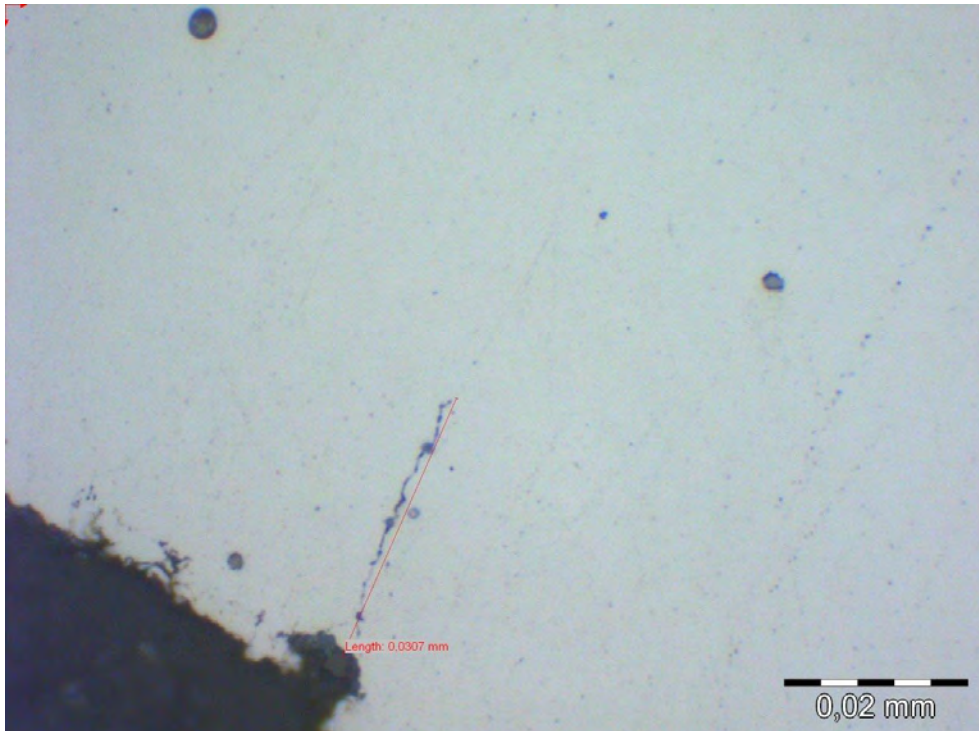


Figure C.69 Cut one in crack at segment A, fourth ridge on barrel no. SFK 0120-A

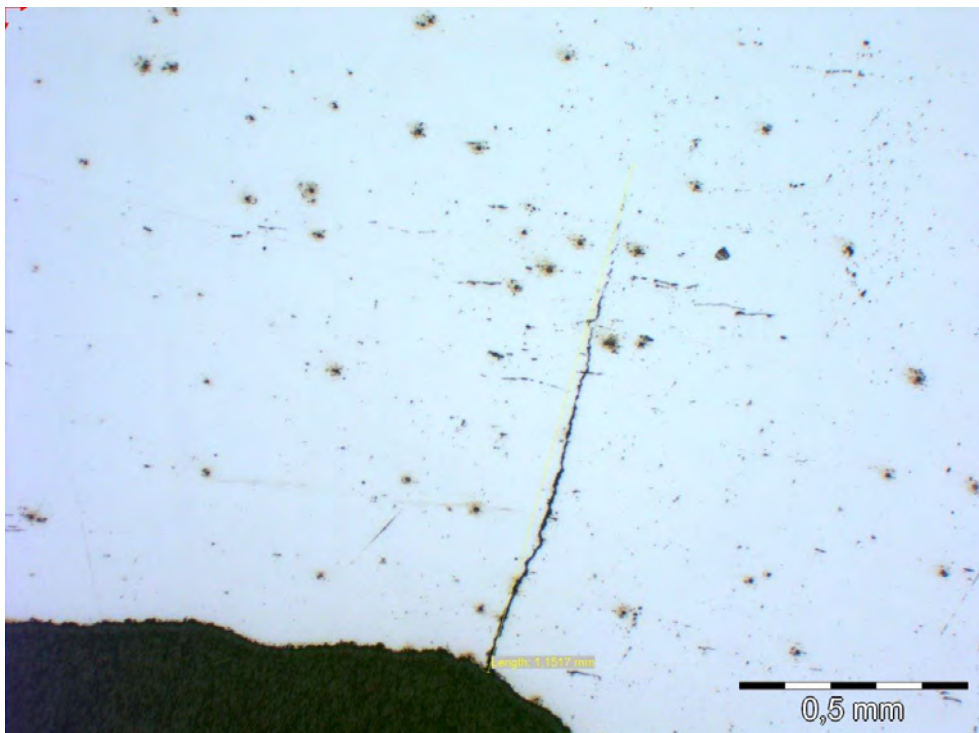


Figure C.70 Cut two in crack at segment B, first ridge on barrel no. SFK 0120-A

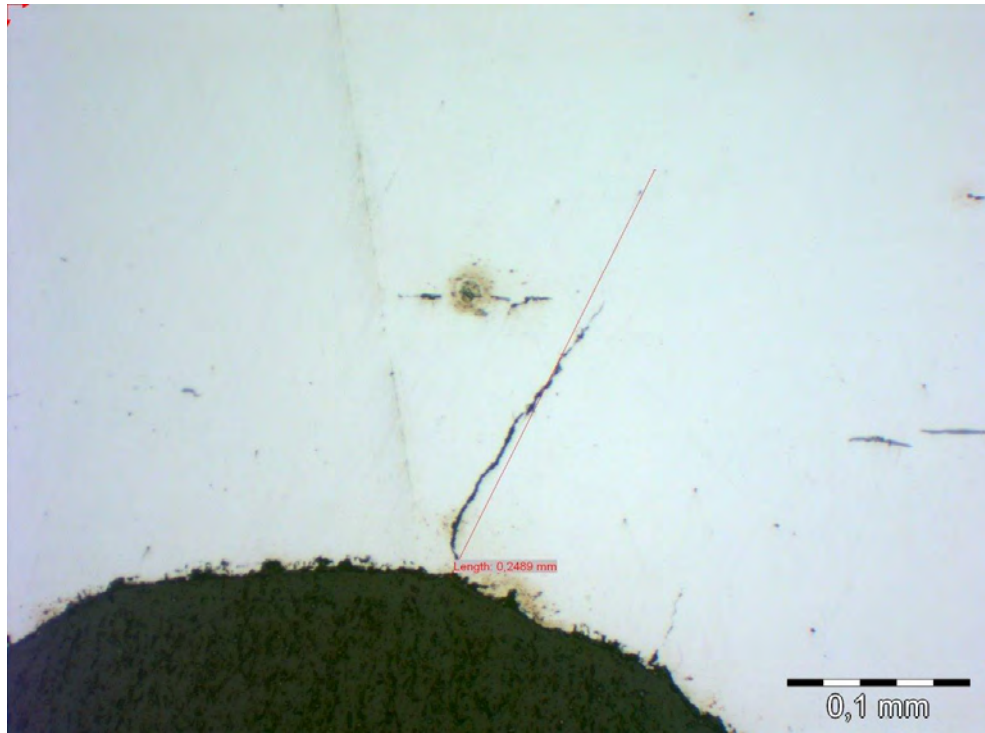


Figure C.71 Cut two in crack at segment B, second ridge on barrel no. SFK 0120-A

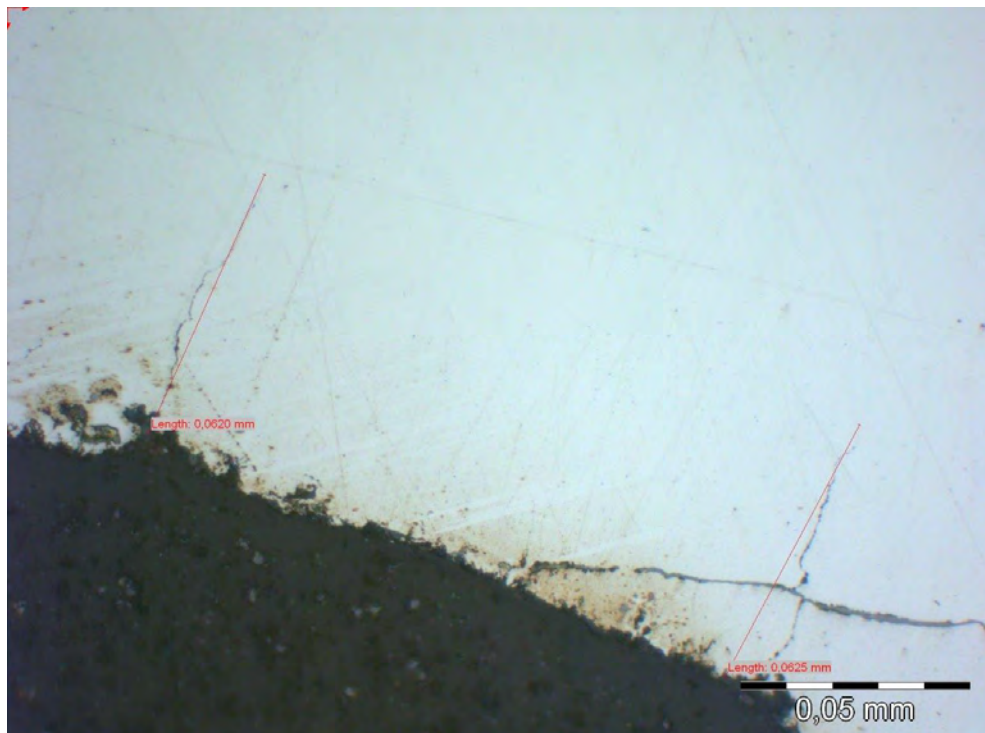


Figure C.72 Cut two in crack at segment B, third ridge on barrel no. SFK 0120-A

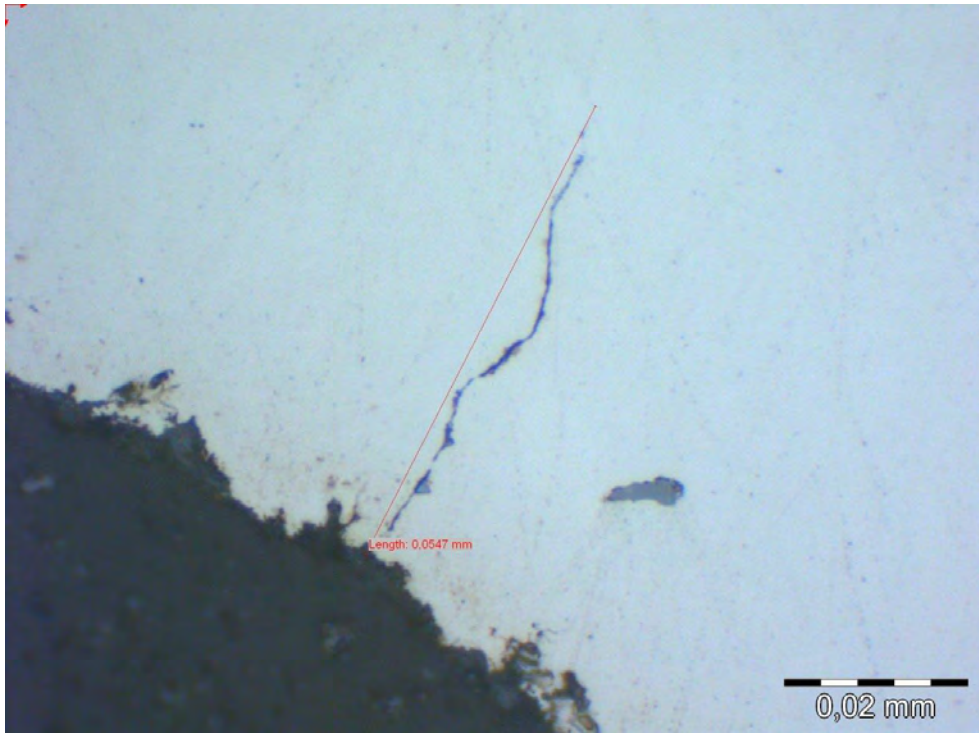


Figure C.73 Cut two in crack at segment B, fourth ridge on barrel no. SFK 0120-A

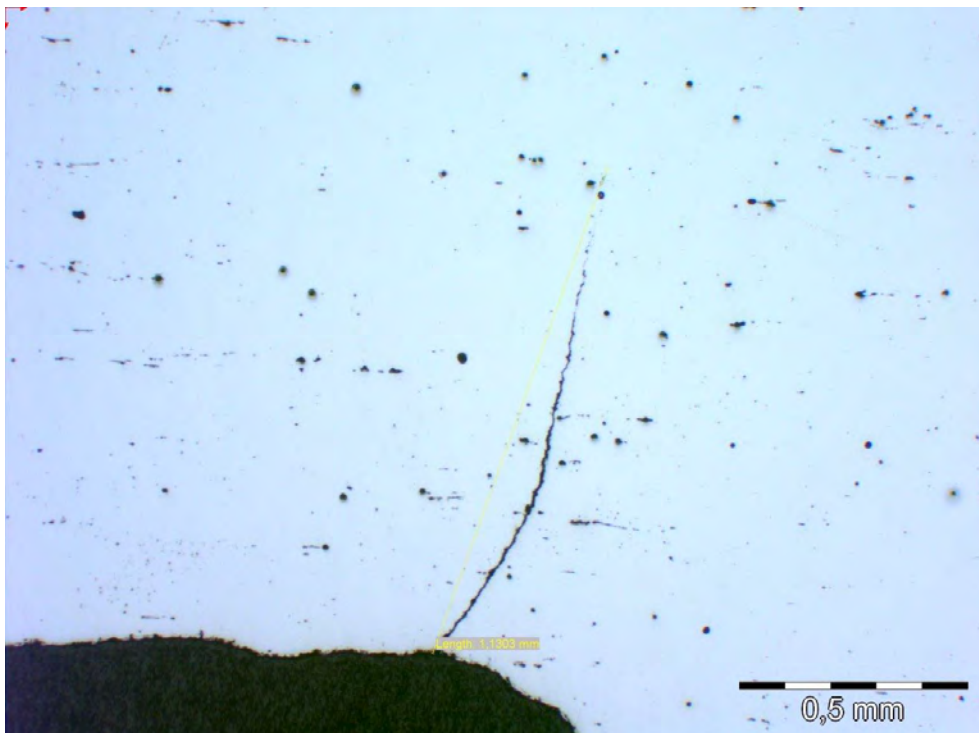


Figure C.74 Cut three in crack at segment A, first ridge on barrel no. SFK 0120-A

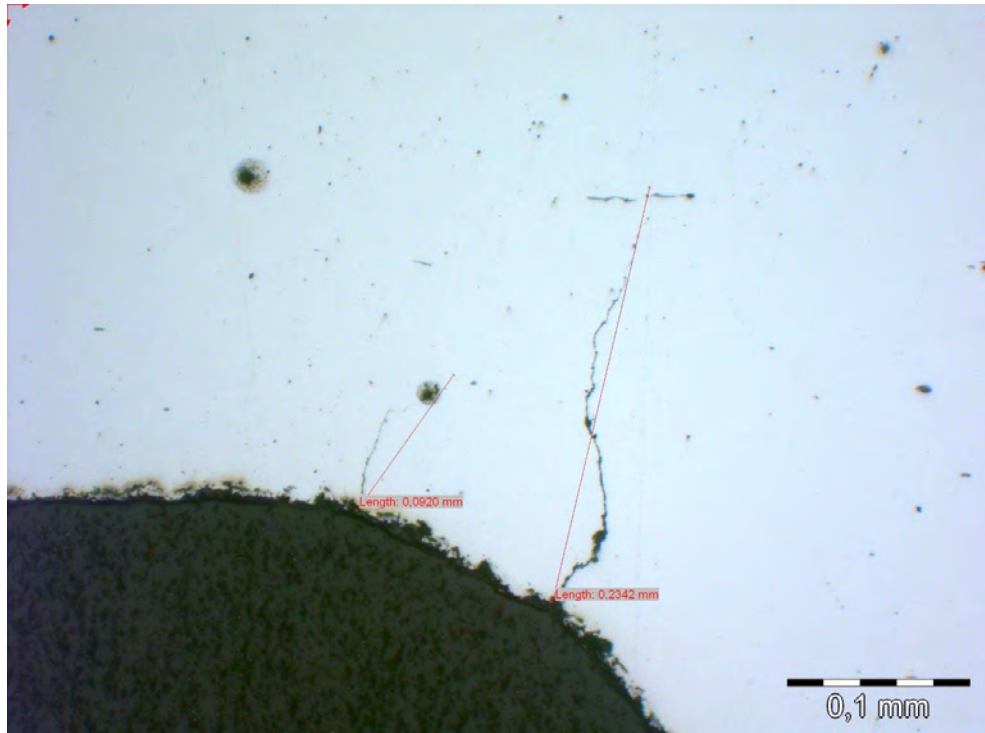


Figure C.75 Cut three in crack at segment A, second ridge on barrel no. SFK 0120-A

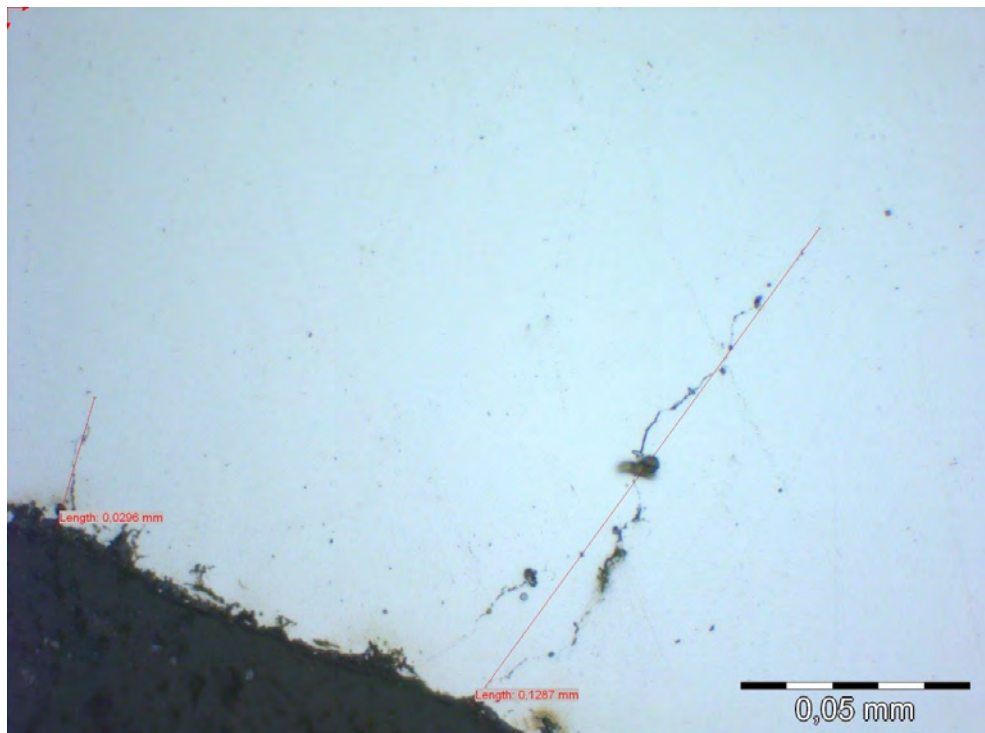


Figure C.76 Cut three in crack at segment A, third ridge on barrel no. SFK 0120-A

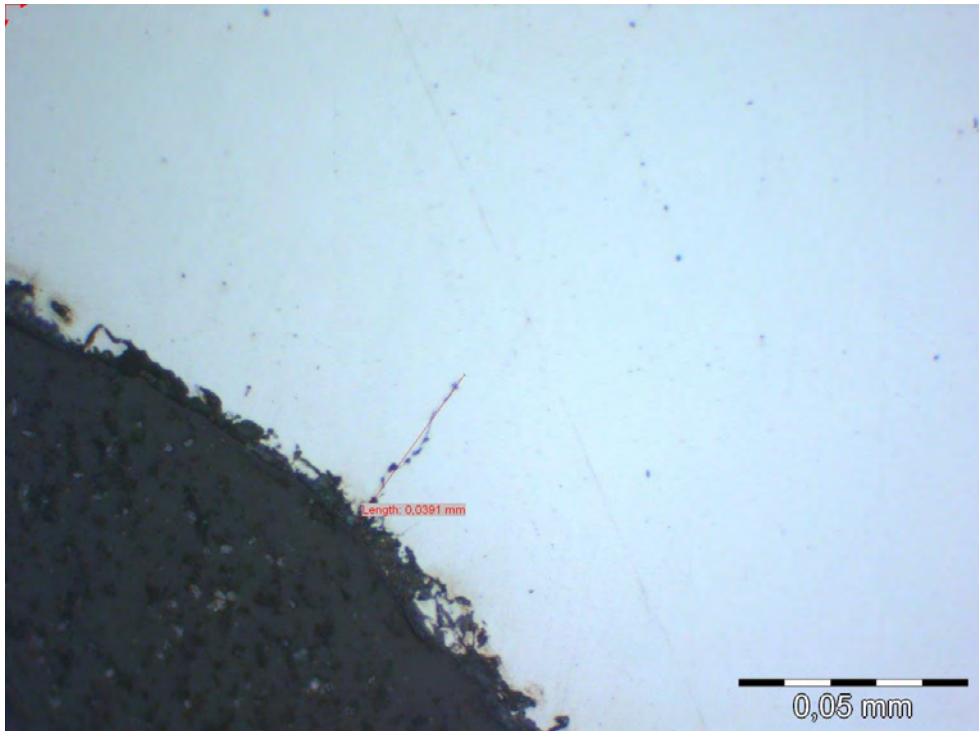


Figure C.77 Cut three in crack at segment A, fourth ridge on barrel no. SFK 0120-A

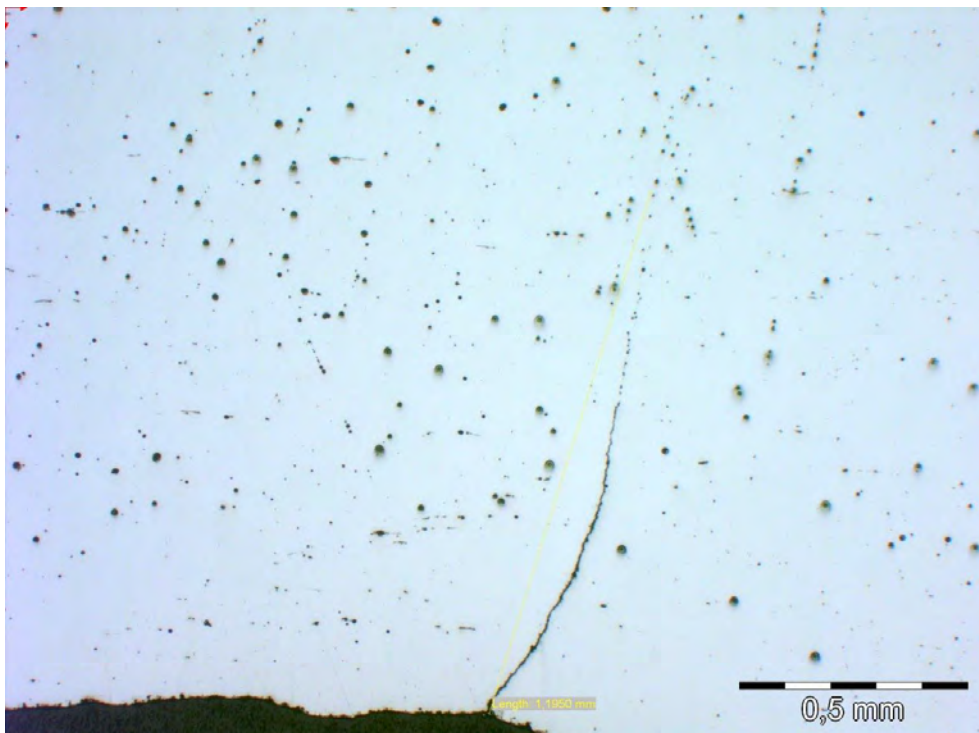


Figure C.78 Cut four in crack at segment B, first ridge on barrel no. SFK 0120-A

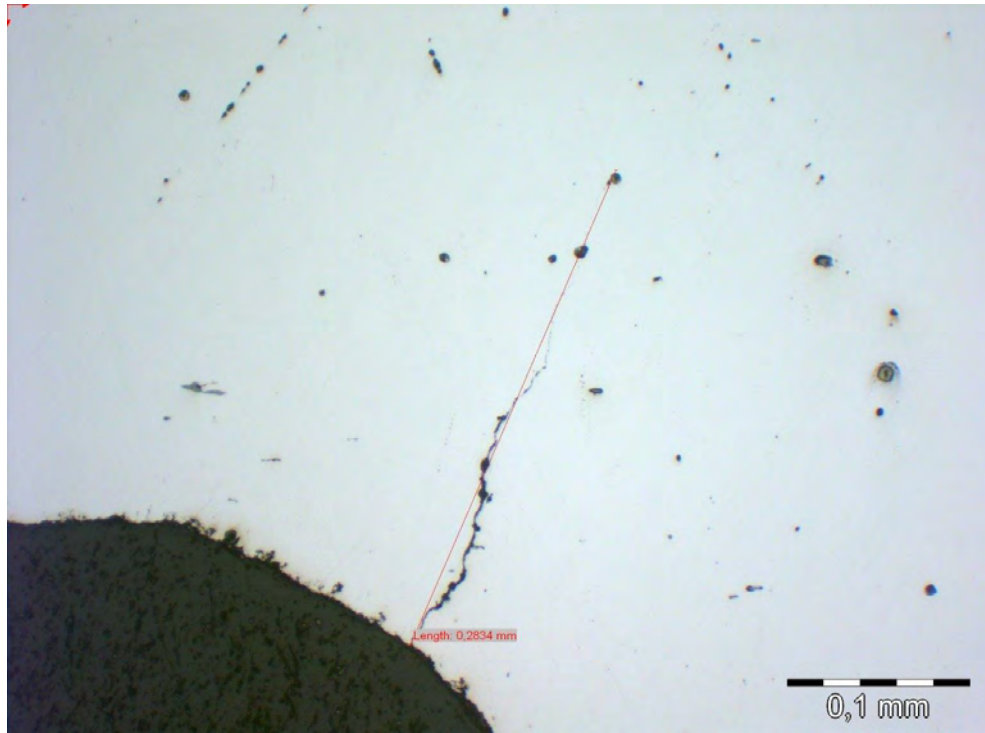


Figure C.79 Cut four in crack at segment B, second ridge on barrel no. SFK 0120-A

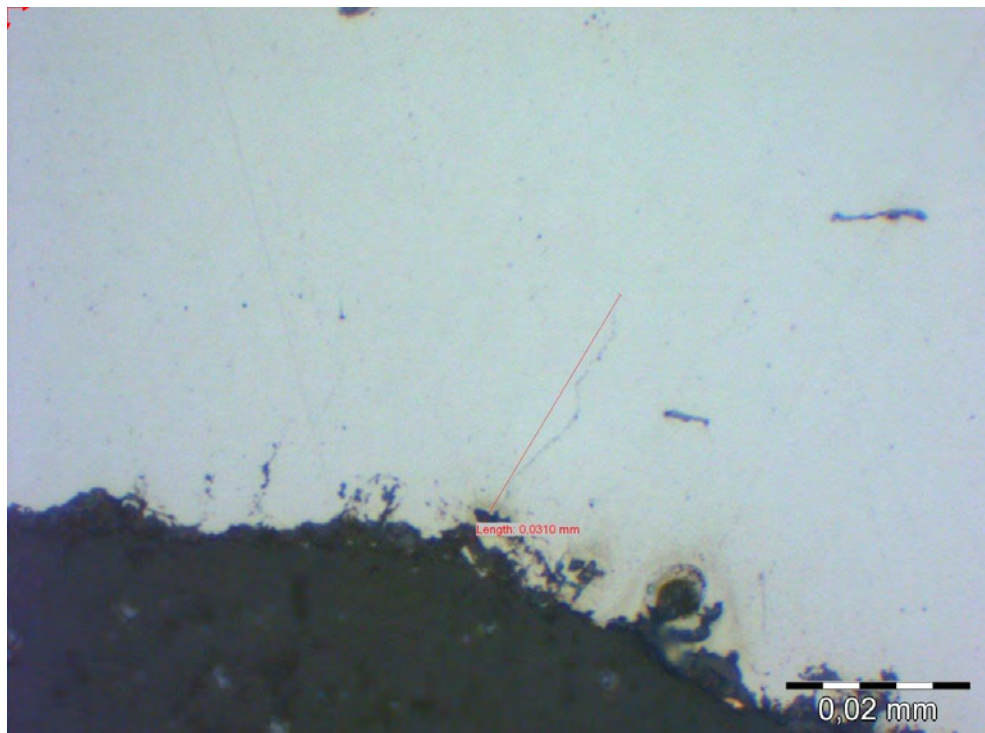


Figure C.80 Cut four in crack A at segment B, third ridge on barrel no. SFK 0120-A

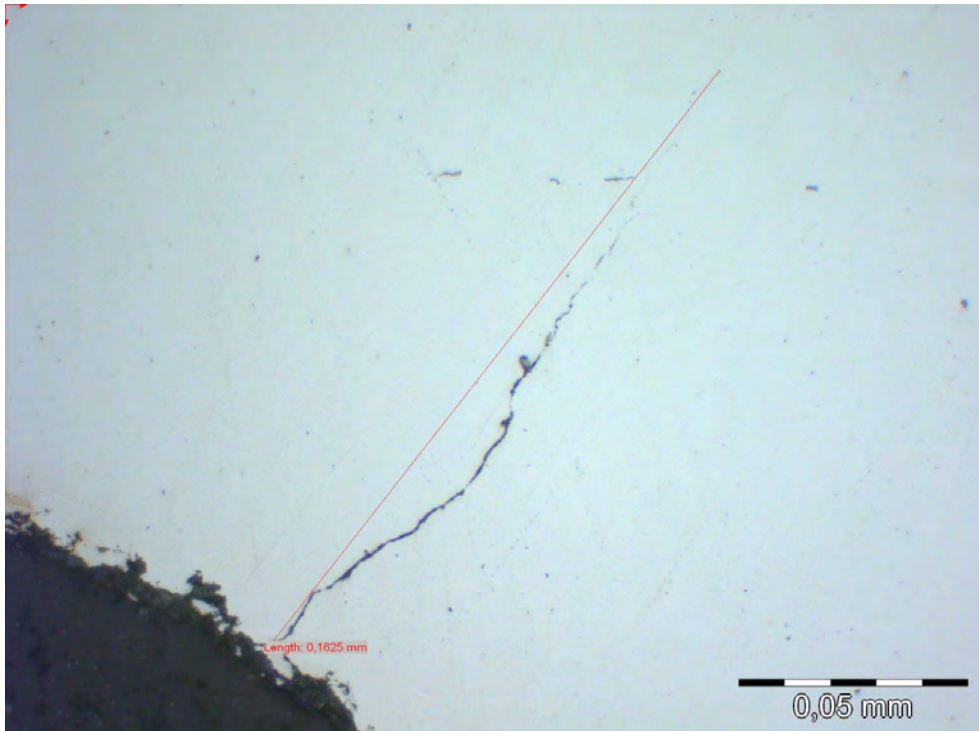


Figure C.81 Cut four in crack B at segment B, third ridge on barrel no. SFK 0120-A

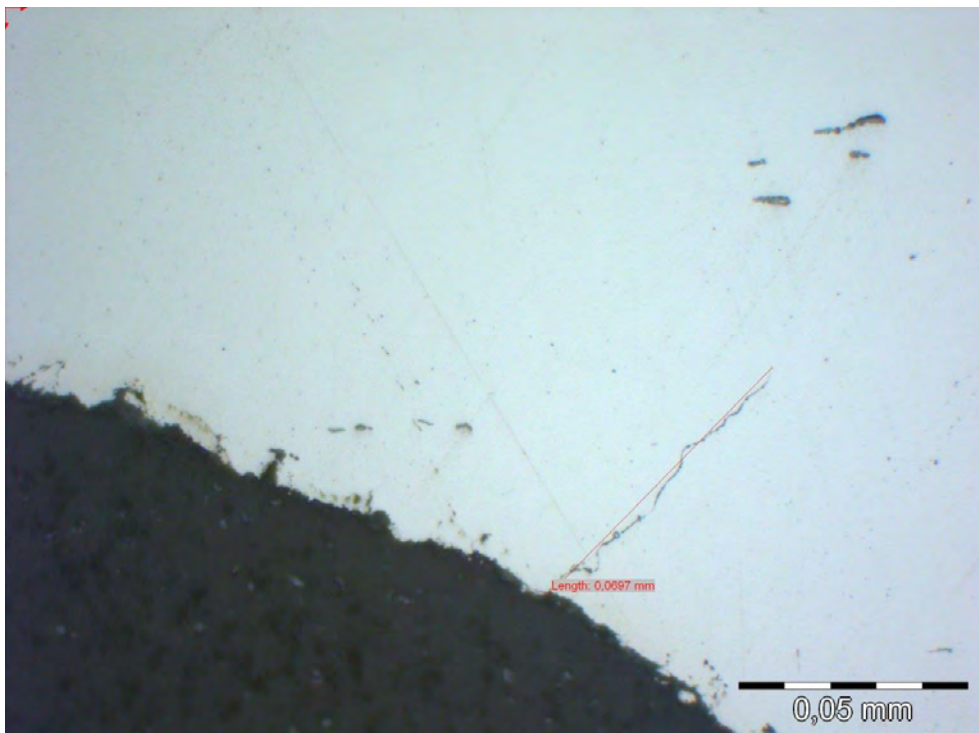


Figure C.82 Cut four in crack at segment B, fourth ridge on barrel no. SFK 0120-A

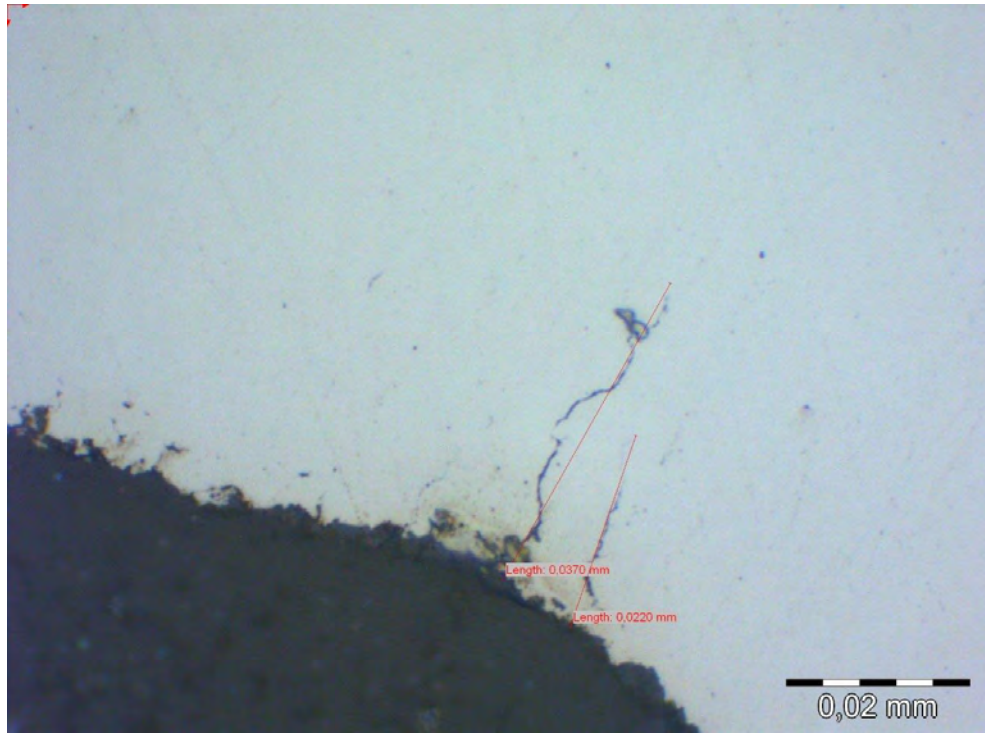


Figure C.83 Cut four in crack at segment B, fifth ridge on barrel no. SFK 0120-A

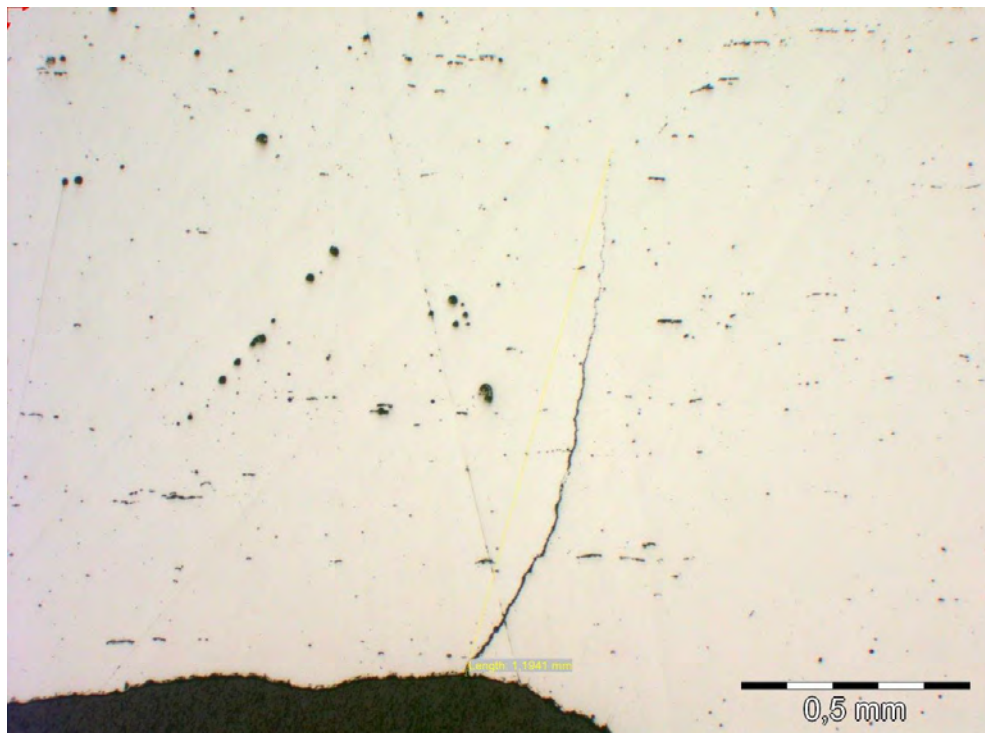


Figure C.84 Cut five in crack at segment B, first ridge on barrel no. SFK 0120-A

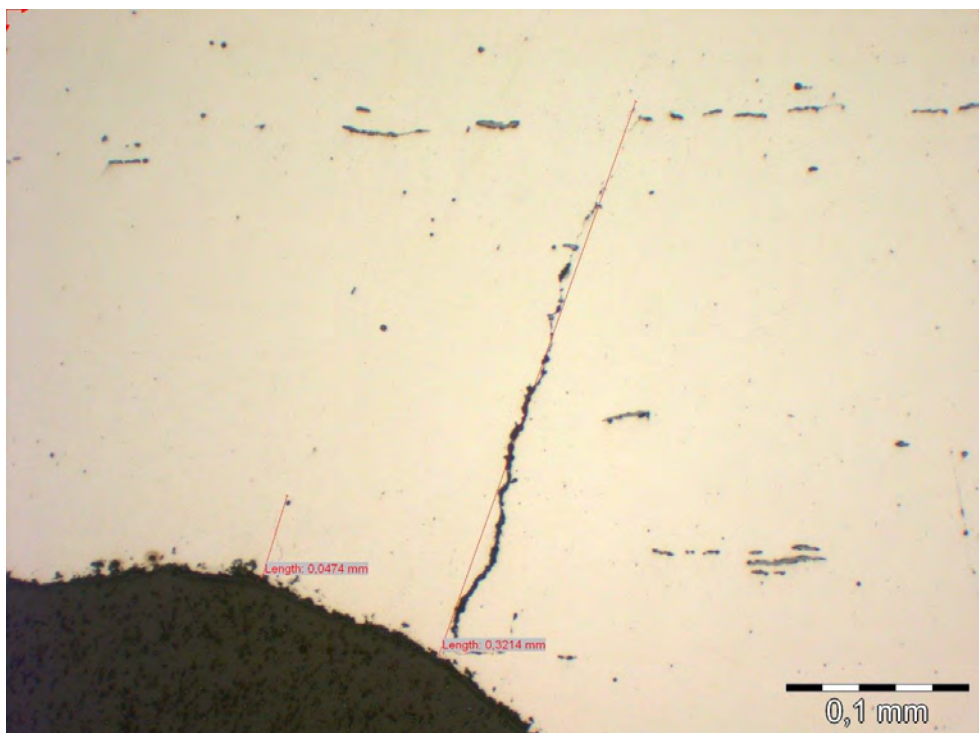


Figure C.85 Cut five in crack at segment B, second ridge on barrel no. SFK 0120-A

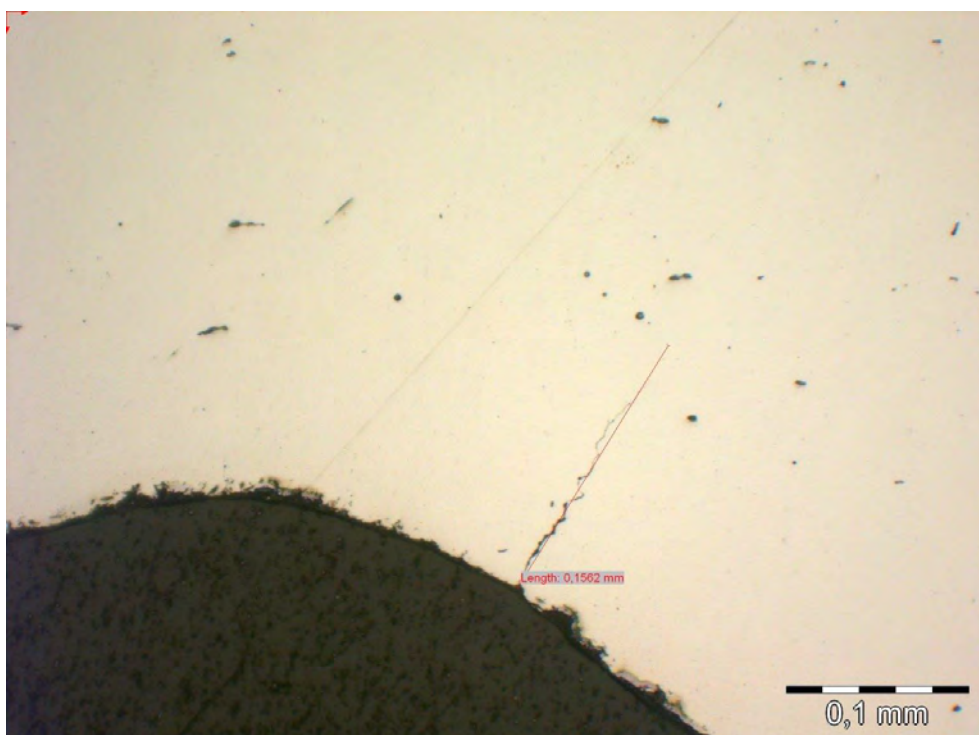


Figure C.86 Cut five in crack at segment B, third ridge on barrel no. SFK 0120-A

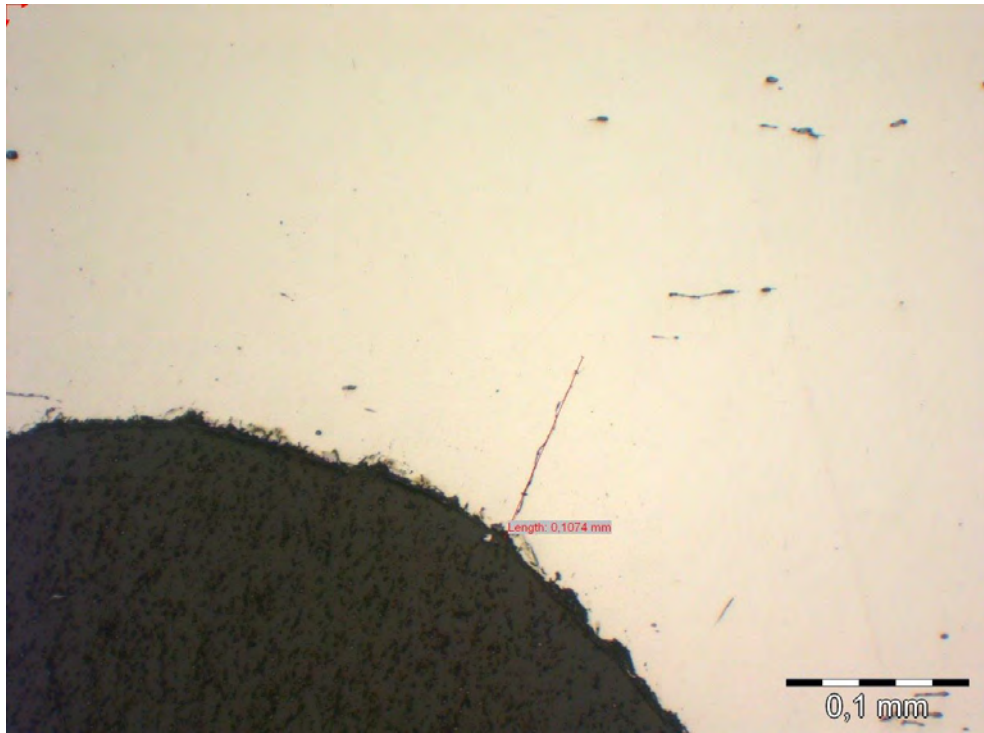


Figure C.87 Cut five in crack at segment B, fourth ridge on barrel no. SFK 0120-A

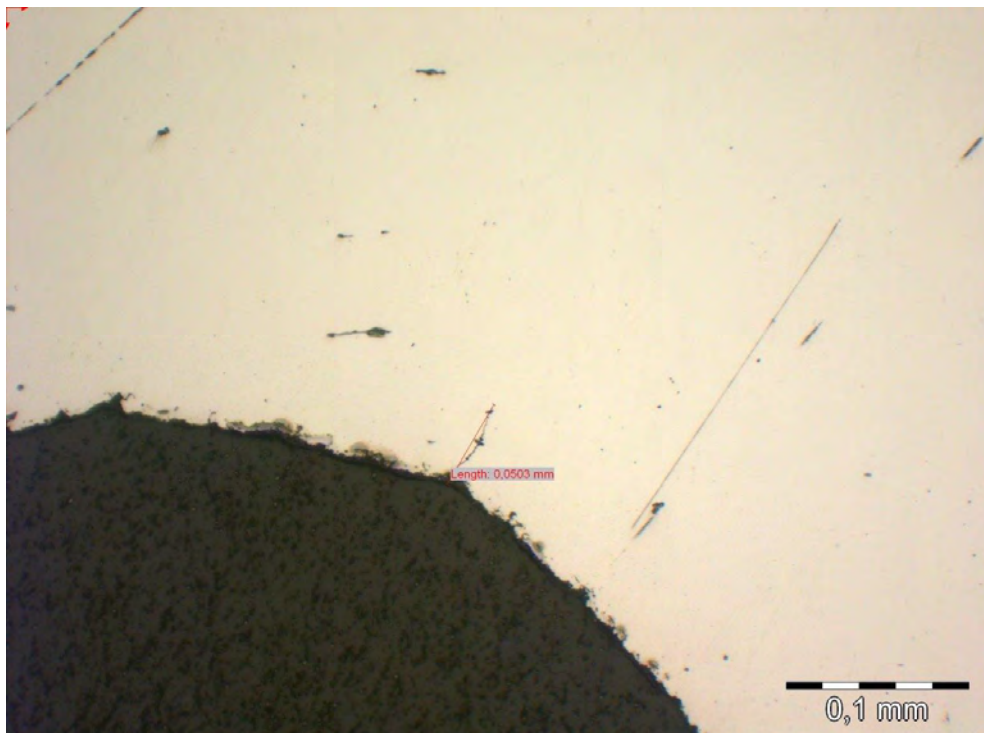


Figure C.88 Cut five in crack at segment B, fifth ridge on barrel no. SFK 0120-A

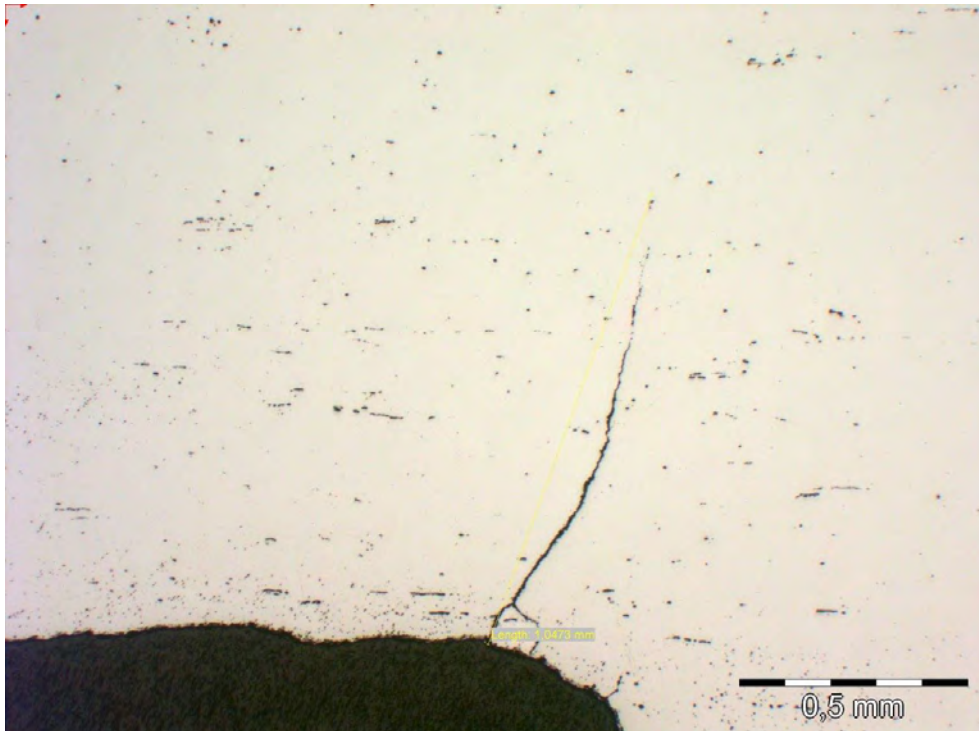


Figure C.89 Cut six in crack at segment B, first ridge on barrel no. SFK 0120-A

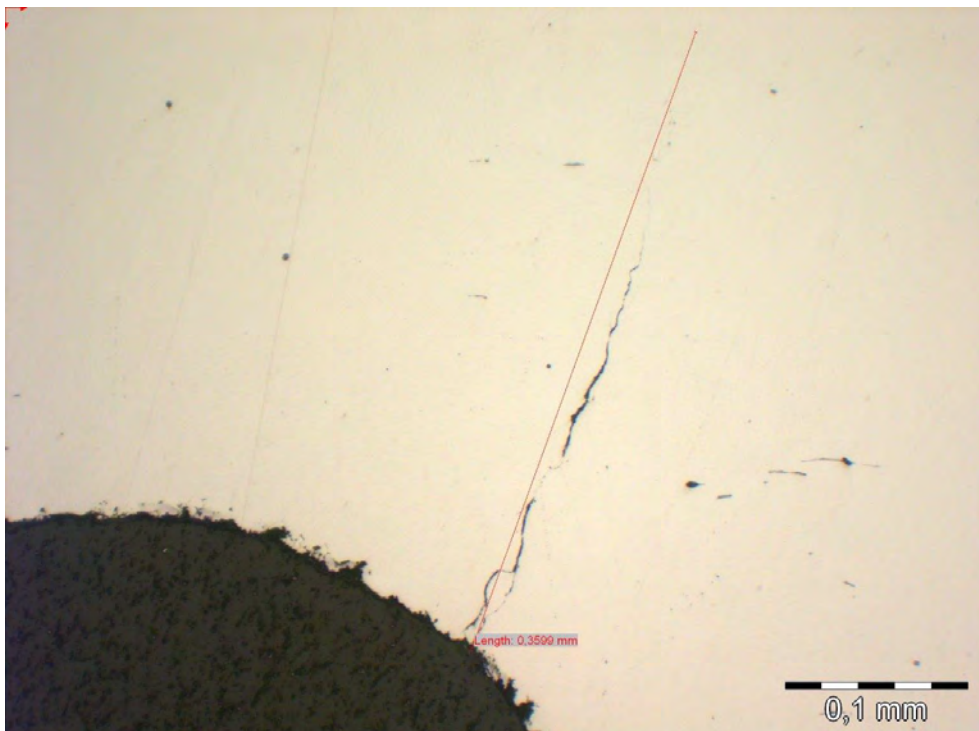


Figure C.90 Cut six in crack at segment B, second ridge on barrel no. SFK 0120-A

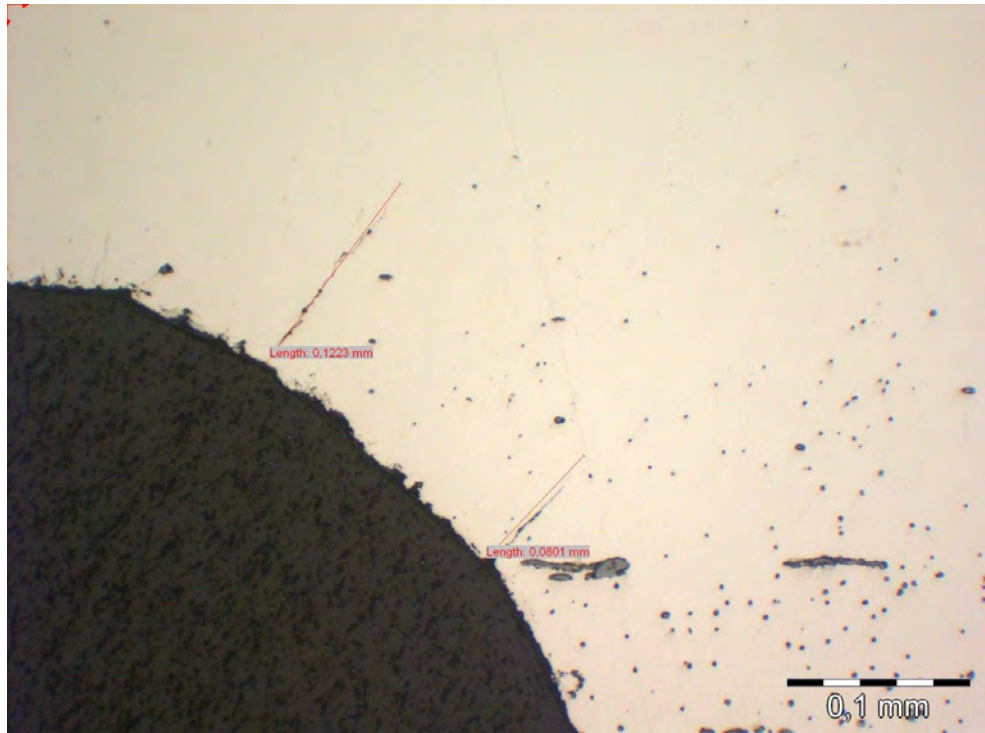


Figure C.91 Cut six in crack at segment B, third ridge on barrel no. SFK 0120-A

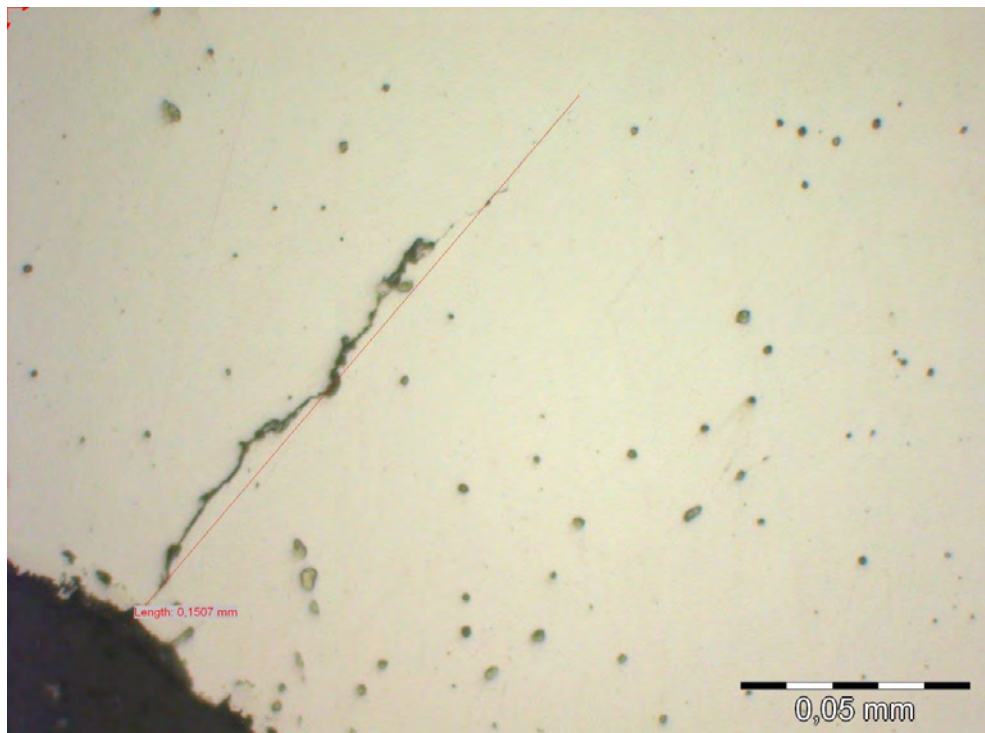


Figure C.92 Cut six in crack at segment B, fourth ridge on barrel no. SFK 0120-A

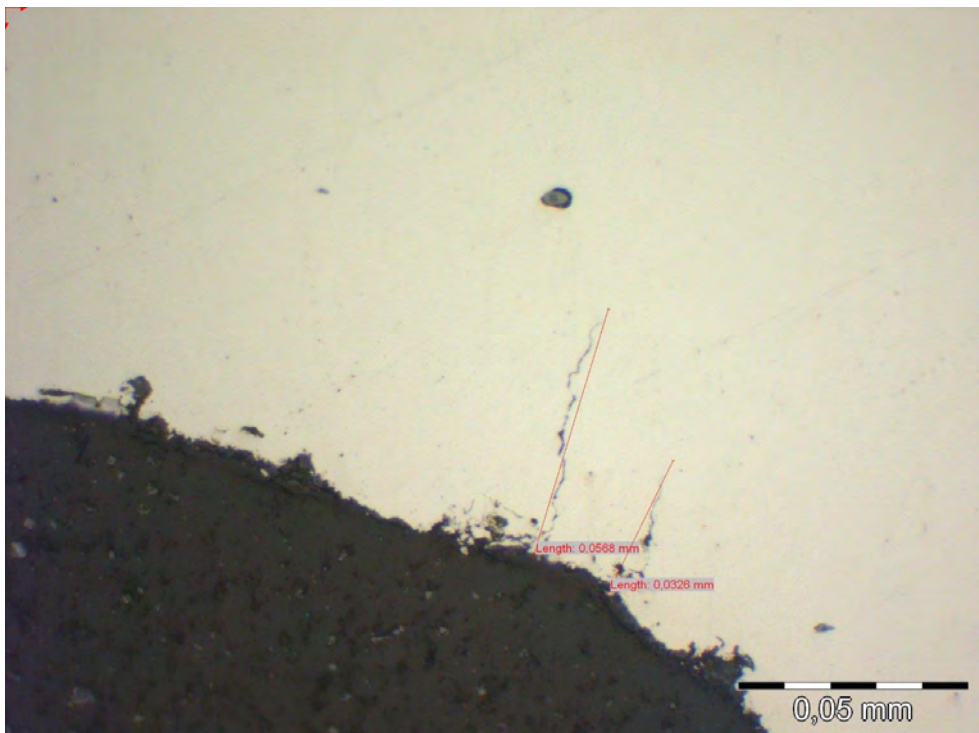


Figure C.93 Cut six in crack at segment B, fifth ridge on barrel no. SFK 0120-A

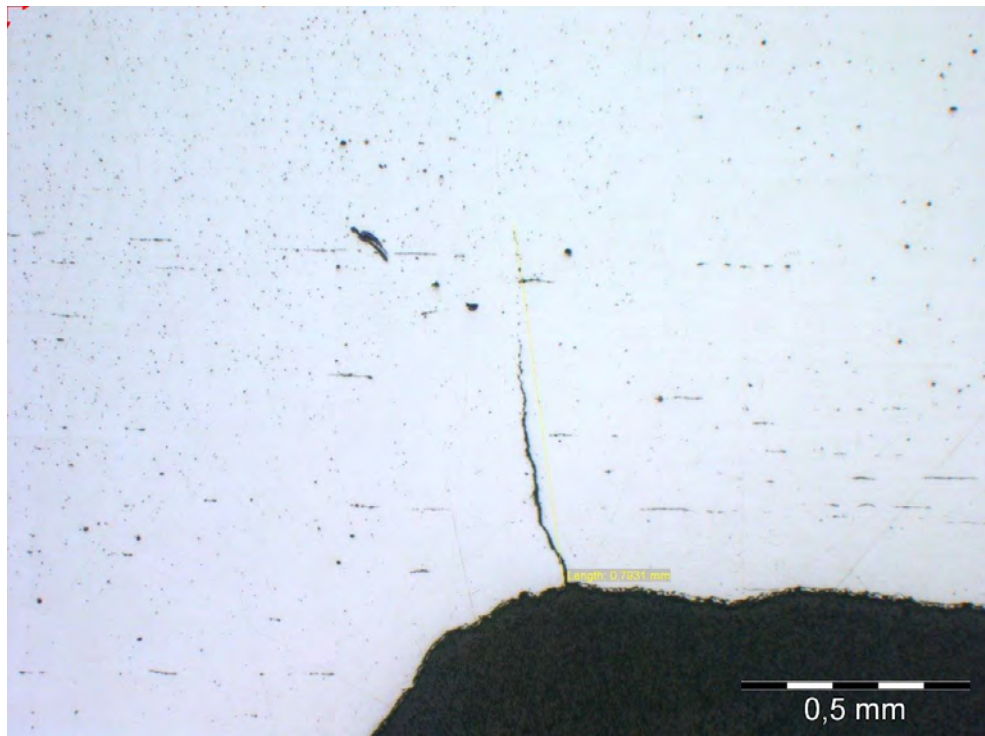


Figure C.94 Crack at segment A, first ridge on barrel no. SFK 0120-A

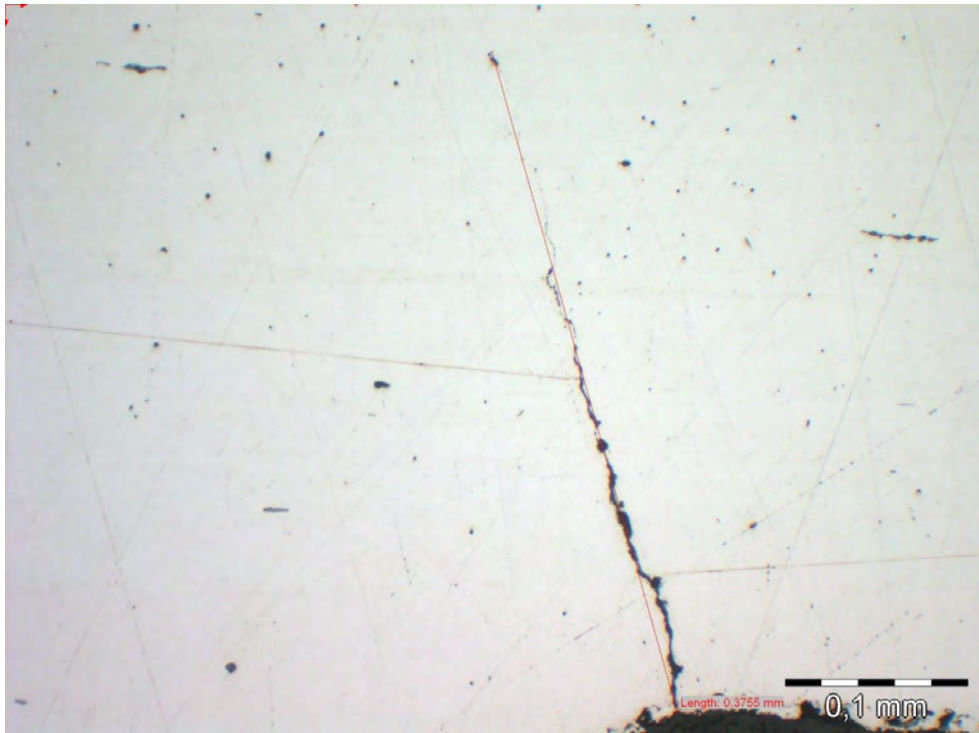


Figure C.95 Crack at segment A, second ridge on barrel no. SFK 0120-A

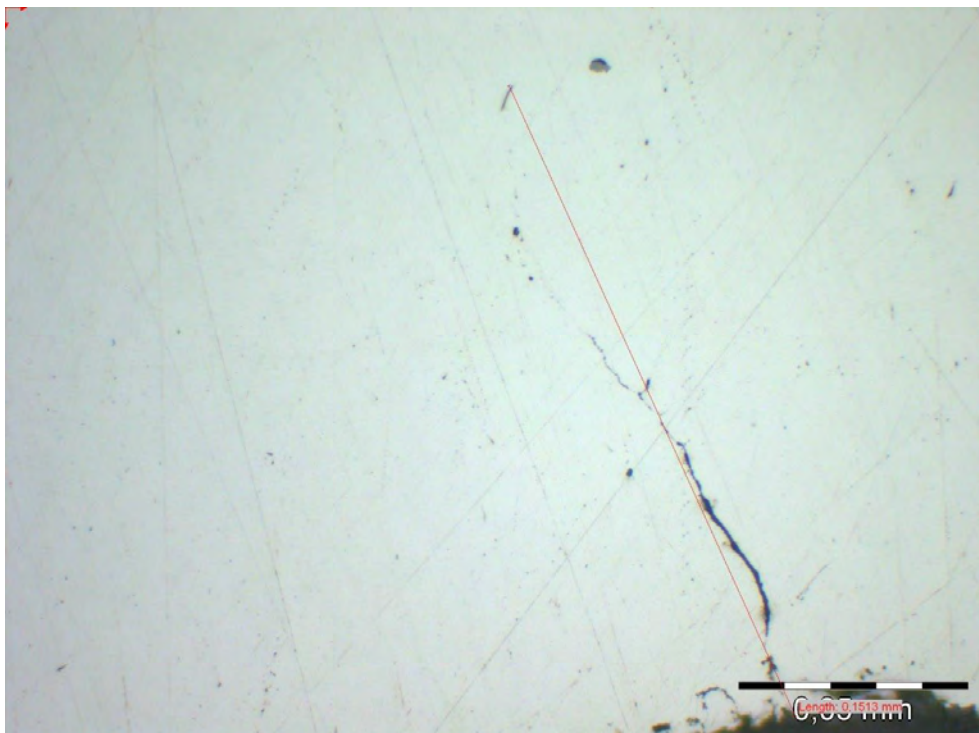


Figure C.96 Crack at segment A, third ridge on barrel no. SFK 0120-A

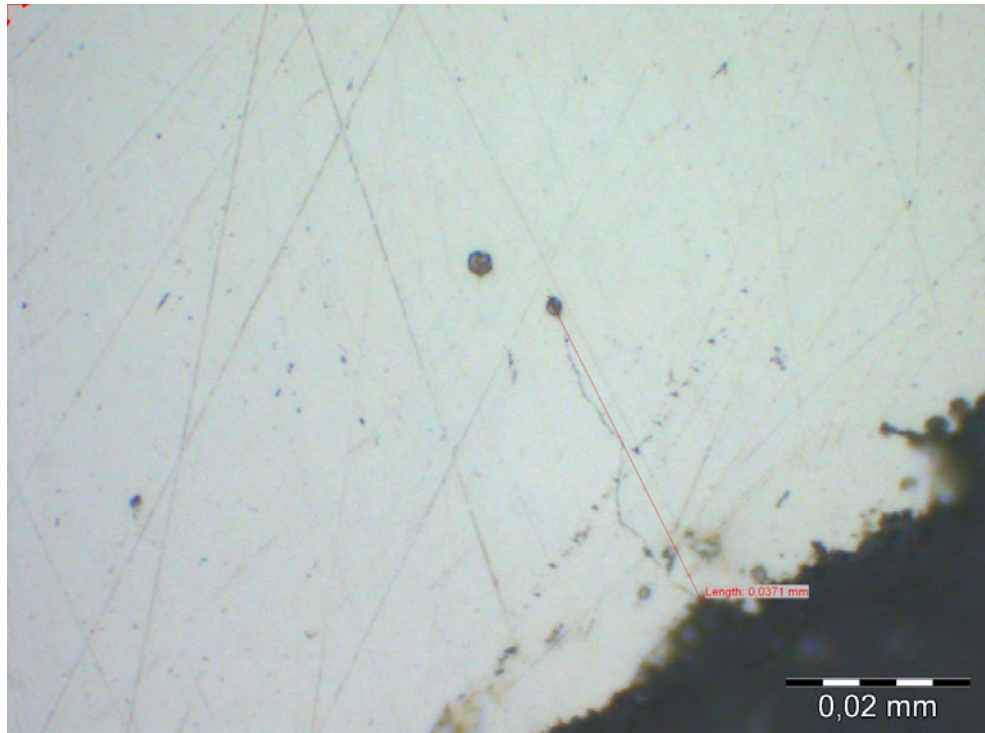


Figure C.97 Crack at segment A, fourth ridge on barrel no. SFK 0120-A

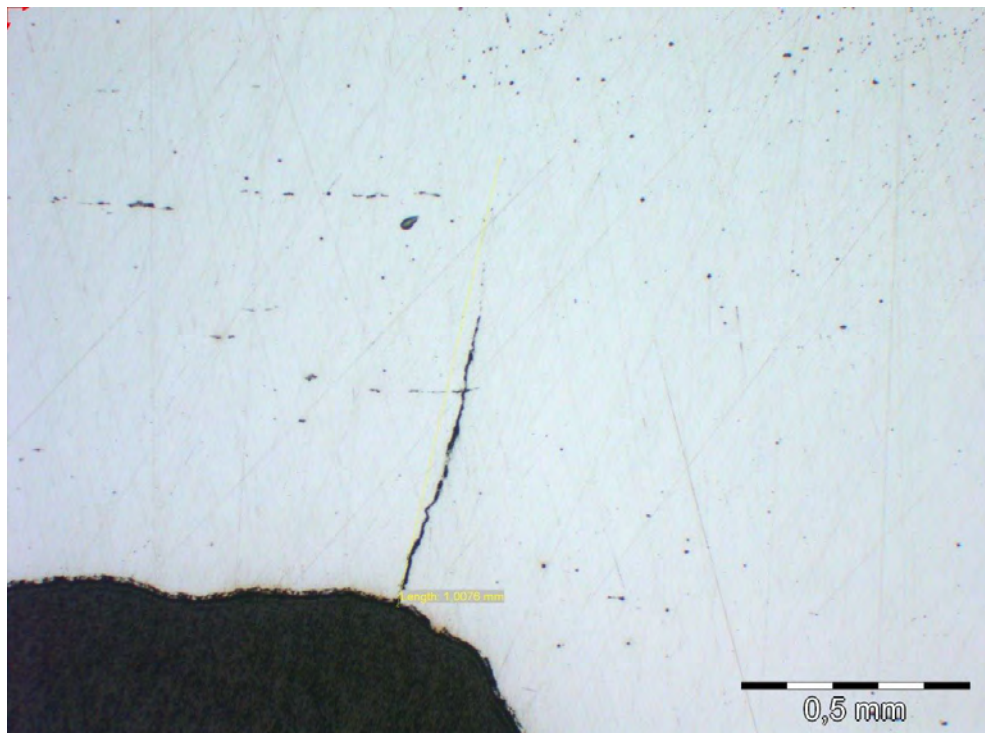


Figure C.98 Crack at segment B, first ridge on barrel no. SFK 0120-A

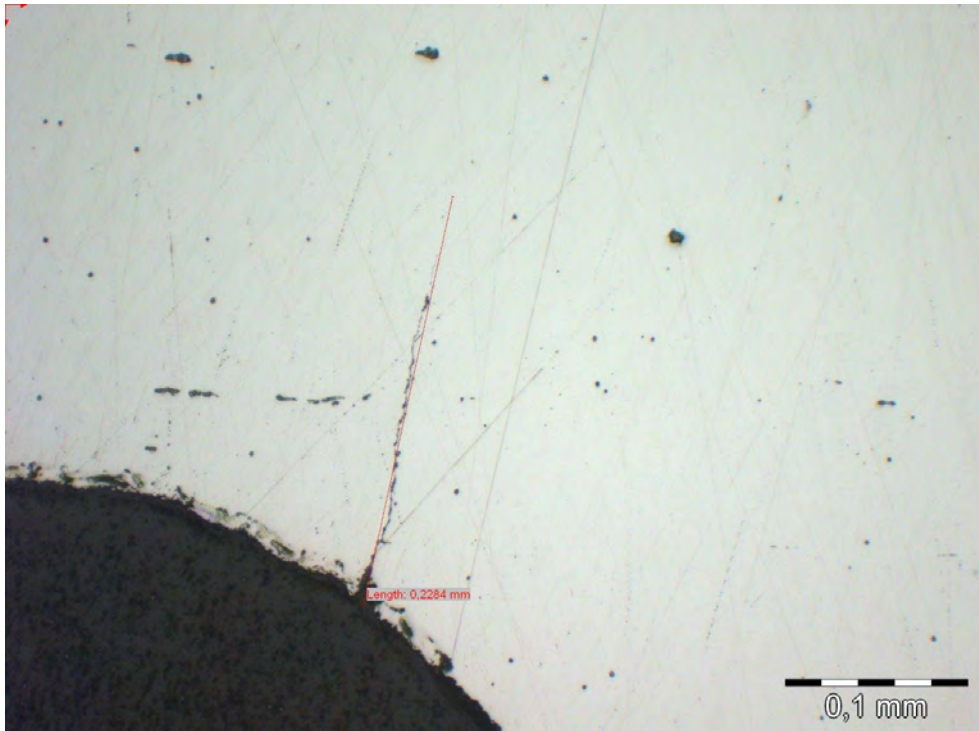


Figure C.99 Crack at segment B, second ridge on barrel no. SFK 0120-A

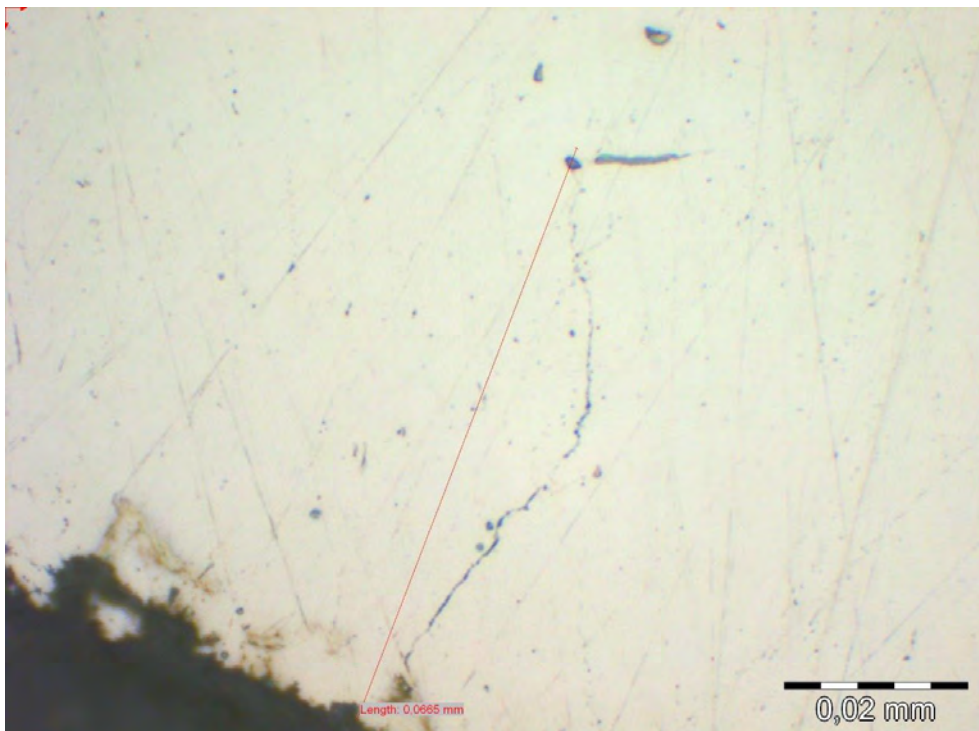


Figure C.100 Crack A at segment B, third ridge on barrel no. SFK 0120-A

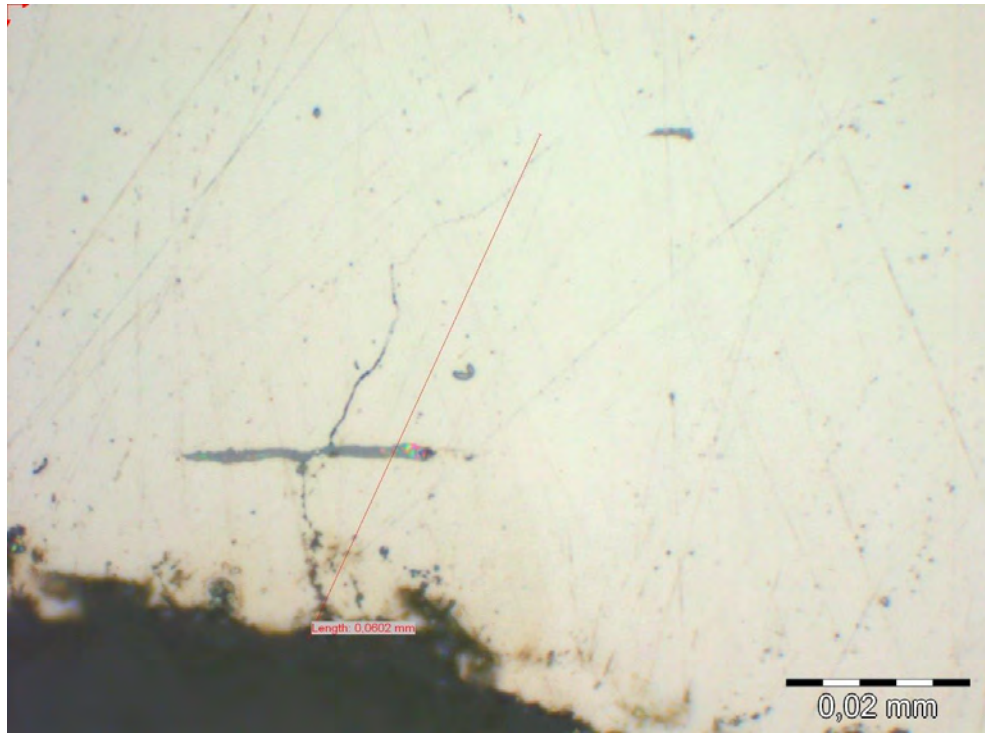


Figure C.101 Crack B at segment B, third ridge on barrel no. SFK 0120-A

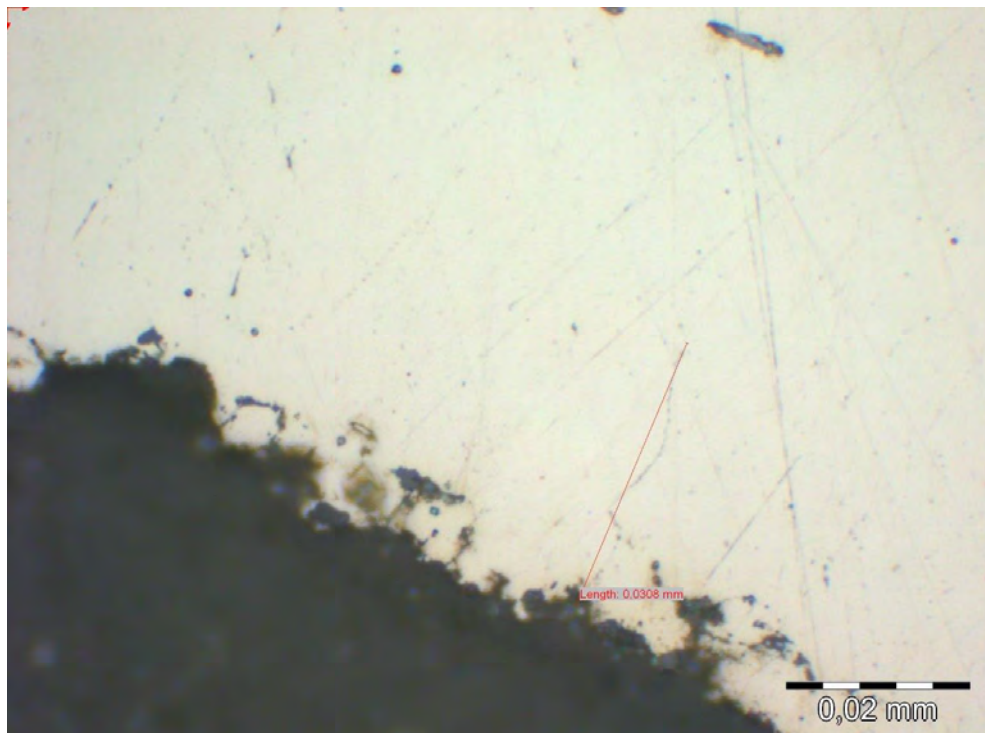


Figure C.102 Crack at segment B, fourth ridge on barrel no. SFK 0120-A

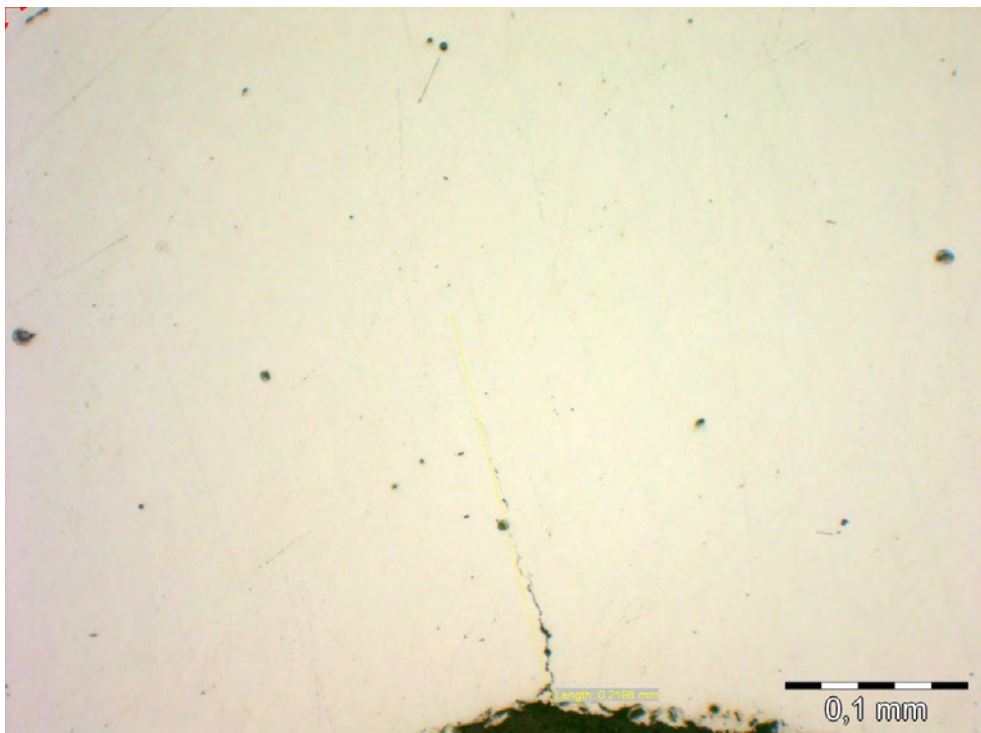


Figure C.103 Crack at segment C, first ridge on barrel no. SFK 0120-A

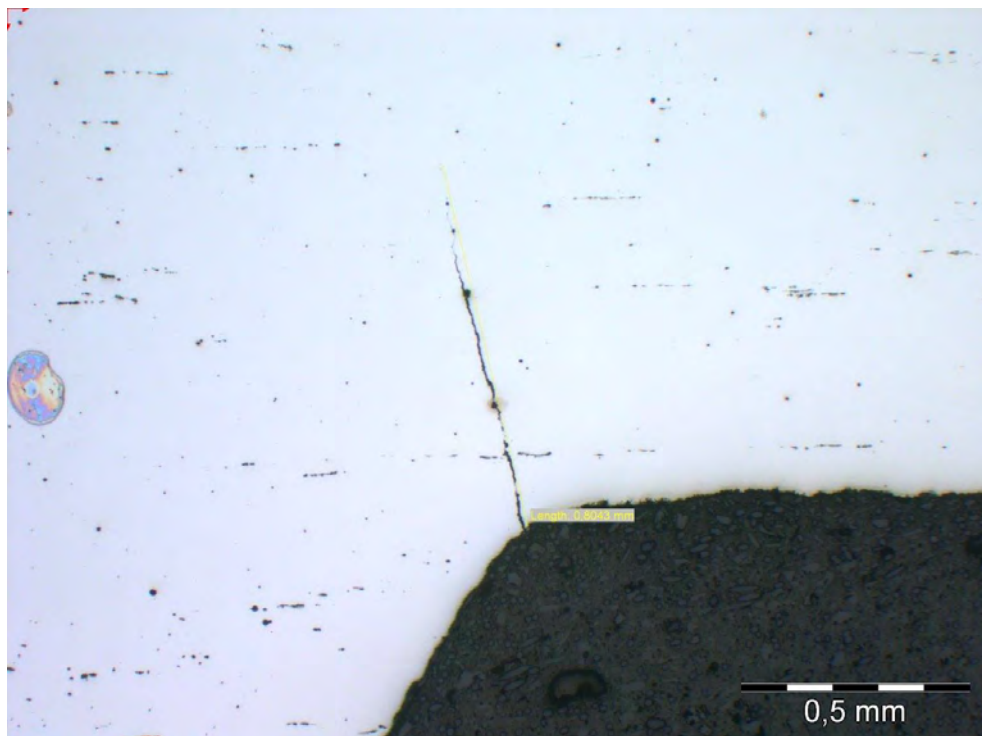


Figure C.104 Crack at segment A, first ridge on barrel no. SFK 0123-A

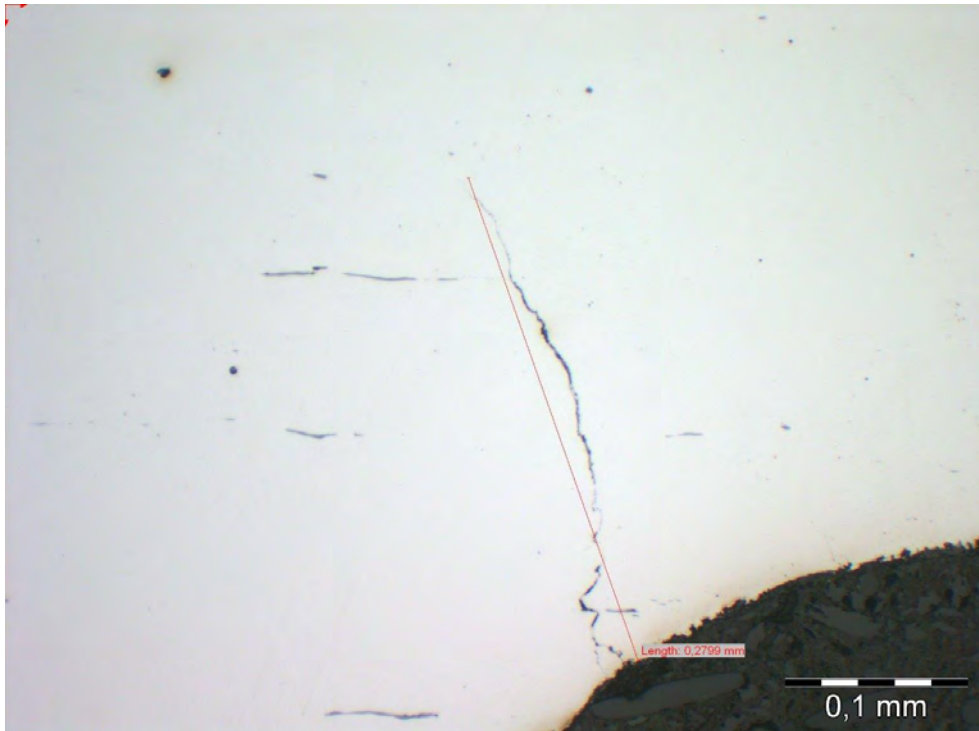


Figure C.105 Crack at segment A, second ridge on barrel no. SFK 0123-A

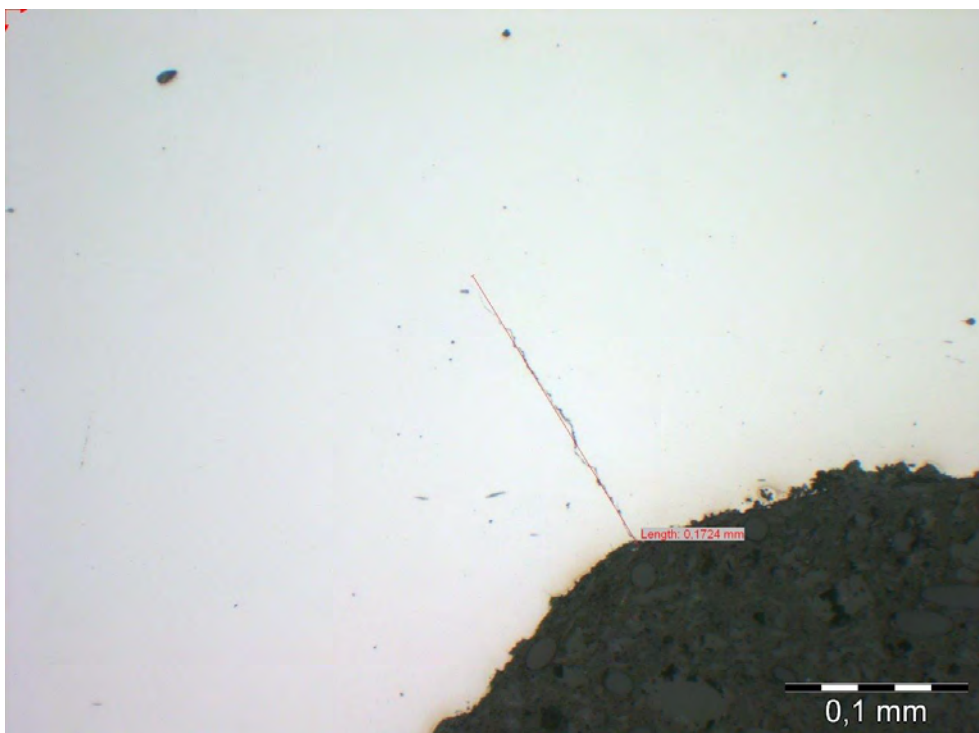


Figure C.106 Crack at segment A, third ridge on barrel no. SFK 0123-A

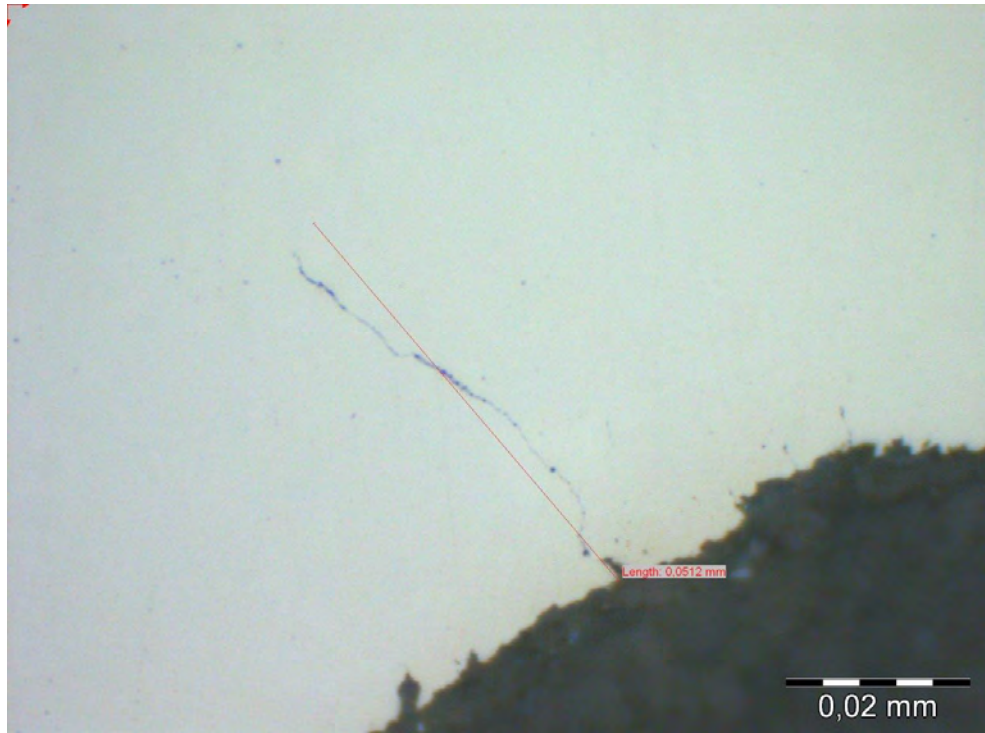


Figure C.107 Crack at segment A, fourth ridge on barrel no. SFK 0123-A

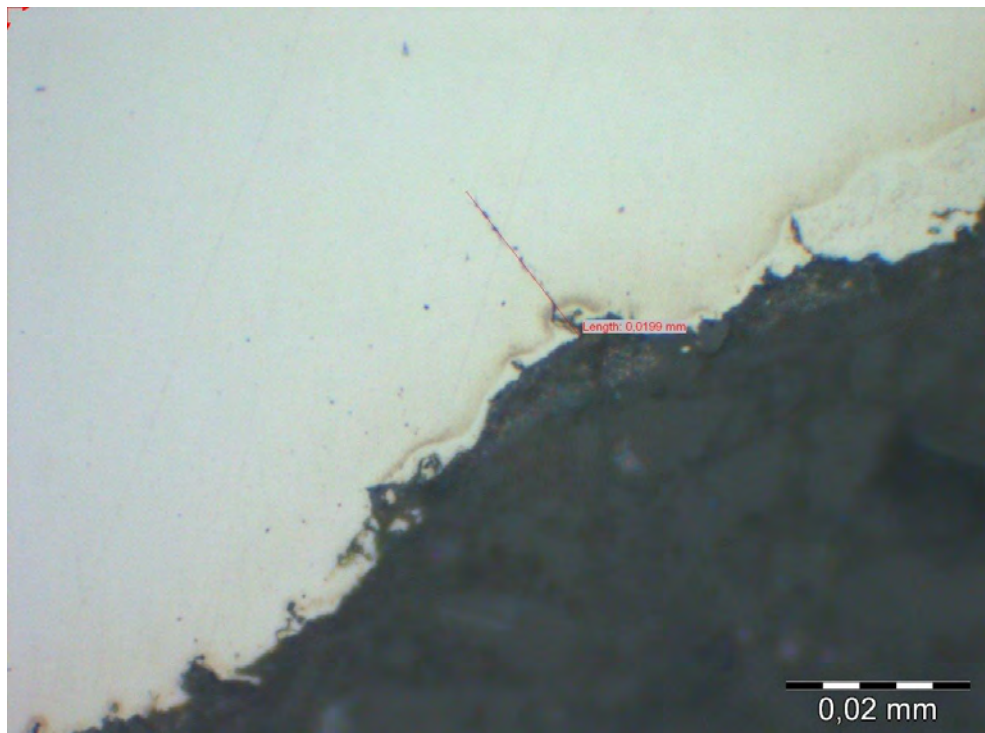


Figure C.108 Crack at segment A, fifth ridge on barrel no. SFK 0123-A

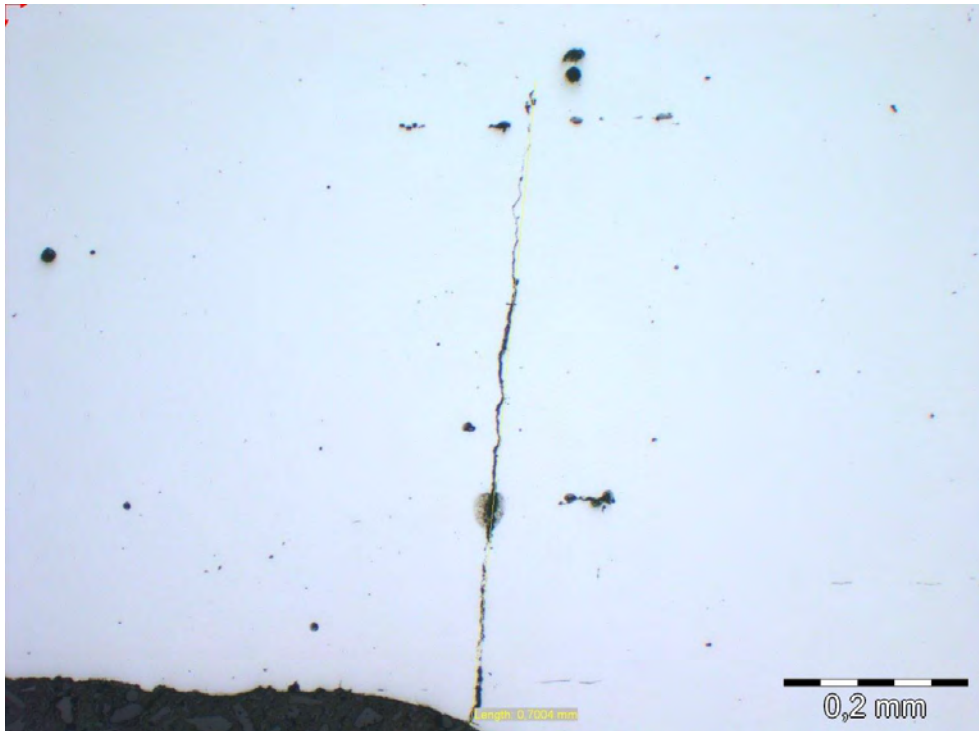


Figure C.109 Crack at segment B, first ridge on barrel no. SFK 0123-A

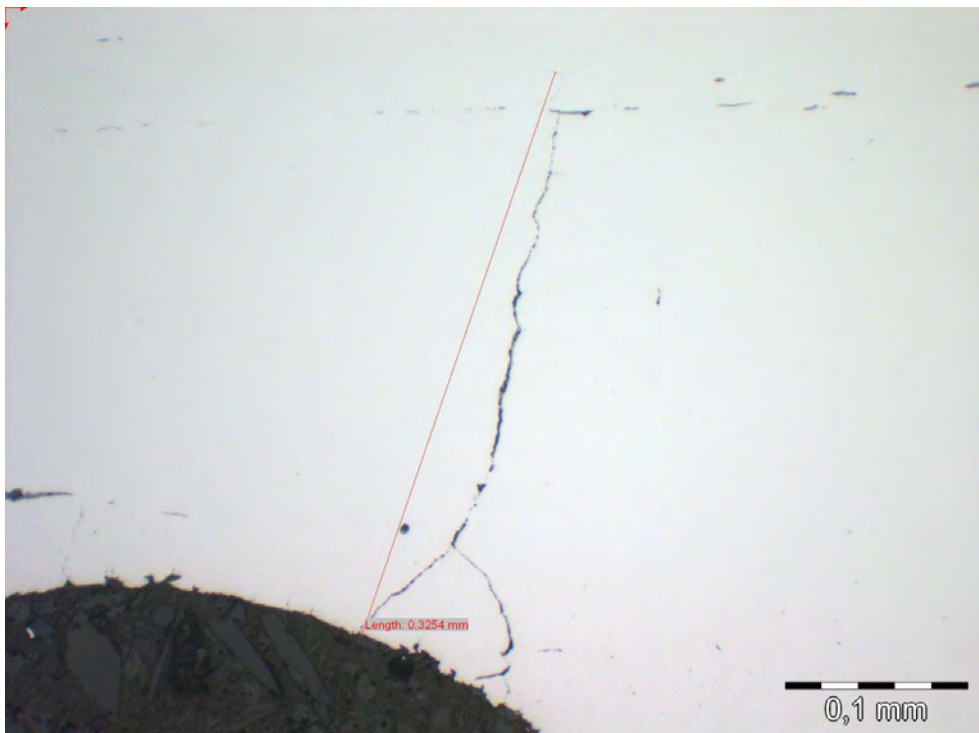


Figure C.110 Crack at segment B, second ridge on barrel no. SFK 0123-A

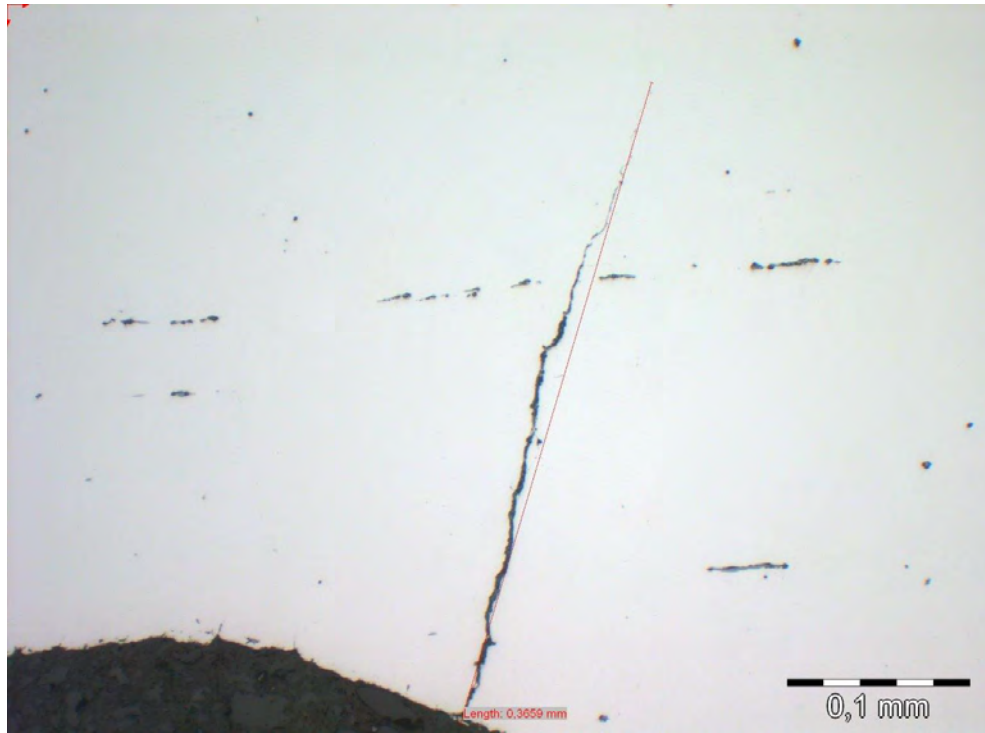


Figure C.111 Crack at segment B, third ridge on barrel no. SFK 0123-A

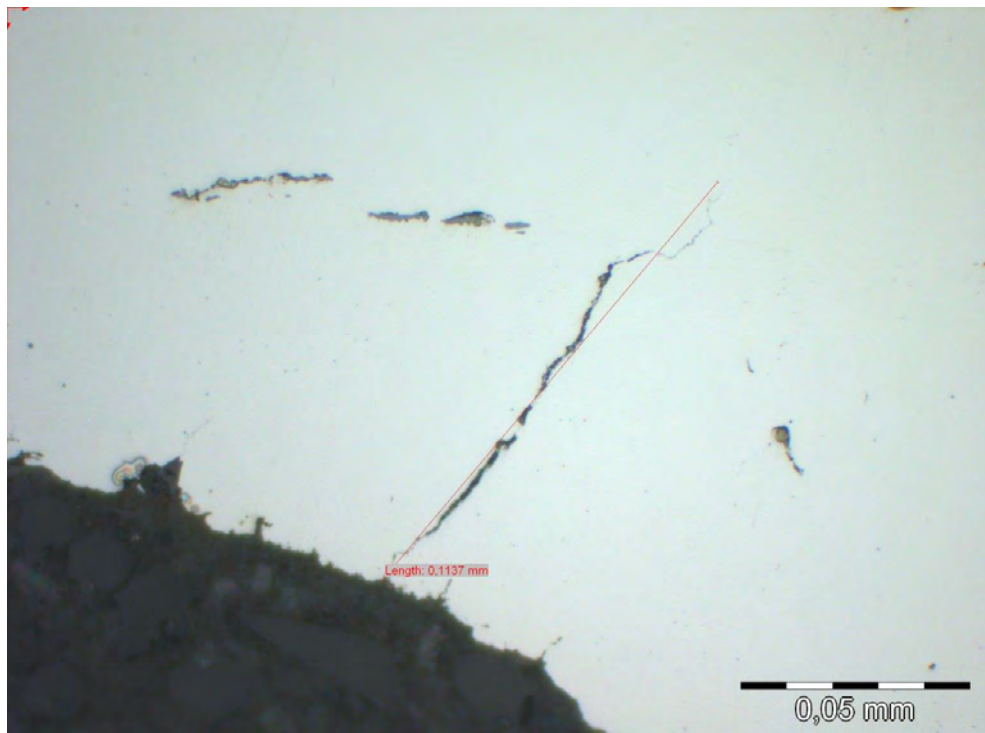


Figure C.112 Crack at segment B, fourth ridge on barrel no. SFK 0123-A

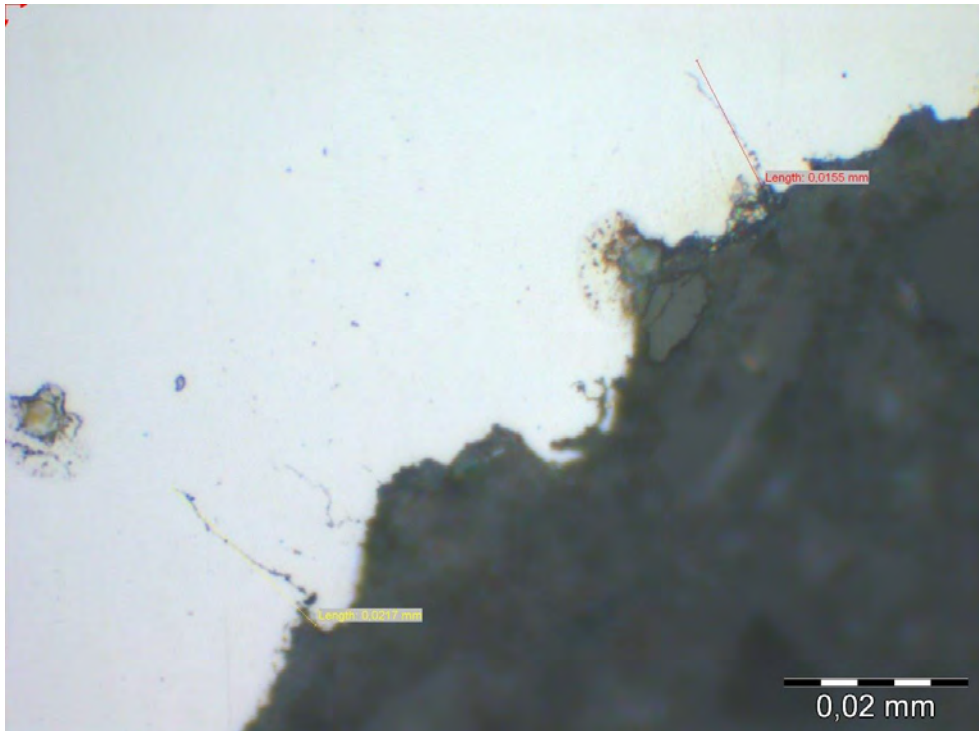


Figure C.113 Crack at segment C, third ridge on barrel no. SFK 0123-A

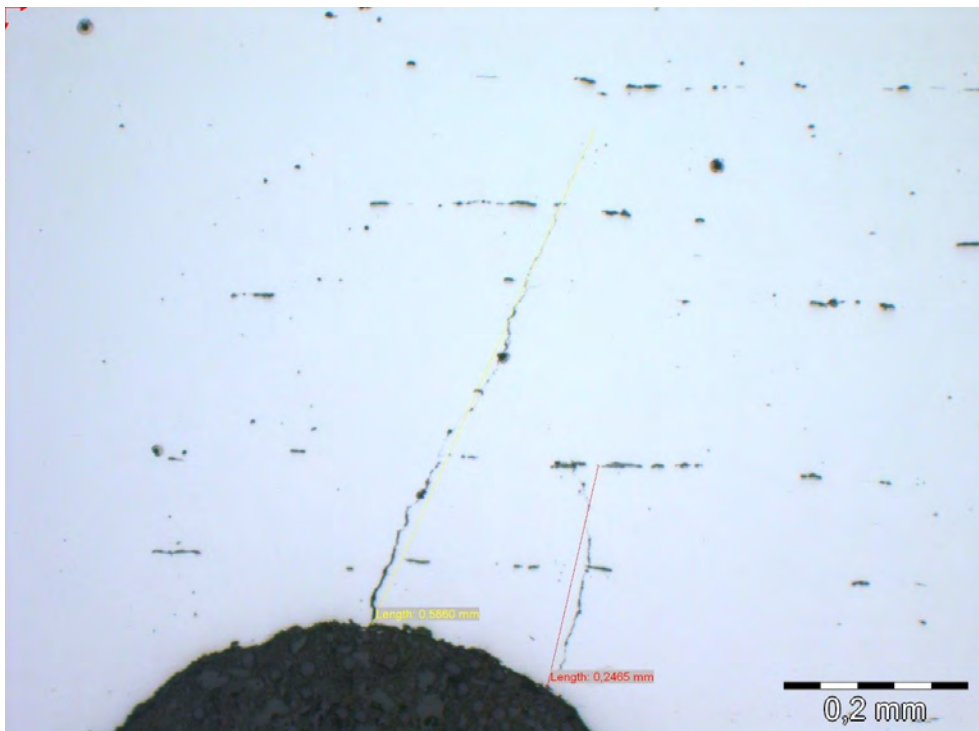


Figure C.114 Crack at segment C, second ridge on barrel no. SFK 0123-A

D Brake opening of crack at FOLAT



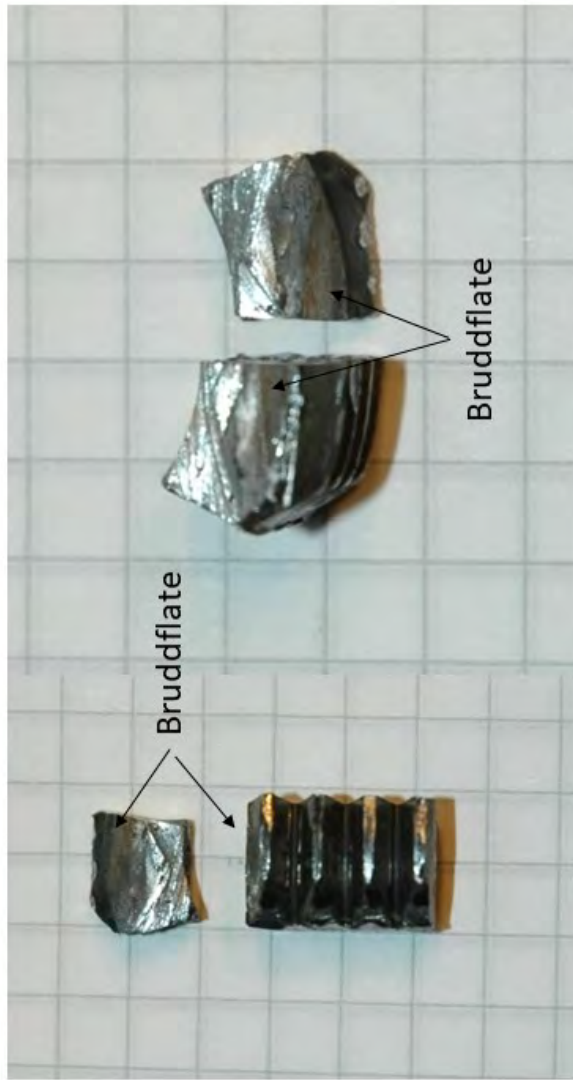
**NORWEGIAN
ARMED FORCES**

NORWEGIAN DEFENCE LOGISTICS ORGANISATION

Norwegian Defence Laboratories
Chemistry and Materials

M-18-054

Marianne E. Andreassen (mariandreasse@mil.no) Phone: 63808755
Øyvind Frigaard (ofrigaard@mil.no) Phone: 90957729



Bruddflate 14389, segment B, lamelle



Bruddflate 14389, segment B, lamelle



Bruddflate 14389, segment B, lamelle



Bruddflate 14389, segment B, lamelle



References

- [1] Avsluttende rapport 12,7 prosjekt - Funksjonsstudie maskingevær 12,7 x 99 NM 214 QCB og NM 218 Åpen bolt, 2013.
- [2] Ammunisjonsoppvarming på midtblokk NM218. Technical Report 2014102802, 2014.
- [3] Brudd i låseramme M2 HB fremme på høyre side. Technical-report MT-2014-0323, SINTEF Raufoss manufacturing, 2014.
- [4] Observasjoner for 12.7 mm mitraljøse. Technical-report 2014-0030, SINTEF Raufoss manufacturing, 2014.
- [5] Skadeundersøkelse på 12.7 mm mitraljøse. Technical-report 2014-0012, SINTEF Raufoss manufacturing, 2014.
- [6] 12,7 mm TUG, Skyteforsøk. Technical-report 2066390, NAMMO, 2015.
- [7] Sammenligning av materialegenskaper for pipe og låseramme, 12.7 mm MITR. Technical-report 150128-03, Forsvarets laboratorietjeneste, 2015.
- [8] Test Report. Kraftmåling M2 12,7. Vinghøg AS - Part of Rheinmetall AG, 2015.
- [9] Undersøkelse av sprekker i pipe og låseramme, 12.7 mm MTR. Technical-report 161116-01, Forsvarets laboratorietjeneste, 2016.
- [10] Sprekkundersøkelse 12.7 mm MITR. Technical-report Q-0737, 2017.
- [11] Aerospace Industrial Maintenance Norway (AIM). Magnetical Particle Testing Report. Technical-report AIM-MT-R-15-01, 2015.
- [12] NATO Army Armaments Group (NAAG). *Multi Calibre Manual of Proof and Inspection (M-C MOPI)*, AC/255(DSS)D(2013)0014 (PFP), Draft AEP-97, Edition A, Version 1 edition.

About FFI

The Norwegian Defence Research Establishment (FFI) was founded 11th of April 1946. It is organised as an administrative agency subordinate to the Ministry of Defence.

FFI's MISSION

FFI is the prime institution responsible for defence related research in Norway. Its principal mission is to carry out research and development to meet the requirements of the Armed Forces. FFI has the role of chief adviser to the political and military leadership. In particular, the institute shall focus on aspects of the development in science and technology that can influence our security policy or defence planning.

FFI's VISION

FFI turns knowledge and ideas into an efficient defence.

FFI's CHARACTERISTICS

Creative, daring, broad-minded and responsible.

Om FFI

Forsvarets forskningsinstitutt ble etablert 11. april 1946. Instituttet er organisert som et forvaltningsorgan med særskilte fullmakter underlagt Forsvarsdepartementet.

FFIs FORMÅL

Forsvarets forskningsinstitutt er Forsvarets sentrale forskningsinstitusjon og har som formål å drive forskning og utvikling for Forsvarets behov. Videre er FFI rådgiver overfor Forsvarets strategiske ledelse. Spesielt skal instituttet følge opp trekk ved vitenskapelig og militærteknisk utvikling som kan påvirke forutsetningene for sikkerhetspolitikken eller forsvarsplanleggingen.

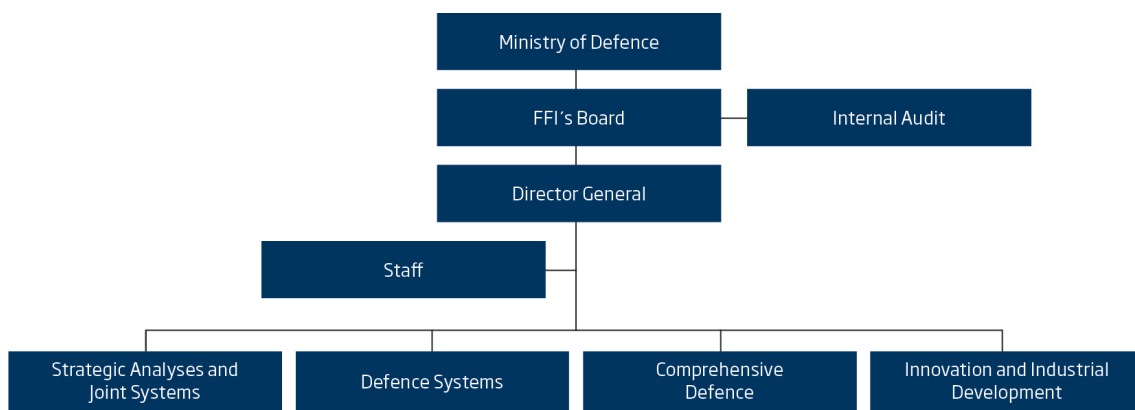
FFIs VISJON

FFI gjør kunnskap og ideer til et effektivt forsvar.

FFIs VERDIER

Skapende, drivende, vidsynt og ansvarlig.

FFI's organisation



Forsvarets forskningsinstitutt
Postboks 25
2027 Kjeller

Besøksadresse:
Instituttveien 20
2007 Kjeller

Telefon: 63 80 70 00
Telefaks: 63 80 71 15
Epost: ffi@ffi.no

Norwegian Defence Research Establishment (FFI)
P.O. Box 25
NO-2027 Kjeller

Office address:
Instituttveien 20
N-2007 Kjeller

Telephone: +47 63 80 70 00
Telefax: +47 63 80 71 15
Email: ffi@ffi.no